Journal of Nanotechnology

Surface-Enhanced Raman Scattering

Guest Editors: Mustafa Çulha, Nickolay Lavrik, Brian M. Cullum, and Simion Astilean

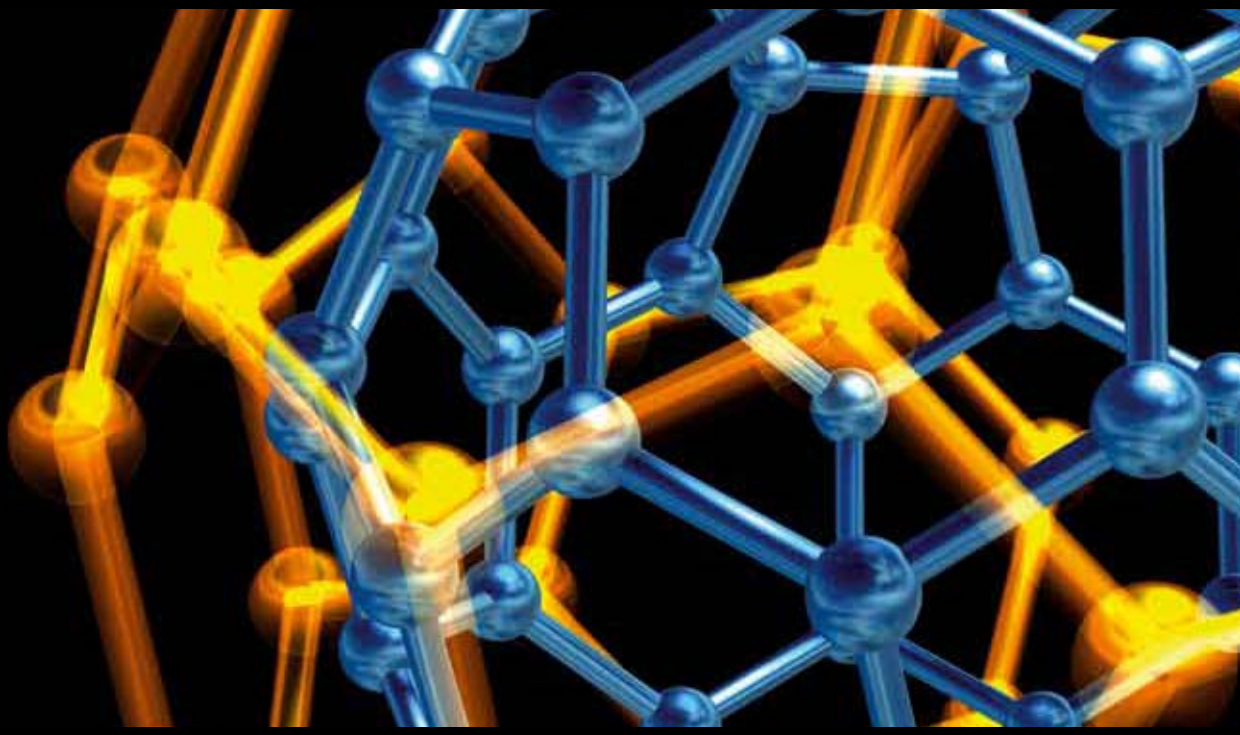

Surface-Enhanced Raman Scattering

Journal of Nanotechnology

Surface-Enhanced Raman Scattering

Guest Editors: Mustafa Çulha, Nickolay Lavrik,
Brian M. Cullum, and Simion Astilean

Editorial Board

Contents

Surface-Enhanced Raman Scattering, Mustafa Çulha, Nickolay Lavrik, Brian M. Cullum, and Simion Astilean
Volume 2012, Article ID 413156, 2 pages

Surface-Enhanced Raman Scattering as an Emerging Characterization and Detection Technique, Mustafa Culha, Brian Cullum, Nickolay Lavrik, and Charles K. Klutse
Volume 2012, Article ID 971380, 15 pages

Surface-Enhanced Raman Scattering of Bacteria in Microwells Constructed from Silver Nanoparticles, Mustafa Çulha, M. Müge Yazici, Mehmet Kahraman, Fikrettin Sahin, and Sesin Kocagöz
Volume 2012, Article ID 297560, 7 pages

SERS Substrates by the Assembly of Silver Nanocubes: High-Throughput and Enhancement Reliability Considerations, Oded Rabin and Seung Yong Lee
Volume 2012, Article ID 870378, 12 pages

Applications of Self-Assembled Monolayers in Surface-Enhanced Raman Scattering, Charles K. Klutse, Adam Mayer, Julia Wittkamper, and Brian M. Cullum
Volume 2012, Article ID 319038, 10 pages

Surface-Enhanced Raman Spectroscopy of Dye and Thiol Molecules Adsorbed on Triangular Silver Nanostructures: A Study of Near-Field Enhancement, Localization of Hot-Spots, and Passivation of Adsorbed Carbonaceous Species, Manuel R. Gonçalves, Fabian Enderle, and Othmar Marti
Volume 2012, Article ID 173273, 15 pages

Designing Gold Nanoparticle-Ensembles as Surface Enhanced Raman Scattering Tags inside Human Retinal Cells, Sanda Boca, Dumitrita Rugina, Adela Pintea, Nicolae Leopold, and Simion Astilean
Volume 2012, Article ID 961216, 10 pages

Relationship between Length and Surface-Enhanced Raman Spectroscopy Signal Strength in Metal Nanoparticle Chains: Ideal Models versus Nanofabrication, Kristen D. Alexander, Shunping Zhang, Angela R. Hight Walker, Hongxing Xu, and Rene Lopez
Volume 2012, Article ID 840245, 7 pages

Sensing Properties of a Fabry-Perot Dielectric Structure and Dimer Nanoparticles, A. Polemi and K. L. Shuford
Volume 2012, Article ID 745390, 7 pages

Hindawi Publishing Corporation
Journal of Nanotechnology
Volume 2012, Article ID 413156, 2 pages
doi:10.1155/2012/413156

Editorial
Surface-Enhanced Raman Scattering

Mustafa Çulha,[1] Nickolay Lavrik,[2] Brian M. Cullum,[3] and Simion Astilean[4]

[1] *Department of Genetics and Bioengineering, Yeditepe University, Atasehir, Kadıkoy, 34755 Istanbul, Turkey*
[2] *Center for Nanophase Materials Sciences, Oak Ridge National Laboratory, Oak Ridge, TN 37830, USA*
[3] *Department of Chemistry and Biochemistry, University of Maryland Baltimore County, 1000 Hilltop Circle, Baltimore, MD 21250, USA*
[4] *Nanobiophotonics Center, Institute for Interdisciplinary Experimental Research in Nanobioscience, Faculty of Physics, Babes-Bolyai University, T. Laurian 42, 400271 Cluj-Napoca, Romania*

Correspondence should be addressed to Mustafa Çulha, mculha@yeditepe.edu.tr

Received 10 June 2012; Accepted 10 June 2012

Surface-enhanced Raman scattering (SERS) is welcomed by researchers in a wide range of fields from physics to medicine. The reason behind this broad interest in SERS is a number of its unique features, such as high sensitivity, capability to provide chemically specific information about components of a sample, and applicability to a range of biological and nonbiological samples. The most important factor in its exponential growth is the interdisciplinary nature of the technique. Indeed, this issue covers a number of diverse and promising applications of SERS and further demonstrates its interdisciplinary landscape.

K. D. Alexander et al. investigated the relationship between length and SERS signal strength in gold nanoparticle (AuNP) chains. The spherical AuNPs with 60 nm sizes were brought into 1–9 nanoparticle chains in the channels (80 nm in width and 70 nm in depth) patterned on an SiO_2 substrate by applying capillary force deposition. The SERS enhancement factor strength for the chains was compared to the numerical predictions. It was found that while dimer nanoparticles offered large enhancement over single particles, increasing the chain length more than two nanoparticles does not appreciably improve the SERS enhancement. It was also stated that the surface morphology could be an important contributing factor that cannot be controlled with the current technology.

A. Polemi et al. reported "Sensing properties of a Fabry-Perot dielectric structure and dimer nanoparticles." In their study, the Fabry-Perot structures, disc dimers, and bowtie elements, are prepared by placing a superstrate with a high permittivity on a substrate with a very low permittivity to establish the resonance condition. They demonstrated that the array of disc dimers and bowties could effectively increase the SERS gain. They conclude their report by suggesting that other nanoparticle geometries and new array arrangements could be used for sensing.

There is a strong interest to employ the technique for microbial detection and identification. However, there are still a number of problems that need to be addressed before SERS can be efficiently used for identification of real microbial and cellular samples. One of the most important issues in its microbial applications is the reproducibility. M. Çulha et al. describes a novel substrate constructed from silver nanoparticles (AgNPs) to obtain more reproducible SERS spectra for bacterial identification. They compared the results of the study to their previously reported results obtained from the samples prepared with simple mixing and convective assembly. They concluded that the prepared SERS substrate generates similar reproducibility to the convective assembly but more improved reproducibility over simple mixing.

M. R. Goncalves et al. reported the investigation of hotspot formations on triangular silver nanostructures fabricated by thermal evaporation by examining the SERS of thiols and dye molecules adsorbed on these nanostructures. They observed that the hotspots were localized at the edges and corners of the silver triangular particles. They found that the strong and fast fluctuating SERS activity on the fabricated structures is due to the contamination of the nanostructure with amorphous carbon during the thermal evaporation process. They also observed that the adsorption of thiols and dye molecules on the newly prepared surfaces could reduce the undesired SERS activity.

S. Boca et al. reported a strategy to prepare small aggregates of dimers or trimers of AuNPs by capturing from solution and interlocking them into a polymeric cage of thiol-modified poly(ethylene) glycol (PEG-SH). Then, these small aggregates are used as sensing units by transferring into living cells as SERS tags. They demonstrated the usefulness of the approach by using human retinal cells.

O. Rabin and S. Lee reported the variations in SERS enhancement in clusters of assembled silver nanocubes with different sizes and configurations, and laser frequency and polarization. The assembly of silver nanocubes into small clusters on patterned silicon substrate by either vertical deposition or electrophoretic deposition was achieved. The study concluded that the face-to-face linear configuration of the nanocube clusters was not effective for the improvement in SERS enhancement as compared to the linear clusters where nanocubes are located along to an edge.

C. K. Klutse et al. reviewed "Applications of self-assembled monolayers (SAMs) in SERS." SAMs can enhance analytical capacity of SERS substrates improving their long-term stability, selectivity, and reproducibility. The authors focus on the use of SAMs to improve SERS enhancement further. They demonstrate the applicability of the approach from the novel multilayered SERS substrates developed in their laboratory. They claim that SERS enhancement could be greater than 20-fold compared to conventional single layer SERS substrates.

In this special issue, the editors also reviewed several promising but less frequently highlighted trends in preparation of SERS active substrates as well as some biological applications of SERS. While there is a consensus that SERS substrates fabricated using deterministic nanoscale patterning and wafer-level processing are very promising, broader analytical applications of such substrates are lagging behind compared to SERS-active systems prepared according to more conventional colloidal synthesis and assembly routes. This trend is particularly strong in biological applications of SERS, including detection and identification of proteins, microorganisms, and cellular samples; selected recent examples of which are highlighted in the review.

Mustafa Çulha
Nickolay Lavrik
Brian M. Cullum
Simion Astilean

Hindawi Publishing Corporation
Journal of Nanotechnology
Volume 2012, Article ID 971380, 15 pages
doi:10.1155/2012/971380

Review Article

Surface-Enhanced Raman Scattering as an Emerging Characterization and Detection Technique

Mustafa Culha,[1] Brian Cullum,[2] Nickolay Lavrik,[3] and Charles K. Klutse[2]

[1] *Department of Genetics and Bioengineering, Yeditepe University, Atasehir, Kadıkoy, 34755 Istanbul, Turkey*
[2] *Department of Chemistry and Biochemistry, University of Maryland, Baltimore County, 1000 Hilltop Circle, Baltimore, MD 21250, USA*
[3] *Center for Nanophase Materials Sciences, Oak Ridge National Laboratory, Oak Ridge, TN 37831, USA*

Correspondence should be addressed to Mustafa Culha, mculha@yeditepe.edu.tr and Nickolay Lavrik, lavriknv@ornl.gov

Received 3 March 2012; Accepted 27 April 2012

Academic Editor: Simion Astilean

While surface-enhanced Raman spectroscopy (SERS) has been attracting a continuously increasing interest of scientific community since its discovery, it has enjoyed a particularly rapid growth in the last decade. Most notable recent advances in SERS include novel technological approaches to SERS substrates and innovative applications of SERS in medicine and molecular biology. While a number of excellent reviews devoted to SERS appeared in the literature over the last two decades, we will focus this paper more specifically on several promising trends that have been highlighted less frequently. In particular, we will briefly overview strategies in designing and fabricating SERS substrates using deterministic patterning and then cover most recent biological applications of SERS.

1. Introduction

SERS is a Raman spectroscopic technique, which takes advantage of localized surface plasmon resonance (LSPR) in nanoscale systems based on coinage metals, such as silver and gold. As a result, Raman cross-sections of molecules on SERS-active substrates can reach values comparable to those of fluorescence spectroscopy [1–4]. Respectively, enhancements of Raman scattering signals ranging from a factor of 10^6 to 10^{16} have been reported in various studies [5–7]. The mechanisms for this enhancement in SERS are attributed largely to electromagnetic field enhancement due to LSPR and also to chemical interactions of the analyte with the substrate. As a result of these enhancements, SERS can have the sensitivity sufficient for the detection of ultratrace levels of analytes down to single molecules [3, 8]. This level of sensitivity is particularly useful for the detection of a small number of analyte molecules normally encountered in a single cell. Apart from the sensitivity, the inherent unique attributes of Raman are retained in SERS. Thus, it distinguishes vibrational signatures of molecular bonds, enabling label-free positive identification of analytes in complex cellular environments. Analyte detection can be multiplexed without spectral overlap because SERS provides spectra with narrow bandwidth. It is also very sensitive to slight changes in the orientation and structure of the molecules, allowing for structural elucidation. These characteristics, coupled with the weak Raman scattering of water, make SERS an ideal technique for analyzing complex biological samples that require little or no sample preparation. Importantly, SERS is achieved using a wide range of excitation frequencies, allowing for the selection of less energetic excitation (NIR to red) in order to reduce photodamage and background autofluorescence. Additionally, the analyte detection takes place at a close proximity to the SERS-active metal surface, thereby further reducing background autofluorescence through quenching. Therefore, SERS addresses most of the challenges of fluorescence detection for biological applications while providing comparable sensitivity.

Nanostructured metal surfaces or metal nanoparticle assemblies (commonly referred to as SERS substrates) are required for SERS measurements and their SERS activity and

measurement reproducibility largely influence the extent of SERS applications. As a result of this, the development of high-performing SERS substrates is an ongoing investigation.

A remarkably wide variety of SERS active substrates and media have been explored in the last few decades. While roughened noble metal surfaces [9] and noble metal colloids were among historically first SERS active objects, more complex and optimized plasmonic systems prepared by using elaborate chemical synthesis [10–12], template-directed deposition [13–15] and nanosphere self-assembly [16, 17] have subsequently set the standard in the area of SERS active substrates. In general, all technological strategies of creating SERS active substrates can be broadly divided into the three main categories: (i) chemical synthesis, (ii) template-assisted methods, and (iii) deterministic (lithographic) patterning. The former two strategies can be referred to as a "bottom-up" approach, while lithographic patterning is a typical "top-down" approach. Since each of these strategies has its own advantages and limitations, a notable recent trend in creating SERS substrates with improved performance consists in combining top-down and bottom-up technological strategies [18].

Metal colloids in suspensions or aggregation have widely been used for SERS measurements due to their ease of preparation by chemical synthesis and the high SERS activities they exhibit especially at the interparticle spacing [19–22]. SERS enhancement factors as much as 10^{16} have been reported with such substrates, allowing for single-molecule detection [23–26]. When these colloids are immobilized on solid supports using chemical or electrostatic interaction, their reproducibility is tremendously improved. This is due to the ability to control interparticle spacing between the immobilized metal colloids. Additionally, such control of interparticle spacing has been exploited in the investigation of some fundamental concepts of SERS [27–29]. Template-assisted SERS substrates development have largely been aided by the advances in nanotechnology, leading to existence of a broad range of such substrates in recent years. One advantage of this group of substrates involves the use of nanostructure templates to control the interparticle distance and improve the reproducibility. Nanosphere lithography, for example, involves the deposition of a metal film on nanosphere templates arranged on a solid platform followed by the removal of the template. This leaves a regular of array of SERS-active metal nanostructures on the solid platforms [30, 31]. Substrates derived from metal film on nanostructures (MFON) are another template method except in this case; the nanostructures are not removed after the metal deposition. Thus, both the underlying nanostructures and the metal film deposited serve as the SERS substrates [32, 33]. These types of substrate are easily controlled based on the thickness of the metal film deposited and the size of the templates used, yielding highly reproducible SERS substrates. Importantly, by depositing several layers of SERS-active metal films separated by dielectric spacers, MFONs can be used in a multilayer geometry for improved SERS enhancement by as much as 2 orders of magnitude, showing that the SERS enhancement of conventional substrates can be further increased [34–36]. Since SERS discovery, a large variety of substrates has been reported for its measurements as captured in recent reviews [37–40], and all of them could not be covered in this paper. Although experimental work on SERS of biological objects has relied predominantly on "bottom up" approaches, such as colloidal assembly and synthesis, SERS substrates implemented using "top down" strategies, such as EBL, are likely to yield to the most reproducible SERS substrates in the future. Therefore, the following section will review several specific deterministic patterning strategies that offer great promise for fabricating high-performance SERS substrates.

2. SERS Substrates Created Using Deterministic Patterning Strategies

It is worthy to note that, while chemical synthesis and template-directed methods have prevailed in creating intricate plasmonic structures with remarkable SERS performance [10, 41–44], deterministic patterning approaches, in particularly electron beam lithography (EBL), has been explored in the area of SERS far less extensively. This trend can be explained by the historically limited availability of EBL tools as well as the high cost of nanoscale lithographic processing compared to chemical synthesis. Nonetheless, notable examples of successful applications of EBL to SERS active substrates can be traced back to studies by Liao et al. in the early 1980s [45, 46]. A growing number of promising results on SERS active substrates prepared using lithography-derived processing have been reported more recently [18, 47–58].

In the section below, we will briefly discuss the recent advances in high-performance SERS substrates prepared using primarily EBL and wafer level cleanroom processing. Comprehensive discussions of conventional wafer level processes can be found in the literature [59]. Patterning of a substrate material by means of EBL is a multistep process that starts with designing patterns using computer-assisted design (CAD) software. EBL tool provides a programmable exposure of substrates coated with e-beam resist to a focused electron beam. As a result, the pattern is transferred onto a thin layer of e-beam resist that plays a role of a mask in the subsequent selective removal of the substrate material by dry or wet etching or in the subsequent selective removal of a deposited metal film by a liftoff process. Soft lithography relies on a patterned master to create morphologies complimentary to those present on the master in a single step, such as embossing or molding. Various modifications of anisotropic reactive ion etching (RIE) enable formation of grooves, wells, pillars, and other nonplanar structures on Si, SiO_2, and polymeric substrates with excellent control of the sidewall profile and characteristic sizes ranging from tens of nanometers [59]. As applied to SERS substrates, the main advantage of EBL patterning is its ability to create arbitrary 2D shapes with high fidelity on the spatial scale relevant to noble metal structures that exhibit localized plasmon resonance (LSPR) in the visible region of the

electromagnetic spectrum [60]. These features, combined with the wider availability of EBL tools to the research community, have facilitated efforts towards combinatorial [60] as well as model-driven [18, 51, 61–63] SERS active substrates.

The most notable types of deterministically patterned SERS substrates include (i) dense periodic arrays and gratings, [35, 46, 61] (ii) plasmonic structures with extremely small (5 nm or less) nanogaps [48, 52, 64, 65], and (iii) multiscale structures and structures with complex 3D architectures [18, 51, 57, 58, 66]. Silver-coated gratings [61] and dense periodic arrays of nanoscale pillars [45, 46] were among historically first SERS substrates created by means of EBL. Fabrication of such substrates involved three main processing steps: EBL patterning of the resist layer, RIE of the substrate material to the desired depth (typically several hundred nanometers), and physical vapor deposition (PVD) of a 25 to 50 nm silver layer. The SERS enhancements of the resulting structures were reported to be at least one order of magnitude larger than that of silver island films [52]. Subsequently, several modifications of this processing sequence was adapted to create various highly optimized SERS substrates [55, 57, 58].

Plasmonic dimers shaped as nanoscale bowtie antennas [54] represent another interesting class of structures that can be precisely fabricated using EBL and utilized as very promising high-performance SERS substrates [52]. These substrates were characterized by SERS enhancement factor exceeding 10^{11}. An alternative approach to plasmonic structures with sub-10 nm gaps that give rise to very strong local enhancements of optical fields relied on photolithographic patterning and an alumina sacrificial spacer layer deposited using atomic layer deposition [55]. Such vertically oriented plasmonic nanogap arrays were characterized by local SERS enhancements of up to 10^9. Yet another type of SERS substrates with plasmonic dimers with few nm gaps was fabricated by creating discontinuities in EBL-patterned bridge structures using electromigration [48]. Electromigrated nanoscale gaps exhibited extremely strong SERS.

More recently, several modifications of the fabrication sequence that combines EBL, RIE, and PVD have been used to create sombrero-shaped [58] and disc-on-pillar plasmonic architectures further optimized to achieve strong local field enhancements [63].

SERS signal enhancements sufficient for detection of few molecules in vicinity of hot spots were reported for the sombrero-shaped structures [58] while the disk on-pillar structures exhibited averaged SERS enhancement factors above 10^9 [57].

A very interesting concept of aperiodic multiscale structures that takes advantage of the cascade enhancement effect was implemented using EBL patterning and subsequent in situ spatially selective reduction of gold. These two successive steps resulted in hierarchal formation of plasmonic nanoparticles with two characteristic sizes of approximately 200 nm and 30 nm, respectively. These multiscale structures exhibited reproducible spatially averaged SERS enhancements similar to 10^8 [18].

Although fabrication of the majority of the SERS active substrates discussed above relied on EBL, similar structures could be created using alternative approaches, such as optical interference [66, 67], nanostensil [68] lithographies, and laser-induced synthesis [68, 69]. Compared to these latter techniques, advantages of EBL include its wider availability and applicability to patterning both periodic [40] and aperiodic patterns [18, 50] of arbitrary shapes, a particularly useful feature at the research stage. A relatively low throughput and high cost of EBL tools makes them less attractive for scaled-up fabrication of SERS substrates. In order to make deterministic patterning of SERS substrates scalable, more flexible and less expensive advantages of EBL can be further augmented by nanoimprinting, nanoembossing [70], and nanotransfer stamping/printing approaches [53, 54]. For instance, a small-area silicon master with nanoscale patterns can be created using a combination of EBL and RIE and then used in a step-and-repeat process to pattern larger areas and/or a number of SERS substrates in a cost- and time-efficient manner.

3. Design of SERS-Based Nanosensors for Cellular Applications

In addition to lithographically produced or patterned substrate fabrication, SERS has also seen several significant advances in its application to biological and intracellular analyses over the pat decade. Such analyses take advantage of the inherent nanoscale size of the SERS active substrates to perform highly localized chemical-specific investigations. During the past couple of decades, such analyses have advanced from the pioneering work of inserting gold colloidal probes inside a cell for SERS-based chemical imaging of whatever species were present at the probes surface, to more recent versions of SERS-based sensors with various biological receptors for added specificity. In such analyses, the highly enhancing nature of the substrate must be retained as well as the addition of specific receptors. Figure 1 represents the general model of a typical SERS-based nanosensing showing a SERS nanosensor made of a SERS-active nanoparticle with a recognition elements tethered to it. The particle is a nanostructure small enough to be inserted into a living cell without significant perturbation or toxicity. It is also capable of supporting the induction of localized electromagnetic field when excited so that the molecular information of analyte closer to it can be obtained by SERS. Nanostructures made from gold and silver are often used as SERS-active particles because they provide the most enhanced SERS signals especially in the visible to NIR region. To promote analyte specificity, the SERS-active nanostructure can be attached with analyte recognition elements (e.g., enzymes, aptamers, and Fabs) or a Raman reporter. For intracellular analyte detection, the SERS nanosensor is inserted into the cell (through cellular uptake or physical injection). The targeted analyte interacts with the recognition elements and is brought closer to the SERS-active particle. The nanosensor is interrogated with an

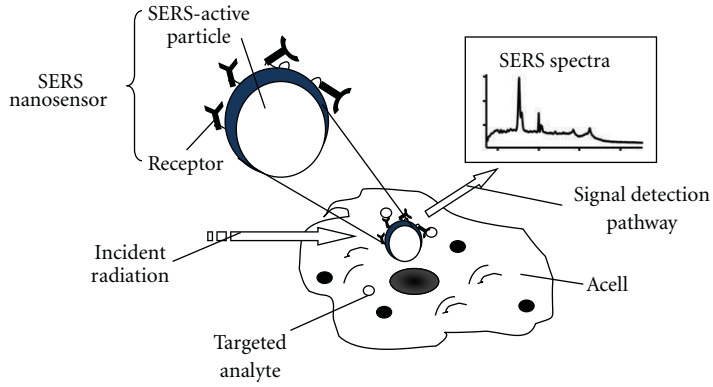

Figure 1: A general concept of SERS-based intracellular nanosensing.

appropriate excitation source and the scattered radiation is collected and detected by a photodetector.

3.1. Application of SERS in Intracellular Analyses. Colloidal plasmonic gold nanoparticles are commonly used for SERS-based intracellular analyses due to their small sizes, SERS-activity, and biocompatibility [71, 72]. Kneipp and coworkers were among the pioneers of SERS-based individual live cells monitoring [73–76]. In one study, gold nanoparticles with sizes ranging from 30 to 50 nm were introduced into immortalized rat renal proximal tubule (IRPT) cells and mouse microphage cell line (J774), via endocytosis. To minimize background autofluorescence, 786 nm was used for excitation source for the measurement of SERS spectra at different time points. Remarkably, it was noticed that the pattern of SERS fingerprints changed over time, with the spectra taken two hours after particles internalization showing the largest number of bands and highest intensity [63]. From these study, the potential of SERS as a sensitive method for label-free analyte detection inside an individual living cell was demonstrated. However, because any species in contact with the metal surface could potentially provide a signal, a significant background problem with such studies was found to exist. Furthermore, the strong interaction of some biological molecules with metal surfaces often resulted in biological fouling, as biomolecules randomly adsorbed onto the metal surfaces [73, 75, 77].

To selectively detect specific analytes in complex biological environments, nanoparticles have been immobilized with chemical receptors to form SERS-based nanosensors. Most of such SERS-based nanosensors have been developed for pH monitoring [78–82]. In one study, 4-mercaptobenzoic acid with pH sensitive COO^- vibration (1430 cm^{-1}) was self-assembled on SERS-active nanoparticles. By monitoring the intensity of COO^- vibration, it was possible to monitor pH in Chinese hamster ovary cells at physiological concentrations [83]. Recently, functionalized gold nanoparticles have been used to monitor intracellular redox potential changes in NIH/3T3 fibroblast cells [75]. SERS-active nanoparticles made of 125 nm silica core and 25 nm thick gold shells were modified with redox-active SERS molecules (e.g. 2-mercaptobenzene-1, 2-diol). The redox-active molecules responded to the concentration of oxidative and reductive species in the cell through reversible redox reaction leading to slight changes in structure, which was reflected in SERS spectra [84].

3.2. SERS-Based Immunonanosensors. With increasing development of different types of SERS-active nanomaterials, it became clear that improvement in the specific analyte detection capability of these nanomaterials can rapidly advance SERS intracellular nanosensing technology. In view of this, various biorecognition molecules (including enzymes, Fabs, and aptamers) were earmarked for the development of SERS bionanosensors [85–88]. Efforts in this direction have led to the development of SERS bionanosensors employing antibodies for analyte recognition [89–92]. These SERS immunonanosensors developed by Cullum and coworkers employed metal film over nanostructure (MFON) SERS-active nanoparticles to provide uniform sensitivity [93] without the need for particle aggregation. Antibodies for specific antigens were immobilized on these nanoparticles to broaden the classes of analytes that can be interrogated to include proteins/peptides [91, 92] and other immunogenically recognized biomolecules (e.g., glucose, insulin, etc.) [89, 94].

Insulin receptive immunonanosensors were fabricated by immobilizing anti-human insulin receptors on MFON SERS-active particles via crosslinkers. Suitable crosslinkers were identified by characterizing several crosslinkers. Figure 2 shows the spectra of 2-mercapto-4-methyl-5-thiazoacetic acid (MMT), which was the preferred crosslinker because it exhibited rigidity and minimal spectral peaks while providing significant bands for use as internal standards. After attachment of the receptor (i.e., antibody) via traditional EDC chemistry, evaluation of the fabricated immunonanosensors in the cell culture media revealed significant and reproducible changes in the SERS spectra physiological concentrations of human insulin.

This was because antibody-analyte interaction led to changes in the conformation of the antibody. The spectra showing the various stages of nanosensor evaluation are shown in Figure 3. That specific Raman bands (443, 808, 1625 cm^{-1}), which are associated with the antibody, were

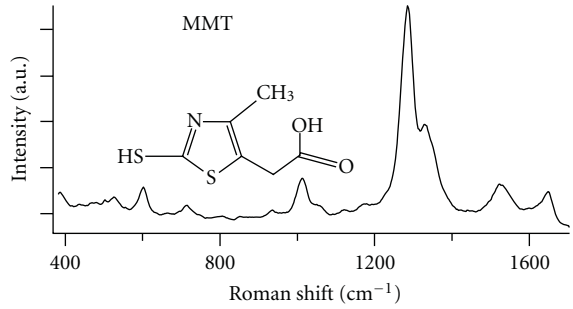

Figure 2: SERS spectra and structure of the cross-linker MMT.

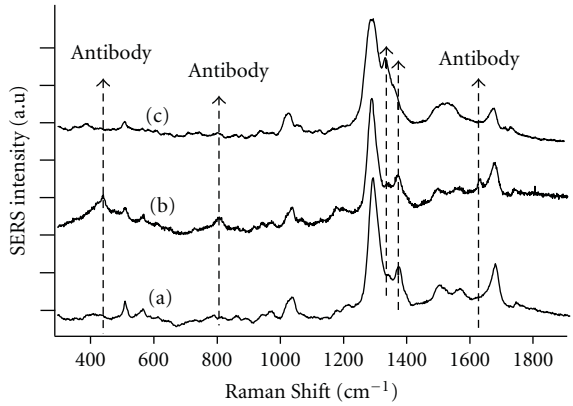

Figure 3: SERS spectra of (a) activated MMT bound to silver-coated nanosphere with 40% surface coverage, (b) after binding anti-human insulin to the MMT, and (c) of (b) (immunonanosensors) in the presence of 10 μg/mL of insulin.

not present when the analyte interacted with the receptor. By attaching interleukin II (IL-2) receptors to SERS nanosensor surfaces through the same attachment process, it was possible to fabricate different types of nanosensors for the detection of IL-2 to a level as low as 10 μg/mL [92, 95] indicating that the nanosensors could be modified for a wide range of applications.

3.3. SERS-Based Nanoimaging. Besides achieving sensitivity for ultratrace intracellular analyte detection, extracellular SERS imaging of cellular and bacterial surfaces has recently seen significant interest. Such extracellular imaging is capable of providing important chemical specific spatial information (e.g., size and distribution) of the macromolecules present. Such analyses significantly improve our understanding of how macromolecules are transported and assembled at specific sites particularly if rapid dynamic imaging is possible. To achieve such analyses, SERS methods with high-spatial resolution are required. A commonly used configuration for improving the spatial resolution of SERS is the tip-enhanced Raman spectroscopy (TERS). This takes advantage of a precise positioning of a nanotip SERS-active substrate to achieve localized SERS enhancement with subdiffraction-limited spatial resolution. TERS is normally achieved by modifying the tips of scanning probe microscopy (SPM) with SERS-active metals. For example, SERS has been coupled with near-field scanning optical microscopy (NSOM), to provide highly resolved chemical images of multiple trace species [96–98]. Other SPMs that have been coupled with SERS to provide the subdiffraction-limited chemical imaging are atomic force microscopy AFM and scanning tunneling microscopy STM [99, 100]. For example, silver coated AFM-tip has been used to gather both topographical and SERS spectral information of a bacterial membrane. The SERS spectral showed the peptide and sugar components of the cell surface [100]. However, TERS is only useful for static images as it typically requires long periods of time to scan across the entire sampling area.

To provide a nanosensor/nanoprobe capable of obtaining dynamic images, a novel nanoimaging probe has been developed whereby coherent fiber optic imaging bundles were coupled with SERS for real-time subdiffraction-limited chemical imaging [68, 101–104]. This SERS nanoimaging probe has an advantage of providing both temporal and spatial resolution, thereby allowing the monitoring of the movement of macromolecules across membranes. The technique takes advantage of a tapered fiber optic with a large collection of fiber elements (30 000). The coherent nature of the packed bundle is retained during the tapering process, which is controlled in order to vary the diameter of the entire tip. This variation in diameter yields predictable spatial resolution that can be varied from microscopic to subdiffraction-limited levels. The SERS surface is produced on the tip through a controlled chemical etching process followed by selective deposition of silver or gold, which creates reproducible hexagonal spikes for the roughness (Figure 4). For this reason, uniform SERS enhancements across the surface of the probe are achieved.

In proof-of-principle studies, such probes have been used for chemical differentiation of various samples with <100 nm spatial resolution [68, 101–104]. In one such study, gelatin was homogenously mixed with brilliant cresyl blue (BCB), while benzoic acid was spotted at various locations around the edge. By tuning to the appropriate wavelength, each of the two analytes was selectively imaged in the sample as shown in the images and the spectra in Figure 5. Additionally, time-lapse images actually allowed for the diffusion of the chemicals to be monitored with millisecond temporal resolution [68, 101]. Using these SERS nanoimaging probes, dynamic visualization of biochemical species associated with cell membrane components have been measured, demonstrating the potential of such probes for providing a deeper understanding of the various physiological processes in cellular membranes [105].

4. Detection, Identification, and Characterization of Biomacromolecules and Microorganisms

There is an enormous interest to use SERS for the solution of problems in biorelated fields such as medicine, molecular biology, and microbiology. The advantage of SERS over other techniques such as fluorescence, IR, and mass spectroscopy

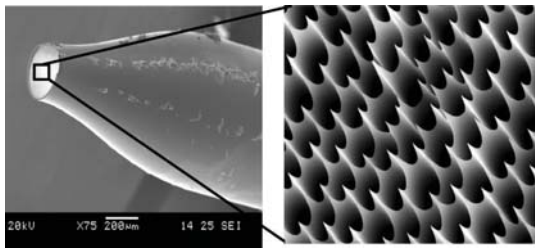

Figure 4: SEM images of (a) a tapered optic fiber probe and (b) its etched tip which is coated with SERS-active metal.

is already stated above. Although all these techniques have distinct advantages, SERS could be a proper replacement for certain applications. For example, narrow-spectral bandwidth, detection and identification of a molecule without an external label, insensitivity to water, nondestructive nature, and low cost for instrumentation can be given the advantages over the mentioned techniques. However, the several issues inherent to the nature of the technique, mainly reproducibility, still persist and lower the applicability to its wide spread use in biological applications.

The detection and identification of several biological molecules such as proteins [106–110], DNA [111–114], and RNA [115, 116] and molecular organizations such as bacteria [117–126], yeast [127–129], and viruses [130, 131] using SERS were reported. The detection scheme could be based on either using the intrinsic fingerprint information of the molecules or molecular structures or the use of an external label. Although the use of the molecules' fingerprint spectrum is highly desirable for identification and detection, obtaining a healthy spectrum from a biological molecule such as proteins could be difficult. In this section, the detection and identification of proteins, DNA/RNA and whole microorganisms will be discussed. There are several reviews [132–134] in literature summarizing the developments in previous years and only most recent and some of the important reports are discussed here.

In most of the indirect protein detection assays, SERS is used as a replacement of either fluorescence or staining step. There are several reports regarding the use of the technique in immunoassays format for protein or microorganism detection [135–141]. In immunoassay-based approaches, a recognition element, an antibody, captures the target and a transducer converts the biological recognition to readout. The transducer could be a radiological, electrochemical, or optical. SERS is generally used as a replacement of these transducers types. The high sensitivity and the multiplexing properties of the technique can be given as its advantages over other transducer types.

In a one-step homogenous immunoassay, label-free detection of human IgG down to 0.1 μg/mL without using an external label was reported [126]. In another report, a photobleaching-resistant immunoassay system was developed for the detection of protein A, which is the surface antigen of *Staphylococcus aureus*. The achieved detection limit for this protein was 1 pg/mL [136].

In a recent study, a SERS-based sandwich immunoassay coupled with an optoelectronic microfluidic system for the detection of human tumor marker, alphafetoprotein, was reported. A detection limit down to 0.1 ng/mL using a 500 nL sample droplet in 5 minutes was accomplished [137]. Figure 6 illustrates the optoelectronic sandwich immunoassay procedure.

In another recent report, immunoassay-based SERS method for the detection of cancer marker, angiogenin (ANG), and alpha-fetoprotein (AFP), was successfully demonstrated with a detection limit of 0.1 pg/mL and 1.0 pg/mL, respectively [138]. Wang et al. demonstrated the detection of MUC4 in real samples, which is a pancreatic cancer marker, using a SERS-based immunoassay platform [139]. The detection of bacteria based on SERS immunoassay is also attracting interest. In a heterogeneous immunoassay, the detection of *E. coli* concentration in range of 10^1–10^5 cfu/mL was demonstrated [140]. The same group also demonstrated the detection of *E coli* down to 8 cfu mL^{-1} using a sandwich immunoassay [141].

The detection and identification of proteins have a critical importance in several fields including medicine, biotechnology, and pharmacology. The conventional approaches such as immunoassay-based techniques and mass spectroscopy are powerful but they have certain drawbacks such a low sensitivity with immunoassay-based techniques and high-cost with mass spectroscopic approach. With the proven high sensitivity, SERS can be a complementary technique, even alternative to some applications, for the protein detection and identification. As mentioned earlier, SERS can be used as replacement for fluorescence or radiolabeling. However, the potential of the technique for label-free detection and identification of biomacromolecules has not been fully explored yet. Among the biomcaromolecules, the proteins are the most important group, and their detection and identification have a great importance. Therefore, the use of SERS as label-free detection and identification of proteins is pursued. Han et al. recently reviewed the detection of proteins using SERS [142]. The biggest obstacle with the label-free detection of proteins is the diversity of the protein shape, size, and surface charge properties. When colloidal noble metal nanoparticles are used in the SERS experiment, it is very difficult to control the aggregation behavior of the protein-NP structures during drying process. When a simple mixing and drying approach is used for the sample preparation, only proteins with a chromophore/heme group provide reasonably rich spectra. Otherwise, a very poor spectrum is obtained. Therefore, a more systematic approach must be followed to obtain good spectra from proteins. For example, Zhou et al. reported fast label-free semiquantitative detection of proteins down to submonolayer coverage using nitrate ion [143].

Kahraman et al. recently used "convective-assembly" approach for label-free detection of proteins regardless of their size, shape, and surface charge [108]. In this approach, mixture of protein-AgNP colloid is spotted at the cross-section of two glass slides, which one is placed on a moving stage and other is located with an angle of 23° on top of the other at a fixed position. Figure 7 shows the

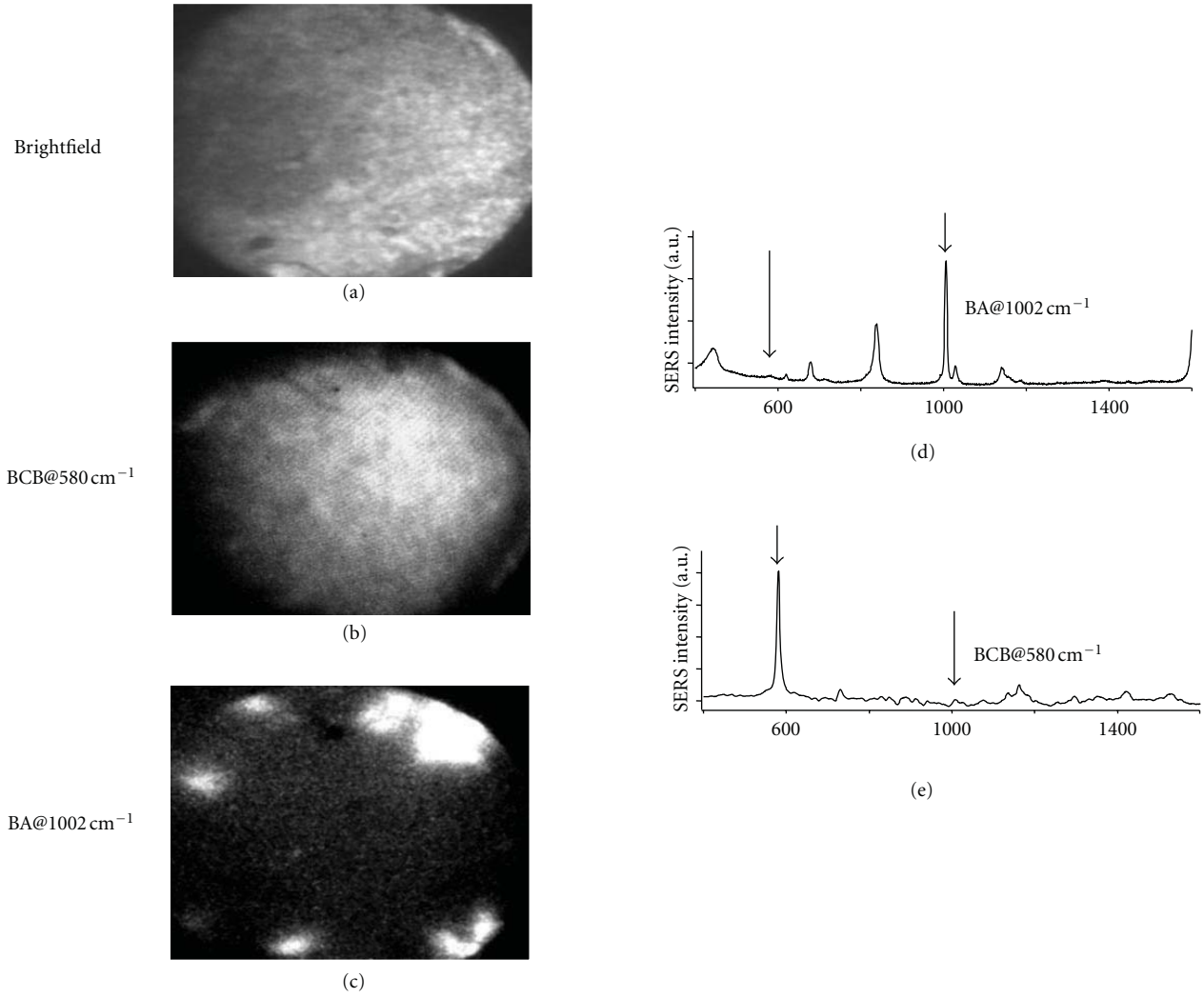

Figure 5: Chemical differentiation using SERS imaging probe tapered down to 140 nm. (a) A brightfield image of the gelatin, (b) a SERS image of the localized benzoic acid, and (c) a SERS image of the BCB, and (d) and (e) are the corresponding spectra of images (b) and (c), respectively.

"convective-assembly" set-up and process. As the stage moves, the droplet at the cross-section is slowly dragged. During the dragging process, the evaporation forces the protein-AgNP structures to form a thin film in a more controlled manner. During the drying process AgNP and proteins are forced to stay close to each other, which has a dramatic effect on SERS spectra. Using this approach, a more reproducible sample preparation was possible. The detection limit using this approach was estimated as 0.50 μg/mL for all proteins used in the study, which was about one order of magnitude lower than the previously reported detection limits. The same group later also demonstrated the differential separation of the binary and ternary protein mixtures using convective assembly process and detection and identification of proteins in these mixtures [110].

Whole microorganism detection and identification using SERS is another research area where the fingerprint spectra obtained from whole microorganisms can be used. There are a number of studies demonstrating the feasibility of technique for whole bacterial detection and identification [117–126]. The identification and classification of bacteria causing urinary tract infections were demonstrated by Goodacre group using citrate reduced AgNPs [123]. The use of gold-coated silica nanoparticles as substrate and a barcoding approach was later used for the bacterial identification by Zeigler group [144]. The major problem with the application of SERS as a technique for microorganism identification is the spectral reproducibility. When the fact that the microorganisms are living systems is taken into account besides the number of parameters influencing the ultimate spectrum due to the nature of the technique, it becomes more confusing. Therefore, a solid protocol is obligatory for healthy interpretation of the obtained results. In this regard, Kahraman et al. followed several different approaches to obtained reproducible spectra from bacteria and studied the parameters influencing spectral reproducibility such as laser wavelength and colloidal nanoparticle concentration used for sample preparation [145].

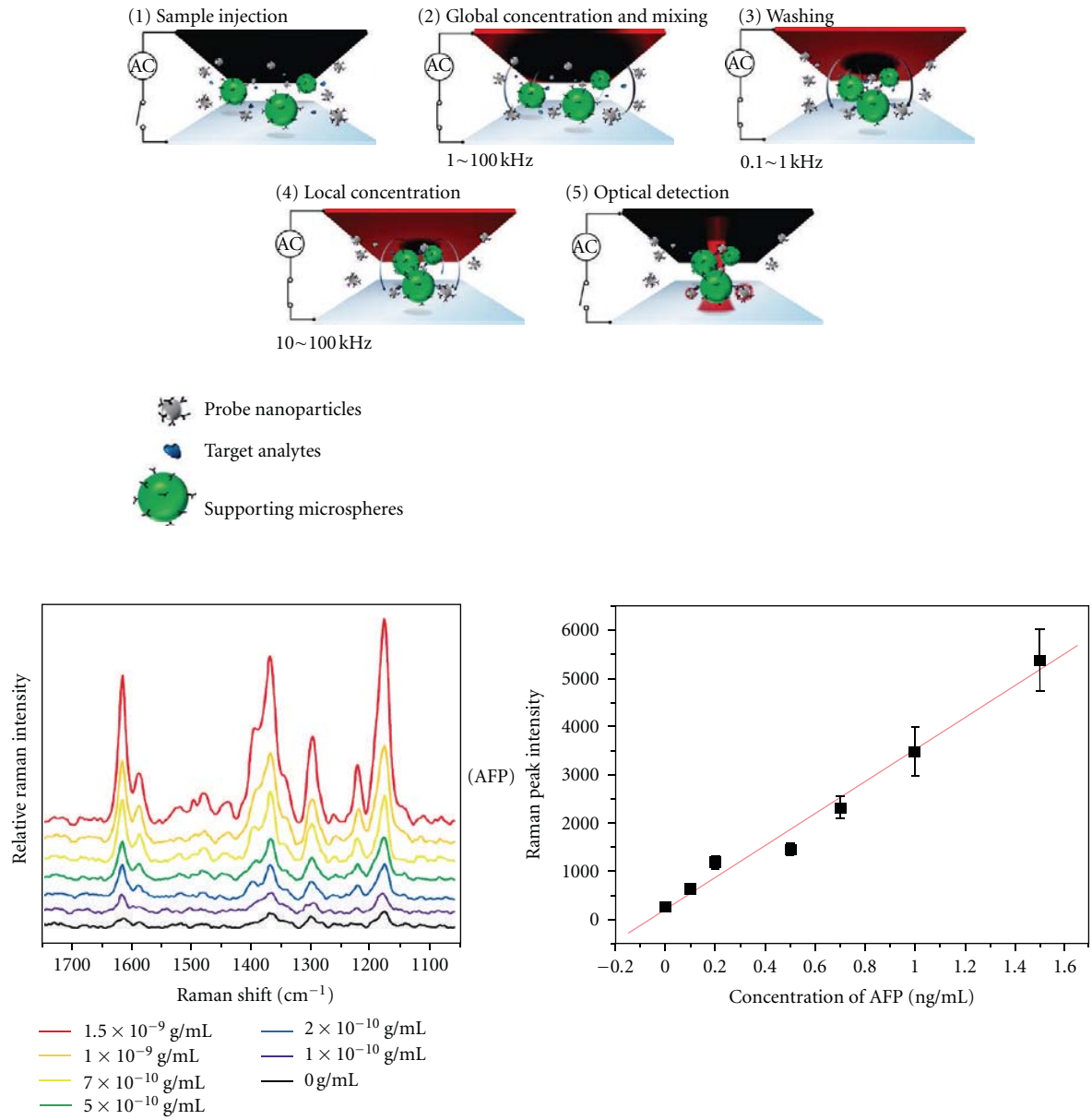

Figure 6: Illustration of optoelectronic sandwich immunoassays procedure, SERS spectra at decreasing AFP concentrations, and calibration curve at 1615 cm^{-1}, reprinted with permission from [137].

For example increasing the colloidal AgNP concentration before mixing with the bacterial sample improved the sample-to-sample spectral reproducibility [126]. In another example, the bacteria and AgNPs were assembled into a thin film with "convective-assembly" method in order to generate a more uniform sample on a surface [146]. Figure 8 shows the SEM image of a sample assembled onto a glass surface using convective assembly. As it was stated above, there are several parameters that may affect the SERS spectra of microorganisms. In addition to the parameters pertaining to the SERS experimental conditions such as substrate and laser wavelength, the microorganisms are living things and they may show variations in their biochemical structure as they continue to grow in their life cycle. Besides the reproducibility issues, the origin of the spectral bands has not been completely understood yet.

When colloidal AgNPs or AuNPs are mixed with a complex biological sample, the molecular or ionic species that have an affinity for the noble metal surface preferentially interacts with the metal surface. From this point, one can easily conclude that the SERS spectra from such a complex mixture are dominated by the vibrational bands originating from those molecules or species preferentially bound to the metal surface. This leads to the striking similarity in the spectral pattern of biological samples, even though they are completely from different origins. For example, the growth media for bacterial has striking similarity with some bacteria such as *E. coli*. Keeping this point in mind, one needs to be

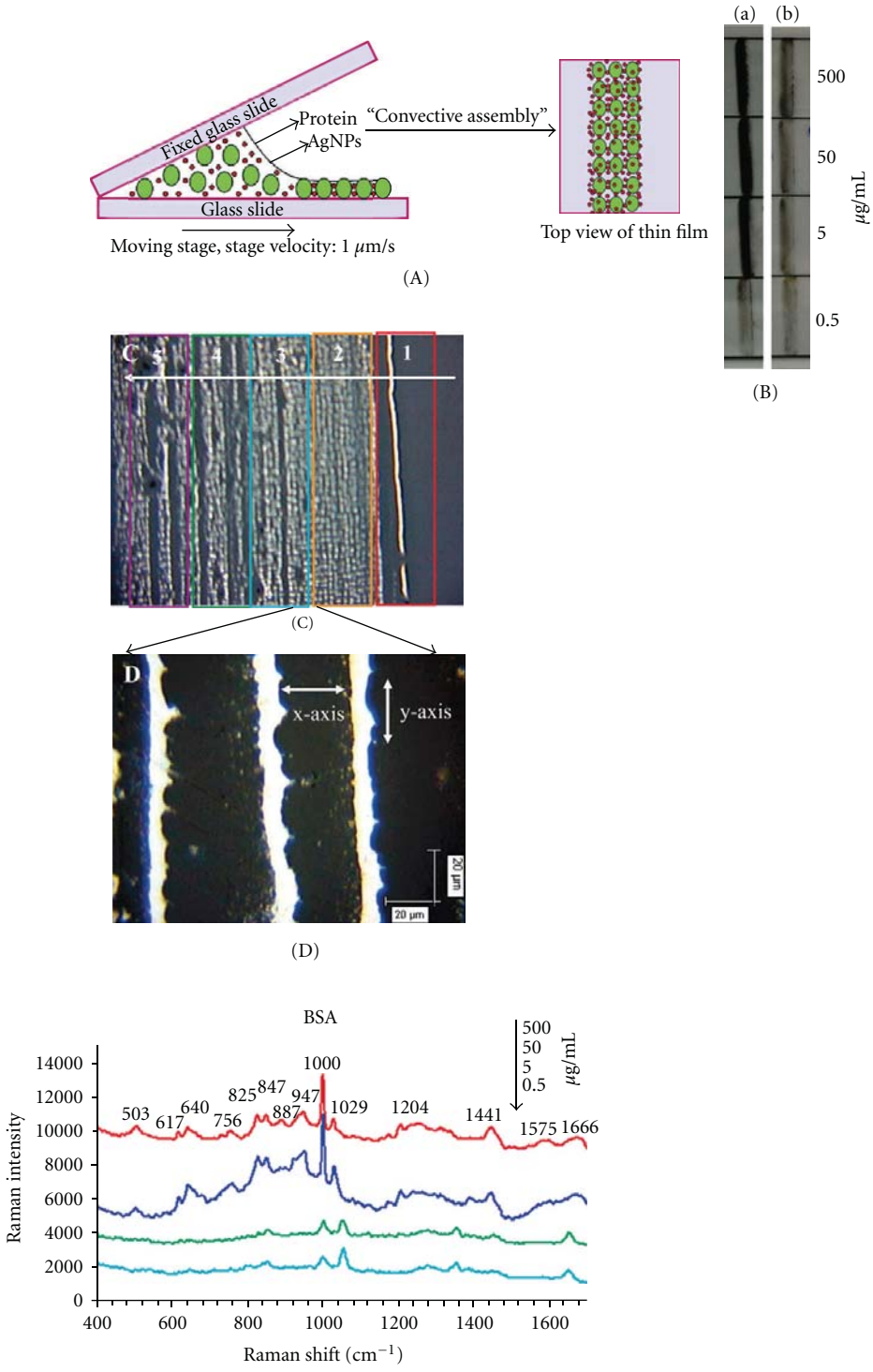

Figure 7: Illustration of process of convective assembly of protein-AgNP mixtures (A), photograph of lysozyme (a) and BSA (b) thin films (B), thin film images of BSA-AgNP film structures under 5x (C) and 50x objectives (D). SERS spectra of BSA-AgNP with decreasing concentrations, reprinted with permission from [108].

very careful with the experimental design and should have a very good knowledge of the sample composition and sample handling for a healthy interpretation of the experimental result. The origin of the bands that appeared on the SERS spectra of bacteria was independently investigated by two groups. Kahraman et al. demonstrated that the SERS spectra obtained from a bacterial sample after several washing steps originate from the bacterial structures on the bacteria wall with some contribution from metabolites released during the sample preparation, mixing, and drying [147]. Premasiri

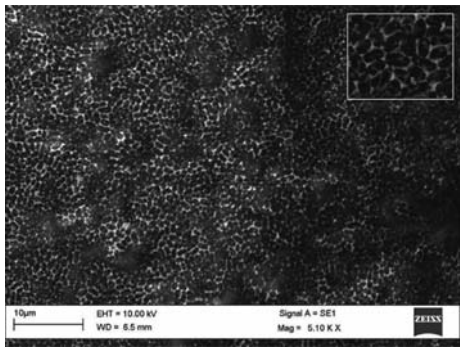

Figure 8: "Convectively assembled" *E. coli* on glass surface, reprinted with permission from [146].

et al. showed that the bacteria grown in different culture media resulted with the same SERS spectrum indicating the source of spectral features on the spectrum were from bacteria [148].

5. Conclusions

The investigation and optimization of high performing SERS substrates remains a very active area pursued by a number of cross-disciplinary research teams. The evidence, that SERS can be used for single-molecule detection and clear understanding of the relationship between LSPR and SERS enhancement mechanism, has inspired many recent studies focused on design and fabrication of new types of SERS substrates [149–151].

A number of recent studies indicate that SERS is a viable analytical technique for detection and differentiation of chemical species in biological cells and biologically relevant samples. Chemically synthesized noble metal nanoparticles and colloidal systems have been among SERS substrates with the highest reported values of SERS signal enhancement. Chemically synthesized noble metal colloids are also the most suitable SERS substrates for biological assays. This is largely due to their stability in aqueous media, inexpensive synthesis, and wide availability of precursor chemicals. On the other hand, a combination of deterministic (lithographic) patterning and wafer level processing offers a very attractive alternative route to SERS substrates that can be rationally designed and further optimized using theoretical models. It can be anticipated that this latter approach will ultimately lead to highly reproducible SERS substrates suitable for analysis of biological samples.

Although applications of lithographically patterned SERS substrates to detection of biological analytes remain relatively rare, ongoing efforts that bridge distinct technological strategies will likely bring a series of breakthroughs in this area in the nearest future. Already an impressive reproducibility and stability have been achieved in SERS analysis of biological samples using recently implemented SERS substrates. In many cases, however, the sensitivity needs to be improved in order to achieve the same level of success as with fractal colloidal aggregates. Further substantial advances can also be anticipated in SERS-based imaging with applications to live biological cells and microorganisms.

Acknowledgments

N. Lavrik acknowledges support by the Scientific User Facilities Division, Office of Basic Energy Sciences, U.S. Department of Energy. M. Culha acknowledges support by Scientific and Technological Research Council of Turkey (TUBITAK) and Yeditepe University.

References

[1] A. Campion and P. Kambhampati, "Surface-enhanced Raman scattering," *Chemical Society Reviews*, vol. 27, no. 4, pp. 241–250, 1998.

[2] A. Otto, "What is observed in single molecule SERS, and why?" *Journal of Raman Spectroscopy*, vol. 33, no. 8, pp. 593–598, 2002.

[3] K. Kneipp, Y. Wang, H. Kneipp et al., "Single molecule detection using surface-enhanced Raman scattering (SERS)," *Physical Review Letters*, vol. 78, no. 9, pp. 1667–1670, 1997.

[4] I. Pavel, E. McCarney, A. Elkhaled, A. Morrill, K. Plaxco, and M. Moskovits, "Label-free SERS detection of small proteins modified to act as bifunctional linkers," *Journal of Physical Chemistry C*, vol. 112, no. 13, pp. 4880–4883, 2008.

[5] K. L. Kelly, E. Coronado, L. L. Zhao, and G. C. Schatz, "The optical properties of metal nanoparticles: the influence of size, shape, and dielectric environment," *Journal of Physical Chemistry B*, vol. 107, no. 3, pp. 668–677, 2003.

[6] C. L. Haynes and R. P. Van Duyne, "Plasmon-sampled surface-enhanced Raman excitation spectroscopy," *Journal of Physical Chemistry B*, vol. 107, no. 30, pp. 7426–7433, 2003.

[7] S. Nie and S. R. Emory, "Probing single molecules and single nanoparticles by surface-enhanced Raman scattering," *Science*, vol. 275, no. 5303, pp. 1102–1106, 1997.

[8] M. E. Hankus, H. Li, G. J. Gibson, and B. M. Cullum, "Surface-enhanced Raman scattering-based nanoprobe for high-resolution, non-scanning chemical imaging," *Analytical Chemistry*, vol. 78, no. 21, pp. 7535–7546, 2006.

[9] M. Moskovits, "Surface roughness and the enhanced intensity of Raman scattering by molecules adsorbed on metals," *The Journal of Chemical Physics*, vol. 69, no. 9, pp. 4159–4161, 1978.

[10] D. K. Lim, K. S. Jeon, H. M. Kim, J. M. Nam, and Y. D. Suh, "Nanogap-engineerable raman-active nanodumbbells for single-molecule detection," *Nature Materials*, vol. 9, no. 1, pp. 60–67, 2010.

[11] L. J. Sherry, S. H. Chang, G. C. Schatz, R. P. Van Duyne, B. J. Wiley, and Y. Xia, "Localized surface plasmon resonance spectroscopy of single silver nanocubes," *Nano Letters*, vol. 5, no. 10, pp. 2034–2038, 2005.

[12] L. J. Sherry, R. Jin, C. A. Mirkin, G. C. Schatz, and R. P. Van Duyne, "Localized surface plasmon resonance spectroscopy of single silver triangular nanoprisms," *Nano Letters*, vol. 6, no. 9, pp. 2060–2065, 2006.

[13] S. J. Hurst, E. K. Payne, L. Qin, and C. A. Mirkin, "Multisegmented one-dimensional nanorods prepared by hard-template synthetic methods," *Angewandte Chemie*, vol. 45, no. 17, pp. 2672–2692, 2006.

[14] L. D. Qin, S. Park, L. Huang, and C. A. Mirkin, "Matrials science: on-wire lithography," *Science*, vol. 309, no. 5731, pp. 113–115, 2005.

[15] H. Ko and V. V. Tsukruk, "Nanoparticle-decorated nanocanals for surface-enhanced Raman scattering," *Small*, vol. 4, no. 11, pp. 1980–1984, 2008.

[16] C. L. Haynes and R. P. Van Duyne, "Plasmon-sampled surface-enhanced Raman excitation spectroscopy," *Journal of Physical Chemistry B*, vol. 107, no. 30, pp. 7426–7433, 2003.

[17] C. L. Haynes and R. P. Van Duyne, "Nanosphere lithography: a versatile nanofabrication tool for studies of size-dependent nanoparticle optics," *Journal of Physical Chemistry B*, vol. 105, no. 24, pp. 5599–5611, 2001.

[18] A. Gopinath, S. V. Boriskina, W. R. Premasiri, L. Ziegler, B. M. Reinhard, and L. D. Negro, "Plasmonic nanogalaxies: multiscale aperiodic arrays for surface-enhanced Raman sensing," *Nano Letters*, vol. 9, no. 11, pp. 3922–3929, 2009.

[19] K. Kneipp, H. Kneipp, I. Itzkan, R. R. Dasari, and M. S. Feld, "Ultrasensitive chemical analysis by Raman spectroscopy," *Chemical Reviews*, vol. 99, no. 10, pp. 2957–2975, 1999.

[20] K. Kneipp, A. S. Haka, H. Kneipp et al., "Surface-enhanced raman spectroscopy in single living cells using gold nanoparticles," *Applied Spectroscopy*, vol. 56, no. 2, pp. 150–154, 2002.

[21] J. B. Jackson and N. J. Halas, "Surface-enhanced Raman scattering on tunable plasmonic nanoparticle substrates," *Proceedings of the National Academy of Sciences of the United States of America*, vol. 101, no. 52, pp. 17930–17935, 2004.

[22] M. Rycenga, P. H. C. Camargo, W. Li, C. H. Moran, and Y. Xia, "Understanding the SERS effects of single silver nanoparticles and their dimers, one at a time," *Journal of Physical Chemistry Letters*, vol. 1, no. 4, pp. 696–703, 2010.

[23] K. Kneipp, Y. Wang, H. Kneipp et al., "Single molecule detection using surface-enhanced Raman scattering (SERS)," *Physical Review Letters*, vol. 78, no. 9, pp. 1667–1670, 1997.

[24] S. M. Nie and S. R. Emory, "Probing single molecules and single nanoparticles by surface-enhanced Raman scattering," *Science*, vol. 275, no. 5303, pp. 1102–1106, 1997.

[25] S. Corni and J. Tomasi, "Surface enhanced Raman scattering from a single molecule adsorbed on a metal particle aggregate: a theoretical study," *Journal of Chemical Physics*, vol. 116, no. 3, pp. 1156–1164, 2002.

[26] X. M. Qian and S. M. Nie, "Single-molecule and single-nanoparticle SERS: from fundamental mechanisms to biomedical applications," *Chemical Society Reviews*, vol. 37, no. 5, pp. 912–920, 2008.

[27] M. Baia, F. Toderas, L. Baia, D. Maniu, and S. Astilean, "Multilayer structures of self-assembled gold nanoparticles as a unique SERS and SEIRA substrate," *ChemPhysChem*, vol. 10, no. 7, pp. 1106–1111, 2009.

[28] J. F. Li, Y. F. Huang, Y. Ding et al., "Shell-isolated nanoparticle-enhanced Raman spectroscopy," *Nature*, vol. 464, no. 7287, pp. 392–395, 2010.

[29] Y. Han, R. Lupitskyy, T. M. Chou, C. M. Stafford, H. Du, and S. Sukhishvili, "Effect of oxidation on surface-enhanced raman scattering activity of silver nanoparticles: a quantitative correlation," *Analytical Chemistry*, vol. 83, no. 15, pp. 5873–5880, 2011.

[30] J. C. Hulteen, D. A. Treichel, M. T. Smith, M. L. Duval, T. R. Jensen, and R. P. Van Duyne, "Nanosphere lithography: size-tunable silver nanoparticle and surface cluster arrays," *Journal of Physical Chemistry B*, vol. 103, no. 19, pp. 3854–3863, 1999.

[31] M. D. Malinsky, K. Lance Kelly, G. C. Schatz, and R. P. van Duyne, "Nanosphere lithography: effect of substrate on the localized surface plasmon resonance spectrum of silver nanoparticles," *Journal of Physical Chemistry B*, vol. 105, no. 12, pp. 2343–2350, 2001.

[32] L. A. Dick, A. D. McFarland, C. L. Haynes, and R. P. Van Duyne, "Metal film over nanosphere (MFON) electrodes for surface-enhanced Raman spectroscopy (SERS): improvements in surface nanostructure stability and suppression of irreversible loss," *Journal of Physical Chemistry B*, vol. 106, no. 4, pp. 853–860, 2002.

[33] J. Stropp, G. Trachta, G. Brehm, and S. Schneider, "A new version of AgFON substrates for high-throughput analytical SERS applications," *Journal of Raman Spectroscopy*, vol. 34, no. 1, pp. 26–32, 2003.

[34] H. Li and B. M. Cullum, "Dual layer and multilayer enhancements from silver film over nanostructured surface-enhanced Raman substratess," *Applied Spectroscopy*, vol. 59, no. 4, pp. 410–417, 2005.

[35] H. Li, C. E. Baum, J. Sun, and B. M. Cullum, "Multilayer enhanced gold film over nanostructure surface-enhanced Raman," *Applied Spectroscopy*, vol. 60, no. 12, pp. 1377–1385, 2006.

[36] C. K. Klutse and B. M. Cullum, "Optimization of SAM-based multilayer SERS substrates for intracellular analyses: the effect of terminating functional groups," in *Smart Biomedical and Physiological Sensor Technology VIII*, vol. 8025 of *Proceedings of SPIE 8025*, Orlando, Fla, USA, April 2011.

[37] B. M. Cullum, H. Li, M. V. Schiza, and M. E. Hankus, "Characterization of multilayer-enhanced surface-enhanced Raman scattering (SERS) substrates and their potential for SERS nanoimaging," *Nanobiotechnology*, vol. 3, no. 1, pp. 1–11, 2007.

[38] J. A. Dieringer, A. D. McFarland, N. C. Shah et al., "Surface enhanced Raman spectroscopy: new materials, concepts, characterization tools, and applications," *Faraday Discussions*, vol. 132, pp. 9–26, 2006.

[39] K. Hering, D. Cialla, K. Ackermann et al., "SERS: a versatile tool in chemical and biochemical diagnostics," *Analytical and Bioanalytical Chemistry*, vol. 390, no. 1, pp. 113–124, 2008.

[40] M. Fan, G. F. S. Andrade, and A. G. Brolo, "A review on the fabrication of substrates for surface enhanced Raman spectroscopy and their applications in analytical chemistry," *Analytica Chimica Acta*, vol. 693, no. 1-2, pp. 7–25, 2011.

[41] L. Qin, S. Zou, C. Xue, A. Atkinson, G. C. Schatz, and C. A. Mirkin, "Designing, fabricating, and imaging Raman hot spots," *Proceedings of the National Academy of Sciences of the United States of America*, vol. 103, no. 36, pp. 13300–13303, 2006.

[42] W. Y. Li, P. H. C. Camargo, X. Lu, and Y. Xia, "Dimers of silver nanospheres: facile synthesis and their use as hot spots for surface-enhanced raman scattering," *Nano Letters*, vol. 9, no. 1, pp. 485–490, 2009.

[43] M. L. Pedano, S. Li, G. C. Schatz, and C. A. Mirkin, "Periodic electric field enhancement along gold rods with nanogaps," *Angewandte Chemie*, vol. 49, no. 1, pp. 78–82, 2010.

[44] R. Kodiyath, J. Wang, Z. A. Combs et al., "SERS effects in silver-decorated cylindrical nanopores," *Small*, vol. 7, no. 24, pp. 3452–3457, 2011.

[45] A. Wokaun, J. P. Gordon, and P. F. Liao, "Radiation damping in surface-enhanced Raman scattering," *Physical Review Letters*, vol. 48, no. 14, pp. 957–960, 1982.

[46] P. F. Liao, J. G. Bergman, D. S. Chemla et al., "Surface-enhanced raman scattering from microlithographic silver particle surfaces," *Chemical Physics Letters*, vol. 82, no. 2, pp. 355–359, 1981.

[47] M. A. De Jesús, K. S. Giesfeldt, J. M. Oran, N. A. Abu-Hatab, N. V. Lavrik, and M. J. Sepaniak, "Nanofabrication of densely packed metal-polymer arrays for surface-enhanced raman spectrometry," *Applied Spectroscopy*, vol. 59, no. 12, pp. 1501–1508, 2005.

[48] D. R. Ward, N. K. Grady, C. S. Levin et al., "Electromigrated nanoscale gaps for surface-enhanced Raman spectroscopy," *Nano Letters*, vol. 7, no. 5, pp. 1396–1400, 2007.

[49] N. A. Abu Hatab, J. M. Oran, and M. J. Sepaniak, "Surface-enhanced Raman spectroscopy substrates created via electron beam lithography and nanotransfer printing," *ACS Nano*, vol. 2, no. 2, pp. 377–385, 2008.

[50] S. M. Wells, S. D. Retterer, J. M. Oran, and M. J. Sepaniak, "Controllable nanofabrication of aggregate-like nanoparticle substrates and evaluation for surface-enhanced Raman spectroscopy," *ACS Nano*, vol. 3, no. 12, pp. 3845–3853, 2009.

[51] B. Yan, A. Thubagere, W. R. Premasiri, L. D. Ziegler, L. D. Negro, and B. M. Reinhard, "Engineered SERS substrates with multiscale signal enhancement: nanoparticle cluster arrays," *ACS Nano*, vol. 3, no. 5, pp. 1190–1202, 2009.

[52] N. A. Hatab, C. H. Hsueh, A. L. Gaddis et al., "Free-standing optical gold bowtie nanoantenna with variable gap size for enhanced Raman spectroscopy," *Nano Letters*, vol. 10, no. 12, pp. 4952–4955, 2010.

[53] D. Bhandari, I. I. Kravchenko, N. V. Lavrik, and M. J. Sepaniak, "Nanotransfer printing using plasma etched silicon stamps and mediated by in situ deposited fluoropolymer," *Journal of the American Chemical Society*, vol. 133, no. 20, pp. 7722–7724, 2011.

[54] D. Bhandari, S. M. Wells, A. Polemi, I. I. Kravchenko, K. L. Shuford, and M. J. Sepaniak, "Stamping plasmonic nanoarrays on SERS-supporting platforms," *Journal of Raman Spectroscopy*, vol. 42, no. 11, pp. 1916–1924, 2011.

[55] J. D. Caldwell, O. Glembocki, F. J. Bezares et al., "Plasmonic nanopillar arrays for large-area, high-enhancement surface-enhanced Raman scattering sensors," *ACS Nano*, vol. 5, no. 5, pp. 4046–4055, 2011.

[56] A. S. P. Chang, M. Bora, H. T. Nguyen et al., "Nanopillars array for surface enhanced Raman scattering," in *Advanced Environmental, Chemical, and Biological Sensing Technologies VIII*, vol. 8024 of *Proceedings of the SPIE*, pp. 802401–802409, 2011.

[57] S. M. Wells, A. Polemi, N. V. Lavrik, K. L. Shuford, and M. J. Sepaniak, "Efficient disc on pillar substrates for surface enhanced Raman spectroscopy," *Chemical Communications*, vol. 47, no. 13, pp. 3814–3816, 2011.

[58] J.-S. Wi, E. S. Barnard, R. J. Wilson et al., "Sombrero-shaped plasmonic nanoparticles with molecular-level sensitivity and multifunctionality," *ACS Nano*, vol. 5, no. 8, pp. 6449–6457, 2011.

[59] M. J. Madou, *Fundamentals of Microfabrication: The Science of Miniaturization*, CRC, Boca Raton, Fla, USA, 2002.

[60] E. Hao and G. C. Schatz, "Electromagnetic fields around silver nanoparticles and dimers," *Journal of Chemical Physics*, vol. 120, no. 1, pp. 357–366, 2004.

[61] M. Kahl, E. Voges, S. Kostrewa, C. Viets, and W. Hill, "Periodically structured metallic substrates for SERS," *Sensors and Actuators B*, vol. 51, no. 1–3, pp. 285–291, 1998.

[62] K. R. Li, M. I. Stockman, and D. J. Bergman, "Self-similar chain of metal nanospheres as an efficient nanolens," *Physical Review Letters*, vol. 91, no. 22, pp. 227402/1–227402/4, 2003.

[63] A. Polemi, S. M. Wells, N. V. Lavrik, M. J. Sepaniak, and K. L. Shuford, "Local field enhancement of pillar nanosurfaces for SERS," *Journal of Physical Chemistry C*, vol. 114, no. 42, pp. 18096–18102, 2010.

[64] H. Duan, A. I. Fernández-Domínguez, M. Bosman, S. A. Maier, and J. K. W. Yang, "Nanoplasmonics: classical down to the nanometer scale," *Nano Letters*, vol. 12, no. 3, pp. 1683–1689, 2012.

[65] H. Im, K. C. Bantz, N. C. Lindquist, C. L. Haynes, and S. H. Oh, "Vertically oriented sub-10-nm plasmonic nanogap arrays," *Nano Letters*, vol. 10, no. 6, pp. 2231–2236, 2010.

[66] M. R. Gartia, Z. Xu, E. Behymer et al., "Rigorous surface enhanced Raman spectral characterization of large-area high-uniformity silver-coated tapered silica nanopillar arrays," *Nanotechnology*, vol. 21, no. 39, Article ID 395701, 2010.

[67] J. Henzie, M. H. Lee, and T. W. Odom, "Multiscale patterning of plasmonic metamaterials," *Nature Nanotechnology*, vol. 2, no. 9, pp. 549–554, 2007.

[68] S. Aksu, M. Huang, A. Artar et al., "Flexible plasmonics on unconventional and nonplanar substrates," *Advanced Materials*, vol. 23, no. 38, pp. 4422–4430, 2011.

[69] K. Herman, L. Szabó, L. F. Leopold, V. Chiş, and N. Leopold, "In situ laser-induced photochemical silver substrate synthesis and sequential SERS detection in a flow cell," *Analytical and Bioanalytical Chemistry*, vol. 400, no. 3, pp. 815–820, 2011.

[70] J. M. Yao, A. P. Le, M. V. Schulmerich et al., "Soft embossing of nanoscale optical and plasmonic structures in glass," *ACS Nano*, vol. 5, no. 7, pp. 5763–5774, 2011.

[71] J. Kneipp, "Nanosenors based on SERS for application in living cells," in *Surface-Enhanced Raman Scattering*, K. Kneipp, M. Moskovits, and H. Kneipp, Eds., vol. 103, Springer, Heidelberg, Germany, 2006.

[72] J. Kneipp, H. Kneipp, B. Wittig, and K. Kneipp, "Novel optical nanosensors for probing and imaging live cells," *Nanomedicine*, vol. 6, no. 2, pp. 214–226, 2010.

[73] J. Kneipp, H. Kneipp, M. McLaughlin, D. Brown, and K. Kneipp, "In vivo molecular probing of cellular compartments with gold nanoparticles and nanoaggregates," *Nano Letters*, vol. 6, no. 10, pp. 2225–2231, 2006.

[74] K. Kneipp, A. S. Haka, H. Kneipp et al., "Surface-enhanced raman spectroscopy in single living cells using gold nanoparticles," *Applied Spectroscopy*, vol. 56, no. 2, pp. 150–154, 2002.

[75] J. Kneipp, H. Kneipp, W. L. Rice, and K. Kneipp, "Optical probes for biological applications based on surface-enhanced Raman scattering from indocyanine green on gold nanoparticles," *Analytical Chemistry*, vol. 77, no. 8, pp. 2381–2385, 2005.

[76] K. Kneipp, H. Kneipp, I. Itzkan, R. R. Dasari, and M. S. Feld, "Ultrasensitive chemical analysis by Raman spectroscopy," *Chemical Reviews*, vol. 99, no. 10, pp. 2957–2975, 1999.

[77] R. M. Jarvis, N. Law, I. T. Shadi, P. O'Brien, J. R. Lloyd, and R. Goodacre, "Surface-enhanced raman scattering from intracellular and extracellular bacterial locations," *Analytical Chemistry*, vol. 80, no. 17, pp. 6741–6746, 2008.

[78] M. A. Ochsenkühn, P. R. T. Jess, H. Stoquert, K. Dholakia, and C. J. Campbell, "Nanoshells for surface-enhanced raman spectroscopy in eukaryotic cells: cellular response and sensor development," *ACS Nano*, vol. 3, no. 11, pp. 3613–3621, 2009.

[79] S. W. Bishnoi, C. J. Rozell, C. S. Levin et al., "All-optical nanoscale pH meter," *Nano Letters*, vol. 6, no. 8, pp. 1687–1692, 2006.

[80] K. L. Nowak-Lovato, B. S. Wilson, and K. D. Rector, "SERS nanosensors that report pH of endocytic compartments

during FcεRI transit," *Analytical and Bioanalytical Chemistry*, vol. 398, no. 5, pp. 2019–2029, 2010.

[81] J. Kneipp, H. Kneipp, B. Wittig, and K. Kneipp, "Following the dynamics of pH in endosomes of live cells with SERS nanosensors," *Journal of Physical Chemistry C*, vol. 114, no. 16, pp. 7421–7426, 2010.

[82] J. P. Scaffidi, M. K. Gregas, V. Seewaldt, and T. Vo-Dinh, "SERS-based plasmonic nanobiosensing in single living cells," *Analytical and Bioanalytical Chemistry*, vol. 393, no. 4, pp. 1135–1141, 2009.

[83] C. E. Talley, L. Jusinski, C. W. Hollars, S. M. Lane, and T. Huser, "Intracellular pH sensors based on surface-enhanced raman scattering," *Analytical Chemistry*, vol. 76, no. 23, pp. 7064–7068, 2005.

[84] C. A. R. Auchinvole, P. Richardson, C. McGuinnes et al., "Monitoring intracellular redox potential changes using SERS nanosensors," *ACS Nano*, vol. 6, no. 1, pp. 888–896, 2012.

[85] H. Cho, B. R. Baker, S. Wachsmann-Hogiu et al., "Aptamer-based SERRS sensor for thrombin detection," *Nano Letters*, vol. 8, no. 12, pp. 4386–4390, 2008.

[86] N. Hamaguchi, A. Ellington, and M. Stanton, "Aptamer beacons for the direct detection of proteins," *Analytical Biochemistry*, vol. 294, no. 2, pp. 126–131, 2001.

[87] D. Saerens, L. Huang, K. Bonroy, and S. Muyldermans, "Antibody fragments as probe in biosensor development," *Sensors*, vol. 8, no. 8, pp. 4669–4686, 2008.

[88] K. L. Brogan, K. N. Wolfe, P. A. Jones, and M. H. Schoenfisch, "Direct oriented immobilization of F(ab′) antibody fragments on gold," *Analytica Chimica Acta*, vol. 496, no. 1-2, pp. 73–80, 2003.

[89] C. R. Yonzon, C. L. Haynes, X. Zhang, J. T. Walsh, and R. P. Van Duyne, "A glucose biosensor based on surface-enhanced Raman scattering: improved partition layer, temporal stability, reversibility, and resistance to serum protein interference," *Analytical Chemistry*, vol. 76, no. 1, pp. 78–85, 2004.

[90] H. Li, J. Sun, T. Alexander, and B. M. Cullum, "Implantable SERS nanosensors for pre-symptomatic detection of BW agents," in *Chemical and Biological Sensing VI*, Proceedings of SPIE, pp. 8–18, March 2005.

[91] H. Li, J. Sun, and B. M. Cullum, "Label-free detection of proteins using SERS-based immuno-nanosensors," *Nanobiotechnology*, vol. 2, no. 1-2, pp. 17–28, 2006.

[92] H. Li, J. Sun, and B. M. Cullum, "Nanosphere-based SERS immuno-sensors for protein analysis," in *Smart Medical and Biomedical Sensor Technology II*, Proceedings of SPIE, pp. 19–30, October 2004.

[93] M. Litorja, C. L. Haynes, A. J. Haes, T. R. Jensen, and R. P. Van Duyne, "Surface-enhanced Raman scattering detected temperature programmed desorption: optical properties, nanostructure, and stability of silver film over SiO_2 nanosphere surfaces," *Journal of Physical Chemistry B*, vol. 105, no. 29, pp. 6907–6915, 2001.

[94] D. A. Stuart, J. M. Yuen, N. Shah et al., "In vivo glucose measurement by surface-enhanced Raman spectroscopy," *Analytical Chemistry*, vol. 78, no. 20, pp. 7211–7215, 2006.

[95] H. Li, J. Sun, and B. M. Cullum, "Label-free detection of proteins using SERS-based immuno-nanosensors," *Nanobiotechnology*, vol. 2, no. 1-2, pp. 17–28, 2006.

[96] E. Betzig, A. Lewis, A. Harootunian, M. Isaacson, and E. Kratschmer, "Near-field scanning optical microscopy (NSOM)—development and biophysical applications," *Biophysical Journal*, vol. 49, no. 1, pp. 269–279, 1986.

[97] V. Deckert, D. Zeisel, R. Zenobi, and T. Vo-Dinh, "Near-field surface-enhanced Raman imaging of dye-labeled DNA with 100-nm resolution," *Analytical Chemistry*, vol. 70, no. 13, pp. 2646–2650, 1998.

[98] D. Zeisel, V. Deckert, R. Zenobi, and T. Vo-Dinh, "Near-field surface-enhanced Raman spectroscopy of dye molecules adsorbed on silver island films," *Chemical Physics Letters*, vol. 283, no. 5-6, pp. 381–385, 1998.

[99] B. Ren, G. Picardi, and B. Pettinger, "Preparation of gold tips suitable for tip-enhanced Raman spectroscopy and light emission by electrochemical etching," *Review of Scientific Instruments*, vol. 75, no. 4, pp. 837–841, 2004.

[100] U. Neugebauer, P. Rösch, M. Schmitt et al., "On the way to nanometer-sized information of the bacterial surface by tip-enhanced Raman spectroscopy," *ChemPhysChem*, vol. 7, no. 7, pp. 1428–1430, 2006.

[101] B. M. Cullum and M. E. Hankus, "SERS nanoimaging probes for characterizing extracellular surfaces," in *Smart Biomedical and Physiological Sensor Technology V*, Proceedings of SPIE, September 2007.

[102] M. E. Hankus and B. M. Cullum, "SERS probes for the detection and imaging of biochemical species on the nanoscale," in *Smart Medical and Biomedical Sensor Technology IV*, Proceedings of SPIE, October 2006.

[103] M. E. Hankus, G. Gibson, N. Chandrasekharan, and B. M. Cullum, "Surface-enhanced Raman scattering (SERS)—nanoimaging probes for biological analysis," in *Smart Medical and Biomedical Sensor Technology II*, Proceedings of SPIE, pp. 106–116, October 2004.

[104] M. E. Hankus, G. J. Gibson, and B. M. Cullum, "Characterization and optimization of novel surface-enhanced Raman scattering (SERS)-based nanoimaging probes for chemical imaging," in *Smart Medical and Biomedical Sensor Technology III*, Proceedings of SPIE, October 2005.

[105] B. M. Cullum and M. E. Hankus, "SERS nanoimaging probes for characterizing extracellular surfaces," in *Smart Biomedical and Physiological Sensor Technology V*, Proceedings of SPIE, September 2007.

[106] X. Yang, C. Gu, F. Qian, Y. Li, and J. Z. Zhang, "Highly sensitive detection of proteins and bacteria in aqueous solution using surface-enhanced raman scattering and optical fibers," *Analytical Chemistry*, vol. 83, no. 15, pp. 5888–5894, 2011.

[107] M. Çulha, M. Altunbek, S. Keskin, and D. Saatçi, "Manipulation of silver nanoparticles in a droplet for label-free detection of biological molecules using surface-enhanced Raman scattering," in *Plasmonics in Biology and Medicine VIII*, Proceedings of SPIE, January 2011.

[108] M. Kahraman, I. Sur, and M. Çulha, "Label-free detection of proteins from self-assembled protein-silver nanoparticle structures using surface-enhanced raman scattering," *Analytical Chemistry*, vol. 82, no. 18, pp. 7596–7602, 2010.

[109] Z. A. Combs, S. Chang, T. Clark, S. Singamaneni, K. D. Anderson, and V. V. Tsukruk, "Label-free raman mapping of surface distribution of protein A and IgG biomolecules," *Langmuir*, vol. 27, no. 6, pp. 3198–3205, 2011.

[110] S. Keskin, M. Kahraman, and M. Çulha, "Differential separation of protein mixtures using convective assembly and label-free detection with surface enhanced Raman scattering," *Chemical Communications*, vol. 47, no. 12, pp. 3424–3426, 2011.

[111] E. Papadopoulou and S. E. J. Bell, "Label-free detection of single-base mismatches in DNA by surface-enhanced raman spectroscopy," *Angewandte Chemie*, vol. 50, no. 39, pp. 9058–9061, 2011.

[112] D. Van Lierop, K. Faulds, and D. Graham, "Separation free DNA detection using surface enhanced raman scattering," *Analytical Chemistry*, vol. 83, no. 15, pp. 5817–5821, 2011.

[113] Z. Zhang, Y. Wen, Y. Ma, J. Luo, L. Jiang, and Y. Song, "Mixed DNA-functionalized nanoparticle probes for surface-enhanced Raman scattering-based multiplex DNA detection," *Chemical Communications*, vol. 47, no. 26, pp. 7407–7409, 2011.

[114] J. A. Dougan, D. MacRae, D. Graham, and K. Faulds, "DNA detection using enzymatic signal production and SERS," *Chemical Communications*, vol. 47, no. 16, pp. 4649–4651, 2011.

[115] J. D. Driskell and R. A. Tripp, "Label-free SERS detection of microRNA based on affinity for an unmodified silver nanorod array substrate," *Chemical Communications*, vol. 46, no. 19, pp. 3298–3300, 2010.

[116] L. Sun and J. Irudayaraj, "Quantitative surface-enhanced Raman for gene expression estimation," *Biophysical Journal*, vol. 96, no. 11, pp. 4709–4716, 2009.

[117] S. Efrima and B. V. Bronk, "Silver colloids impregnating or coating bacteria," *Journal of Physical Chemistry B*, vol. 102, no. 31, pp. 5947–5950, 1998.

[118] L. Zeiri, B. V. Bronk, Y. Shabtai, J. Eichler, and S. Efrima, "Surface-enhanced Raman spectroscopy as a tool for probing specific biochemical components in bacteria," *Applied Spectroscopy*, vol. 58, no. 1, pp. 33–40, 2004.

[119] L. Zeiri and S. Efrima, "Surface-enhanced Raman spectroscopy of bacteria: the effect of excitation wavelength and chemical modification of the colloidal milieu," *Journal of Raman Spectroscopy*, vol. 36, no. 6-7, pp. 667–675, 2005.

[120] A. Sengupta, M. L. Laucks, and E. James Davis, "Surface-enhanced Raman spectroscopy of bacteria and pollen," *Applied Spectroscopy*, vol. 59, no. 8, pp. 1016–1023, 2005.

[121] A. Sengupta, M. Mujacic, and E. J. Davis, "Detection of bacteria by surface-enhanced Raman spectroscopy," *Analytical and Bioanalytical Chemistry*, vol. 386, no. 5, pp. 1379–1386, 2006.

[122] M. L. Laucks, A. Sengupta, K. Junge, E. J. Davis, and B. D. Swanson, "Comparison of psychro-active arctic marine bacteria and common mesophillic bacteria using surface-enhanced raman spectroscopy," *Applied Spectroscopy*, vol. 59, no. 10, pp. 1222–1228, 2005.

[123] R. M. Jarvis and R. Goodacre, "Discrimination of bacteria using surface-enhanced Raman spectroscopy," *Analytical Chemistry*, vol. 76, no. 1, pp. 40–47, 2004.

[124] R. M. Jarvis, A. Brooker, and R. Goodacre, "Surface-enhanced Raman spectroscopy for bacterial discrimination utilizing a scanning electron microscope with a Raman spectroscopy interface," *Analytical Chemistry*, vol. 76, no. 17, pp. 5198–5202, 2004.

[125] W. R. Premasiri, D. T. Moir, M. S. Klempner, N. Krieger, G. Jones, and L. D. Ziegler, "Characterization of the surface enhanced Raman scattering (SERS) of bacteria," *Journal of Physical Chemistry B*, vol. 109, no. 1, pp. 312–320, 2005.

[126] M. Kahraman, M. M. Yazıcı, F. Sahin, O. F. Bayrak, and M. Culha, "Reproducible surface-enhanced Raman scattering spectra of bacteria on aggregated silver nanoparticles," *Applied Spectroscopy*, vol. 61, no. 5, pp. 479–485, 2007.

[127] I. Sayin, M. Kahraman, F. Sahin, D. Yurdakul, and M. Culha, "Characterization of yeast species using surface-enhanced Raman scattering," *Applied spectroscopy*, vol. 63, no. 11, pp. 1276–1282, 2009.

[128] M. Culha, M. Kahraman, D. Çam, I. Sayin, and K. Keseroğlu, "Rapid identification of bacteria and yeast using surface-enhanced raman scattering," *Surface and Interface Analysis*, vol. 42, no. 6-7, pp. 462–465, 2010.

[129] A. Sujith, T. Itoh, H. Abe et al., "Imaging the cell wall of living single yeast cells using surface-enhanced raman spectroscopy," *Analytical and Bioanalytical Chemistry*, vol. 394, no. 7, pp. 1803–1809, 2009.

[130] P. Negri, A. Kage, A. Nitsche, D. Naumann, and R. A. Dluhy, "Detection of viral nucleoprotein binding to anti-influenza aptamers via SERS," *Chemical Communications*, vol. 47, no. 30, pp. 8635–8637, 2011.

[131] S. Shanmukh, L. Jones, J. Driskell, Y. Zhao, R. Dluhy, and R. A. Tripp, "Rapid and sensitive detection of respiratory virus molecular signatures using a silver nanorod array SERS substrate," *Nano Letters*, vol. 6, no. 11, pp. 2630–2636, 2006.

[132] S. D. Hudson and G. Chumanov, "Bioanalytical applications of SERS (surface-enhanced Raman spectroscopy)," *Analytical and Bioanalytical Chemistry*, vol. 394, no. 3, pp. 679–686, 2009.

[133] S. Xu, X. Ji, W. Xu et al., "Surface-enhanced Raman scattering studies on immunoassay," *Journal of biomedical optics*, vol. 10, no. 3, pp. 1–12, 2005.

[134] M. Y. Sha, H. Xu, S. G. Penn, and R. Cromer, "SERS nanoparticles: a new optical detection modality for cancer diagnosis," *Nanomedicine*, vol. 2, no. 5, pp. 725–734, 2007.

[135] J. W. Chen, Y. Lei, X. J. Liu, J. H. Jiang, G. L. Shen, and R. Q. Yu, "Immunoassay using surface-enhanced Raman scattering based on aggregation of reporter-labeled immunogold nanoparticles.," *Analytical and bioanalytical chemistry*, vol. 392, no. 1-2, pp. 187–193, 2008.

[136] C. C. Lin, Y. M. Yang, Y. F. Chen, T. S. Yang, and H. C. Chang, "A new protein A assay based on Raman reporter labeled immunogold nanoparticles," *Biosensors and Bioelectronics*, vol. 24, no. 2, pp. 178–183, 2008.

[137] H. Hwang, H. Chon, J. Choo, and J. K. Park, "Optoelectrofluidic sandwich immunoassays for detection of human tumor marker using surface-enhanced raman scattering," *Analytical Chemistry*, vol. 82, no. 18, pp. 7603–7610, 2010.

[138] M. Lee, S. Lee, J. H. Lee et al., "Highly reproducible immunoassay of cancer markers on a gold-patterned microarray chip using surface-enhanced Raman scattering imaging," *Biosensors and Bioelectronics*, vol. 26, no. 5, pp. 2135–2141, 2011.

[139] G. Wang, R. J. Lipert, M. Jain et al., "Detection of the potential pancreatic cancer marker MUC4 in serum using surface-enhanced Raman scattering," *Analytical Chemistry*, vol. 83, no. 7, pp. 2554–2561, 2011.

[140] E. Temur, I. H. BoyacI, U. Tamer, H. Unsal, and N. Aydogan, "A highly sensitive detection platform based on surface-enhanced Raman scattering for Escherichia coli enumeration," *Analytical and Bioanalytical Chemistry*, vol. 397, no. 4, pp. 1595–1604, 2010.

[141] B. Guven, N. Basaran-Akgul, E. Temur, U. Tamer, and I. H. Boyaci, "SERS-based sandwich immunoassay using antibody coated magnetic nanoparticles for Escherichia coli enumeration," *Analyst*, vol. 136, no. 4, pp. 740–748, 2011.

[142] X. X. Han, B. Zhao, and Y. Ozaki, "Surface-enhanced Raman scattering for protein detection," *Analytical and Bioanalytical Chemistry*, vol. 394, no. 7, pp. 1719–1727, 2009.

[143] Z. Zhou, G. G. Huang, and Y. Ozaki, "Label-free rapid semi-quantitative detection of proteins down to sub-monolayer coverage by using surface-enhanced raman scattering of

nitrate ion," *Chemistry Letters*, vol. 39, no. 11, pp. 1203–1205, 2010.

[144] I. S. Patel, W. R. Premasiri, D. T. Moir, and L. D. Ziegler, "Barcoding bacterial cells: a SERS-based methodology for pathogen identification," *Journal of Raman Spectroscopy*, vol. 39, no. 11, pp. 1660–1672, 2008.

[145] M. Kahraman, M. M. Yazici, F. Şahin, and M. Çulha, "Experimental parameters influencing surface-enhanced Raman scattering of bacteria," *Journal of Biomedical Optics*, vol. 12, no. 5, Article ID 054015, 2007.

[146] M. Kahraman, M. M. Yazici, F. Şahin, and M. Çulha, "Convective assembly of bacteria for surface-enhanced Raman scattering," *Langmuir*, vol. 24, no. 3, pp. 894–901, 2008.

[147] M. Kahraman, K. Keseroğlu, and M. Çulha, "On sample preparation for surface-enhanced Raman scattering (SERS) of bacteria and the source of spectral features of the spectra," *Applied Spectroscopy*, vol. 65, no. 5, pp. 500–506, 2011.

[148] W. R. Premasiri, Y. Gebregziabher, and L. D. Ziegler, "On the difference between surface-enhanced Raman scattering (SERS) spectra of cell growth media and whole bacterial cells," *Applied Spectroscopy*, vol. 65, no. 5, pp. 493–499, 2011.

[149] D. Bhandari, S. M. Wells, A. Polemi, I. I. Kravchenko, K. L. Shuford, and M. J. Sepaniak, "Stamping plasmonic nanoarrays on SERS-supporting platforms," *Journal of Raman Spectroscopy*, 2011.

[150] A. J. Pasquale, B. M. Reinhard, and L. Dal Negro, "Engineering photonic-plasmonic coupling in metal nanoparticle necklaces," *ACS Nano*, vol. 5, no. 8, pp. 6578–6585, 2011.

[151] M. Kahraman, N. Tokman, and M. Çulha, "Silver nanoparticle thin films with nanocavities for surface-enhanced Raman scattering," *ChemPhysChem*, vol. 9, no. 6, pp. 902–910, 2008.

Hindawi Publishing Corporation
Journal of Nanotechnology
Volume 2012, Article ID 297560, 7 pages
doi:10.1155/2012/297560

Research Article

Surface-Enhanced Raman Scattering of Bacteria in Microwells Constructed from Silver Nanoparticles

Mustafa Çulha,[1] M. Müge Yazıcı,[1] Mehmet Kahraman,[1] Fikrettin Şahin,[1] and Sesin Kocagöz[2]

[1] *Genetics and Bioengineering Department, Faculty of Engineering and Architecture, Yeditepe University, Istanbul 34755, Turkey*
[2] *Acıbadem University, School of Medicine, Department of Infectious Diseases, Büyükdere Cad. No. 40, Maslak, Istanbul 34457, Turkey*

Correspondence should be addressed to Mustafa Çulha, mculha@yeditepe.edu.tr

Received 2 February 2012; Revised 19 April 2012; Accepted 1 May 2012

Academic Editor: Nickolay Lavrik

Whole bacterial cell characterization is critically important for fast bacterial identification. Surface-enhanced Raman scattering (SERS) is proven to be powerful technique to serve such a goal. In this study, the characterization of whole bacterial cells in the microwells constructed from colloidal silver nanoparticles (AgNPs) with "convective-assembly" method is reported. The proper size of the microwells for the model bacteria, *Escherichia coli* and *Staphylococcus cohnii*, is determined to be 1.2 μm from their electron microscopy images. A minimum dilution factor of 20 is necessary for the bacterial samples collected from growth media to diminish the bacterial aggregation to place the bacterial cells into the microwells. The constructed microwell structures are tested for their bacterial SERS performance and compared to the SERS spectra obtained from the samples prepared with a simple mixing of bacteria and AgNPs for the same bacteria. The results indicate that microwell structures not only improve the spectral quality but also increase the reproducibility of the SERS spectra.

1. Introduction

The spectroscopic characterization of biological structures such as bacterial and living eukaryotic cells as a whole is an important concept to understand not only the biochemical structure of organization in their natural environment but also cellular processes inside of living cells. The surface-enhanced Raman scattering (SERS) is an emerging and promising technique to achieve such a goal and its potential has not fully explored to study bacterial and eukaryotic cells as whole yet. The supremacy of SERS mostly comes from its capability to provide molecular information from molecules or molecular structures located very close to nanostructured surfaces of silver or gold with a very limited influence of water, which is a significant component of biological structures.

The several groups explored the utility of SERS for bacterial characterization, discrimination and identification [1–13]. A simple mixing of bacterial cells and colloidal nanoparticles provides a straightforward way of preparing samples. However, due to the nonuniform nature of the prepared sample with the simple mixing, the acquired SERS spectra show variation from sample-to-sample and spot-to-spot on the same sample. Although there is strong evidence that the certain locations on the bacterial cell wall preferably strongly interact with AgNPs, the variations due to the sample preparation must be minimized for proper interpretation of the SERS spectra. Therefore, a more systematic approach is necessary to collect interpretable spectra from bacteria.

A patterned surface may provide a more suitable environment for bacterial cells to experience the surface plasmons of noble metal nanoparticles used to construct the patterned surfaces. The "convective-assembly" is a technique used to control assembly of nano- and micrometer size particles into two-dimensional (2D) and three-dimensional (3D) structures. The self-assembly of colloidal particles in thin evaporating films is the basis of the technique [14, 15]. During the assembly process, the small, nanometer size, gold or silver nanoparticles fill the voids around the large, micrometer size, latex particles forming a colloidal crystal.

After the assembly process is completed, the latex particles can be washed from the surface with an organic solvent. The remaining porous three-dimensional structure can be used as a SERS substrate [16]. The use of this technique was also reported to prepare coatings from sterically protected and silica-encapsulated nanoparticles and porous 3D gold structures for SERS [16–20].

In this study, we prepared microwells on glass surfaces constructed from AgNPs with "convective-assembly" method. The surfaces structured with microwells were used for as a SERS substrate to characterize whole bacteria cells. The SERS spectra obtained from the bacterial cells located into microwells and simply mixed with the AgNPs for two model bacteria, *E. coli* and *S. cohnii,* were compared.

2. Experimental

2.1. Chemicals. $AgNO_3$ (99.5%) and nutrient broth were purchased from Fluka (Seelze, Germany). Sodium citrate (99%) was purchased from Merck (Darmstadt, Germany). The latex microspheres were purchased from Invitrogen (Eugene, OR) as surfactant-free white sulfate latex. Microscope slide was purchased from Citoglass (China). HPLC grade dichloromethane stabilized with ethanol was purchased from Labkim (Istanbul, Turkey).

2.2. Preparation of Colloidal AgNPs. The colloidal AgNPs were prepared with a method reported by Lee and Meisel method [21]. In this, a 90 mg of $AgNO_3$ was dissolved in 500 mL of distilled water and heated until boiling. Then, a 10 mL of 1% sodium citrate solution was added into this boiling solution. This mixture was kept boiling until final volume is reached 250 mL. The obtained AgNP colloidal suspension was characterized by using UV spectroscopy and SEM. The maximum absorption wavelength of the AgNP colloidal suspension is typically at around 420 nm with an average size of 60 nm. The density of the AgNPs in the suspension was estimated as 2.0×10^{11} particles/mL.

2.3. Colloidal Suspension Concentration. An increased colloidal AgNP suspension concentration is required to construct the microwell structures. Therefore, a 100-fold increase in AgNP colloidal suspension concentration from its original concentration was needed. This was achieved by centrifuging a 200 mL of the AgNP colloidal suspension 5500 rpm for 30 min and removing the supernatant to leave only 2 mL of concentrated suspension.

2.4. Preparation of Bacteria Samples. *Escherichia coli* (35218 ATCC) and *Staphylococcus cohnii* samples were obtained from our microorganism collection (Yeditepe University, Genetics and Bioengineering Department). Before using the bacteria, their identification was verified by Sherlock Microbial Identification System version 4.5 (MIDI, Newark, Delaware). The bacteria were cultivated for 24 h at 37°C on nutrient broth. The collected bacteria washed three times by adding 20 mL of deionized water at centrifuging at 5000 rpm for ten 10 min and by discarding the supernatant. For the simple mixing method, a 5 μL of each washed bacterium was added into 100 μL AgNPs suspension. Then, they were mixed with a vortex and 5 μL of this homogeneous mixture was spotted onto a CaF_2 slide. The spot was allowed to dry at room temperature about 15 min before the analysis.

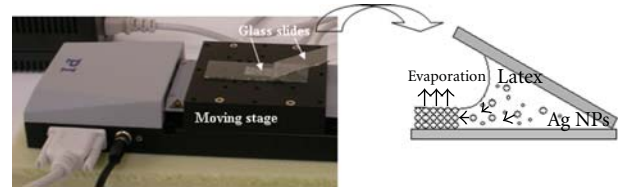

Figure 1: The "convective-assembly" setup used to construct the microwells in this study.

2.5. Preparation of Microwells. The AgNPs and latex micro spheres (1.2 μm) were mixed and coated onto glass slides using "convective-assembly." First, the glass slides were washed with chromic acid to clean the surface. Then, the washed slides were rinsed with deionized water and dried before coating procedure at ambient temperature. The mixture containing silver and latex nanoparticles was located at the cross-section of two glasses meeting with an angle of ~23 and the lower glass slide fixed on the moving stage was moved with a certain speed with the help of a controller (PI, Germany). Figure 1 shows the "convective-assembly" setup. The details of the experimental setup were also explained elsewhere [22]. As different from the reported setup, the glass slide attached to the moving stage was mobile other than the glass slide placed with an angle. The concentrated AgNPs and a desired size of latex microparticle suspension can be used to construct the preferred size of microwells. Due to the size of the bacteria used in this study, the 1.2 μm latex microspheres were used to construct the microwells. The ratio of latex colloidal suspension to AgNPs was 1 : 9 in final mixture before spotting at the cross-section of two glass slides. The speed of the stage that the glass slide was placed was in the range of 1.0–2.0 μm/s.

2.6. Preparation of Bacterial Samples on Surfaces. The initial bacterial counts were calculated with a dilution method and found as 1.3×10^7 and 7.4×10^7 CFU/mL for *S. cohnii* and *E. coli*, respectively. From this sample, 5 μL was taken and completed to 100 μL with distilled water. Then, a 2 μL-aliquot was spotted on the microwell-structured surface. This procedure generated enough bacteria in the microwells and the SERS experiments were performed on these surfaces. The area where bacterial suspension spotted remained in the range of $2.5 \pm 0.4\,\mu\text{m} \times 1.5 \pm 0.3\,\mu\text{m}$ for both bacterial samples. The number of bacteria in each microwell changes depending on the aggregation characteristics of the bacterial cells. Since the shape of *S. cohnii* cells is spherical with an average diameter of 0.8 μm, it is possible to locate about 4 cells into one 1 μm size well. The shape of *E. coli* cells is rod-like with an average length and diameter of 1.8 and 0.9 μm, respectively. Thus, only one or two cells can fit into one

microwell depending on the orientation of the cells. Note that the localization of the bacterial cells in the microwells seemed trivial.

2.7. Raman Instrumentation. All measurements were performed using a Renishaw inVia Reflex Raman spectroscopy system (Renishaw Plc., New Mills, Wotton-under-Edge Gloucestershire, UK) An 830 nm laser was used for all SERS experiments. The laser power on the sample was 3 mW with a time 10 sec exposure time. The spot size of the laser is about 1 micron when the 50x (NA = 0.75) objective is used. The wavelength of the instrument was automatically calibrated using an internal silicon wafer, and the spectrum was centered at 520 cm^{-1}.

2.8. Scanning Electron Microscope. The characterization of the prepared surfaces was performed with a Karl Zeiss EVO 40 model SEM instrument. The SEM images of the bacterial cells in the microwells were acquired upon drying at ambient temperature. For simple mixing experiments, the images were acquired after mixing the colloidal suspension and bacterial cells and drying on a scanning electron microscope sample stub at ambient temperature. The accelerating voltage was 10 kV for all experiments.

3. Results and Discussion

We previously investigated the parameters influencing the SERS spectra of bacteria when a simple mixing of bacterial cells with colloidal nanoparticles was employed as a sample preparation method [11, 12]. One of the principle requirements in a SERS experiment is to bring the noble metal nanoparticles or nanostructures close contact with molecules and molecular structures. This necessity is set by the mechanism of Raman signal enhancement due to the fact that the major contribution to the enhancement mechanism comes from the surface plasmons (SPs). Therefore, molecular structures such as bacterial cells must be at close contact with as many as noble metal nanoparticles when a noble metal colloidal suspension is used for the SERS experiment. In our earlier study, we demonstrated that increasing the colloidal suspension concentration four times (4x) improved not only the reproducibility but also the quality of SERS spectra due to the increased density of AgNPs in the sample compared to the previous reports [11]. Figure 2(a) shows the SEM image of *E. coli* sample prepared with 4x colloidal suspension and Figure 2(b) shows the SERS spectra acquired from ten different spots on the sample. As seen, the AgNPs are heterogeneously distributed among the bacterial cells, which results with variations on the spectra as the laser beam is moved on the sample. The microwells are expected to provide a three-dimensional (3D) environment generating many contact points for the bacterial cells to sense the SPs, which could improve the spot-to-spot variations and obtain more reproducible SERS spectra. Figure 3 shows a typical microwell-constructed surface containing *S. cohnii* cells. Considering size of *S. cohnii* (~0.8 μm) obtained from the SEM images, a size relationship between bacterial cells and microwell size (1.2 μm) can be correlated. However, the aggregation tendency of the bacterial cells influence the uniform distribution of bacterial cells in the microwells and prevents filling all microwells with bacterial cells. Therefore, a dilution step is necessary to have the bacterial cells distribute appropriately in the microwells as explained in the experimental section.

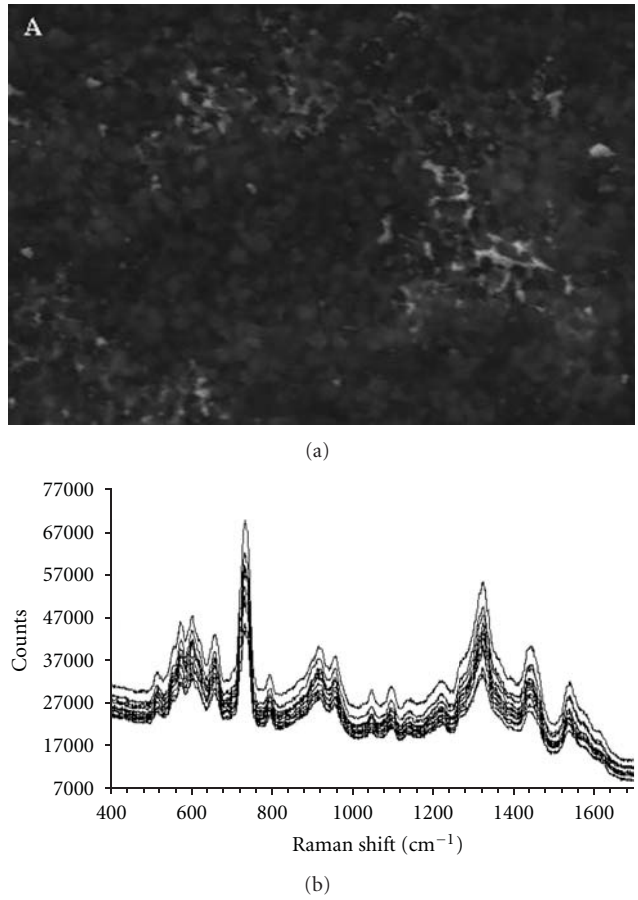

Figure 2: SEM image of an *E. coli* sample prepared with 4x colloidal suspension (a) and the ten SERS spectra generated from this sample from different locations (b).

Figure 4(a) shows the SEM images of microwells containing *E. coli* cells. A size relationship between *E. coli* and microwells can also be defined based on the possible orientation of the *E. coli* cells in the microwells. The average size of *E. coli* cells is measured from their SEM images (see Figure 4(b)) as 1.8 × 0.9 μm, length and diameter, respectively. Either 1 or 2 E. coli cells in each microwell can fit depending on the orientation of *E. coli* cells on the substrate surface. Although it was not possible to clearly visualize the *E. coli* cells in the microwells on the SEM images, the presence of bacterial cells on the substrate was confirmed with AFM as seen on Figure 4(b). In addition, obtaining SERS spectra from the surfaces verifies the presence of the bacterial cells in the microwells. The difficulty to visualize the *E. coli* cell on the samples prepared with simple mixing was also observed (see Figure 2(a)).

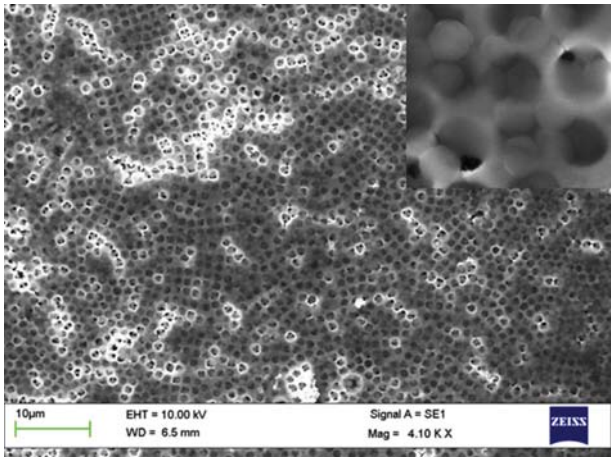

Figure 3: SEM image of *S. cohnii* in the microwells constructed from AgNPs. Inset image shows a closer caption of the bacterial cells.

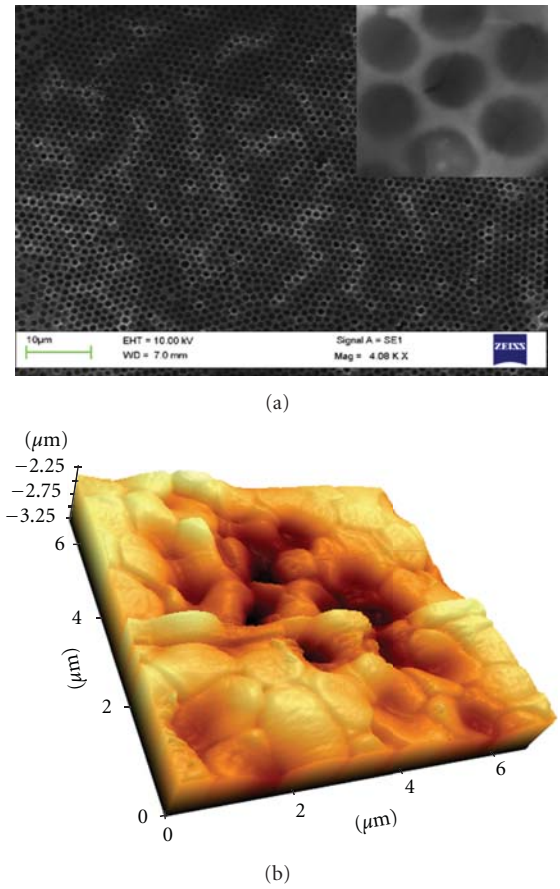

Figure 4: SEM (a) and AFM (b) image of *E. coli* cells in microwells. Inset image shows a closer caption of the bacterial cells.

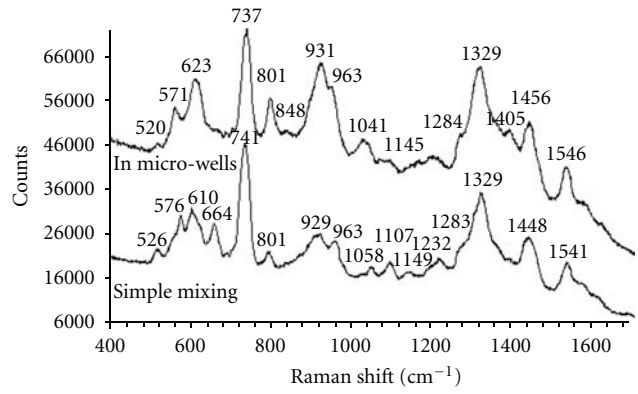

Figure 5: Comparison of SERS spectra of *E. coli* obtained in microwells and with simple mixing.

It is important to select proper laser wavelength for good quality of SERS spectra from bacteria [12]. Efrima and Zeiri also demonstrated the influence of the laser wavelength and power on the SERS of bacteria [23]. The shift of SP excitation to longer wavelengths as the noble metal nanoparticles form aggregates is a well known phenomenon. Therefore, a longer wavelength laser is more suitable to excite the SPs of aggregated AgNPs. It was indeed a laser wavelength at 514 nm did not perform as good as a laser wavelength at 830 nm in this study. Besides, this wavelength is more suitable for study of biological samples since the damage to the sample in NIR region is limited.

Due to the noteworthy differences in both approaches, simple mixing and in microwells, it is important to understand the spectral features on the SERS spectrum generated from each method. Figure 5 shows the comparison of the SERS spectra of *E. coli* taken from a sample prepared with simple mixing of 4x AgNPs and in the microwells.

The comparative inspection of both spectra reveals many spectral differences. However, the major difference is observed in the region from 500 to 700 cm^{-1}. While the five peaks at 526, 564, 582, 610, and 664 cm^{-1} appear in this region on the spectra acquired from the sample prepared with simple mixing, only three peaks at 520, 571, and 621 cm^{-1} are observed in microwells. The peaks around 500 cm^{-1} on the SERS of proteins and peptides were attributed to S–S stretch [24] and the peak around 520 and 526 cm^{-1} on both spectra can be assigned to S–S stretch [25]. Due to the fact that thiol moieties interact strongly with AgNPs, the band shifts may be observed on the SERS spectra upon interaction of such groups on the bacterial cell wall with the AgNPs when considering the free AgNPs present upon mixing with bacterial cells. The peaks on simple mixing spectra at 564, 582, 610, and 664 cm^{-1} and 660 and 630 cm^{-1} could be attributed to carbohydrates [26] and COO^{-} [27], respectively. Note that we earlier determined that the source of spectral features was originating from the bacteria [28]. However, as seen above, even with the use of same laser and type of the NPs, variations on the spectral features are observed.

Figure 6 shows the comparison of SERS spectra of *S. cohnii* obtained from a sample prepared simple mixing of 4x AgNP colloidal suspension and in the microwells. As seen, the SERS spectra obtained from the samples prepared with simple mixing and adding into the microwells are strikingly similar. This similarity can be explained with the

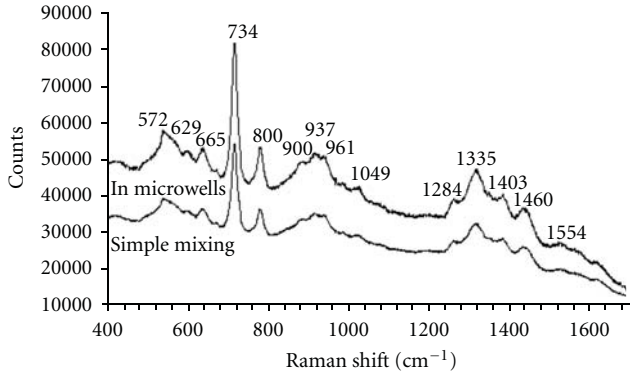

Figure 6: Comparison of SERS spectra of *S. cohnii* obtained in microwells and with simple mixing.

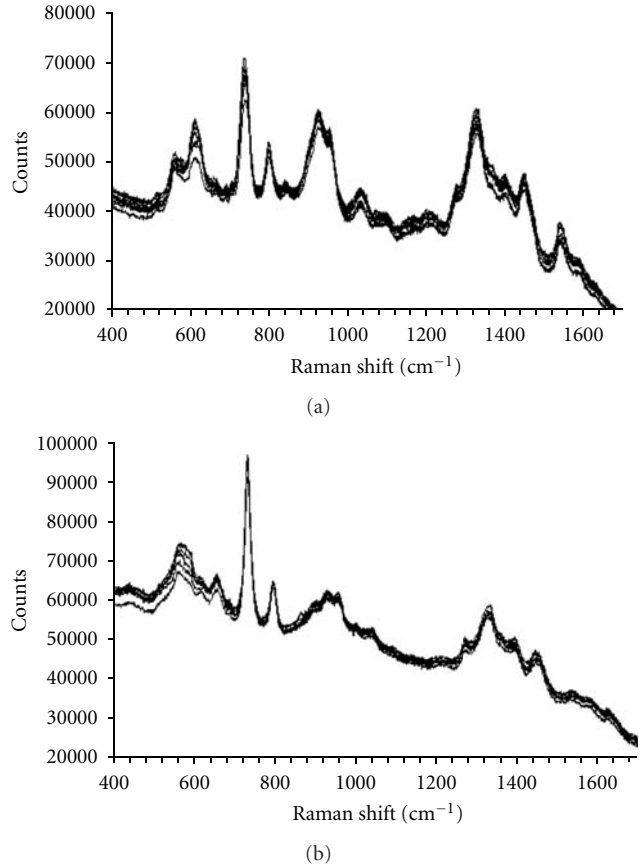

Figure 7: Reproducibility of SERS spectra of *E. coli* (a) and *S.cohnii* (b). SERS spectra acquired from different locations on AgNP microwell structure.

bacterial cell wall structures as well. *S. cohnii* is a Gram-positive bacteria and its cell wall biochemistry is completely different compared to Gram-negative bacteria. The outer wall structure is composed of a thick peptidoglycan structure that is rich in N-acetyl D-glucoseamine (NAG). In addition, this strong structure peptidoglycan structure has a more uniform structure compared to Gram-negative bacterial outer cell wall. The similarity of the spectra may refer to the uniform wall structure of this bacterium. The peaks appearing on the SERS spectra can be assigned to similar bond vibrations as they are in SERS spectra of *E. coli*.

The biochemical structures giving rise to the peaks on the SERS spectra of bacteria are not clearly known yet. There are a number of parameters influencing the spectra of bacteria imposed by the nature of the microbiological materials and the technique. There are several reports from sample preparation to experimental conditions such as laser wavelength, nanoparticle, and substrate type addressing the source of the variations on the SERS spectra of microorganisms [12, 23, 28–30]. From these studies, it is clear that a well-defined protocol is necessary for reproducible and interpretable results.

In order to demonstrate the spot-to-spot reproducibility, several spectra were acquired from different location on the same sample. Figures 7(a) and 7(b) shows reproducibility of SERS spectra of *E. coli* and *S. cohnii*, respectively. The percent coefficient of variation (CV), which is defined as standard deviation (s)/mean (χ) $\times$ 100, can be used to quantify the variation in SERS spectra of the bacteria obtained from the samples. The CV using peak height, absolute intensity, and peak area can be calculated at every frequency for a number of spectra. Either a %CV value at a certain frequency or an average from the calculated %CV at every frequency can be calculated for the quantification of variation. In this study, we used the peak height, absolute intensity, and peak area at around 737 cm^{-1} to express the reproducibility of the spectra through the %CV values. The %CV for the *E. coli* in the microwells using the peak height, absolute intensity, and peak area was calculated as 12, 10, and 10, respectively. However, the %CV with simple mixing method was 17, 18, and 19, respectively. The %CV for the *E. coli* sample prepared with "convective-assembly" process using the peak height, absolute intensity and peak area was calculated as 9, 8, and 8, respectively. The %CV for *S. cohnii* in microwells was 2, 1, and 5, respectively, but it was 12, 11, and 15, respectively, for simple mixing. The %CV for the *S. cohnii* sample prepared with convective assembly process using the peak height, absolute intensity, and peak area was calculated as 6, 6, and 7, respectively. When the two sample preparation methods are compared, the reproducibility of SERS spectra for *E. coli* is quite similar. However, in this method the reproducibility of the SERS spectra for *S. cohnii* is higher than the sample prepared with convective assembly method. With the simple mixing, the %CVs of both bacteria are very similar. However, the reproducibility of the spectra of the *S. cohnii* acquired in the microwells was more reproducible than the *E. coli* due to the size and shape related homogeneity of the cells in the microwells. The shape of the prepared wells is spherical, which is similar in size and shape of *S. cohnii* and they can enter into the wells easily and homogeneously. However, *E. coli* is rod-shaped and its entrance into the wells is hindered. Therefore, the improvement of the reproducibility is lower for the *E. coli*. This can be easily concluded from Figures 3 and 4.

The improvement in percent CV in microwells is higher than 40% for *E. coli* and 70% for *S. cohnii* compared to the simple mixing with 1x colloidal AgNP suspension. The improvement in CV of peak height, area, and absolute intensity was in the range 60–63% for *E. coli* and 58–61% for *S. cohnii* from the sample prepared with 1x colloidal suspension to the sample prepared with "convective-assembly." When the results of this study are compared to our previous study using "convective-assembly" [13], the improvement in reproducibility is rather similar.

4. Conclusion

In this study, the utility of microwell structures constructed from AgNPs for whole bacterial characterization using SERS and an analysis of the obtained bacterial SERS spectra for possible discrimination or identification is demonstrated. Since the size of majority of clinically important bacteria is already known, the SERS substrates with different size of microwells can be preprepared. As the AgNPs form organized aggregates in the well structure, the SP excitation wavelength shifts to longer wavelength. Therefore, a longer wavelength laser light is a proper choice for better quality of bacterial SERS in the prepared structures. The placement of bacterial cells in microwells significantly improves the reproducibility of the SERS spectra of bacteria used in this study. Thus, the SERS spectra can be used for fast bacterial identification.

Acknowledgments

The support of the Scientific and Technological Research Council of Turkey (TUBITAK) and Yeditepe University is gratefully acknowledged.

References

[1] R. E. Holt and T. M. Cotton, "Surface-enhanced resonance Raman and electrochemical investigation of Glucose Oxidase catalysis at a silver electrode," *Journal of the American Chemical Society*, vol. 111, no. 8, pp. 2815–2821, 1989.

[2] S. Efrima and B. V. Bronk, "Silver colloids impregnating or coating bacteria," *Journal of Physical Chemistry B*, vol. 102, no. 31, pp. 5947–5950, 1998.

[3] L. Zeiri, B. V. Bronk, Y. Shabtai, J. Eichler, and S. Efrima, "Surface-enhanced Raman spectroscopy as a tool for probing specific biochemical components in bacteria," *Applied Spectroscopy*, vol. 58, no. 1, pp. 33–40, 2004.

[4] L. Zeiri and S. Efrima, "Surface-enhanced Raman spectroscopy of bacteria: the effect of excitation wavelength and chemical modification of the colloidal milieu," *Journal of Raman Spectroscopy*, vol. 36, no. 6-7, pp. 667–675, 2005.

[5] A. Sengupta, M. L. Laucks, and E. James Davis, "Surface-enhanced Raman spectroscopy of bacteria and pollen," *Applied Spectroscopy*, vol. 59, no. 8, pp. 1016–1023, 2005.

[6] A. Sengupta, M. Mujacic, and E. J. Davis, "Detection of bacteria by surface-enhanced Raman spectroscopy," *Analytical and Bioanalytical Chemistry*, vol. 386, no. 5, pp. 1379–1386, 2006.

[7] M. L. Laucks, A. Sengupta, K. Junge, E. J. Davis, and B. D. Swanson, "Comparison of psychro-active arctic marine bacteria and common mesophillic bacteria using surface-enhanced raman spectroscopy," *Applied Spectroscopy*, vol. 59, no. 10, pp. 1222–1228, 2005.

[8] R. M. Jarvis and R. Goodacre, "Discrimination of bacteria using surface-enhanced Raman spectroscopy," *Analytical Chemistry*, vol. 76, no. 1, pp. 40–47, 2004.

[9] R. M. Jarvis, A. Brooker, and R. Goodacre, "Surface-enhanced Raman spectroscopy for bacterial discrimination utilizing a scanning electron microscope with a Raman spectroscopy interface," *Analytical Chemistry*, vol. 76, no. 17, pp. 5198–5202, 2004.

[10] W. R. Premasiri, D. T. Moir, M. S. Klempner, N. Krieger, G. Jones, and L. D. Ziegler, "Characterization of the surface enhanced Raman scattering (SERS) of bacteria," *Journal of Physical Chemistry B*, vol. 109, no. 1, pp. 312–320, 2005.

[11] M. Kahraman, M. M. Yazici, F. Şahin, Ö. F. Bayrak, and M. Çulha, "Reproducible surface-enhanced Raman scattering spectra of bacteria on aggregated silver nanoparticles," *Applied Spectroscopy*, vol. 61, no. 5, pp. 479–485, 2007.

[12] M. Kahraman, M. M. Yazici, F. Şahin, and M. Çulha, "Experimental parameters influencing surface-enhanced Raman scattering of bacteria," *Journal of Biomedical Optics*, vol. 12, no. 5, Article ID 054015, 2007.

[13] M. Kahraman, M. M. Yazici, F. Şahin, and M. Çulha, "Convective assembly of bacteria for surface-enhanced Raman scattering," *Langmuir*, vol. 24, no. 3, pp. 894–901, 2008.

[14] N. D. Denkov, O. D. Velev, P. A. Kralchevsky, I. B. Ivanov, H. Yoshimura, and K. Nagayama, "Mechanism of formation of two-dimensional crystals from latex particles on substrates," *Langmuir*, vol. 8, no. 12, pp. 3183–3190, 1992.

[15] N. D. Denkov, O. D. Velev, P. A. Kralchevsky, I. B. Ivanov, H. Yoshimura, and K. Nagayama, "Two-dimensional crystallization," *Nature*, vol. 361, no. 6407, p. 26, 1993.

[16] P. M. Tessier, S. D. Christesen, K. K. Ong et al., "Online spectroscopic characterization of sodium cyanide with nanostructured gold surface-enhanced Raman spectroscopy substrates," *Applied Spectroscopy*, vol. 56, no. 12, pp. 1524–1530, 2002.

[17] M. Brust, D. Bethell, C. J. Kiely, and D. J. Schiffrin, "Self-assembled gold nanoparticle thin films with nonmetallic optical and electronic properties," *Langmuir*, vol. 14, no. 19, pp. 5425–5429, 1998.

[18] T. Ung, L. M. Liz-Marzán, and P. Mulvaney, "Gold nanoparticle thin films," *Colloids and Surfaces A*, vol. 202, no. 2-3, pp. 119–126, 2002.

[19] P. M. Tessier, O. D. Velev, A. T. Kalambur, A. M. Lenhoff, J. F. Rabolt, and E. W. Kaler, "Structured metallic films for optical and spectroscopic applications via colloidal crystal templating," *Advanced Materials*, vol. 13, no. 6, pp. 396–400, 2001.

[20] P. M. Tessier, O. D. Velev, A. T. Kalambur, J. F. Rabolt, A. M. Lenhoff, and E. W. Kaler, "Assembly of gold nanostructured films templated by colloidal crystals and use in surface-enhanced Raman spectroscopy," *Journal of the American Chemical Society*, vol. 122, no. 39, pp. 9554–9555, 2000.

[21] P. C. Lee and D. Meisel, "Adsorption and surface-enhanced Raman of dyes on silver and gold sols," *The Journal of Physical Chemistry*, vol. 88, p. 3391, 1982.

[22] B. G. Prevo and O. D. Velev, "Controlled, rapid deposition of structured coatings from micro- and nanoparticle suspensions," *Langmuir*, vol. 20, no. 6, pp. 2099–2107, 2004.

[23] S. Efrima and L. Zeiri, "Understanding SERS of bacteria," *Journal of Raman Spectroscopy*, vol. 40, no. 3, pp. 277–288, 2009.

[24] S. Steward and P. M. Fredericks, "Surface-enhanced Raman spectroscopy of peptides and proteins adsorbed on an electrochemically prepared silver surface," *Spectrochimica Acta Part A*, vol. 55, p. 1615, 1999.

[25] K. Maquelin, C. Kirschner, L. P. Choo-Smith et al., "Identification of medically relevant microorganisms by vibrational spectroscopy," *Journal of Microbiological Methods*, vol. 51, no. 3, pp. 255–271, 2002.

[26] R. Keir, D. Sadler, and W. E. Smith, "Preparation of stable, reproducible silver colloids for use as surface-enhanced resonance Raman scattering substrates," *Applied Spectroscopy*, vol. 56, no. 5, pp. 551–559, 2002.

[27] K. C. Schuster, I. Reese, E. Urlaub, J. R. Gapes, and B. Lendl, "Multidimensional information on the chemical composition of single bacterial cells by confocal Raman microspectroscopy," *Analytical Chemistry*, vol. 72, no. 22, pp. 5529–5534, 2000.

[28] M. Kahraman, K. Keseroğlu, and M. Çulha, "On sample preparation for surface-enhanced Raman scattering (SERS) of bacteria and the source of spectral features of the spectra," *Applied Spectroscopy*, vol. 65, no. 5, pp. 500–506, 2011.

[29] W. R. Premasiri, Y. Gebregziabher, and L. D. Ziegler, "On the difference between surface-enhanced Raman scattering (SERS) spectra of cell growth media and whole bacterial cells," *Applied Spectroscopy*, vol. 65, no. 5, pp. 493–499, 2011.

[30] T. Smith-Palmer, C. Douglas, and P. Fredericks, "Rationalizing the SER spectra of bacteria," *Vibrational Spectroscopy*, vol. 53, no. 1, pp. 103–106, 2010.

Hindawi Publishing Corporation
Journal of Nanotechnology
Volume 2012, Article ID 870378, 12 pages
doi:10.1155/2012/870378

Research Article

SERS Substrates by the Assembly of Silver Nanocubes: High-Throughput and Enhancement Reliability Considerations

Oded Rabin[1,2] and Seung Yong Lee[1]

[1] *Department of Materials Science and Engineering, University of Maryland, College Park, MD 20742, USA*
[2] *Institute for Research in Electronics and Applied Physics, University of Maryland, College Park, MD 20742, USA*

Correspondence should be addressed to Oded Rabin, oded@umd.edu

Received 3 February 2012; Accepted 21 March 2012

Academic Editor: Mustafa Çulha

Small clusters of nanoparticles are ideal substrates for SERS measurements, but the SERS signal enhancement by a particular cluster is strongly dependent on its structural characteristics and the measurement conditions. Two methods for high-throughput assembly of silver nanocubes into small clusters at predetermined locations on a substrate are presented. These fabrication techniques make it possible to study both the structure and the plasmonic properties of hundreds of nanoparticle clusters. The variations in SERS enhancement factors from cluster to cluster were analyzed and correlated with cluster size and configuration, and laser frequency and polarization. Using Raman instruments with 633 nm and 785 nm lasers and linear clusters of nanocubes, an increase in the reproducibility of the enhancement and an increase in the average enhancement values were achieved by increasing the number of nanocubes in the cluster, up to 4 nanocubes per cluster. By examining the effect of cluster configuration, it is shown that linear clusters with nanocubes attached in a face-to-face configuration are not as effective SERS substrates as linear clusters in which nanocubes are attached along an edge.

1. Introduction

The assembly of plasmonic nanoparticles is a simple and inexpensive method for the production of nanoscale gaps between metallic surfaces that generate hot-spots (small volumes with intense electric field strength) when illuminated [1, 2]. The oscillating electric field in the gap can couple to electronic and vibrational modes of molecules present in the hot-spot. A possible outcome of these interactions is a change in the vibrational state of the molecule and the inelastic scattering of a photon—an event that is detected with a Raman spectrometer. Since the inelastic (Raman) scattering rate is approximately proportional to the 4th power of the amplitude of the electric field at the site of the molecule and the hot-spots typically enhance the field by a factor of 10^1-10^2, the Raman spectrum (or Raman map) may be dominated by photons scattered by the few molecules located in the hot-spots, in what is referred to as Surface-Enhanced Raman Scattering or Surface-Enhanced Raman Spectroscopy (SERS) [3, 4].

Knowing the geometry of the assembly and the optical properties of the nanoparticle material and the surrounding medium, the enhancement of the electric field on and near the surface of the nanoparticles can be calculated by solving Maxwell's equations [5, 6]. Such calculations, as well as methodic experiments, show that there are many factors that determine whether a nanoscale gap between metallic nanoparticles will act as an effective SERS site. Local geometry parameters, such as the gap size and the curvature of the surfaces, and electronic factors, such as the frequency-dependent dielectric constant of the metal, are particularly important [7]. Changes in the structure and composition of the surface away from the hot-spot (at distances comparable to the wavelength) can also affect the enhancement. In addition, the experimentalists' choices regarding wavelength and polarization greatly influence the effectiveness of SERS [8–10]. Lastly, the ability of targeted molecules to reach the hot-spot and their orientation(s) once there also affect the SERS signal. Control over many of these factors requires the engineering of crystals, surfaces, and chemical interactions with nanoscale precision.

The consequence of the strong dependence of the Raman scattering process on experimental conditions and

almost-atomistic details of the surface is that the SERS enhancement can vary by several orders of magnitude from site to site on a single substrate [11]. For analytical applications, this problem can be surmounted by increasing the area of signal collection to include a large number of hot-spots and thus relying on the average enhancement of the signal across the entire sampling area. Reproducible results can be obtained this way using laboratory or commercial SERS substrates [8]. However, a key advantage of SERS over other optical spectroscopy methods is the ability to record molecular spectra at *ultra-low* concentrations. Analytical applications that require large sampling areas in order to obtain quantitative results do not make good use of the sensitivity range of the SERS process. Towards creating SERS substrates for quantitative high-sensitivity molecular detection, that is, SERS substrates with high and reproducible enhancements, it is necessary to study the site-to-site variability of the SERS signal of nanofabricated and self-assembly SERS substrates and to understand the reasons for this variability.

With the advent of methods for the synthesis of noble metal nanoparticles with highly uniform shape and size, [12, 13] and the demonstration of single molecule SERS sensing using nanoparticle clusters as enhancing substrates, [14, 15] the two remaining challenges towards quantitative SERS using nanoparticle self-assembly are (i) the robust design of the enhancing element—the nanoparticle cluster—and (ii) the design of a suitable high-throughput fabrication method. These two challenges are intertwined. The *design* of the enhancing element refers to the selection of the size and geometric features of the nanoparticle cluster [16–20]. These include the particle size and shape, the number of nanoparticles in a cluster and their relative positions. These parameters will need to be tailored specifically for the analyte and the Raman spectrometer to be used. The *robustness* of the design refers to whether a set of analytical measurement targets (e.g., a 5 : 1 signal-to-noise ratio when probing a 1 nM sample for 0.5 sec) is achieved when the tolerances associated with the fabrication method are considered. For example, if the selected cluster design is that of pairs of silver nanospheres and the selected fabrication method produces nanospheres of sizes 55 ± 5 nm separated by a 3 ± 1 nm gap, a robust design should meet the analytical targets with any likely combination of sphere sizes and gaps that may result out of said production.

Our current research efforts address the robust design and high-throughput fabrication of SERS substrates based on self-assembly of nanoparticle. The focus of this study is on the generation of SERS substrates each consisting of *one small cluster of silver nanocubes* and the quantification of the enhancement of the SERS signal by these individual clusters. Special procedures were developed in order to quantitatively determine the enhancement factor of hundreds of individual clusters in an efficient manner, without the aid of simulations, and without the need to make assumptions regarding the locations and dimensions of the hot-spots. Using this large pool of data, the robustness of the enhancement by different types of clusters is analyzed. Recommendations regarding silver nanocube cluster design for SERS are provided.

2. Experimental Methods for High-Throughput Assembly of Nanoparticles for SERS Studies

Assemblies of nanoparticles have been examined in great detail by various nanocharacterization tools such as AFM, SEM, and TEM [9, 21–24]. The key technical obstacle for SERS characterization of assemblies of nanoparticles is the need to find and register the locations of the clusters on the substrate in order to perform correlated characterization by Raman spectroscopy and additional characterization tools of the same assemblies [25]. Frequently, the assemblies form in random locations on a substrate, for example, by drop-casting and self-assembly [18]. The substrate needs to be imaged to locate clusters that qualify for the investigation (e.g., isolated from neighboring particles)—a time consuming step that may also alter the effectiveness of the enhancement (e.g., due to radiation damage). As a result, most detailed studies on the SERS effect in nanoparticle clusters have been limited to a small sample population. Alternatively, methods for the preassembly of clusters of nanoparticles in solution have been introduced in recent years, [26] but these clusters often include surface coatings, [22, 24] and still need to be deposited and located by scanning the substrate. In order to achieve high-throughput characterization, our focus is on methods that dictate *a-priori* the sites on the substrate in which clusters will form. We present two methods based on (i) vertical deposition [27–29] and (ii) electrophoretic deposition [30] in *patterned* substrates. In both methods the SERS substrate preparation involves the synthesis of plasmonic nanoparticles as a colloidal solution followed by the templated assembly of the nanoparticles into discrete clusters. The patterned substrates and the deposition method guide the formation of clusters in preselected locations, in this work, a square array with a period (site-to-site separation) of $5\,\mu$m. This pattern geometry was chosen for the time-efficient collection of spectra from hundreds of sites using the x-y stage automatic-mapping function provided with the control software of the Raman spectrometer (LabRAM Jovin-Yvon microRaman system).

2.1. Vertical Deposition in Patterned Substrates. In the vertical deposition method a substrate is held vertically in the colloidal solution and then pulled out in a vertical motion at a constant velocity. Nanoparticles are deposited on the substrate as the air/liquid interface traverses the surface. When the surface of the substrate contains topographic steps, nanoparticle deposition is enhanced at the bottom of these steps [27–29]. In this work, topographic steps were generated by lithographic patterning and etching. Surface wetting and the presence of a meniscus are favorable conditions for the selective deposition of nanoparticles in the patterns.

The substrates used in the vertical deposition were fabricated out of single-side polished (100) Si wafers (Silicon Inc.). E-beam lithography and reactive ion etching with

a SF_6/O_2 gas mixture (100 W power, 50 mTorr pressure, 50 sccm : 10 sccm $SF_6 : O_2$ flow ratio) were used to generate a square array of nanoscale pores, 200 nm in diameter, 100 nm in depth, and 5 μm apart. The dimensions of the pores were chosen to accommodate small clusters of 85 nm silver nanocubes. Larger markers were patterned around the array to allow the user to recognize the position of the columns and rows of the array by optical microscopy. The etched silicon wafer was rinsed with acetone, treated with oxygen plasma, and cleaned with *aqua regia* to remove any residue from the patterning process [31]. An SEM image of the as-prepared substrate is shown in Figure 1. The vertical velocity of the substrate during the deposition and the solvent of the colloidal solution were adjusted to achieve the highest efficiency for filling the pores with nanocubes. The velocities used were in the range of 0.16 to 1.25 mm/hr. The vertical deposition process took between 3 to 10 hours to complete. The colloidal solutions used in the vertical deposition were obtained by resuspending 85 nm silver nanocubes passivated by polyvinylpyrrolidone (see Section 3.2) in DI water to a concentration of 2 mM (based on Ag).

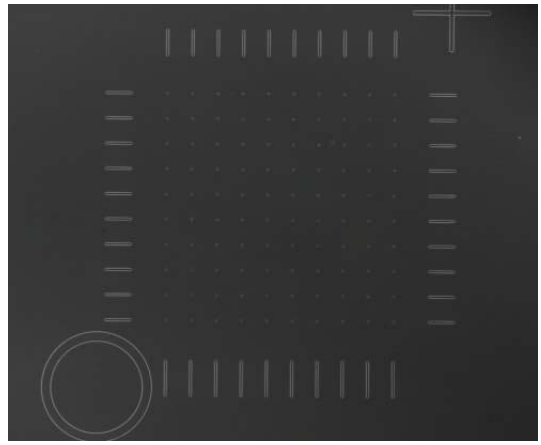

Figure 1: SEM image of the patterned silicon substrate used for the vertical deposition process. The pattern includes one hundred circular pores, 200 nm in diameter, in a square array surrounded by twenty alignment markers identifying the locations of the columns and rows, and auxiliary identification marks (ring and cross). The spacing between adjacent rows and columns is 5 μm.

2.2. Electrophoretic Deposition in Patterned Substrates. In the electrophoretic deposition method charged particles are pulled by electric fields between two electrodes in a low-current electrolytic cell [30, 32–35]. In our experiments, the electrolyte consisted of 110 nm silver nanocubes with a polymeric coating (see Section 3.2) suspended in DI water at a concentration of 0.25–2 mM (based on Ag). No supporting electrolyte was added. The silver nanocubes are negatively charged when suspended in DI water due to the polymer surfactant and can be deposited exclusively on the anode by electrophoresis. A 0.5 cm^2 single-side polished (100) silicon wafer was used as the anode and a steel mesh as the cathode. In order to guide the deposition of the nanocubes to chosen sites, the anode was covered with a sacrificial insulating film patterned by e-beam lithography (Scheme 1). Typically, we used a 200 nm thick PMMA film patterned with an array of 150 nm by 500 nm rectangular pores. During electrophoresis, nanocubes near the anode concentrated and deposited in the areas where the silicon surface was exposed to the solution. A constant voltage of 15 V was applied for a short period of time (10–60 seconds, depending on the concentration of the particles in the electrolyte) to limit the generation of large clusters and minimize parasitic electrochemical reactions. Typical current values were 10–40 μA. Dissolution of the PMMA layer removed all nanocubes except those clustered in direct contact with the silicon surface (Scheme 1).

2.3. Comparison between Deposition Methods. It may be worthy to compare attributes of the vertical deposition and the electrophoretic deposition methods for the purpose of generating small clusters of nanoparticles in predetermined locations on substrates.

(i) *Duration and Cost*. The electrophoretic deposition can be completed in a few minutes, while the vertical deposition is a significantly slower process. However, when the time dedicated to patterning the substrate is also considered, the vertical deposition saves time and cost with a recyclable substrate that can be reused after cleaning (because the pores are permanently etched into the silicon).

(ii) *Filling Efficiency*. The electrophoretic deposition is more reliable in generating clusters in the designated sites, while the efficiency of the vertical deposition process depends on the shape of the pore, and on the wettability of the substrate and the volatility of the solvent. The latter are more difficult to test and optimize.

(iii) *Damage to Nanocubes*. During the electrophoretic deposition, surface reactions involving electroactive species from the solution cannot be excluded, however, to date no detrimental effects on the silver nanocubes were recognized by imaging or spectroscopy. During the vertical deposition, the nanocubes may react on defect sites in the surface of the silicon substrate [31]. These reactions can be prevented by following standard surface cleaning and passivation procedures.

(iv) *Aging*. The rate of degradation of the nanocubes in ambient air is comparable in both methods. Substrates were usually used within 48 hours of nanocube deposition.

3. Experimental Methods for High-Throughput SERS Characterization of Assemblies of Nanoparticles

3.1. The SERS Substrate Enhancement Factor. There are different approaches to calculate the SERS substrate enhancement factor (SSEF), which, regrettably, make it very challenging to compare substrate characteristics and research

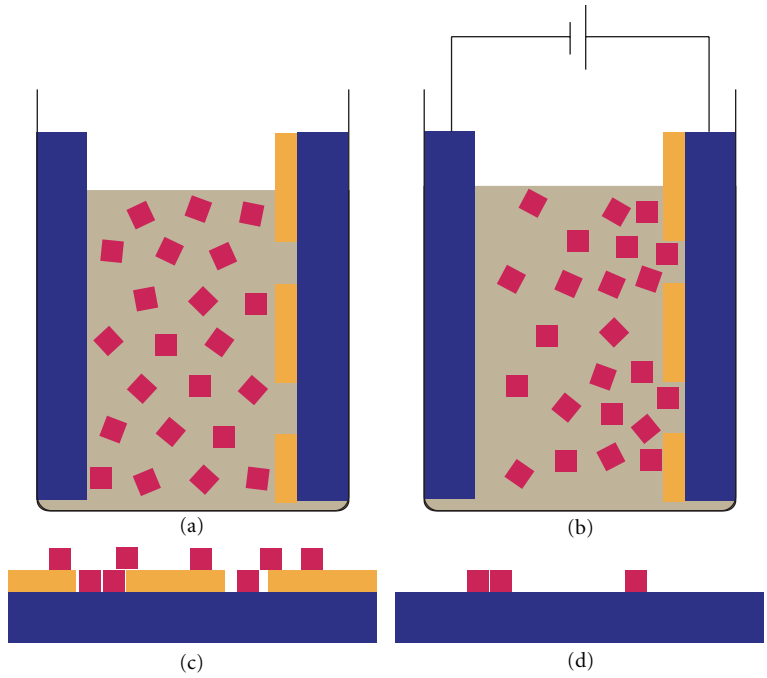

Scheme 1: Illustration of the electrophoretic deposition process. (a) A patterned electrode and a counter electrode are immersed in a colloidal solution of nanoparticles. (b) An electric field is applied, causing the charged nanoparticles to deposit on one electrode. (c) The deposited nanoparticles are primarily concentrated near the patterned openings in the sacrificial insulating layer. (d) The sacrificial insulating layer is removed, leaving nanoparticles only in the patterns.

data reported by different groups [36]. Considering that the probed molecule may be in many possible locations and orientations during the measurement, the enhancement factor measured experimentally should be considered as an average response. Selective targeting of molecules to the hot-spot site may be engineered into the structure and surface chemistry of the SERS substrate, but such examples are rare [37]. Thus, the approach we have taken to generate the most consistent values of SSEF is to saturate the plasmonic surfaces with the analyte and report the average enhancement acting on the ensemble of adsorbed molecules. The number of molecules per cluster in our experiments is on the order of 10^5 to 10^6 when close-packed monolayers are considered. The SSEF values are calculated by comparing the Raman signal from the molecules on the SERS substrate with that from molecules in a concentrated solution (0.5 M in 1,5-pentanediol, corresponding to $\sim 10^{10}$ molecules), taking into account the number of molecules being probed in each experiment. SSEF values calculated by this approach are reproducible and of informative value to the end-user.

3.2. Silver Nanocubes. Single-crystal silver nanocubes were synthesized by the polyol reduction method in 1,5-pentanediol [23, 38]. The as-prepared nanocubes are terminated by the silver crystal 100 planes and are coated with a passivation layer of polyvinylpyrrolidone (PVP). The nanocube size is tunable between 50 nm and 150 nm by the modification of the reaction conditions. We have used suspensions of nanocubes with an average size of 85 nm and 110 nm for the reported SERS experiments.

3.3. Cluster Data Collection and Analysis. Each cluster in the array was probed by Raman spectroscopy after the adsorption of a reporter molecule, 4-aminothiophenol, as a saturated monolayer on all accessible silver surfaces (5 molecules per nm^2). The spectra were collected using a LabRAM Jovin-Yvon microRaman system with a computer-controlled x-y scanning stage. Using a 50× objective (numerical aperture NA = 0.5) the laser was focused to a spot 2.2 μm in diameter. A dispersive grating with 600 lines/mm provided a spectral resolution of $\sim 1\ cm^{-1}$. Measurements with a He-Ne laser (633 nm) took 4 sec at a power of 0.6 mW and 10 sec at a power of 0.06 mW. Measurements with a diode laser (785 nm) took 50 sec with a power of 0.4 mW.

The clusters were then imaged by SEM (Hitachi, SU-70) to deduce the number of nanocubes in each cluster and the relative arrangement of the nanocubes within the cluster. These will be referred to as "cluster size" and "cluster configuration," respectively, in this paper. Sites with a single silver nanocube were also included in the study. The SSEF is calculated from the scattering intensity (as determined from the Raman spectrum) and the total surface area of the silver deduced from the nanoparticle and cluster size. The SSEF values obtained in each experiment cover a wide range. The sensitivity range of the Raman spectrometer was set to quantify the scattering intensity corresponding to SSEFs in the highest range of $\sim 10^4$–10^8. Signals weaker than this range were not determined quantitatively and were set to an arbitrary value of 1, since they can be considered as impractical for analytical measurement purposes. However, *no cluster is ignored in the following analysis*, regardless of

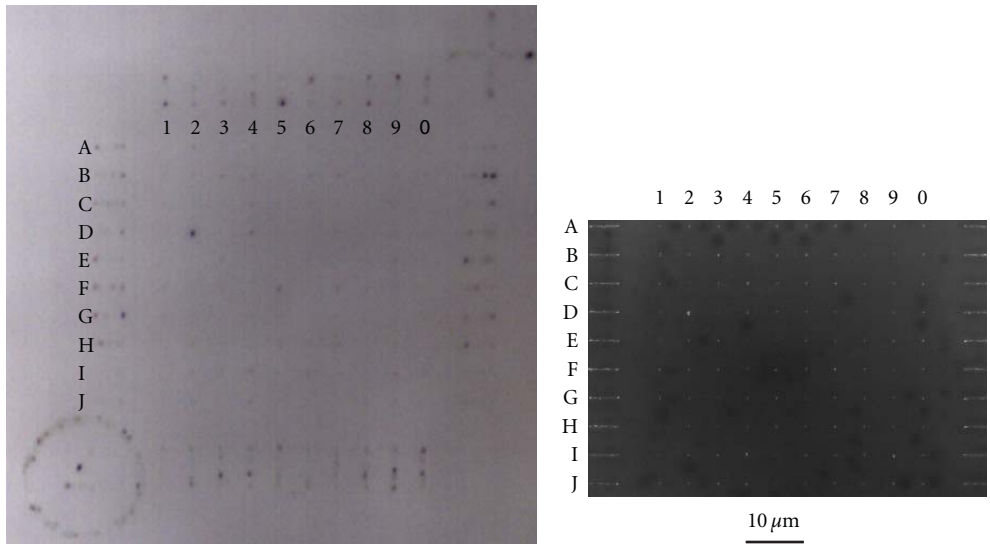

(a) (b)

Figure 2: (a) White-light reflectance microscopy image and (b) SEM image of a patterned array of 85 nm nanocube clusters on silicon. The images were scaled to the same magnification. The row (A–J) and column (1–9, 0) indicators were added to the images using Adobe Illustrator CS3.

how weak the Raman scattering signal may be. The weak enhancement data are extremely important in analyzing the robustness of the cluster design.

Figure 2 shows an optical micrograph of an array of nanocube clusters side-by-side with the corresponding SEM micrograph of the same sample. The images show the area of the square array in which the clusters are organized, as well as the line markers that indicate the positions of the rows and columns. The line markers, which contain a large number of nanocubes, are clearly visible in the optical microscope image. The light scattering intensity contrast from the array points varies. While some cluster sites are easy to pinpoint (e.g., site D2 is the darkest in the image), others generate no contrast in the optical image (e.g., sites D1 and J0). The SEM micrograph confirms that 89 out of the 100 array sites are occupied with nanocubes; however, the optical image would suggest a lower number of occupied sites. This pair of images illustrates a key point in the study of large number of clusters generated by self-assembly: methods based on the use of light scattering to locate clusters randomly placed on a substrate (e.g. by drop-casting) are biased and may fail to detect a portion of clusters that are weak light scatterers. An analysis based on only a segment of the population of clusters may lead to an unintended bias in the depiction of the dispersion of Raman enhancement values. The formation of clusters in predetermined locations prevents this type of bias in the analysis of self-assembly SERS substrates.

The properties of the clusters were studied for their influence on the robustness of the plasmonic design. Our initial studies have focused on the number of nanocubes in the cluster and the configuration of the cluster. For each analysis, the collection of clusters was divided into N categories based on cluster size or configuration using the SEM data. For each category, consisting of n_i ($i = 1$ to N) clusters, the SSEF values were collected and sorted from high to low (Figures 3(a) and 3(b)). For the purpose of comparing sets, the sorted SSEF values were plotted against their normalized list index (ranging from $1/n_i$ to 1). This normalization is necessary because the number of clusters that fall into each category varies significantly ($n_i \neq n_j$). Figure 3(c) illustrates the trendlines that are obtained by following the above-mentioned data analysis procedure. The y-axis displays the SSEF value and the x-axis can be regarded as the cumulative fraction of the cluster population. A testimony to the robustness of the plasmonic cluster design is for all the clusters in a given category to have similar (and large) SSEF values. Thus, we are seeking plots that show a nearly horizontal trendline.

4. Results and Discussion

As part of our investigation of cluster configurations, we have studied the effect of the azimuth orientation of linear silver nanocube clusters on their SERS response. Because of the relevance of this study to the design of the patterned substrates used in all the subsequent experiments, it is presented first.

4.1. The Azimuth Angle of a Pair of Nanocubes. The vertical deposition into circular pores provided us with many isolated pairs of silver nanocubes (dimers) for this study. These dimers are distinguishable due to variations in the gap distance between the cubes (limited by the size of the cavity and the size of the cubes), in the orientation of the dimer axis (i.e., the azimuth angle θ in the plane of the silicon wafer, measured with respect to the positive y-axis, as shown in Figures 4(a) and 4(c)), and in the orientation of the nanocubes in the pair with respect to

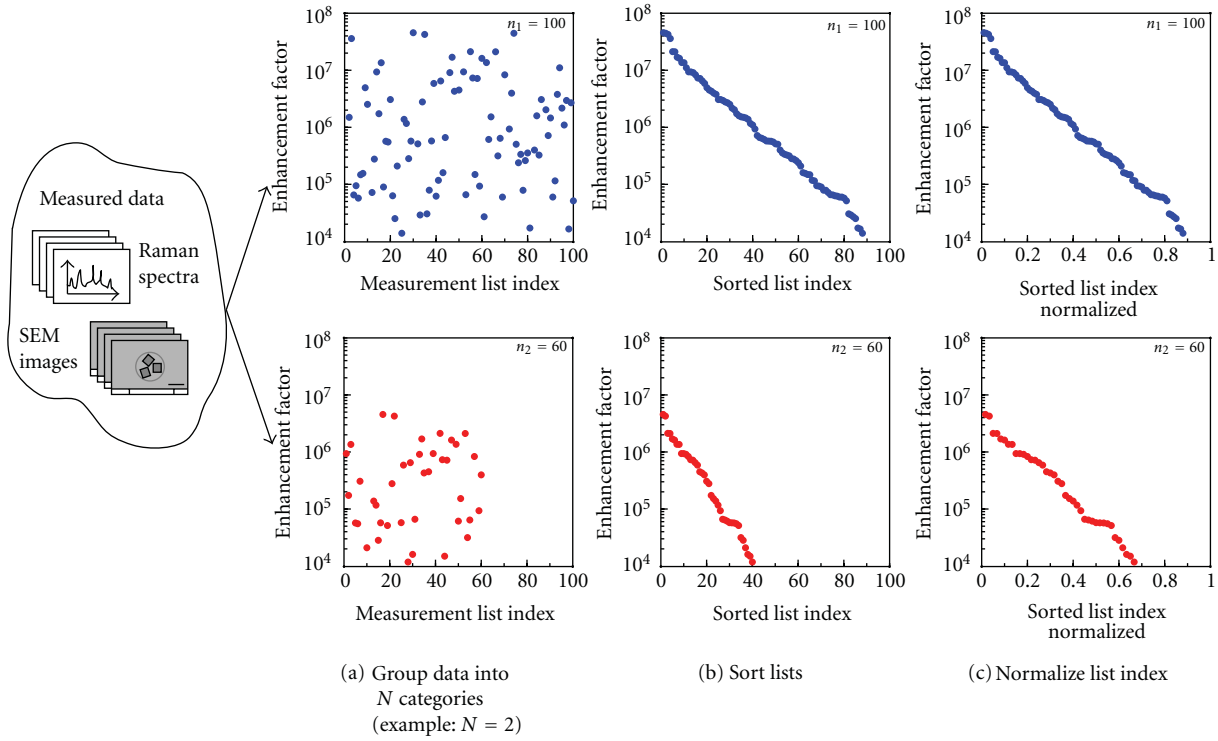

FIGURE 3: Analysis of SSEF data. (a) The data is grouped into N categories ($N = 2$): set 1 consists of a list of $n_1 = 100$ values (blue), and set 2 consists of a list of $n_2 = 60$ values (red). The list content is plotted against the list index that indicates the sequence in which the data was collected and has no physical meaning. (b) The values within each category are sorted in descending order. (c) The list index is normalized to allow a direct comparison between the lists. The normalized list indices are $0.01, 0.02, \ldots, 1$ for set 1 with $n_1 = 100$ (blue) and $1/60, 1/30, 1/20, \ldots, 1$ for set 2 with $n_2 = 60$ (red). Note that 12% of the SSEF values in set 1 and 33% of the values in set 2 are lower than 10^4 and thus are not displayed in any of the plots.

each other. An analysis of the dependence of the SSEF on the azimuth angle of the dimer axis revealed that tight control of this parameter is vital for a robust design. Figure 4 displays the oscillatory trend of the Raman enhancement on the azimuth angle. The root of this behavior is the linear polarization of the incident laser of the Raman spectrometer and the selective coupling between far-field radiation and plasmon modes that are dipolar in nature. The coupling strength is proportional to $|(\vec{D} \cdot \vec{E})|^2$, the square of the projection of the E-field vector on the direction of the dipole associated with the plasmon mode. In the case of a dimer, the vector $\vec{D}$ is oriented either parallel to the dimer axis (with magnitude D_{ax}) or perpendicular to it (with magnitude D_{orth}). When the orientation of the E-field vector is set parallel to the y axis of the sample plane, the scattering intensity $I_y(\theta)$ is proportional to $(D_{\text{ax}} \cos\theta + D_{\text{orth}} \sin\theta)^2$. When the orientation of the E-field vector is set parallel to the x axis of the sample plane, the scattering intensity $I_x(\theta)$ is proportional to $(D_{\text{ax}} \sin\theta + D_{\text{orth}} \cos\theta)^2$. If a strong hot-spot exists in the gap between the particles, $D_{\text{ax}} \gg D_{\text{orth}}$ and the SSEF(θ) is large and anisotropic. Otherwise, SSEF(θ) is weak and more isotropic. These trends are observed in Figure 4(b). The data, plotted as the SERS signal change in response to a $\pi/2$ change in the incident light polarization versus the dimer axis orientation, are concentrated in two quadrants of the plot. The measurements match well with the theoretical curve that assumes $D_{\text{orth}} = 0$. This assumption is justified only if there is good coupling between the plasmons of the nanoparticles in the dimer, and if the excitation wavelength matches the resonance frequency of the coupled plasmon mode. These conditions should also lead to a strong SERS signal. Data from dimers with a strong SERS enhancement therefore fit better to the theoretical curve.

The orientation of the nanocubes of the dimer relative to each other has a more subtle influence on the SSEF [23]. Consequently, our study on the effect of the azimuth angle is fairly insensitive to and unobstructed by variations in the nanocube dimer configuration. In the following studies on the effect of cluster size (Section 4.2) and cluster configuration (Section 4.3) on the SSEF it was important to exclude the effect of variations in the azimuth angle. Thus, in the following experiments only linear silver nanocube clusters of uniform orientation were utilized.

4.2. The Number of Nanocubes in the Cluster. Researchers have undoubtedly demonstrated that strong hot-spots occur at narrow junctions between metallic nanoparticles [2]. There is less certainty regarding the parameters that make those hot-spots most effective towards the SERS process. In particular, a fundamental question which has not yet been

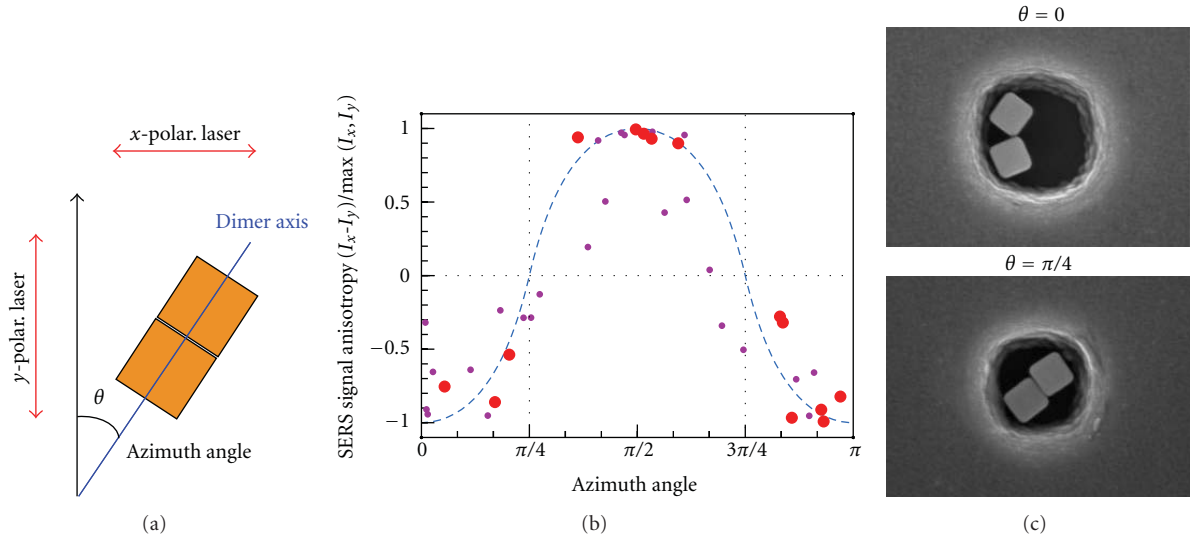

FIGURE 4: (a) Schematic of the azimuth angle θ between the positive y-axis and the dimer axis, traced clockwise. (b) The dependence of the SERS signal on the orientation of the polarization of the laser with respect to the orientation of the axis of the dimer of silver nanocubes. The SERS signal anisotropy is calculated as $(I_x(\theta) - I_y(\theta))/\max(I_x, I_y)$ (see definitions in text). The theoretical relation $(\sin^2\theta - \cos^2\theta)/\max(\sin^2\theta, \cos^2\theta)$ is indicated by the blue dashed line. Data from dimers with SSEF $> 10^5$ (large circles) is closer to the theoretical trend than data from dimers with SSEF $< 10^5$ (small circles). (c) Examples of two dimers of silver nanocubes, oriented at $\theta = 0$ and $\theta = \pi/4$, respectively. The nanocube size is 85 nm. Each dimer is located inside a pore.

resolved is whether increasing the number of nanoparticles in a cluster, and therefore the number of junctions between particles, leads to an increase in the enhancement factor. Increasing the number of nanoparticles in a cluster increases the metallic surface area; without a concomitant increase in the scattering intensity the SSEF will decrease. Detrimental retardation effects also become more pronounced as the plasmonic structure increases in size [39, 40]. Additionally, the change in the cluster size may bring the plasmon mode in *or* out of resonance with the laser of the Raman spectrometer.

We have studied the effect of the cluster size on the SSEF. To eliminate the effect of the azimuth angle, we have concentrated on the study of linear clusters and therefore have chosen the electrophoretic deposition method to deposit nanocubes within aligned rectangular pores. Representative images of plasmonic clusters consisting of linear assemblies of 2–4 silver nanocubes are shown in Figure 5. The four categories used for the data analysis reflect the number of cubes per site: monomers, dimers, trimers, and tetramers.

While the cluster size has been considered in the context of obtaining the largest enhancement factor, the reproducibility of these SSEF measurements is often overlooked. Indeed, we find that the largest SSEF value recorded for a category of clusters is not a good indicator for the SSEF values of similarly structured clusters. Figures 6(a) and 6(b) present the SSEF data for independently measured clusters of 110 nm silver nanocubes, using excitation wavelengths of 633 nm and 785 nm, respectively. The data was grouped by cluster size, with 7–124 clusters per category. The data shows a dramatic difference in the SSEF values of monomers and multiparticle clusters. Monomeric silver nanocube SERS substrates lack the narrow gaps that effectively generate hotspots. The SSEF values of monomers are the lowest, and at least 80% of the monomers have an SSEF value lower than 10^4. The comparison between enhancements by dimers, trimers, and tetramers leads to the conclusion that the most notable advantage of engineering larger clusters is that the reproducibility of the measurements is improved. The slope of the trendline decreases with cluster size. The trendline for tetramers is the most horizontal. The incorporation of additional nanocubes into the clusters results in improved robustness for the linear-cluster SERS substrate design. Similarly, the portion of unusable clusters diminishes as clusters contain more nanocubes. Of the dimers, at least 10% at 633 nm and 60% at 785 nm were ineffective SERS substrates with SSEF below 10^4. In comparison, we have not detected tetramers with SSEF below 10^4. The robustness of the trimeric structures is in between that of the tetramers and the dimers.

The data of Figure 6 indicate that the SSEF reproducibility is sensitive to the excitation wavelength. When a plasmon resonance matches with the excitation laser frequency, a boost in the SERS signal is plausible. While the resonance frequency of the plasmon modes depends on the cluster configuration, particularly on the gap sizes over which there is very limited control in the self-assembly methods used here, these frequency variations are small compared to the red-shift occurring when an additional nanoparticle is added to the cluster. Thus, while dipolar plasmons in dimers resonate near the 633 nm wavelength, they are far from resonance with the 785 nm wavelength. For this reason the trendline for dimer SSEF values slopes down more

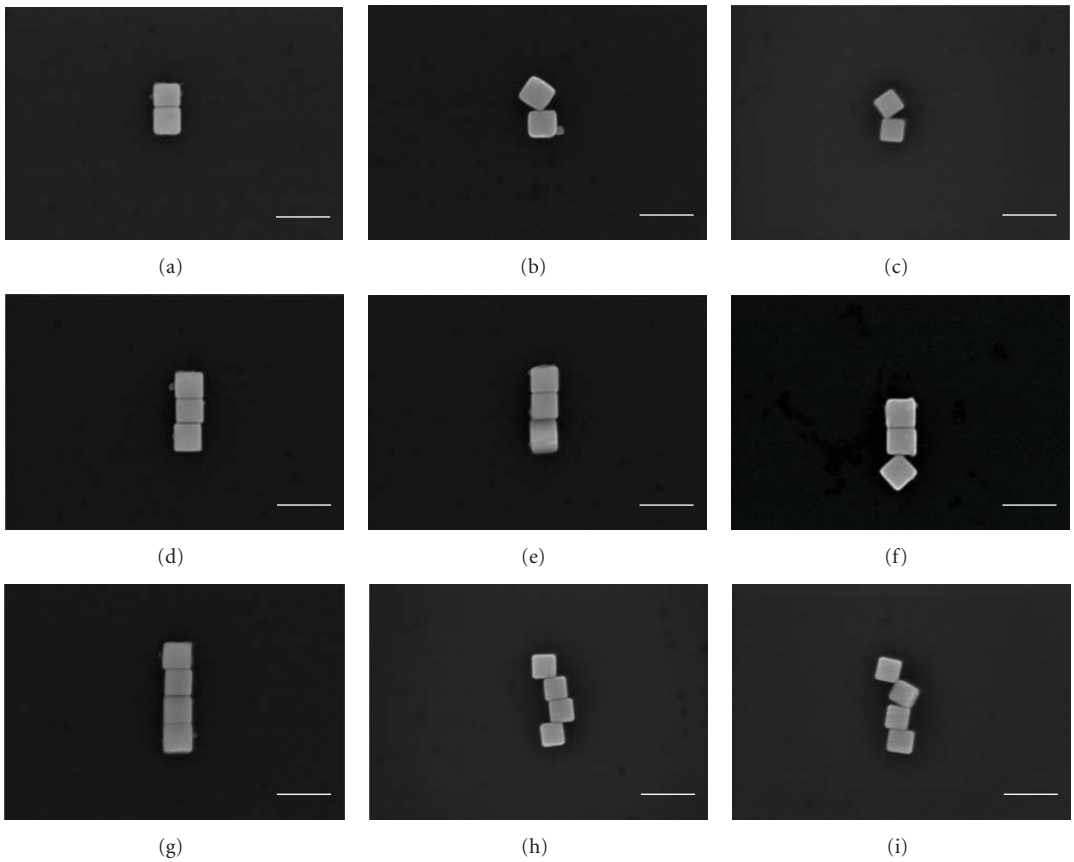

Figure 5: Collection of SEM images of silver nanocube dimers, trimers, and tetramers on silicon formed by the electrophoresis deposition method. The scale bar size is 200 nm. Images (a), (d) and (g) show examples of nanocube clusters with face-to-face configuration.

sharply as we increase the wavelength of the excitation laser (Figure 6(b) versus Figure 6(a)) and the enhancement of a large portion of the dimers decreases below the practical threshold. A similar trend is seen with monomers which resonate near 520 nm.

The number of trimers and tetramers studied is not large enough to reliably determine that the *maximum* SSEF achieved with the larger clusters is lower than that of dimers. However, the data collected thus far clearly indicates that the enhancements from the larger clusters are more reproducible and less susceptible to the lack of precise positioning control during assembly (i.e., structural variations).

A few monomers have surprisingly high SSEF values $>10^4$. We postulate the presence of a hot-spot in the junction between the nanocube and the silicon wafer. Using chemical manipulations designed to direct more molecules to this junction, we were able to increase the percentage of monomers with SSEF $>10^4$ to 40% (see Section 4.3).

4.3. The Relative Position and Orientation of the Nanocubes in the Cluster. Several experimental results and theoretical calculations with nanocube dimers have predicted the largest plasmonic enhancements for nanocubes arranged face-to-face with a gap of few nanometers between them [23, 41]. Calculations show that strong fields are predicted to extend over the entire face of the nanocube forming the narrow gap. In other configurations the strongest fields are located along cube edges or near its corners. In other words, in the face-to-face configuration the hot-spot contains more silver surface area than in other configurations, and thus more signal-generating molecules experience the strongest fields.

Our results do not reproduce these expectations. We have alluded to this result in our previous study on dimers in circular pores [23], and new data from SERS substrates produced by the electrophoretic method (Figure 5) reinforce the unexpected trend. The analysis of the new data proceeded by dividing the plasmonic structures into 3 categories of clusters: (1) clusters with nanocubes attached face-to-face (FF), (2) clusters of nanocubes attached in a non-face-to-face manner (non-FF), that is, along an edge, and (3) clusters of any configuration with at least one gap between the nanocubes that could be resolved by SEM (i.e., gap >3 nm). The gaps between nanocubes in the clusters selected for the first two categories were all less than 3 nm. This categorization was implemented with data sets from nanocube dimers and nanocube trimers, as shown in Figures 7(a) and 7(b). The SSEF values of face-to-face (FF) dimers are collectively lower than those of non-face-to-face (non-FF) dimers and the SSEF values of FF trimers are collectively lower than those of non-FF trimers. Strikingly, the FF clusters are comparable

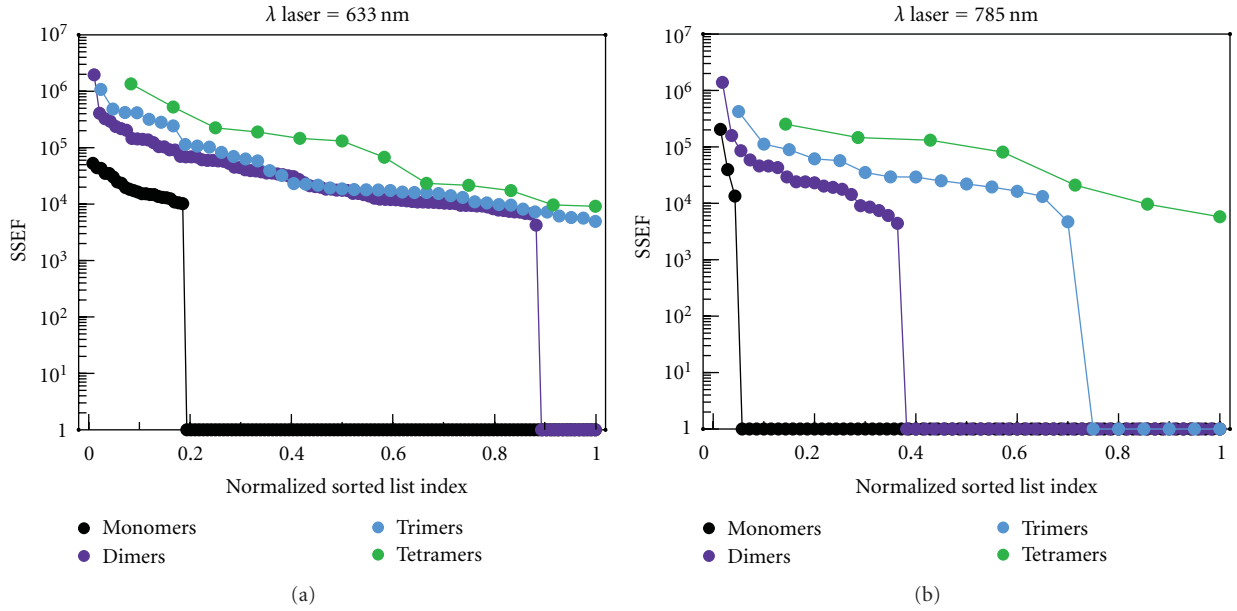

Figure 6: Cluster size analysis. Sorted SSEF data from silver nanocube monomers (black), dimers (violet), trimers (cyan), and tetramers (green). Excitation laser wavelength: (a) 633 nm and (b) 785 nm. Nanocube size: 110 nm.

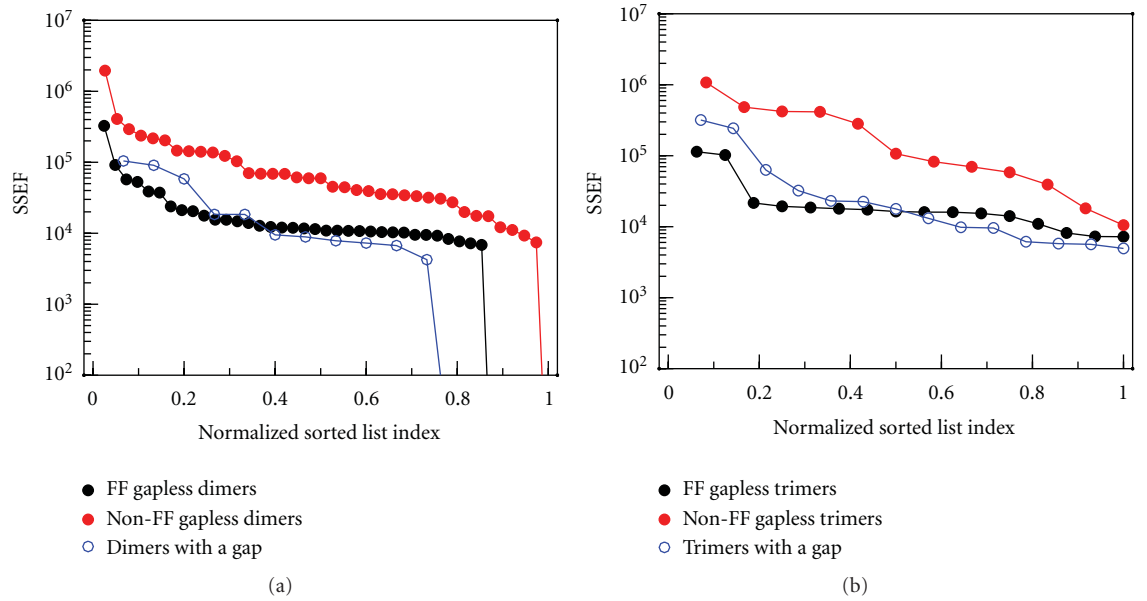

Figure 7: Cluster configuration analysis. Sorted SSEF data from (a) silver nanocube dimers and (b) silver nanocube trimers. The categories are FF clusters with no gaps (black), non-FF clusters with no gaps (red), and clusters with a gap (blue, open circles). Excitation wavelength: 633 nm. Nanocube size: 110 nm.

in their SSEF to clusters in which we can observe a sizeable gap (>3 nm).

The data in Figure 7 indicate that the FF-type junctions produce smaller Raman scattering enhancements than the non-FF junctions. There are several possible explanations for these observations. The most intuitive hypothesis is that there are no Raman dye molecules in the FF-type junctions. The Raman dye molecules are more likely to adsorb on the metal surface areas that are more accessible to the solution. The dye solution cannot easily access the surfaces that form the FF-type junctions, since these faces are separated by a gap less than 3 nm in size that is also occupied by surface-passivating PVP molecules. To examine the hypothesis that the FF-type clusters have an average low SSEF because of the low surface concentration of the Raman reporter in their gaps, we have compared the SSEF data reported in Figure 6 and Figure 7 with SSEF data obtained from clusters formed with nanocubes that have been treated by adsorption of

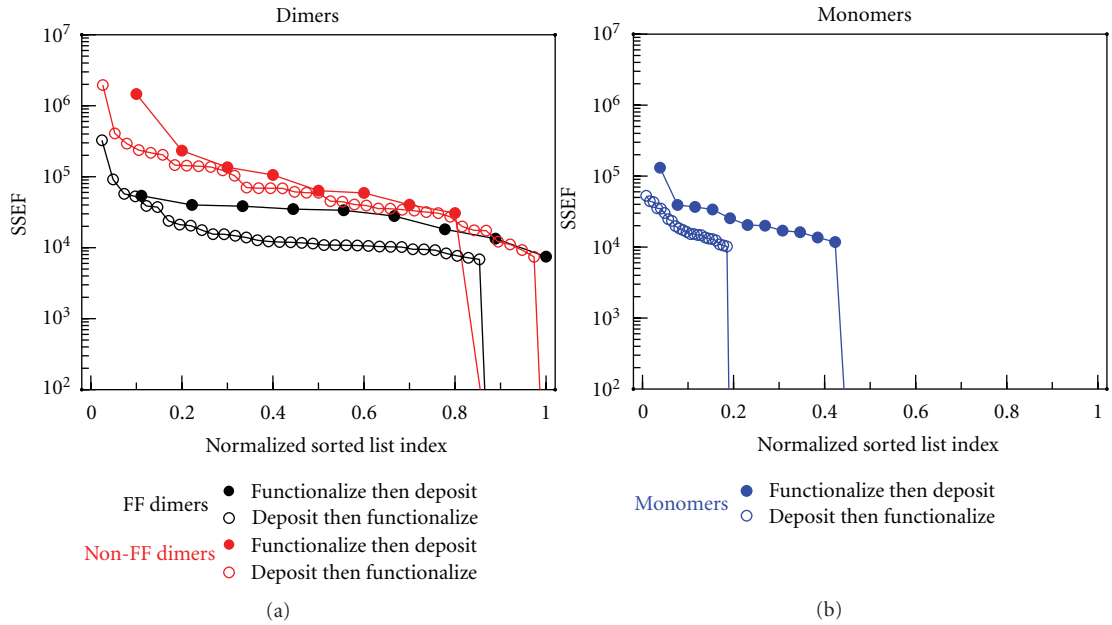

Figure 8: Pre- and post-deposition functionalization of silver nanocubes. Sorted SSEF data from (a) silver nanocube dimers and (b) silver nanocube monomers. The categories are FF dimer with no gaps (black), non-FF dimers with no gaps (red), and monomers (blue). Excitation wavelength: 633 nm. Nanocube size: 110 nm.

the Raman dye *before* they were allowed to cluster. Briefly, the silver nanocubes were dispersed in a 1 mM ethanoic solution of 4-aminothiophenol. After 3 hours, the nanocubes were separated and cleaned by repeated centrifugation in ethanol and in DI water. These functionalized nanocubes were deposited on substrates coated with a patterned PMMA layer (with an array of rectangular nanopores) by drop-casting. Following the removal of the PMMA layer, substrates with clusters of nanocubes in predetermined locations were obtained. In these experiments, no electric fields were applied during the deposition of the cubes because we had found that the Raman reporter molecule is not compatible with the electrophoretic deposition conditions. As a result, a comparatively low number of clusters were obtained for this study, most of them monomers and dimers.

Figure 8 presents the comparison between SERS data obtained with pre-deposition functionalization and post-deposition functionalization of the silver nanocubes with the Raman reporter. The SERS data from dimers were grouped according to cluster configuration (FF versus non-FF). The trendlines for FF dimers indicate that the collective SSEFs are higher when the functionalization precedes the deposition. Still, the same is true for non-FF dimers and even more significantly for monomers. The trendline for FF dimers is still lower than that of non-FF dimers, even after pre-deposition functionalization. Taken together, these observations suggest that there is an increase in the surface concentration of the Raman dye in pre- versus post-deposition functionalized nanocubes. However, the similarities in the results recorded for monomers and for FF dimers suggest that the most significant difference in the surface concentration is in the gaps between the nanocubes and the silicon substrate. These gaps are narrower than the lateral gaps in the FF dimers, are presumably the least accessible to the solution, and are the most plausible location for the hot-spots in monomers. The increase in the SSEF values of all the clusters regardless of cluster configuration (Figure 8) can be accounted for by the increase in the surface concentration of 4-aminothiophenol in all the gaps between silver nanocubes and the silicon substrate. The fact that the increase in SSEF values is the *least significant* in the non-FF dimers could indicate that the molecules in the junctions between the nanocubes are significantly more radiant than the molecules on the bottom surface of these dimers. The hypothesis that lower SSEF values in FF dimers are due to lower surface concentration of molecules in the gap is probably incorrect. Other hypotheses, relating the SSEF values to the effect of cluster configuration on the plasmon resonance frequencies and the field intensity distribution around the nanocubes, are more plausible and should be examined further [23].

5. Conclusions

The analysis of the distribution of the SSEF values is a direct method to probe the reliability of an SERS substrate design with respect to fabrication tolerances. We have demonstrated the acquisition of SERS signals from hundreds of SERS substrates, each consisting of a small cluster of nanoparticles and produced by self-assembly techniques (either vertical deposition or electrophoretic deposition using patterned substrates). The analysis of the distribution of the SSEF values from these substrates provided insightful information regarding the important parameters that lead to high and reproducible SSEFs using silver nanocubes.

Our results reproduce the SSEF dependence on the polarization of the incident laser beam commonly reported in the literature. The azimuth angle studies indicate that linear clusters of silver nanocubes should be prepared with their long axis parallel to the laser polarization. This linear alignment was achieved by clustering the nanocubes within rectangular nanopores.

By increasing the cluster size, from monomers to tetramers, the average SSEF values increased, both with 633 nm and 785 nm incident laser light. Furthermore, the distribution of SSEF values from same-size clusters becomes narrower with increasing cluster size. In contrast, no clear correlation between maximum SSEF value and cluster size could be established from the data.

Our experimentation with various cluster configurations indicates that better sensitivity could be achieved in SERS by avoiding the assembly of nanocubes into close-packed linear clusters with face-to-face arrangement. This guideline for cluster design can be satisfied using our fabrication methods by introducing nanoscale corrugations to the base or the side-walls of the nanopores in the substrate.

For most of the practical applications of SERS in chemical and biomolecule sensing, the plasmonic nanostructured substrate has to be assembled prior to the exposure to the analyte. Adsorption of the analyte following the assembly of the cluster may not lead to the highest possible concentration of molecules on the surface of the nanocubes. The face of the nanocube adjacent to the flat silicon substrate is potentially depleted of Raman reporters, and thus it could be challenging to effectively utilize hot-spots in the gap between the silicon and the silver nanocubes for SERS.

Acknowledgments

The authors acknowledge financial support from ONR (N000140911190). The support of the Maryland NanoCenter and its NispLab is appreciated. The NispLab is supported in part by the NSF as a MRSEC Shared Experimental Facility.

References

[1] H. Xu, E. J. Bjerneld, M. Käll, and L. Börjesson, "Spectroscopy of single hemoglobin molecules by surface enhanced raman scattering," *Physical Review Letters*, vol. 83, no. 21, pp. 4357–4360, 1999.

[2] J. P. Camden, J. A. Dieringer, Y. Wang et al., "Probing the structure of single-molecule surface-enhanced Raman scattering hot spots," *Journal of the American Chemical Society*, vol. 130, no. 38, pp. 12616–12617, 2008.

[3] M. Moskovits, "Surface-enhanced Raman spectroscopy: a brief retrospective," *Journal of Raman Spectroscopy*, vol. 36, no. 6-7, pp. 485–496, 2005.

[4] F. J. García-Vidal and J. B. Pendry, "Collective theory for surface enhanced Raman scattering," *Physical Review Letters*, vol. 77, no. 6, pp. 1163–1166, 1996.

[5] K. L. Kelly, E. Coronado, L. L. Zhao, and G. C. Schatz, "The optical properties of metal nanoparticles: the influence of size, shape, and dielectric environment," *Journal of Physical Chemistry B*, vol. 107, no. 3, pp. 668–677, 2003.

[6] I. D. Mayergoyz, D. R. Fredkin, and Z. Zhang, "Electrostatic (plasmon) resonances in nanoparticles," *Physical Review B*, vol. 72, no. 15, pp. 1–15, 2005.

[7] N. Grillet, D. Manchon, F. Bertorelle et al., "Plasmon coupling in silver nanocube dimers: resonance splitting induced by edge rounding," *ACS Nano*, vol. 5, no. 12, pp. 9450–9462, 2011.

[8] W. Lee, S. Y. Lee, R. M. Briber et al., "Self-assembled SERS substrates with tunable surface plasmon resonances," *Advanced Functional Materials*, vol. 21, no. 18, pp. 3424–3429, 2011.

[9] D. K. Lim, K. S. Jeon, H. M. Kim, J. M. Nam, and Y. D. Suh, "Nanogap-engineerable raman-active nanodumbbells for single-molecule detection," *Nature Materials*, vol. 9, no. 1, pp. 60–67, 2010.

[10] T. Dadosh, J. Sperling, G. W. Bryant et al., "Plasmonic control of the shape of the raman spectrum of a single molecule in a silver nanoparticle dimer," *ACS Nano*, vol. 3, no. 7, pp. 1988–1994, 2009.

[11] Y. Fang, N. H. Seong, and D. D. Dlott, "Measurement of the distribution of site enhancements in surface-enhanced raman scattering," *Science*, vol. 321, no. 5887, pp. 388–392, 2008.

[12] Y. Sun and Y. Xia, "Shape-controlled synthesis of gold and silver nanoparticles," *Science*, vol. 298, no. 5601, pp. 2176–2179, 2002.

[13] I. Ojea-Jimenez, N. G. Bastus, and V. Puntes, "Influence of the sequence of the reagents addition in the citrate-mediated synthesis of gold nanoparticles," *Journal of Physical Chemistry C*, vol. 115, no. 32, pp. 15752–15757, 2011.

[14] S. Nie and S. R. Emory, "Probing single molecules and single nanoparticles by surface-enhanced Raman scattering," *Science*, vol. 275, no. 5303, pp. 1102–1106, 1997.

[15] K. Kneipp, Y. Wang, H. Kneipp et al., "Single molecule detection using surface-enhanced Raman scattering (SERS)," *Physical Review Letters*, vol. 78, no. 9, pp. 1667–1670, 1997.

[16] H. Chen, Z. Sun, W. Ni et al., "Plasmon coupling in clusters composed of two-dimensionally ordered gold nanocubes," *Small*, vol. 5, no. 18, pp. 2111–2119, 2009.

[17] J. A. Fan, C. Wu, K. Bao et al., "Self-assembled plasmonic nanoparticle clusters," *Science*, vol. 328, no. 5982, pp. 1135–1138, 2010.

[18] L. Chuntonov and G. Haran, "Trimeric plasmonic molecules: the role of symmetry," *Nano Letters*, vol. 11, no. 6, pp. 2440–2445, 2011.

[19] F. S. Ou, M. Hu, I. Naumov et al., "Hot-spot engineering in polygonal nanofinger assemblies for surface enhanced Raman spectroscopy," *Nano Letters*, vol. 11, no. 6, pp. 2538–2542, 2011.

[20] S. C. Yang, H. Kobori, C. L. He et al., "Plasmon hybridization in individual gold nanocrystal dimers: direct observation of bright and dark modes," *Nano Letters*, vol. 10, no. 2, pp. 632–637, 2010.

[21] D. S. Kim, J. Heo, S. H. Ahn, S. W. Han, W. S. Yun, and Z. H. Kim, "Real-space mapping of the strongly coupled plasmons of nanoparticle dimers," *Nano Letters*, vol. 9, no. 10, pp. 3619–3625, 2009.

[22] K. L. Wustholz, A. I. Henry, J. M. McMahon et al., "Structure-activity relationships in gold nanoparticle dimers and trimers for surface-enhanced raman spectroscopy," *Journal of the American Chemical Society*, vol. 132, no. 31, pp. 10903–10910, 2010.

[23] S. Y. Lee, L. Hung, G. S. Lang, J. E. Cornett, I. D. Mayergoyz, and O. Rabin, "Dispersion in the SERS enhancement with silver nanocube dimers," *ACS Nano*, vol. 4, no. 10, pp. 5763–5772, 2010.

[24] G. Chen, Y. Wang, M. Yang et al., "Measuring ensemble-averaged surface-enhanced Raman scattering in the hotspots of colloidal nanoparticle dimers and trimers," *Journal of the American Chemical Society*, vol. 132, no. 11, pp. 3644–3645, 2010.

[25] M. Rycenga, P. H. C. Camargo, W. Li, C. H. Moran, and Y. Xia, "Understanding the SERS effects of single silver nanoparticles and their dimers, one at a time," *Journal of Physical Chemistry Letters*, vol. 1, no. 4, pp. 696–703, 2010.

[26] J. M. Romo-Herrera, R. A. Alvarez-Puebla, and L. M. Liz-Marzán, "Controlled assembly of plasmonic colloidal nanoparticle clusters," *Nanoscale*, vol. 3, no. 4, pp. 1304–1315, 2011.

[27] J. A. Liddle, Y. Cui, and P. Alivisatos, "Lithographically directed self-assembly of nanostructures," *Journal of Vacuum Science and Technology B*, vol. 22, no. 6, pp. 3409–3414, 2004.

[28] K. D. Alexander, M. J. Hampton, S. Zhang, A. Dhawan, H. Xu, and R. Lopez, "A high-throughput method for controlled hotspot fabrication in SERS-active gold nanoparticle dimer arrays," *Journal of Raman Spectroscopy*, vol. 40, no. 12, pp. 2171–2175, 2009.

[29] Y. Yin, Y. Lu, B. Gates, and Y. Xia, "Template-assisted self-assembly: a practical route to complex aggregates of monodispersed colloids with well-defined sizes, shapes, and structures," *Journal of the American Chemical Society*, vol. 123, no. 36, pp. 8718–8729, 2001.

[30] Q. Zhang, T. Xu, D. Butterfield et al., "Controlled placement of CdSe nanoparticles in diblock copolymer templates by electrophoretic deposition," *Nano Letters*, vol. 5, no. 2, pp. 357–361, 2005.

[31] S. Y. Lee and O. Rabin, "A unique solid-solid transformation of silver nanoparticles on reactive-ion-etching processed silicon," *Nanotechnology*, vol. 23, no. 6, article 065301, 2012.

[32] L. Besra and M. Liu, "A review on fundamentals and applications of electrophoretic deposition (EPD)," *Progress in Materials Science*, vol. 52, no. 1, pp. 1–61, 2007.

[33] N. Chandrasekharan and P. V. Kamat, "Assembling gold nanoparticles as nanostructured films using an electrophoretic approach," *Nano Letters*, vol. 1, no. 2, pp. 67–70, 2001.

[34] M. A. Islam, Y. Xia, M. L. Steigerwald et al., "Addition, suppression, and inhibition in the electrophoretic deposition of nanocrystal mixture films for CdSe nanocrystals with γ-Fe_2O_3 and Au Nanocrystals," *Nano Letters*, vol. 3, no. 11, pp. 1603–1606, 2003.

[35] R. C. Bailey, K. J. Stevenson, and J. T. Hupp, "Assembly of micropatterned colloidal gold thin films via microtransfer molding and electrophoretic deposition," *Advanced Materials*, vol. 12, no. 24, pp. 1930–1934, 2000.

[36] E. C. Le Ru, E. Blackie, M. Meyer, and P. G. Etchegoint, "Surface enhanced raman scattering enhancement factors: a comprehensive study," *Journal of Physical Chemistry C*, vol. 111, no. 37, pp. 13794–13803, 2007.

[37] L. Rodríguez-Lorenzo, R. A. Álvarez-Puebla, I. Pastoriza-Santos et al., "Zeptomol detection through controlled ultrasensitivesitive surface-enhanced raman scattering," *Journal of the American Chemical Society*, vol. 131, no. 13, pp. 4616–4618, 2009.

[38] A. Tao, P. Sinsermsuksakul, and P. Yang, "Polyhedral silver nanocrystals with distinct scattering signatures," *Angewandte Chemie*, vol. 45, no. 28, pp. 4597–4601, 2006.

[39] M. Inoue and K. Ohtaka, "Surface enhanced Raman scattering by metal spheres. I. Cluster effect," *Journal of the Physical Society of Japan*, vol. 52, no. 11, pp. 3853–3864, 1983.

[40] D. A. Genov, A. K. Sarychev, V. M. Shalaev, and A. Wei, "Resonant field enhancements from metal nanoparticle arrays," *Nano Letters*, vol. 4, no. 1, pp. 153–158, 2004.

[41] P. H. C. Camargo, L. Au, M. Rycenga, W. Li, and Y. Xia, "Measuring the SERS enhancement factors of dimers with different structures constructed from silver nanocubes," *Chemical Physics Letters*, vol. 484, no. 4-6, pp. 304–308, 2010.

Hindawi Publishing Corporation
Journal of Nanotechnology
Volume 2012, Article ID 319038, 10 pages
doi:10.1155/2012/319038

Review Article

Applications of Self-Assembled Monolayers in Surface-Enhanced Raman Scattering

Charles K. Klutse, Adam Mayer, Julia Wittkamper, and Brian M. Cullum

Department of Chemistry and Biochemistry, University of Maryland, Baltimore County, 1000 Hilltop Circle, Baltimore, MD 21250, USA

Correspondence should be addressed to Brian M. Cullum, cullum@umbc.edu

Received 8 February 2012; Accepted 16 March 2012

Academic Editor: Mustafa Çulha

The increasing applications of surface-enhanced Raman scattering (SERS) has led to the development of various SERS-active platforms (SERS substrates) for SERS measurement. This work reviews the current optimization techniques available for improving the performance of some of these SERS substrates. The work particularly identifies self-assembled-monolayer- (SAM-) based substrate modification for optimum SERS activity and wider applications. An overview of SERS, SAM, and studies involving SAM-modified substrates is highlighted. The focus of the paper then shifts to the use of SAMs to improve analytical applications of SERS substrates by addressing issues including long-term stability, selectivity, reproducibility, and functionalization, and so forth. The paper elaborates on the use of SAMs to achieve optimum SERS enhancement. Specific examples are based on novel multilayered SERS substrates developed in the author's laboratory where SAMs have been demonstrated as excellent dielectric spacers for improving SERS enhancement more than 20-fold relative to conventional single layer SERS substrates. Such substrate optimization can significantly improve the sensitivity of the SERS method for analyte detection.

1. Introduction

There is a great interest in the development of SERS-based analytical techniques for real-time monitoring of intracellular events due to the advantages SERS has compared to other commonly used optical techniques in biological analyses. SERS provides narrow spectral bands, thereby allowing multiplex detection of analytes in complex sampling environments. It also has potential for quenching autofluorescence that can interfere with SERS measurements. SERS is the enhancement of Raman intensity of analytes which are in close proximity to nanoscaled roughened metallic surfaces (normally referred to as SERS substrates) [1, 2]. The ratio of such Raman scattering intensities of a given number of analyte molecules to the intensities of the same number of molecules in the absence of the SERS substrates is the SERS enhancement factor (EF) [3]. SERS EF is a widely accepted parameter for estimating the SERS activity of the SERS substrates, with larger SERS EFs indicating highly SERS-active substrates. While the commonly reported SERS EFs can range from 10^6 to 10^8, SERS EF can reach 10^{14} on certain special substrates, making SERS capable of single molecule detection [4–6].

In recent years, SERS has been demonstrated as a powerful tool for a wide range of analyses. Critical to the quality of the SERS analyses is the characteristic of the SERS substrates on which the SERS is conducted. As a result of this, the development and optimization of the SERS substrate for routine analytical purposes has become a very attractive area of research. In this paper, the recent development on SERS substrates involving the use of SAMs for various forms of modifications is discussed. The discussion begins with an overview of SERS and its analytical importance, followed by the identification of a broad category of SERS substrates that are commonly employed for SERS measurements. A brief description of SAM and how it features in SERS is given. The main subject for the paper then focuses on the use of thiolated organic molecules for the optimization of SERS. The discussion on SAM-based optimization of SERS will involve the modification of the

SERS-active surface with SAMs to improve selectivity, long-term stability, reproducibility, substrate functionalization, and so forth. The paper will also discuss the SAM-based multilayer SERS substrate optimization for the enhancement of SERS activity. The area of SERS substrate development is extensive and cannot be exhausted in this paper. Therefore, the paper will focus on some of the most commonly used SERS substrates which include metal colloids and metal-coated nanostructures.

2. Overview of SERS

Raman spectroscopy has various analytical applications, especially in research fields requiring high analyte specificity, because it is capable of providing molecular structural information about analytes of interest without the need for exogenous labels. Additionally, as a result of the weak Raman scattering of water, Raman spectroscopy can be applied to aqueous complex biological samples with little or no sample preparation, making it an ideal analytical tool for monitoring biomolecules within individual living cells. However, Raman lacks the sensitivity for the detection of analytes at ultratrace level due to extremely small Raman cross-section. In 1974, Fleischmann and coworkers observed very intense Raman scattering of pyridine adsorbed on electrochemically roughened silver electrodes, which was attributed to the large surface area of the roughened electrode [7, 8]. Later, Jeanmaire and Van Duyne and Albrecht and Creighton working independently observed that the enhanced Raman scattering on the roughened surface exceeds what is expected from the increase in surface area arising from the roughening of the electrode. Their work led to the proposal of SERS mechanisms (broadly categorized as electromagnetic (EM) and chemical mechanisms) to explain the enhancement of Raman scattering on roughened metal surfaces [9, 10]. Thus, the phenomenon of achieving enhanced Raman scattering on specialized surfaces became known as SERS. Importantly, it became clear that other metals including gold and copper can be used as SERS-active surfaces [11, 12]. By using SERS, it is now possible to achieve high sensitivity in addition to the various Raman advantages, making SERS a powerful tool for a broad range of analyses. In recent years, SERS has been applied in biomedical research, defense and security, diseases diagnosis and prevention, single-cell analysis, and for quantitative detection of analytes in various samples [13–26].

3. SERS Substrates

The quest for standardized SERS substrates capable of routine SERS-based chemical analysis and the need for deeper understanding of SERS have contributed largely to the advances in SERS substrate development. As a result, since the discovery of SERS, various techniques have been applied for the fabrication of these substrates [27–29]. Progress in SERS substrates development, which is not the focus of this work, has been reviewed elsewhere [27, 30, 31], and therefore only a brief overview will be discussed. Electrochemically roughened metal electrodes were the earliest types of SERS substrates. However, advances in nanofabrication have significantly influenced SERS substrates development. Colloidal metal nanoparticles are some of the commonly used SERS substrates. They are normally used as suspensions and their plasmonic properties can easily be modified using their sizes and shapes in order to improve their SERS activities [2, 23, 32–36]. Although colloidal metal nanoparticles are notable for high SERS activities at their junctions, they exhibit large variations in SERS signals due to the random occurrence of these junctions. To minimize such variations, the colloids can sometimes be self-assembled on planar platforms to create relatively regular junctions among the colloids [36–39]. Nanolithographic methods are also commonly used to fabricate highly ordered SERS substrates by forming nanostructures directly on a small area of a solid support. Such nanostructures can be achieved by selective etching of the specialized surface using an ultraviolet light or electron beam and then coating the etched surface with a SERS-active metal film [40–42]. Orderly structured SERS substrates can also be derived through a method commonly referred to as nanosphere lithography. In this method, metal films are deposited (using either physical or chemical means) on nanospheres arranged on a solid support. The removal of the nanospheres leaves a regular array of nanostructures, forming the SERS substrates [43–45]. While lithographically produced SERS substrates are highly reproducible, they are difficult and time consuming to produce in mass quantities.

A highly ordered SERS substrate which can easily be produced in mass quantities is based on nanostructures arranged on solid planar support followed by the deposition of a thin layer of metal film on the nanostructures. Unlike nanosphere lithography, it is the metal-coated nanostructures that are used as the SERS substrates, normally referred to as metal film on nanostructures (MFONs). A schematic representation of MFON substrates fabrication is shown in Figure 1. Other unique features of these types of SERS substrates include a combination of the advantages of 3D nanosized metal colloids for probing microsampling environments and the highly ordered and regularly arranged nanostructures on solid platforms for reproducible SERS measurements. Thus, as shown in Figure 1, the metal-coated nanostructured platform can be used as a planar SERS substrate for routine SERS analyses [30, 46, 47]. Importantly, the individual metal film-coated nanospheres can also be used as sensor supports for SERS-based bio-nanosensors, which will be discussed later [19, 26].

4. Self-Assembled Monolayers

Although SERS substrates with very large SERS EFs have demonstrated the high sensitivity of SERS-based analysis, the bare substrates lack the selectivity that will allow their use in complex samples. However, by using SAMs to modify substrates, it is possible to make the SERS substrates selective as well as tailor other desirable qualities that allow them to be used for various analytical purposes. SAMs are derived from the adsorption of organic molecules onto surfaces of metals, metal oxides, semiconductors, and other platforms, to form a thin layer. SAMs can affect the interface properties

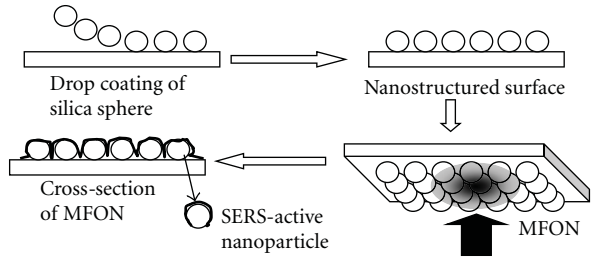

Figure 1: A flow diagram of MFON fabrication.

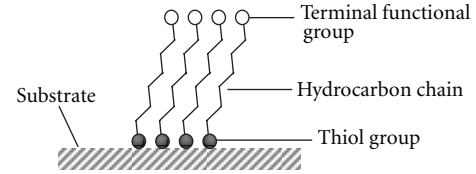

Figure 2: Schematic representation of the individual molecules adsorbed on metal substrate to form SAM.

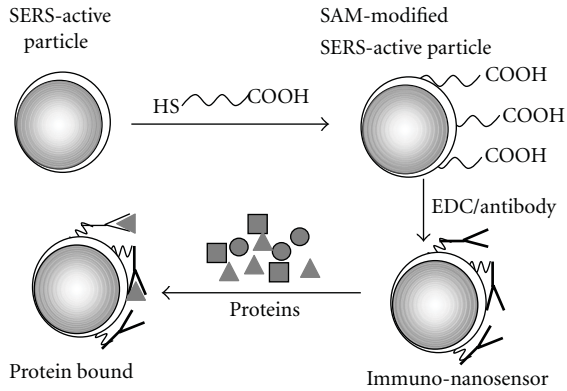

Figure 3: Schematic representation of the SERS-based immuno-nanosensor via –COOH– terminated SAM for label-free protein detection.

in many ways including insulation of conducting surfaces, creating hydrophobic surfaces, allowing them to be used for the modification and study of interfacial phenomena [48–51]. There are widespread examples of SAMs with equally widespread uses. However, this paper will focus on SAMs involving thiol-modified organic molecules (e.g., alkylthiols) that have been specifically employed in SERS to improve the SERS substrates characteristics. An idealized representation of molecules used for SAM formation is shown schematically in Figure 2. A typical example of a molecule used for SAM formation is made up of a thiol group, which attaches to the substrates, and the hydrocarbon tail which can be varied in order to vary the thickness of the SAM. An essential part of the molecule is the terminal functional group which can be varied in order to confer a specific surface chemistry to suit the intended application of the monolayer.

5. SAMs Applications in SERS

SAMs applications in SERS are diverse and include surface chemistry and substrates modifications. The unique attribute of SAMs to affect surfaces and the SERS ability to probe surface chemistry has been exploited as investigative tools in various ways. For example, SAM has been used to verify the EM mechanisms of SERS [52, 53]. Halas et al. used various lengths of labeled DNA self-assembled on SERS substrate as molecular rulers to investigate the EM field effect on SERS. By varying the lengths of SAMs and measuring Raman intensities of the Raman labels positioned at the tail ends of these rulers, it was observed that the shorter chains showed more intense Raman scattering. This was because the labels attached to the shorter chains were nearer to the metal surface and therefore exhibited better interaction with the EM field relative to the longer chain lengths [50, 53–55]. Conversely, SERS has been applied to study SAMs including verifying the mechanism of thiol-metal surface interaction [54, 56–59]. By doing Raman and SERS measurements of several alkylthiols, it was found that the S–H vibration at 2575 cm^{-1} was absent when the molecules adsorbed on the metal surface. However, the Raman band at 200 cm^{-1} associated with Ag–S vibrations appeared, confirming the formation of SAM via the cleavage of the S–H bond. Another confirmation of the formation of SAM on SERS substrates is the high intensity of the C–S band at 650 cm^{-1} due to its proximity to the SERS-active surface [54, 60].

The most widespread application of SAMs in SERS is their use for SERS substrates modification as shown in Figure 3. Metal colloids are often protected with SAMs in order to preserve the integrity of the particles and prevent them from aggregating. SAMs have been shown to influence the absorption characteristics of metal colloids. Thus, SAMs can be used to controllably tailor the wavelength of surface plasmon absorption of substrates to match the excitation wavelength, thereby improving the SERS activity of the metal colloids [50, 61]. Functionalization of SERS substrates has been seen as a means of improving analyte specificity and reducing random adsorption of untargeted molecules. SAMs have been employed as cross-linkers primarily to aid functionalization of SERS substrates [55, 62–65]. Used in this way, SAMs with specially functionalized tail groups can be immobilized on the bare SERS substrate before attaching recognition elements for specific analytes [19, 66]. Culha et al. have used SAM-modified SERS platforms as models for gene diagnostics. In these models, the tail functional group of 1-mercaptohexane was modified with Rhodamine B-labeled single-stranded DNA complementary to breast cancer gene (BRCA1). To prevent the long HS–$(CH_2)_6$–ssDNA-RhB strands from folding, they were interspaced with 6-mercaptohexanol. The SAM-modified SERS platform was capable of specifically detecting the breast cancer gene by complementary paring [62]. SERS substrates have also been functionalized via SAMs for label-free detection of proteins in modeled environments at physiological concentrations. As shown in Figure 3, the SERS-active nanoparticles which were derived from MFON SERS substrates were first immobilized with carboxylic acid-terminated SAMs. Molecules of anti-human insulin (IgG) were then bound to the SAM via the commonly used EDC chemistry to develop SERS-based

immuno-nanosensors. The immuno-nanosensors were then used to detect insulin in cell lysates at a concentration of 10 μg/mL [25, 67, 68].

Applications SAMs in the optimization of SERS substrate have been done specifically to improve various substrates characteristics, including long-term stability, analyte selectivity, and precision across the sampling volume. Due to their unique abilities of influencing interfacial properties of substrates, SAMs can be used to modify the affinity of SERS substrates towards specific analytes, thereby improving their selectivity. For instance, SAM-modified SERS substrates have been used to partition analyte from known matrices and concentrate them on the SERS substrate for detection [69–71]. Such substrates have been used as SERS platforms for the detection of polycyclic aromatic hydrocarbons (PAHs). PAHs adsorbed on the bare gold SERS-active surface are known to undergo surface-induced decomposition due to the catalytic properties of the roughened gold surface. By modifying the surface with 1-propanethiol, it was possible to selectively concentrate PAHs on the substrate, reduce decomposition, and improve reproducibility and stability [72]. Apart from improving selectivity, SAMs have been used to increase the long-term stability of the substrates by means of partial coverage of the SERS-active surface with the SAM [73].

One major drawback of SERS is its lack of reproducibility due to the random distribution of the SERS hot spots across the substrate surface. SAMs have been used as forms of internal standards to account for the variations in the SERS signals [74–81]. In one such study, SERS intensities of analytes were taken on SERS substrates modified with labeled SAMs. It was assumed that both the labeled SAM and the analyte experienced the same excitation and substrate conditions during a particular SERS measurement. For this reason, although the SERS intensities of the analytes varied from spot to spot on the SERS substrates, ratios of the labeled SAM intensity to the analyte intensity did not vary significantly. Thus, the SAM is used in this case as an internal standard to normalize the SERS intensity of the analytes. Despite these optimization processes, there are issues concerning the reduction of the SERS effect on the analyte due to the coverage of the SERS active platforms with SAM, effectively reducing the sensitivity of SAM-modified SERS substrates [52].

6. SAM Multilayer SERS Substrate Optimization

With the increasing potential application of SERS, the search for optimized SERS substrates that lack the limitations of most conventional SERS substrates has become a priority. In 2005, Cullum's group discovered that MFON SERS substrates can be optimized to achieve larger SERS EFs by using SERS substrates based on multiple layers of SERS-active surfaces separated by dielectric spacers (i.e., metal oxide) [82]. As shown in Figure 4, the first reported multilayer SERS substrate consisted of multiple layers of silver film separated by silver oxide. Using the multilayer geometry, SERS substrates can be optimized without making the SERS-active surface less accessible to analytes. Although it has generally been observed that SERS enhancement is significantly affected by the dielectric constant around the SERS substrate, how this observation relates to the multilayer SERS enhancement is still under investigation. However, it is thought that the optimum interaction of the EM fields generated on the multiple SERS-active surfaces largely contributed to the observed multilayer SERS enhancement. Additionally, the results of the multilayer SERS studies suggested that efficient separation of the SERS-active surfaces, the type of dielectric spacer used, and the thickness of this spacer can significantly affect the multilayer SERS enhancement [83, 84]. For this reason, our laboratory has been investigating other forms of dielectric spacers (e.g., polymers, silica, and SAMs) and SERS-active metal films for the systematic multilayer SERS optimization [84, 85].

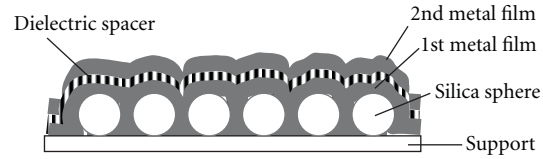

Figure 4: An idealized multilayer SERS substrate.

Systematic optimization of multilayer SERS requires control of the dielectric spacer and a thorough understanding of its effect on the SERS enhancement. Since 2007, data gathered on the optimization of multilayer SERS using SAMs as the main dielectric spacers have generated interesting yet nonsystematic results. To provide a more systematic evaluation, SAMs have recently been employed to vary spacer thickness and dielectric constant in a more controlled fashion, based on the choice of the hydrocarbon chain length and tail functional group, respectively. To form SAM multilayer SERS substrates, a single-layer MFON, referred to as single film on nanostructure (SFON), was immersed in 1 mM solutions containing the appropriate alkylthiol for SAM formation. The substrate was retrieved and rinsed to remove unattached molecules of the spacers. After the removal of the unattached molecules, a second layer of metal film was deposited to form dual-layer SERS substrate as shown in Figure 4, with the SAM as the dielectric spacer. The procedure can be repeated to form multiple layers of SERS-active surfaces. In first reported results of SAM multilayer SERS enhancement, SAMs were formed on gold-coated SFON substrates. Another layer of gold was then deposited on these SAMs. A solution of Rhodamine 6G was drop-coated and measured on this substrate. For comparison, SERS measurement of the same concentration of the model analyte was done on a SFON SERS substrate with the amount of SERS-active metal film equal to the total amount of metal film deposited on the multilayer substrates. As shown in Figure 5, a 4-layered SERS substrate having 11-mercaptoundecanoic acid as the dielectric spacer exhibited SERS EF of $(1.15 \pm 0.06) \times 10^6$ which is more than a 15-fold increase over the SERS EF ($(7.4 \pm 0.6) \times 10^4$) of optimized SFON substrates. Various studies conducted confirmed that SAM multilayer SERS can be used to optimize SERS activities [86]. In a similar study, SAM multilayer SERS enhancement was also applied to SERS nanoprobes, showing that SAM

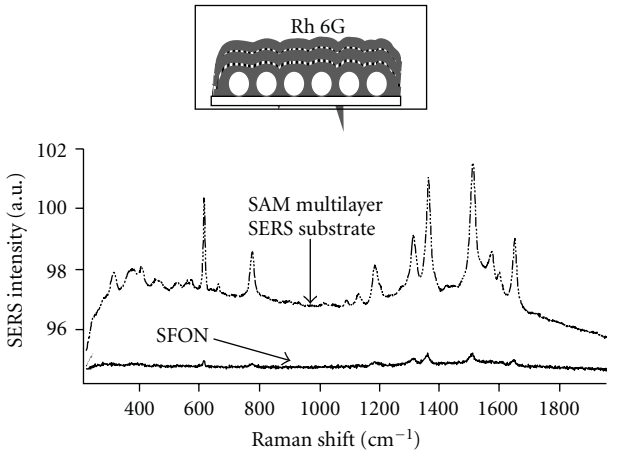

Figure 5: SERS spectra of 1 μM Rhodamine 6G measured on SFON and SAM multilayer SERS substrates. Insert is the schematic of SAM multilayer SERS substrates.

multilayer SERS can be applied to different types of SERS substrates [86, 87].

Following that observation, a comprehensive investigation on the SAM multilayer SERS substrates enhancement was performed. The results of these studies confirmed current mechanistic understandings of the multilayer SERS enhancement phenomenon. For instance, they clearly revealed the need for the formation of a compact and uniform dielectric spacer for achieving multilayer SERS enhancement. This is because multilayer SERS substrates made from orderly packed SAMs showed larger SERS enhancement relative to those made from SAM with considerable defect sites. That is, when the adjacent SERS-active surfaces are well separated with minimum points of direct contact, it leads to the optimum interaction of the EM fields generated on the SERS-active surfaces and enhances the SERS activity beyond what is expected of conventional SERS substrates. SAM multilayer SERS substrates clearly indicated that SAM can be used to improve the SERS EFs of SERS substrates, thus offering even higher sensitivity for SERS-based analyses. Importantly, the achievable SAM multilayer SERS enhancement can be systematically controlled based on several factors that include the structure of the SAMs and the condition under which the SAMs were formed. Figure 6 shows that the SAM multilayer SERS enhancement can be varied by varying the hydrocarbon chain length of the alkylthiol used to form the SAM dielectric spacer. In this case three types of carboxylic-acid-terminated alkylthiols having 2, 11, or 16 carbon atoms in their hydrocarbon chain lengths were used as dielectric spacers. When benzoic acid was analyzed on these SAM multilayer SERS substrates, there was chain length-dependent SERS enhancement. The chain length-dependent SERS enhancement was attributed to the more uniform SAM formed by the longer hydrocarbon chains [85, 86, 88].

Apart from the hydrocarbon chain length, it was shown that terminal functional group can be used to vary the dielectric constant of the dielectric spacer and hence control the SERS enhancement. The conditions under which the SAM dielectric spacers are deposited on substrate were also used to control the SERS enhancement. For example, the solvent used for SAM preparation can significantly affect the orderly packing of the SAM. Polar solvents which exhibit less attractive interactions toward the nonpolar hydrocarbon chain can lead to an orderly packed SAM and therefore larger SERS enhancement. The result shown in Figure 7 is spectra of 1, 2-Bis(2-pyridyl)ethylene (BPE) measured on SAM multilayer SERS substrates which were fabricated using the same amount of SERS-active metal film and type of SAM dielectric spacer. However, the pH under which the monolayers were formed was varied. The variation of the pH had a tremendous effect on the SAM multilayer SERS enhancement. Apparently, the carboxylic acid-terminated SAM dielectric spacer used in this case formed more carboxylate ions under basic conditions. As result, there were relative repulsive interactions among the carboxylate ions, leading to defects in the dielectric spacer which affected the SERS enhancement. This became obvious when alkyl-terminated SAM used in similar study showed no preference to the pH condition in terms of the SERS enhancement [85, 88, 89].

SAM multilayer SERS offers other unique characteristics which can be exploited to improve analytical capabilities of SERS. As indicated by the arrows in the spectra in Figure 6, the SERS fingerprint of the underlying SAM appears together with the SERS bands of the analyte (benzoic acid). This suggests that the SAM can be used as an internal standard to normalize the SERS intensity of the analytes, thereby improving SERS signal reproducibility. SAM multilayer SERS offers another unique advantage of substrate modification relative to other SAM-modified SERS substrates. That is, SAM multilayer fabrication involves the capping of the SAM with SERS-active metal films. Thus, the entire SERS-active surface is still accessible to the analyte, making SAM multilayer SERS substrate more sensitive relative to other SAM-modified substrates. In effect, it has been shown that multilayer SERS substrate can be greatly optimized in a predictive manner by appropriate choice of the SAM chain length, the tail terminal group, and the solvent used for SAM formation [85, 86].

Long-term stability (especially for silver-coated substrates) and reproducibility have been the traditional issues with SERS. The effect of the introduction of the dielectric spacer between adjacent metal films on the substrate stability was therefore considered in the multilayer substrates. Studies conducted with both gold- and silver-coated multilayer SERS substrates showed that the stability and reversibility of the SERS substrates were largely dependent on the metal film overlayer. Both SFON and multilayer substrates lost their SERS activities over the same period of time in a similar manner. It was also possible to reuse the both sets of substrates the same number of times before losing significant level of SERS signals. Thus, the introduction of the SAM dielectric spacer does not significantly affect the long-term stability of the multilayer SERS substrates [82, 86, 90]. It is widely accepted that surface morphology of the substrate plays a significant role in the SERS activity of the SERS substrates as well as the

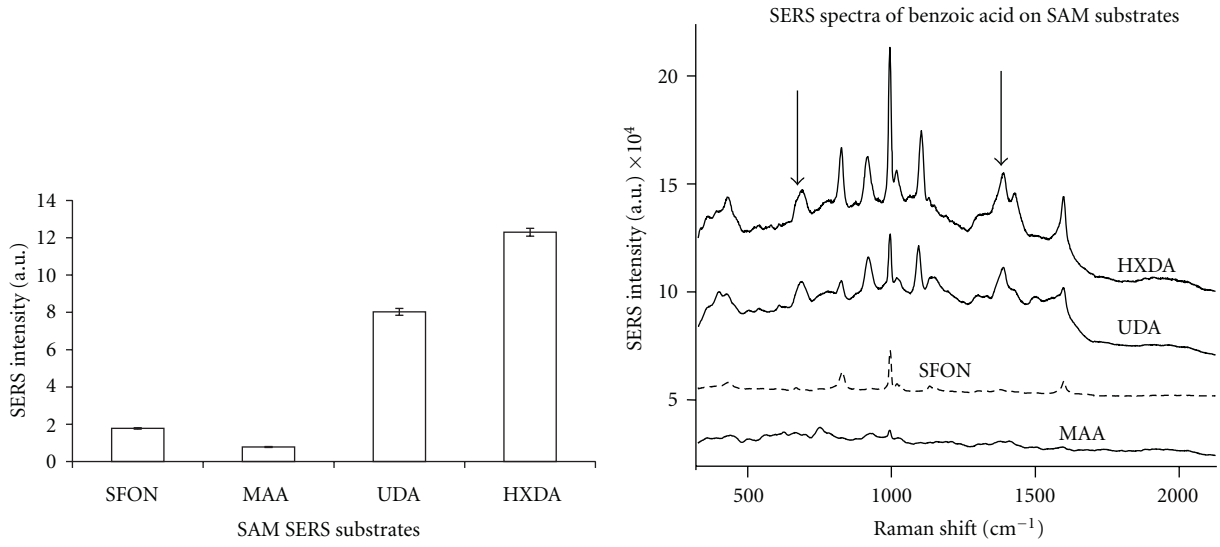

Figure 6: (a) The relative SERS intensities 1 mM benzoic acid obtained on dual-layer coated substrates separated by different types of self-assembled monolayers (MAA, UDA, and HXDA represent 2, 11, and 16 carbon chains, resp.) and optimized SFON substrates. (b) The spectra showing the 1000 cm^{-1} band of 1 mM benzoic acid used for the measurement.

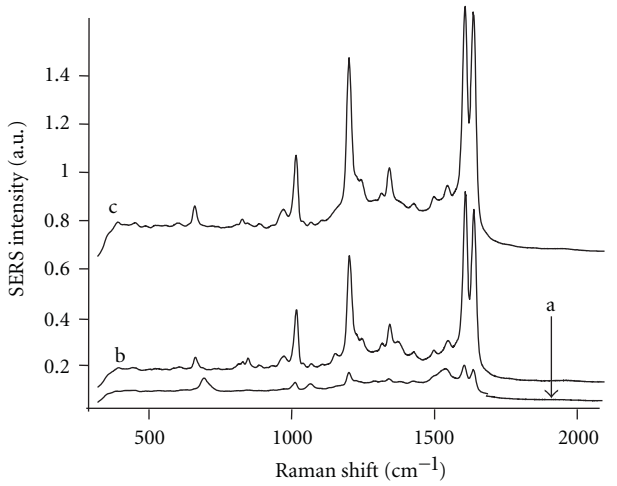

Figure 7: A comparison of the SERS intensities of 0.126 mM BPE on –COOH– terminated SAM multilayer SERS substrates fabricated in pH (a) 12, (b) 7.8, and (c) 2.

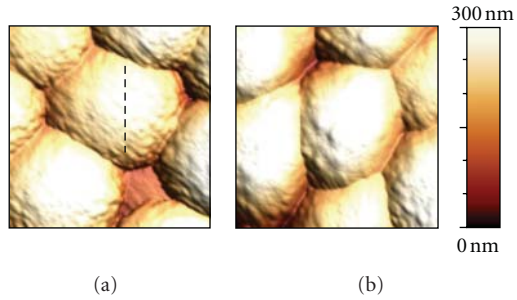

Figure 8: AFM images of (a) SFON and (b) octadecanethiol multilayer SERS substrates showing substructural features. The individual nanostructures were 390 nm in diameter and the scan size was 800 nm by 800 nm.

reproducibility of their SERS measurements. For the MFON SERS substrates, the surface morphology depends on the nanostructures beneath the metal film and the substructures on these metal-coated nanostructures [91]. Studies have shown that roughness due to the nanostructures was not significantly affected by the introduction of the dielectric spacers [86, 90]. For this reason, attention was given to the effect of the dielectric spacer on the substructural features on the individual nanostructures. AFM images of typical SFON and SAM multilayer substrates in Figure 8 show the substructures on the individual nanostructures. The roughness values were estimated by drawing several horizontal and vertical lines across these individual nanostructures. The average roughness values for the SFON substrates and SAM multilayer SERS substrate were 3.1 ± 0.6 and 2.8 ± 0.7, respectively, showing that there was no significant effect on the sub-structural features relative to the SFON substrates irrespective of the introduction of the SAM. Remarkably, the relative standard deviation of multilayer SERS measurement was less than half that of the SFON substrates, indicating an improvement in reproducibility. Although the reason for the improved reproducibility is still being investigated, multilayer SERS has clearly illustrated a number of improvements that can be made on any SERS substrates. Thus, SERS activity (i.e., enhancement factors) of SERS substrates can be increased by as much as 20-fold and their reproducibility improved by using multiple layers of SERS-active metal films interspaced with appropriate dielectric spacers [89]. Using an appropriate SAM, the SERS fingerprints of the dielectric

spacer can serve as internal standards to minimize spot-to-spot variation of SERS signals on a substrate. Importantly, multilayer SERS has demonstrated that SERS substrate can be optimized in various ways without compromising the existing substrate qualities.

7. Conclusion

This paper provides an overview of the various ways by which conventional SERS substrates can be optimized in order to achieve enhanced analytical performance. SAMs play an important role in SERS substrates optimization and adaptation for various analytical purposes. Using SAM multilayer SERS substrates, SERS can be optimized to provide SERS enhancement about 20-fold larger than that derived from conventional SERS substrates, thereby improving the sensitivity of the SERS method of analysis. Apart from improving SERS activity, SAMs can also be used to improve long-term stability, reproducibility, and selectivity of the SERS substrates. They provide excellent routes for functionalization of SERS substrates and introduction of internal standard for selective, specific, and reproducible analyte detection in complex samples. The increasing research attention that SERS is attracting is leading to the development of various types of SERS-active platforms for SERS measurement. However, the determining factor in the eventual application of these platforms will be determined on the basis of how their SERS activities can be optimized without losing other desirable SERS substrates properties as well as how the substrates can be tailored for specific applications.

Acknowledgments

This work was supported by University of Maryland, Baltimore County and US Army Research Office.

References

[1] M. Moskovits, "Surface-enhanced spectroscopy," *Reviews of Modern Physics*, vol. 57, no. 3, pp. 783–826, 1985.

[2] K. Kneipp, H. Kneipp, I. Itzkan, R. R. Dasari, and M. S. Feld, "Ultrasensitive chemical analysis by Raman spectroscopy," *Chemical Reviews*, vol. 99, no. 10, pp. 2957–2975, 1999.

[3] E. C. Le Ru, E. Blackie, M. Meyer, and P. G. Etchegoint, "Surface enhanced raman scattering enhancement factors: a comprehensive study," *Journal of Physical Chemistry C*, vol. 111, no. 37, pp. 13794–13803, 2007.

[4] K. Kneipp, Y. Wang, H. Kneipp et al., "Single molecule detection using surface-enhanced Raman scattering (SERS)," *Physical Review Letters*, vol. 78, no. 9, pp. 1667–1670, 1997.

[5] S. M. Nie, "Probing single molecules and single nanoparticles by surface- enhanced Raman scattering," *Abstracts of Papers American Chemical Society*, vol. 221, p. 110-PHYS, 2001.

[6] S. Nie and S. R. Emory, "Probing single molecules and single nanoparticles by surface-enhanced Raman scattering," *Science*, vol. 275, no. 5303, pp. 1102–1106, 1997.

[7] M. Fleischmann, P. J. Hendra, and A. J. McQuillan, "Raman spectra of pyridine adsorbed at a silver electrode," *Chemical Physics Letters*, vol. 26, no. 2, pp. 163–166, 1974.

[8] A. J. McQuillan, "The discovery of surface-enhanced Raman scattering," *Notes and Records of the Royal Society*, vol. 63, no. 1, pp. 105–109, 2009.

[9] D. L. Jeanmaire and R. P. Van Duyne, "Surface Raman spectroelectrochemistry Part I. Heterocyclic, aromatic, and aliphatic amines adsorbed on the anodized silver electrode," *Journal of Electroanalytical Chemistry*, vol. 84, no. 1, pp. 1–20, 1977.

[10] M. G. Albrecht and J. A. Creighton, "Anomalously intense Raman spectra of pyridine at a silver electrode," *Journal of the American Chemical Society*, vol. 99, no. 15, pp. 5215–5217, 1977.

[11] R. L. Garrell, "Surface-enhanced Raman spectroscopy," *Analytical Chemistry*, vol. 61, no. 6, pp. 401A–411A, 1989.

[12] E. J. Zeman and G. C. Schatz, "An accurate electromagnetic theory study of surface enhancement factors for silver, gold, copper, lithium, sodium, aluminum, gallium, indium, zinc, and cadmium," *The Journal of Physical Chemistry*, vol. 91, no. 3, pp. 634–643, 1987.

[13] A. M. Alak and T. Vo-Dinh, "Surface-enhanced Raman spectrometry of organophosphorus chemical agents," *Analytical Chemistry*, vol. 59, no. 17, pp. 2149–2153, 1987.

[14] P. D. Enlow, M. Buncick, R. J. Warmack, and T. Vo-Dinh, "Detection of nitro polynuclear aromatic compounds by surface-enhanced Raman spectrometry," *Analytical Chemistry*, vol. 58, no. 6, pp. 1119–1123, 1986.

[15] V. A. Narayanan, J. M. Bello, D. L. Stokes, and T. Vo-Dinh, "Surface-enhanced raman analysis of vitamin B complex: quantitative detection of p-aminobenzoic acid," *Journal of Raman Spectroscopy*, vol. 22, pp. 327–331, 1991.

[16] N. Taranenko, J. P. Alarie, D. L. Stokes, and T. Vo-Dinh, "Surface-enhanced Raman detection of nerve agent simulant (DMMP and DIMP) vapor on electrochemically prepared silver oxide substrates," *Journal of Raman Spectroscopy*, vol. 27, no. 5, pp. 379–384, 1996.

[17] T. Vo-Dinh, L. R. Allain, and D. L. Stokes, "Cancer gene detection using surface-enhanced Raman scattering (SERS)," *Journal of Raman Spectroscopy*, vol. 33, no. 7, pp. 511–516, 2002.

[18] N. R. Isola, D. L. Stokes, and T. Vo-Dinh, "Surface-rnhanced Raman gene probe for HIV detection," *Analytical Chemistry*, vol. 70, no. 7, pp. 1352–1356, 1998.

[19] D. A. Stuart, J. M. Yuen, N. Shah et al., "In vivo glucose measurement by surface-enhanced Raman spectroscopy," *Analytical Chemistry*, vol. 78, no. 20, pp. 7211–7215, 2006.

[20] X. Zhang, M. A. Young, O. Lyandres, and R. P. Van Duyne, "Rapid detection of an anthrax biomarker by surface-enhanced Raman spectroscopy," *Journal of the American Chemical Society*, vol. 127, no. 12, pp. 4484–4489, 2005.

[21] D. A. Stuart, C. R. Yonzon, X. Zhang et al., "Glucose sensing using near-infrared surface-enhanced raman spectroscopy: gold surfaces, 10-day stability, and improved accuracy," *Analytical Chemistry*, vol. 77, no. 13, pp. 4013–4019, 2005.

[22] D. A. Stuart, K. B. Biggs, and R. P. Van Duyne, "Surface-enhanced Raman spectroscopy of half-mustard agent," *Analyst*, vol. 131, no. 4, pp. 568–572, 2006.

[23] J. Kneipp, H. Kneipp, M. McLaughlin, D. Brown, and K. Kneipp, "In vivo molecular probing of cellular compartments with gold nanoparticles and nanoaggregates," *Nano Letters*, vol. 6, no. 10, pp. 2225–2231, 2006.

[24] H. Li, J. Sun, T. Alexander, and B. M. Cullum, "Implantable SERS nanosensors for pre-symptomatic detection of BW

agents," in *Chemical and Biological Sensing VI*, vol. 5795 of *Proceedings of the SPIE*, pp. 8–18, March 2005.

[25] H. Li, C. E. Baum, and B. M. Cullum, "Label-free detection of antigens using implantable sers nanosensors," in *Smart Medical and Biomedical Sensor Technology III*, vol. 6007 of *Proceedings of the SPIE*, pp. 58–70, October 2005.

[26] C. E. Talley, L. Jusinski, C. W. Hollars, S. M. Lane, and T. Huser, "Intracellular pH sensors based on surface-enhanced raman scattering," *Analytical Chemistry*, vol. 76, no. 23, pp. 7064–7068, 2005.

[27] M. Fan, G. F. S. Andrade, and A. G. Brolo, "A review on the fabrication of substrates for surface enhanced Raman spectroscopy and their applications in analytical chemistry," *Analytica Chimica Acta*, vol. 693, no. 1-2, pp. 7–25, 2011.

[28] X. M. Lin, Y. Cui, Y. H. Xu, B. Ren, and Z. Q. Tian, "Surface-enhanced raman spectroscopy: substrate-related issues," *Analytical and Bioanalytical Chemistry*, vol. 394, no. 7, pp. 1729–1745, 2009.

[29] K. Hering, D. Cialla, K. Ackermann et al., "SERS: a versatile tool in chemical and biochemical diagnostics," *Analytical and Bioanalytical Chemistry*, vol. 390, no. 1, pp. 113–124, 2008.

[30] T. Vo-Dinh, "Surface-enhanced Raman spectroscopy using metallic nanostructures," *Trends in Analytical Chemistry*, vol. 17, no. 8-9, pp. 557–582, 1998.

[31] G. A. Baker and D. S. Moore, "Progress in plasmonic engineering of surface-enhanced Raman-scattering substrates toward ultra-trace analysis," *Analytical and Bioanalytical Chemistry*, vol. 382, no. 8, pp. 1751–1770, 2005.

[32] K. L. Kelly, E. Coronado, L. L. Zhao, and G. C. Schatz, "The optical properties of metal nanoparticles: the influence of size, shape, and dielectric environment," *Journal of Physical Chemistry B*, vol. 107, no. 3, pp. 668–677, 2003.

[33] S. R. Emory and S. Nie, "Near-field surface-enhanced Raman spectroscopy on single silver nanoparticles," *Analytical Chemistry*, vol. 69, no. 14, pp. 2631–2635, 1997.

[34] A. R. Bizzarri and S. Cannistraro, "SERS detection of thrombin by protein recognition using functionalized gold nanoparticles," *Nanomedicine*, vol. 3, no. 4, pp. 306–310, 2007.

[35] W. E. Doering and S. Nie, "Spectroscopic tags using dye-embedded nanoparticles and surface-enhanced Raman scattering," *Analytical Chemistry*, vol. 75, no. 22, pp. 6171–6176, 2003.

[36] M. Baia, F. Toderas, L. Baia, D. Maniu, and S. Astilean, "Multilayer structures of self-assembled gold nanoparticles as a unique SERS and SEIRA substrate," *ChemPhysChem*, vol. 10, no. 7, pp. 1106–1111, 2009.

[37] J. L. Seung, M. B. Jeong, and M. Moskovits, "Polarization-dependent surface-enhanced raman scattering from a silver-nanoparticle-decorated single silver nanowire," *Nano Letters*, vol. 8, no. 10, pp. 3244–3247, 2008.

[38] H. Wang, J. Kundu, and N. J. Halas, "Plasmonic nanoshell arrays combine surface-enhanced vibrational spectroscopies on a single substrate," *Angewandte Chemie*, vol. 46, no. 47, pp. 9040–9044, 2007.

[39] M. Kahraman, M. M. Yazici, F. Şahin, and M. Çulha, "Convective assembly of bacteria for surface-enhanced Raman scattering," *Langmuir*, vol. 24, no. 3, pp. 894–901, 2008.

[40] M. A. De Jesús, K. S. Giesfeldt, J. M. Oran, N. A. Abu-Hatab, N. V. Lavrik, and M. J. Sepaniak, "Nanofabrication of densely packed metal-polymer arrays for surface-enhanced raman spectrometry," *Applied Spectroscopy*, vol. 59, no. 12, pp. 1501–1508, 2005.

[41] N. A. Abu Hatab, J. M. Oran, and M. J. Sepaniak, "Surface-enhanced Raman spectroscopy substrates created via electron beam lithography and nanotransfer printing," *ACS Nano*, vol. 2, no. 2, pp. 377–385, 2008.

[42] H. Im, K. C. Bantz, N. C. Lindquist, C. L. Haynes, and S. H. Oh, "Vertically oriented sub-10-nm plasmonic nanogap arrays," *Nano Letters*, vol. 10, no. 6, pp. 2231–2236, 2010.

[43] C. L. Haynes and R. P. Van Duyne, "Nanosphere lithography: a versatile nanofabrication tool for studies of size-dependent nanoparticle optics," *Journal of Physical Chemistry B*, vol. 105, no. 24, pp. 5599–5611, 2001.

[44] M. D. Malinsky, K. Lance Kelly, G. C. Schatz, and R. P. van Duyne, "Nanosphere lithography: effect of substrate on the localized surface plasmon resonance spectrum of silver nanoparticles," *Journal of Physical Chemistry B*, vol. 105, no. 12, pp. 2343–2350, 2001.

[45] J. C. Hulteen, D. A. Treichel, M. T. Smith, M. L. Duval, T. R. Jensen, and R. P. Van Duyne, "Nanosphere lithography: size-tunable silver nanoparticle and surface cluster arrays," *Journal of Physical Chemistry B*, vol. 103, no. 19, pp. 3854–3863, 1999.

[46] J. M. Bello, D. L. Stokes, and T. Vo-Dinh, "Silver-coated alumina as a new medium for surfaced-enhanced Raman scattering analysis," *Applied Spectroscopy*, vol. 43, no. 8, pp. 1325–1330, 1989.

[47] M. Litorja, C. L. Haynes, A. J. Haes, T. R. Jensen, and R. P. Van Duyne, "Surface-enhanced Raman scattering detected temperature programmed desorption: optical properties, nanostructure, and stability of silver film over SiO_2 nanosphere surfaces," *Journal of Physical Chemistry B*, vol. 105, no. 29, pp. 6907–6915, 2001.

[48] J. C. Love, L. A. Estroff, J. K. Kriebel, R. G. Nuzzo, and G. M. Whitesides, "Self-assembled monolayers of thiolates on metals as a form of nanotechnology," *Chemical Reviews*, vol. 105, no. 4, pp. 1103–1169, 2005.

[49] N. Muskal, I. Turyan, and D. Mandler, "Self-assembled monolayers on mercury surfaces," *Journal of Electroanalytical Chemistry*, vol. 409, no. 1-2, pp. 131–136, 1996.

[50] M. D. Malinsky, K. L. Kelly, G. C. Schatz, and R. P. Van Duyne, "Chain length dependence and sensing capabilities of the localized surface plasmon resonance of silver nanoparticles chemically modified with alkanethiol self-assembled monolayers," *Journal of the American Chemical Society*, vol. 123, no. 7, pp. 1471–1482, 2001.

[51] C. E. D. Chidsey and D. N. Loiacono, "Chemical functionality in self-assembled monolayers: structural and electrochemical properties," *Langmuir*, vol. 6, no. 3, pp. 682–691, 1990.

[52] B. J. Kennedy, S. Spaeth, M. Dickey, and K. T. Carron, "Determination of the distance dependence and experimental effects for modified sers substrates based on self-assembled monolayers formed using alkanethiols," *Journal of Physical Chemistry B*, vol. 103, no. 18, pp. 3640–3646, 1999.

[53] S. Lal, N. K. Grady, G. P. Goodrich, and N. J. Halas, "Profiling the near field of a plasmonic nanoparticle with Raman-based molecular rulers," *Nano Letters*, vol. 6, no. 10, pp. 2338–2343, 2006.

[54] C. S. Levin, B. G. Janesko, R. Bardhan, G. E. Scuseria, J. D. Hartgerink, and N. J. Halas, "Chain-length-dependent vibrational resonances in alkanethiol self-assembled monolayers observed on plasmonic nanoparticle substrates," *Nano Letters*, vol. 6, no. 11, pp. 2617–2621, 2006.

[55] M. Tsen and L. Sun, "Surface-enhanced Raman scattering from functionalized self-assembled monolayers. Part 1. Distance dependence of enhanced Raman scattering from a terminal phenyl group," *Analytica Chimica Acta*, vol. 307, no. 2-3, pp. 333–340, 1995.

[56] M. Rycenga, Z. Wang, E. Gordon et al., "Probing the photothermal effect of gold-based nanocages with surface-enhanced Raman scattering (SERS)," *Angewandte Chemie*, vol. 48, no. 52, pp. 9769–9927, 2009.

[57] M. Moskovits and J. S. Suh, "Conformation of mono- and dicarboxylic acids adsorbed on silver surfaces," *Journal of the American Chemical Society*, vol. 107, no. 24, pp. 6826–6829, 1985.

[58] K. E. Brown and D. D. Dlott, "High-pressure raman spectroscopy of molecular monolayers adsorbed on a metal surface," *Journal of Physical Chemistry C*, vol. 113, no. 14, pp. 5751–5757, 2009.

[59] C. W. Meuse, G. Niaura, M. L. Lewis, and A. L. Plant, "Assessing the molecular structure of alkanethiol monolayers in hybrid bilayer membranes with vibrational spectroscopies," *Langmuir*, vol. 14, no. 7, pp. 1604–1611, 1998.

[60] M. A. Bryant and J. E. Pemberton, "Surface Raman scattering of self-assembled monolayers formed from 1-alkanethiols: behavior of films at Au and comparison to films at Ag," *Journal of the American Chemical Society*, vol. 113, no. 22, pp. 8284–8293, 1991.

[61] L. Guerrini, I. Izquierdo-Lorenzo, R. Rodriguez-Oliveros et al., "α,ω-aliphatic diamines as molecular linkers for engineering Ag nanoparticle clusters: tuning of the interparticle distance and sensing application," *Plasmonics*, vol. 5, no. 3, pp. 273–286, 2010.

[62] M. Culha, D. Stokes, L. R. Allain, and T. Vo-Dinh, "Surface-enhanced Raman scattering substrate based on a self-assembled monolayer for use in gene diagnostics," *Analytical Chemistry*, vol. 75, no. 22, pp. 6196–6201, 2003.

[63] M. D. Porter, R. J. Lipert, L. M. Siperko, G. Wang, and R. Narayanan, "SERS as a bioassay platform: fundamentals, design, and applications," *Chemical Society Reviews*, vol. 37, no. 5, pp. 1001–1011, 2008.

[64] K. J. Yoon, H. K. Seo, H. Hwang et al., "Bioanalytical application of SERS immunoassay for detection of prostate-specific antigen," *Bulletin of the Korean Chemical Society*, vol. 31, no. 5, pp. 1215–1218, 2010.

[65] J. D. Driskell, R. J. Lipert, and M. D. Porter, "Labeled gold nanoparticles immobilized at smooth metallic substrates: systematic investigation of surface plasmon resonance and surface-enhanced raman scattering," *Journal of Physical Chemistry B*, vol. 110, no. 35, pp. 17444–17451, 2006.

[66] D. S. Grubisha, R. J. Lipert, H. Y. Park, J. Driskell, and M. D. Porter, "Femtomolar detection of prostate-specific antigen: an immunoassay based on surface-enhanced Raman scattering and immunogold labels," *Analytical Chemistry*, vol. 75, no. 21, pp. 5936–5943, 2003.

[67] H. Li, J. Sun, and B. M. Cullum, "Label-free detection of proteins using SERS-based immuno-nanosensors," *Nanobiotechnology*, vol. 2, no. 1-2, pp. 17–28, 2006.

[68] H. Li, J. Sun, and B. M. Cullum, "Nanosphere-based SERS immuno-sensors for protein analysis," in *Smart Medical and Biomedical Sensor Technology II*, vol. 5588 of *Proceedings of the SPIE*, pp. 19–30, October 2004.

[69] C. R. Yonzon, C. L. Haynes, X. Zhang, J. T. Walsh, and R. P. Van Duyne, "A glucose biosensor based on surface-enhanced raman scattering: improved partition layer, temporal stability, reversibility, and resistance to serum protein interference," *Analytical Chemistry*, vol. 76, no. 1, pp. 78–85, 2004.

[70] G. L. De Vault and M. J. Sepaniak, "Spatially focused deposition of capillary electrophoresis effluent onto surface-enhanced Raman-active substrates for off-column spectroscopy," *Electrophoresis*, vol. 22, no. 11, pp. 2303–2311, 2001.

[71] O. Neumann, D. Zhang, F. Tam, S. Lal, P. Wittung-Stafshede, and N. J. Halas, "Direct optical detection of aptamer conformational changes induced by target molecules," *Analytical Chemistry*, vol. 81, no. 24, pp. 10002–10006, 2009.

[72] J. C. S. Costa, A. C. Sant'Ana, P. Corio, and M. L. A. Temperini, "Chemical analysis of polycyclic aromatic hydrocarbons by surface-enhanced Raman spectroscopy," *Talanta*, vol. 70, no. 5, pp. 1011–1016, 2006.

[73] T. O. Deschaines and K. T. Carron, "Stability and surface uniformity of selected thiol-coated SERS surfaces," *Applied Spectroscopy*, vol. 51, no. 9, pp. 1355–1359, 1997.

[74] M. Culha, D. Stokes, L. R. Allain, and T. Vo-Dinh, "Surface-enhanced Raman scattering substrate based on a self-assembled monolayer for use in gene diagnostics," *Analytical Chemistry*, vol. 75, no. 22, pp. 6196–6201, 2003.

[75] M. Culha, D. Stokes, and T. Vo-Dinh, "Surface-enhanced Raman scattering for cancer diagnostics: detection of the BCL2 gene," *Expert Review of Molecular Diagnostics*, vol. 3, no. 5, pp. 669–675, 2003.

[76] T. O. Deschaines and K. T. Carron, "Stability and surface uniformity of selected thiol-coated SERS surfaces," *Applied Spectroscopy*, vol. 51, no. 9, pp. 1355–1359, 1997.

[77] A. Lorén, J. Engelbrektsson, C. Eliasson et al., "Internal standard in surface-enhanced Raman spectroscopy," *Analytical Chemistry*, vol. 76, no. 24, pp. 7391–7395, 2004.

[78] J. C. S. Costa, A. C. Sant'Ana, P. Corio, and M. L. A. Temperini, "Chemical analysis of polycyclic aromatic hydrocarbons by surface-enhanced Raman spectroscopy," *Talanta*, vol. 70, no. 5, pp. 1011–1016, 2006.

[79] D. Zhang, Y. Xie, S. K. Deb, V. J. Davison, and D. Ben-Amotz, "Isotope edited internal standard method for quantitative surface-enhanced raman spectroscopy," *Analytical Chemistry*, vol. 77, no. 11, pp. 3563–3569, 2005.

[80] S. E. J. Bell, J. N. Mackle, and N. M. S. Sirimuthu, "Quantitative surface-enhanced Raman spectroscopy of dipicolinic acid—towards rapid anthrax endospore detection," *Analyst*, vol. 130, no. 4, pp. 545–549, 2005.

[81] P. Kao, N. A. Malvadkar, M. Cetinkaya, H. Wang, D. L. Allara, and M. C. Demirel, "Surface-enhanced raman detection on metalized nanostructured poly(p-xylylene) films," *Advanced Materials*, vol. 20, no. 18, pp. 3562–3565, 2008.

[82] H. Li and B. M. Cullum, "Dual layer and multilayer enhancements from silver film over nanostructured surface-enhanced Raman substratess," *Applied Spectroscopy*, vol. 59, no. 4, pp. 410–417, 2005.

[83] H. Li, C. E. Baum, J. Sun, and B. M. Cullum, "Multilayer enhanced SERS active materials: fabrication, characterization, and application to trace chemical detection," in *Chemical and Biological Sensing VII*, vol. 6218 of *Proceedings of the SPIE*, April 2006.

[84] H. Li, P. H. Patel, and B. M. Cullum, "Novel multilayered SERS substrates for trace chemical and biochemical analysis," in *Smart Medical and Biomedical Sensor Technology II*, vol. 5588 of *Proceedings of the SPIE*, pp. 87–97, October 2004.

[85] C. K. Klutse, H. Li, and B. M. Cullum, "Optimization of multilayer Surface Enhanced Raman Scattering (SERS):Immuno-nanosensors via self-assembled monolayer spacers," in *Smart Biomedical and Physiological Sensor Technology VI*, vol. 7313 of *Proceedings of the SPIE*, April 2009.

[86] B. M. Cullum, H. Li, M. V. Schiza, and M. E. Hankus, "Characterization of multilayer-enhanced surface-enhanced Raman scattering (SERS) substrates and their potential for SERS nanoimaging," *Nanobiotechnology*, vol. 3, no. 1, pp. 1–11, 2007.

[87] M. E. Hankus, H. Li, G. J. Gibson, and B. M. Cullum, "Surface-enhanced Raman scattering-based nanoprobe for high-resolution, non-scanning chemical imaging," *Analytical Chemistry*, vol. 78, no. 21, pp. 7535–7546, 2006.

[88] C. K. Klutse and B. M. Cullum, "Development of SAM-based multi-layer SERS substrates for intracellular analyses," in *Smart Biomedical and Physiological Sensor Technologies VII*, vol. 7674 of *Proceedings of the SPIE*, April 2010.

[89] C. K. Klutse and B. M. Cullum, "Optimization of SAM-based multilayer SERS substrates for intracellular analyses: the effect of terminating functional groups," in *Micro-sensors for Cellular Analyses*, vol. 8025 of *Proceedings of the SPIE*, 2011.

[90] H. Li, C. E. Baum, J. Sun, and B. M. Cullum, "Multilayer enhanced gold film over nanostructure surface-enhanced Raman," *Applied Spectroscopy*, vol. 60, no. 12, pp. 1377–1385, 2006.

[91] L. A. Dick, A. D. McFarland, C. L. Haynes, and R. P. Van Duyne, "Metal film over nanosphere (MFON) electrodes for surface-enhanced Raman spectroscopy (SERS): improvements in surface nanostructure stability and suppression of irreversible loss," *Journal of Physical Chemistry B*, vol. 106, no. 4, pp. 853–860, 2002.

Hindawi Publishing Corporation
Journal of Nanotechnology
Volume 2012, Article ID 173273, 15 pages
doi:10.1155/2012/173273

Research Article

Surface-Enhanced Raman Spectroscopy of Dye and Thiol Molecules Adsorbed on Triangular Silver Nanostructures: A Study of Near-Field Enhancement, Localization of Hot-Spots, and Passivation of Adsorbed Carbonaceous Species

Manuel R. Gonçalves,[1] Fabian Enderle,[2] and Othmar Marti[1]

[1] *Institute of Experimental Physics, Ulm University, Albert-Einstein-Allee 11, 89069 Ulm, Germany*
[2] *Institute of Solid State Physics, Ulm University, Albert-Einstein-Allee 11, 89069 Ulm, Germany*

Correspondence should be addressed to Manuel R. Gonçalves, manuel.goncalves@uni-ulm.de

Received 9 December 2011; Revised 19 February 2012; Accepted 19 February 2012

Academic Editor: Simion Astilean

Surface-enhanced Raman spectroscopy (SERS) of thiols and dye molecules adsorbed on triangular silver nanostructures was investigated. The SERS hot-spots are localized at the edges and corners of the silver triangular particles. AFM and SEM measurements permit to observe many small clusters formed at the edges of triangular particles fabricated by nanosphere lithography. Finite-element calculations show that near-field enhancements can reach values of more than 200 at visible wavelengths, in the gaps between small spherical particles and large triangular particles, although for the later no plasmon resonance was found at the wavelengths investigated. The regions near the particles showing strong near-field enhancement are well correlated with spatial localization of SERS hot-spots done by confocal microscopy. Silver nanostructures fabricated by thermal evaporation present strong and fast fluctuating SERS activity, due to amorphous carbon contamination. Thiols and dye molecules seem to be able to passivate the undesired SERS activity on fresh evaporated silver.

1. Introduction

The purpose of this paper is twofold: to demonstrate the detection of places presenting strong near-field enhancement by surface-enhanced Raman spectroscopy (SERS) combined with confocal microscopy, and to characterize the SERS activity of different molecules confined at edges of silver nanostructures fabricated in arrays.

The Raman enhancement characteristic of SERS [1–3] has two contributions: one of electromagnetic nature [4–7], due to surface plasmons, and other of chemical nature, associated with electronic excitations and charge transfer mechanisms [8–10]. The electromagnetic effect is dominant. For example, single-molecule SERS cannot be explained without a strong optical field enhancement $M = |\mathbf{E}/\mathbf{E}_0| \sim 10^3$ [11, 12]. Conversely, sites in nanostructures presenting strong field enhancement can be localized using surface-enhanced Raman spectroscopy combined with microscopic techniques.

Enhanced Raman scattering can be obtained by two different types of excitation: by far-field illumination of metal nanostructures or rough metal surfaces with molecules absorbed and by illuminating a sharp metal tip, scanning a surface with molecules [13–15]. The later, called tip-enhanced Raman spectroscopy (TERS) is a special type of SERS, where the field enhancement is provided by the confinement of surface plasmons at the metal tip. Despite the lateral resolution achieved, aperture scanning near-field optical microscopy (SNOM) is not adequate for SERS because of the small-field enhancements achieved at the aperture of the probe. SNOM probes are usually coated with aluminum, which has strong absorption at visible wavelengths. The excitation power in aperture SNOM is limited by the

throughput of the aperture. Therefore, far-field illumination methods are preferred. Confocal microscopy improves the lateral resolution over classical optical microscopy and allows to use a wide range of excitation powers.

Molecules investigated by surface-enhanced Raman scattering (SERS) are generally much smaller than the wavelength of light, usually less than 5 nm. Near-fields at metallic protrusions and other nanostructures have a fast decay with distance. They can decrease one or more orders of magnitude in few nm [4, 5, 7]. By placing a small molecule close to a metal surface, where the near-field was enhanced by a factor M, an increase in the Raman scattering cross-section of $G \sim M^4$ is achieved [4–7, 12]. In many theoretical calculations, the field at the molecule is assumed to be locally homogeneous. However, this assumption is not correct if the molecule extends itself over several tens of nm, reaching eventually 1 μm in length. This is the case of polymer and some biomolecules [16–18].

Many research groups have investigated SERS using a single of few molecular species adsorbed at a specific metal structure [19, 20]. These structures, in particular, clusters or roughened surfaces, are usually difficult to characterize in terms of shape and field enhancement and cannot be well reproduced. It is, therefore, valuable to fabricate templates of good reproducibility, where the near-fields and the related Raman enhancements can be calculated, and compare the SERS of different molecules on the same structure. Sensing applications in biology and medicine require reproducibility. Lithography methods are, therefore, often preferred for SERS metal templates.

However, the nanostructures of silver and gold obtained by thermal evaporation processes have a strong drawback. The SERS activity of fresh evaporated films due to amorphous carbon is very large [3, 21–24]. Some techniques have been tried to avoid the carbon contamination and to passivate it [3, 25].

In this paper, we present an SERS study of different molecules using the same type of metal template: triangular particles of silver fabricated by nanosphere lithography. Moreover, we show that solutions of dye molecules, or thiols may passivate the amorphous carbon or carbonaceous species adsorbed on silver and responsible for fast fluctuating spectra. The size of the structures is large enough to by resolved be confocal microscopy.

2. Templates Fabrication and Sample Preparation

The fabrication of metal structures appropriate for SERS applications has followed, mainly, two routes: microfabrication based on electron-beam lithography [26, 27] and nanosphere lithography methods [28–30] and methods based on chemical growth [31–34]. The first allows a flexible tailoring of the structures shape and the replication in arrays at surfaces. The latter may lead to monodisperse particles of well-defined shape or to clusters of colloidal particles of random size [11, 20, 35]. In any approach, it is envisaged to obtain metal structures which can enhance sufficiently optical near-fields. These enhancements can reach several orders of magnitude, depending on the surface-plasmon resonances, structure shape, and size [4, 5, 36, 37].

The nanosphere lithography (NSL) is an appealing fabrication method because of its technical simplicity and near-field enhancements achieved. The method was firstly proposed by Fischer and Zingsheim for fabrication of nanoparticles in surfaces [28]. The particles obtained have, in general, approximate triangular shape and are distributed in hexagonal lattices at the substrate [29]. The triangles have concave sides and sharp corners (see Figures 1(b) and 1(c)). The fabrication steps are presented in Figure 1(a). Particles tailored to be resonant at a specific wavelength enhance strongly near-field at their corners, making them appropriate for SERS [37].

We show in this paper that the particle tailoring to achieve surface-plasmon resonance is not absolutely required. Target molecules in solution can be adsorbed in large metal particles and small clusters. In order to protect the adsorbed molecules and the silver particles, a polymer coating can be used.

Monodisperse suspension of polystyrene (PS) spheres (NIST size standards) were purchased from Duke Scientific. Diameters of 3 μm, 1 μm, and 400 μm were employed. The smallest PS spheres are less useful in the present investigation, because their projected metal patterns cannot be resolved by a confocal microscope. Cover slides of $20 \times 20\,\text{mm}^2$ were used as substrates. Thin films of silver of 50 nm thickness were deposited on top of the colloidal crystals by thermal evaporation at a rate of $\sim$10 Å/s, in a vacuum of 2×10^{-5} mbar. The coated samples were removed from the vacuum chamber and sonicated in ethyl methyl ketone (EMK) and ethanol, in order to remove the coated spheres. The silver projected patterns remain on the substrate. 20 μL of ethanol solutions of rhodamine 6G, fluorescein, and methylene blue (concentration of $\approx 10^{-2}$ M) were put on top the patterned samples. After evaporation of solvent, the samples were firstly sonicated and then rinsed in pure ethanol. Solvent rest was evaporated by nitrogen jet. A droplet of polymethylsiloxane (PDMS), mixing elastomer and curing agent at a ratio of 10 : 1, was cast on top the silver patterns and covered by a cover slide. The viscous liquid spreads to the edges of the substrate and covers completely the patterned surface. The curing process was done in an oven at 50°C for 12 h, at normal pressure. PDMS has a refractive index at optical wavelengths of $n = 1.43$. Some samples fabricated for studying time-resolved spectra were covered by the copolymer polybutadiene-block-polyisoprene (PB-b-PIP) from Aldrich. This elastomer is fluid at room temperature and has a refractive index of $n = 1.519$.

Several recent papers addressed the investigation of SERS on samples fabricated by NSL, using AFM and confocal Raman microscopy to localize hot-spots [38–40]. However, in these reports the size of the structures fabricated is smaller than 1 μm. On the other hand, the convolution between the AFM cantilever tip and sample surface limits the resolution achieved for small objects localized near a larger particle. SEM is recommended to characterize objects of few tens of nm. The differences between AFM measurements and high-resolution scanning electron microscopy can be seen

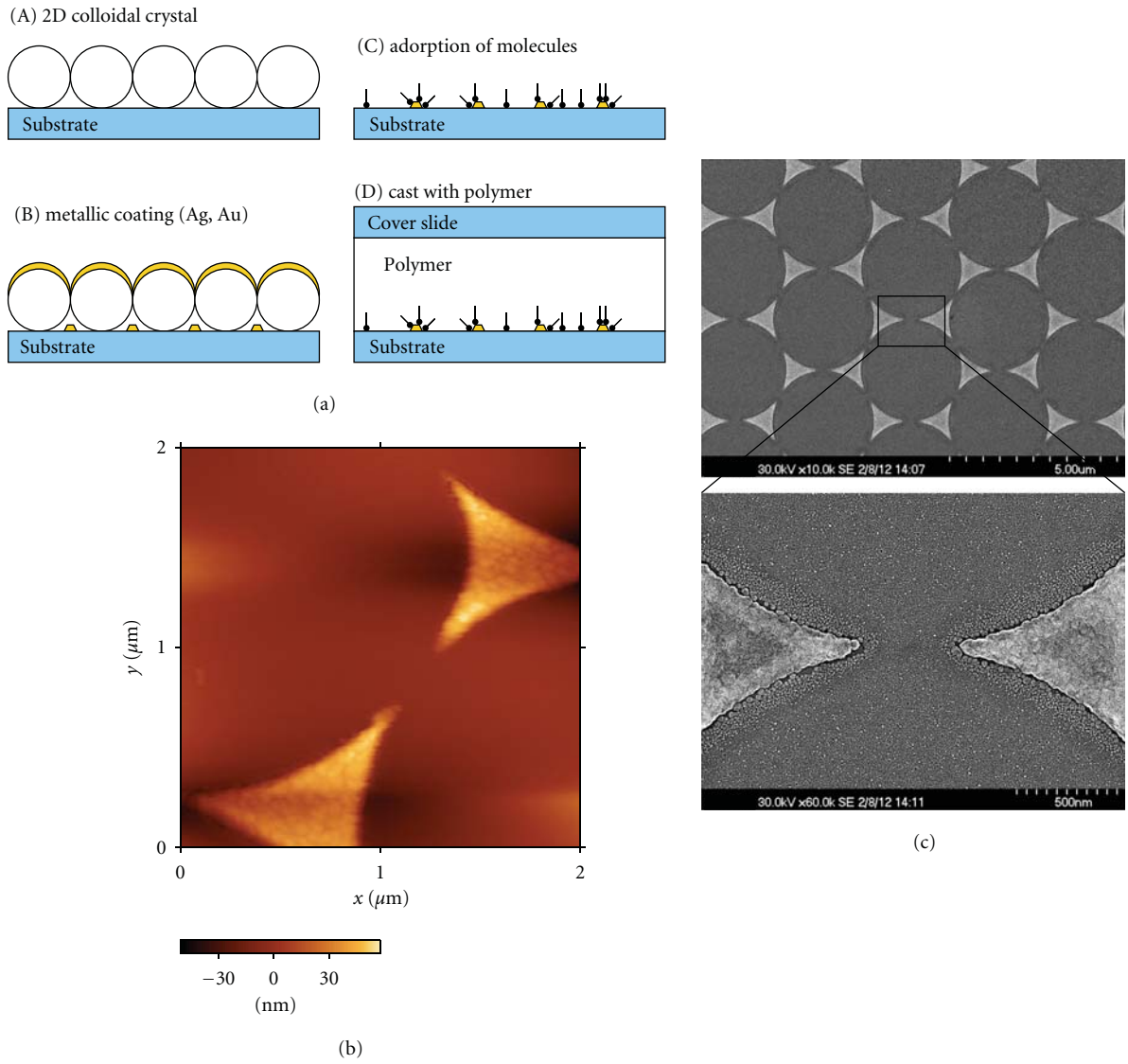

Figure 1: (a) Fabrication steps of metal templates by nanosphere lithography. (A) Colloidal crystals formed by crystallization of PS spheres during solvent evaporation. (B) Metal coating. (C) Molecules in solution adsorbed (physisorbed or chemisorbed) at the metal nanoparticles obtained after spheres lift-off. (D) Polymer cast used to protect the sample and to change refractive index of the medium close to the metal nanoparticles. Using transparent substrates, the illumination of the sample can be done from both sides. (b) AFM topography image of a Ag pattern with 50 nm film thickness. (c) SEM micrographs of a 50 nm thick silver pattern, fabricated using PS spheres of 3 diameter. Small clusters (30 to 50 nm) are found close to the triangular particles. The smaller clusters between the triangles are formed by sputtering of a gold-palladium target, used for the coating required for the scanning electron microscope. This coating has a thickness of 4 nm.

in Figure 1. A Hitachi S-5200 scanning electron microscope was used for the SEM measurements and a WITec Alpha 300 AFM microscope to obtain the topography of the samples.

3. Near-Field of Silver Nanostructures: FEM Simulations

Near-field intensity measured using scanning near-field microscopy (SNOM) [41–43] on small triangular particles present patterns which depend on the excitation wavelength. These patterns may be due to dipolar or multipolar excitations [26]. Moreover, the distribution of the field patterns is sensitive to the polarization of light. Near-fields can be calculated using several numerical methods. Calculations of the optical extinction and near-field on triangular particles, based on the Discrete Dipole Approximation (DDA) [44, 45], were presented in [37]. The enhancement of the near-field intensity $|\mathbf{E}^2|$ can reach values of 3500 or more for isolated particles, while for dimers can surpass 11000.

More recently, methods based on finite-element method (FEM) have been applied to calculate the optical response of metal nanostructures, namely, using COMSOL Multiphysics [49, 50]. Using COMSOL in plasmonics offers several advantages over DDA: size of the structure from few nanometers up

to several light wavelengths (the number of dipoles required for good DDA calculation is extremely large); models for arbitrary dielectric constants can be used (DDA requires small imaginary part of the complex refractive index, or very small inter dipole separation) [45]; nonhomogeneous embedding medium; adaptive meshing.

FEM-based COMSOL Multiphysics version 4.2a with RF module was used to investigate near-fields on different configurations of silver nanoparticles. The particles are embedded in a medium of refractive index $n = 1.5$. The dimensions of the triangular particles were modeled to follow the patterns obtained by NSL. To avoid field artifacts at very sharp edges, the corners and edges of the particles were rounded. For patterns of $3\,\mu$m lattice constant, the corners of the triangular particles are of spherical shape of radius equal to half of the particle thickness. The edges have a circular profile of the same radius. In order to study the effect of close vicinity between two small Ag particles and between a large triangular particle and small spherical particles, three different configurations were modeled: two spherical Ag particles of 60 nm and 50 nm diameter, respectively; a triangular particle of thickness 50 nm and spherical particle of 20 nm at the corner with a gap of 2 nm; a triangular particle and three spheres of 20 nm diameter with the same gap. One of the spheres is placed close to the corner in the symmetry axis of the triangular particle and the other two are at the sides (see Figure 2(e)). This last set of particles is useful to compare the near-field enhancements resulting at the gaps for a specific field polarization.

For each geometric configuration, calculations of the near-field and far-field cross-sections were done for 121 equally spaced wavelengths, between $\lambda = 400$ nm and $\lambda = 1000$ nm. The computational domain, is spherical and the symmetry of the systems of particles for a plane wave illumination was exploited to reduce the amount of mesh elements to 1/2. At the external boundary of the computation domain scattering boundary conditions and perfectly matched layers (PMLs) were used to attenuate back-reflections. The illumination is perpendicular to the plane of the particles and the electric field has an amplitude of 1 V/m. The refractive index of the silver $\tilde{n} = n - ik$ was obtained by interpolation of the experimental data from [51]. The calculation of the extinction cross-section was done by applying the optical theorem [52]. For each geometrical configuration, the near-fields were probed in the middle of the gap between the particles. The results are presented in Figure 2.

In general, the highest field enhancements occur at the corners of the particles. Maxima are reached at the plasmon resonance frequency, given by the far-field extinction. However, the coupling between two particles has a more important contribution to the near-field enhancement, despite the large particle is off-resonance. In the simulations done, no plasmon resonances were found for large triangular particles. They are expected above to be $\lambda = 1000$ nm. Smaller triangular particles have plasmon resonances in the visible and NIR spectral regions [26, 37].

AFM topography and SEM micrographs of silver patterns reveal that small aggregates are formed close to the triangular tips. These aggregates are formed by coalescence of the metal during the evaporation. We simulate the perturbation introduced by small silver aggregates by placing a small spherical particle at short distance to the right corner of the larger triangular particle. Two configuration were investigated: Figures 2(c) and 2(e).

The most typical defects occurring on two-dimensional arrays of triangular patterns, fabricated by NSL, are hexagonal shaped particles, due to vacancies of spheres, and elongated particles due to dislocations in the array of spheres. When the dislocation in the array of spheres is small, the corners of two adjacent triangular particles of the pattern may be almost in contact. Small triangular particles and dimers formed by this way, of size smaller than 100 nm, have plasmon resonances in the visible [37]. Calculations show that large triangular particles, fabricated using sized PS spheres, do not enhance strongly near-fields off their plasmon resonances. Therefore, strong near-fields can only be found on systems formed by a triangular particle and one or more small particles surrounding the first, at a distance of few nanometers. The FEM simulations confirm this assumption. It must be stressed that strong field enhancements only occur for small gaps (less than 5 nm). The field decreases exponentially with distance. These results are in consonance with previous calculations done by other methods [4, 53].

4. Experiments and Results

A scanning confocal Raman microscope (WITec GmbH) was used for the measurements. The microscope is equipped with a laser coupler and edge filter for Raman spectroscopy for wavelength $\lambda = 532$ nm. Acquisition times of only 30 ms are possible with the system. Most of the SERS measurements reported in the literature have acquisition times of several seconds. To limit sample heating by highly focused laser beams, low excitation power is desired. Classical Raman spectroscopy requires a laser power of several to obtain good Raman spectra.

The illumination and collection is done using the same objective. For the measurements, a Nikon oil immersion objective of numerical aperture $NA = 1.25$ was used. At an excitation power of less than $10\,\mu$W, the strongly attenuated Rayleigh scattering for a transparent sample is only slightly above the dark current level of the detector. However, a weak Rayleigh signal is useful as reference to locate SERS active sites close to the metal structures. Fortunately, silver nanoparticles are very good scatterers a visible wavelengths and their contours can be obtained from the Rayleigh peak of the full Raman spectrum. The location of the active Raman sites is only limited by the resolution of the microscope. The spectrometer is equipped with a CCD camera Andor DV401-BV (1024×127 active pixels and quantum efficiency >90%). It has a resolution of $<5\ \text{cm}^{-1}$ and a range of -150 to $3730\ \text{cm}^{-1}$ in the Stokes band.

The illumination of the samples was done from the substrate side, using the oil-immersion objective. Illuminating the sample from top is more difficult because of the thickness

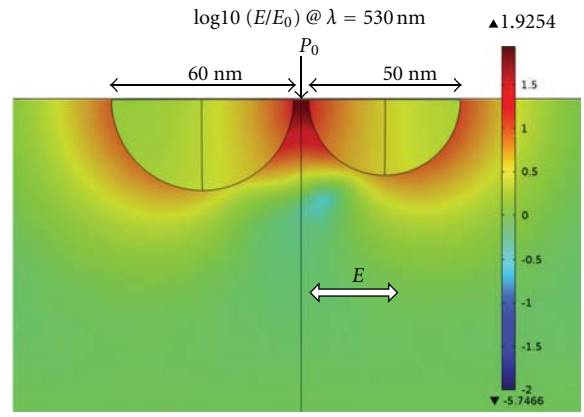

(a)

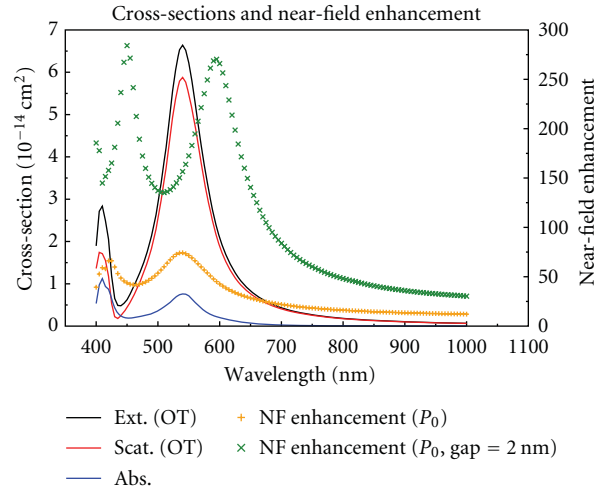

(b)

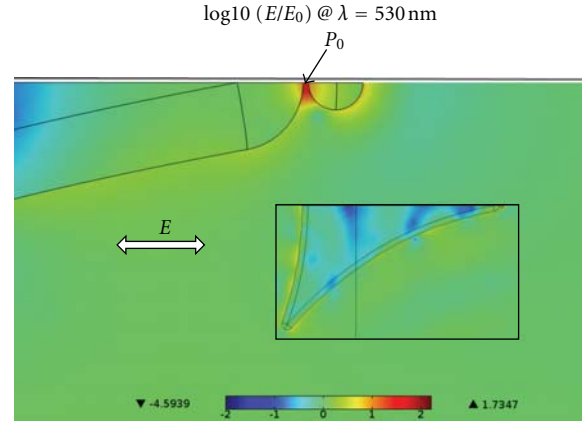

(c)

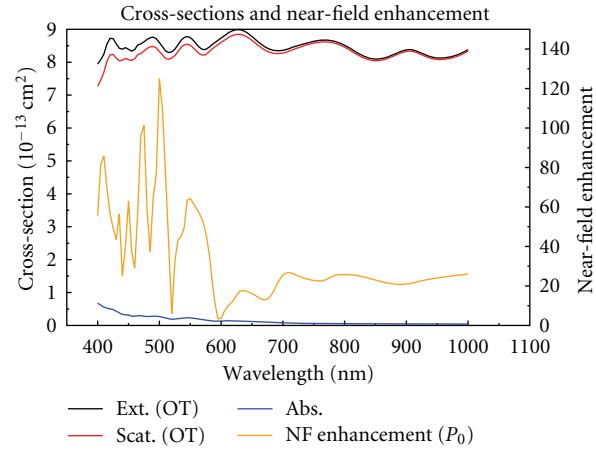

(d)

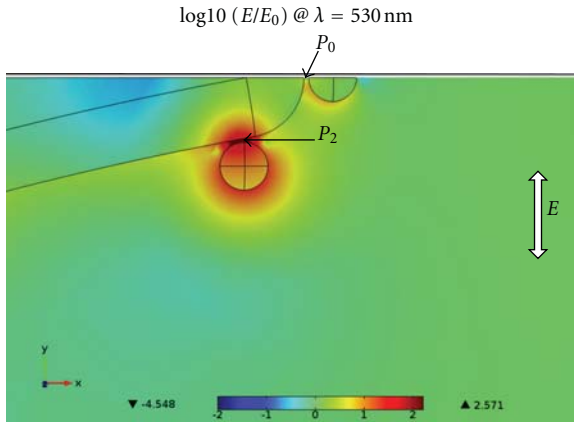

(e)

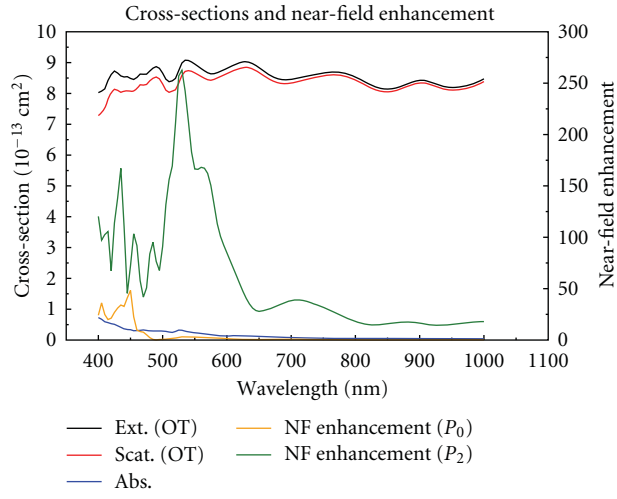

(f)

FIGURE 2: $\log_{10}|\mathbf{E}/\mathbf{E}_0|$ in the symmetry plane of nanoparticles (left column) and extinction, scattering, absorption cross-section and near-field enhancements spectra (right column). (a) and (b) Two Ag spheres of 60 nm and 50 nm diameter, separated by a gap of 5 nm. The near-field at the gap middle point (P_0) marked with × was calculated for a gap of 2 nm. (c) and (d) triangular particle (thickness 50 nm) and small sphere of 20 nm diameter. Gap between the particles is 2 nm. The insert shows half of both particles. (e) and (f) triangular particle and three small spheres of 20 nm diameter (only half geometry is presented in (e)). Gap between triangular particle and each sphere is 2 nm. In all configurations, the refractive index of medium is $n = 1.5$.

of the PDMS film. Four different molecules were used to compare the SERS activity on silver triangular particles: a thiol, 1-dodecanethiol, and three dye molecules. Methylene blue (MB) and fluorescein have only weak absorption at $\lambda = 532$ nm. Their fluorescence is, therefore, low. By contrary, rhodamine 6G (R6G) has an absorption maximum at this wavelength. The Raman cross-section is much smaller than the fluorescence cross-section and thus, in solution, no Raman spectrum can be obtained for R6G at the excitation wavelength of $\lambda = 532$ nm. Skeletal models of the molecules are presented in Figure 3. In Table 1 are presented some of the most important Raman modes and the corresponding wavenumbers.

In the sample preparation, it is not possible to control and quantify the coverage of the Ag particles by each molecular species. For example, 1-dodecanethiol forms self-assembled monolayers with covalent bonds on flat Ag and Au films. However, on highly corrugated surfaces it is not possible to know how many molecules are attached to the corners of Ag particles. The same holds for the other three aromatic molecules. In experiments done to demonstrate single-molecule SERS, volumes of tens of of solutions of dyes were prepared at very low concentrations, 10^{-10} to 10^{-13} M [11, 20]. However, the nanoparticles are prepared by colloidal chemistry methods. They do not suffer from amorphous carbon contamination, though the less controllable shape of the particles and clusters.

Most of the samples prepared were protected with a PDMS film and, thus, PDMS molecules could be also excited by SERS. However, for the integration times used, no typical PDMS Raman peak was found. Raman spectra of bulk PDMS and PB-b-PIP, at fixed focal positions, using the confocal Raman microscope at $\lambda = 532$ nm were acquired (Figure 4). These spectra present characteristic Raman vibrational modes of elastomers in the Stokes band. PDMS has two strong peaks at 2905 and 2960 cm^{-1} corresponding to the symmetric and antisymmetric $-CH_3$ stretching vibrations [54]. The peak at 495 cm^{-1} corresponds to the symmetric Si–O–Si stretching. The band between 150 and 300 cm^{-1} is always present. It corresponds to skeletal C–C bending vibrations [54, 55]. PB-b-PIP has 3 strong peaks between 2800 cm^{-1} and 3000 cm^{-1} and one strong peak at 1665 cm^{-1}.

4.1. SERS on Silver Triangular Patterns. Every sample was scanned at different locations of the projection pattern, at the plane of silver particles. Spectra at single pixels, or arrays of 128×128 pixels were acquired. At each pixel, a full spectrum was acquired with an integration time of 100 ms. The full-frame acquisition time is approximately 32 min. From the data set intensity images of the Rayleigh peak and specific Raman bands can be extracted. The image pixel intensity is calculated by summing the CCD pixel intensity between two specific wavenumbers. For instance, the Rayleigh image pixel intensity was obtained by summing the CCD pixel intensities between -30 and 50 cm^{-1}.

The excitation power required for the Raman spectra of dye molecules is low: 1 to 50 μW. The power was measured at the objective mount in the microscope turret. Low

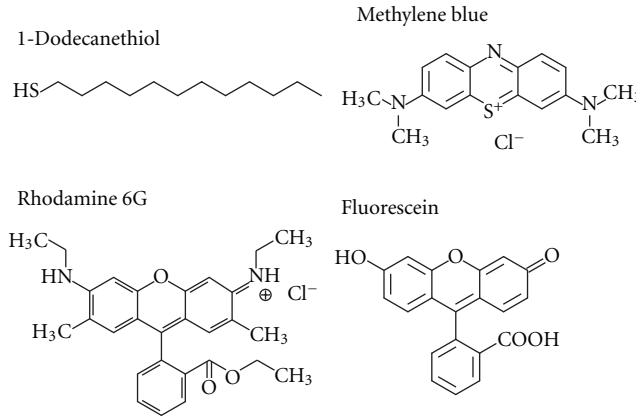

Figure 3: Skeletal models of the molecules used in SERS.

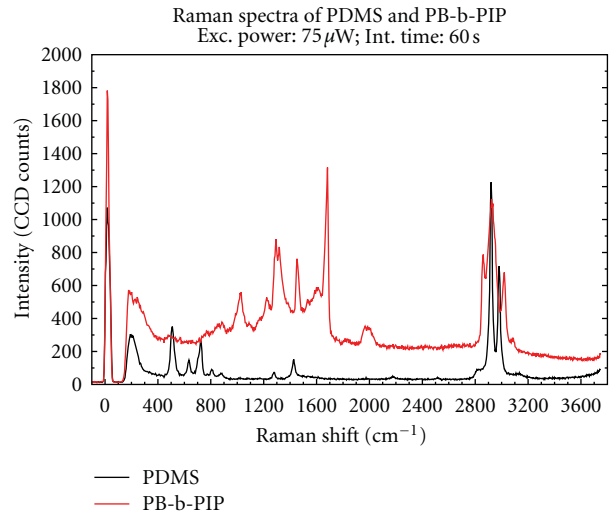

Figure 4: Raman spectra of bulk PDMS and PB-b-PIP.

excitation power avoids sample heating at the scanning region and reduces the probability of molecular degradation. The Raman spectrum changes in intensity from pixel to pixel, depending on the material at the focus. For an excitation powers of 10 to 15 μW Rhodamine 6G generates the strongest spectra (Figure 5). Fluorescein and methylene blue generate successively lower intensity peaks (Figures 6 and 7, resp.). As R6G is at resonant absorption, the Raman scattering is also resonant. The Raman, cross-section of R6G is, at resonance, $\sigma_R \sim 10^{-26}$ cm^2 [56]. Off-resonance the cross-section drops to $\sigma_R \sim 10^{-29}$ cm^2 [56]. In comparison, the fluorescence emission cross-section of R6G, at resonance, is $\sigma_F \sim 10^{-16}$ cm^2 [57]. Thus, Raman spectra of R6G can only be distinguished from the fluorescence if the Stokes cross-section is enhanced to a level of the order or larger than the corresponding fluorescence cross-section, or the fluorescence is suppressed.

An excitation power of P_{exc} 12 μW is sufficient to obtain well-defined Raman peaks of fluorescein. Despite the intensity fluctuation, the Raman peaks characteristic of fluorescein vibrational modes remain at fixed Raman shifts. There is

Table 1: Some of the most strong Raman modes and corresponding wavenumbers. *Data taken from Bryant and Pemberton [46]. **From Vosgröne and Meixner [20]. †From Hildebrandt and Stockburger [47]. ‡From Nuntawong et al. [48].

Molecule	Raman mode assignment	rel. wavenumber/(cm^{-1})
1-Dodecanethiol*	$\nu(C–S)_G$	636
	$\nu(C–S)_T$	707
	$\nu(C–C)_T$	1064–1189
	$\nu(CH_2)$	2852, 2861
	$\nu(CH_3)$	2876–2964
Rhodamine 6G**	aromatic modes	614, 1363, 1512, 1575, 1651
	bend. modes	774, 1124
Fluorescein†	aromatic modes	1176, 1324, 1398, 1548, 1629
Methylene blue‡	inc. aromatic modes	445, 772, 1155, 1392, 1626

low spectral fluctuation. For the dye molecules investigated, no Raman peaks were observed above 1800 cm^{-1}. Typical SERS spectra of fluorescein and R6G have several strong peaks between 1100 and 1700 cm^{-1} and weaker peaks between 400 and 1000 cm^{-1} (plots of Figures 5 and 6). The vibrations modes of the carboxylic group –COOH, in particular the band of the O–H stretching vibrations between 2500 and 3300 cm^{-1}, do not appear in the SERS spectra. The Rayleigh peak is several orders of magnitude weaker.

The fluorescence absorption of R6G molecules has a maximum around $\lambda = 530$ nm. R6G SERS spectra present higher background fluorescence than those of fluorescein and methylene blue. Fluorescence quenching of molecules adsorbed on metal surface can be responsible for the fact that Raman peaks of R6G appear above the fluorescence background. However, the fluorescence of molecules close to metal surfaces is also enhanced [58]. In the study of single, molecule SERS of R6G, Nie and Emory have used a excitation wavelength of $\lambda = 514.5$ nm, close to the maximum of fluorescence absorption. Strong Raman peaks above background were measured on isolated silver islands [11].

Sudden changes of intensity are usually found on adjacent pixels of the same scanning line. The pixel size is 78 nm for 10 μm and 39 nm for 5 μm scan size, respectively. The confocal microscope lateral size of focus is ~250 nm and thus, much wider than the pixel size. Each pixel is illuminated longer than 100 ms. The sudden change of intensity between adjacent pixels can be due to photobleaching.

Intensity images of the Rayleigh peak are required as spacial reference for the location of the SERS hot-sites. The hot spots of dye molecules are at the corners of the triangular particles and some at their edges. Despite the fact that no surface plasmon resonance of the triangular particles is expected for $\lambda = 532$ nm, strong SERS spectra could be measured at low excitation power. The hot-spots localized mostly at the corners of the triangular particles arise due to coupling effects between clusters and between clusters and the triangular particle, as already discussed.

1-dodecanethiol molecules adsorbed on silver triangular particles present smoother intensity transition from pixel to pixel, at the Raman band between 650 and 750 cm^{-1}. Unlike in R6G and fluorescein, in 1-dodecanethiol the Raman band image presents smooth pixel intensity. By one side, no fluorescence excitation is expected at $\lambda = 532$ nm. Due to the covalent bonding, 1-dodecanethiol molecules could be distributed more homogeneously on the surface of silver, both on edge and corner regions.

The typical Raman spectra shown in the plots of Figure 8 have few peaks above the background. Their intensity is comparable with that of the Rayleigh scattering peak. The excitation power was 52 μW, approximately 5× higher than the power used for dye samples. The strongest Raman peak is at 710 cm^{-1}. A broader peak at 2900 cm^{-1}, usually attributed to C–H vibrational modes is also visible. Self-assembled monolayers of several thiols, investigated by Levin et al. [59], present similar Raman peaks.

4.2. Temporal Fluctuation in SERS. Temporal and spectral fluctuations are typical of carbonaceous species, namely, amorphous carbon adsorbed on Ag and Au nanoparticles [21–25, 60]. In fresh evaporated silver patterns after spheres lift-off, we observed often sudden spectral fluctuations and intensity jumps from pixel to pixel in the scanned image were found. The lift-off of silver coated PS spheres was done by sonication in pure ethanol. No other solvent or solution was employed. Similar spectral fluctuations were observed on rough silver films fabricated by thermal evaporation, without using any solvent. Temporal and spectral fluctuations occur for samples of fresh evaporated silver in air as well as for samples covered by polymer films, namely, PDMS and PB-b-PIP.

The temporal evolution of the Raman spectra was investigated at fixed focal points at the silver particles. Sequences of 1000 spectra were acquired with the confocal Raman microscope, with individual integration time of 100 ms, making a total acquisition time of ~100 s. The places of the sample for time-resolved spectra were selected at the edges or corners of the triangular particle using the optical microscope. The time evolution is presented Figure 9(a). Some spectra presented in Figure 9(b) show the typical spectral fluctuation. Traces of peaks between 1200 cm^{-1}

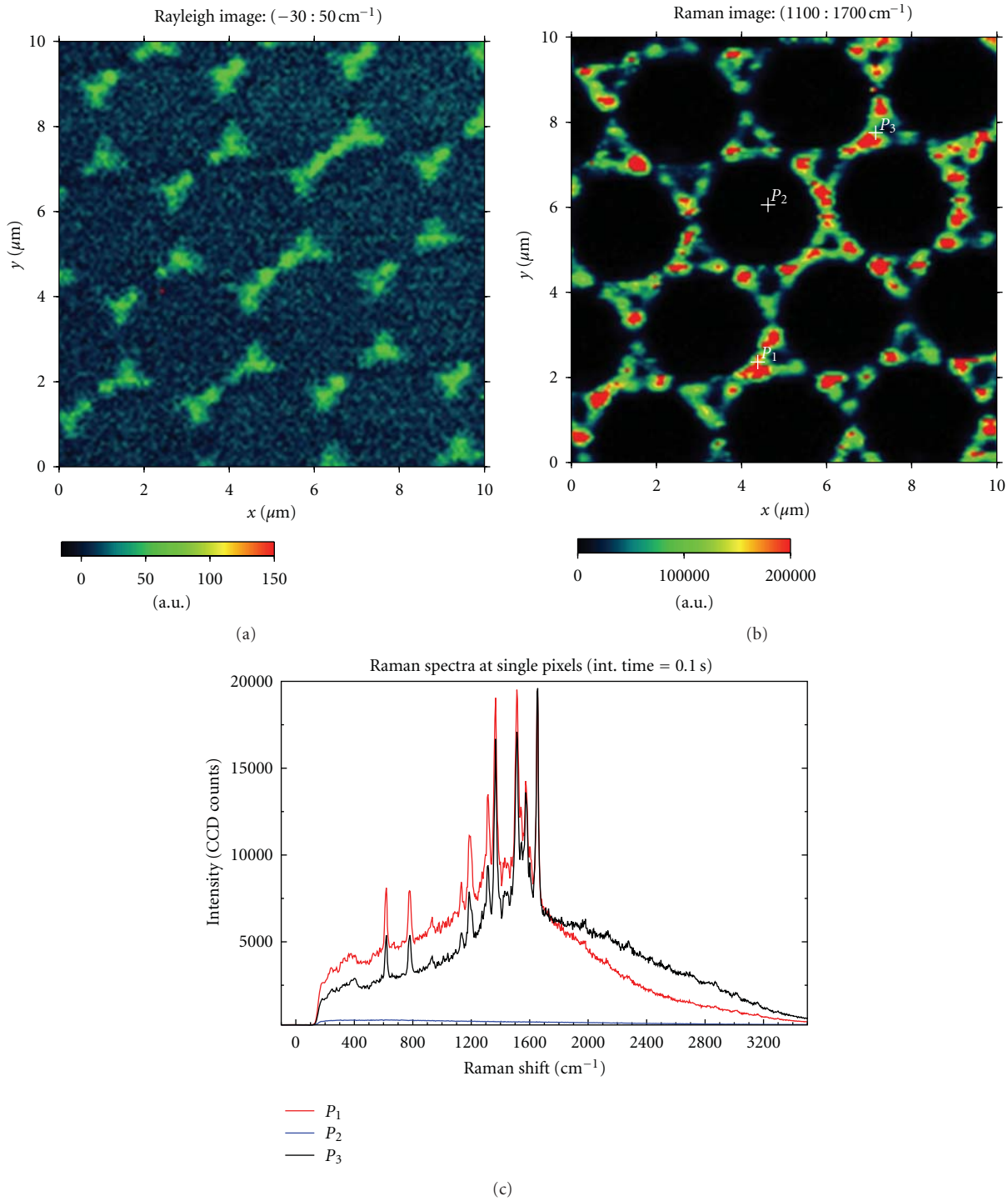

FIGURE 5: SERS of rhodamine 6G molecules on silver patterns of 3 μm diameter and 50 nm thickness. $\lambda = 532$ nm. $P_{exc} = 15\,\mu$W. The spectra below were extracted from the pixels marked. Whereas for point P_2 only background was detected, at the edge of triangular particles, strong SERS spectra of R6G were measured (P_1 and P_3).

and 1600 cm^{-1} are interrupted abruptly in the temporal sequence. By contrary, the spectra of a sample prepared with MB on Ag triangular patterns are stationary along 100 s (Figures 9(c) and 9(d)).

Sudden intensity jumps of short duration (few hundreds of ms) with strong spectral richness are common (see bright lines of Figure 9(a)). Spectral fluctuations and blinking have been discussed in the context of single-molecule SERS [11, 24, 61]. However, here there are no fixed Raman peaks that could be assigned to PB-b-PIP or other target molecule. However, the most strong peaks occurring between 1300 to 1650 cm^{-1} are atributed to amorphous carbon [62]. The

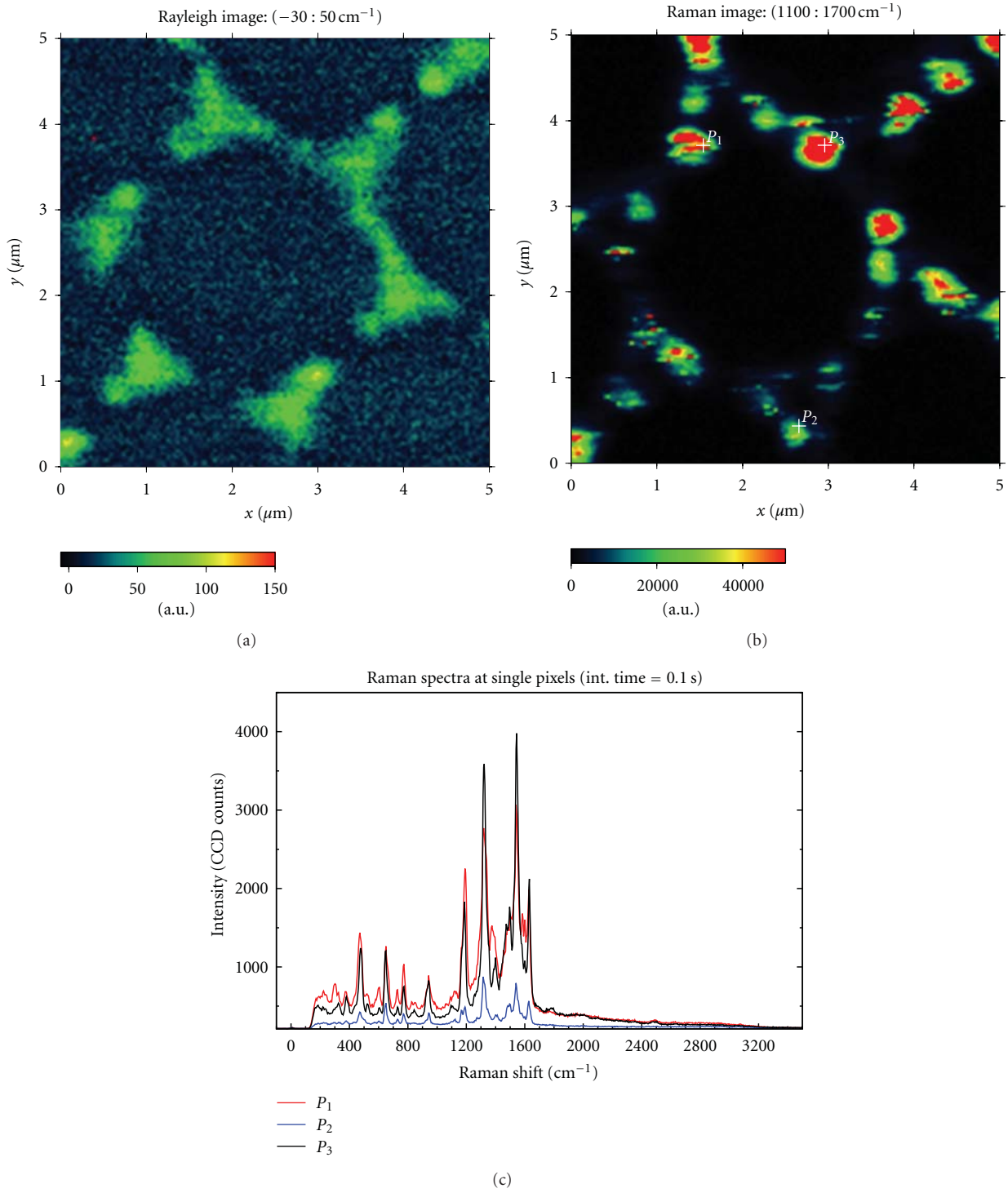

FIGURE 6: SERS of fluorescein molecules on silver patterns of 3 μm diameter and 50 nm thickness. $\lambda = 532$ nm. $P_{exc} = 12\,\mu$W. Three spectra below were extracted from the pixels marked.

mean intensity of the spectra increases with the laser power. Only few μW excitation power is enough to observe spectral fluctuation and blinking, at integration times of 100 ms. Measurements done on older samples show a drop in the mean intensity, but many hot-spots remain active.

Several solvents, namely water, organic solvents as EMK, methanol, and toluene where used, unsuccessfully, to remove or passivate the species responsible for the strong fluctuation. The only method to remove or passivate the silver sample is by using concentrated solutions of dyes (as those referred

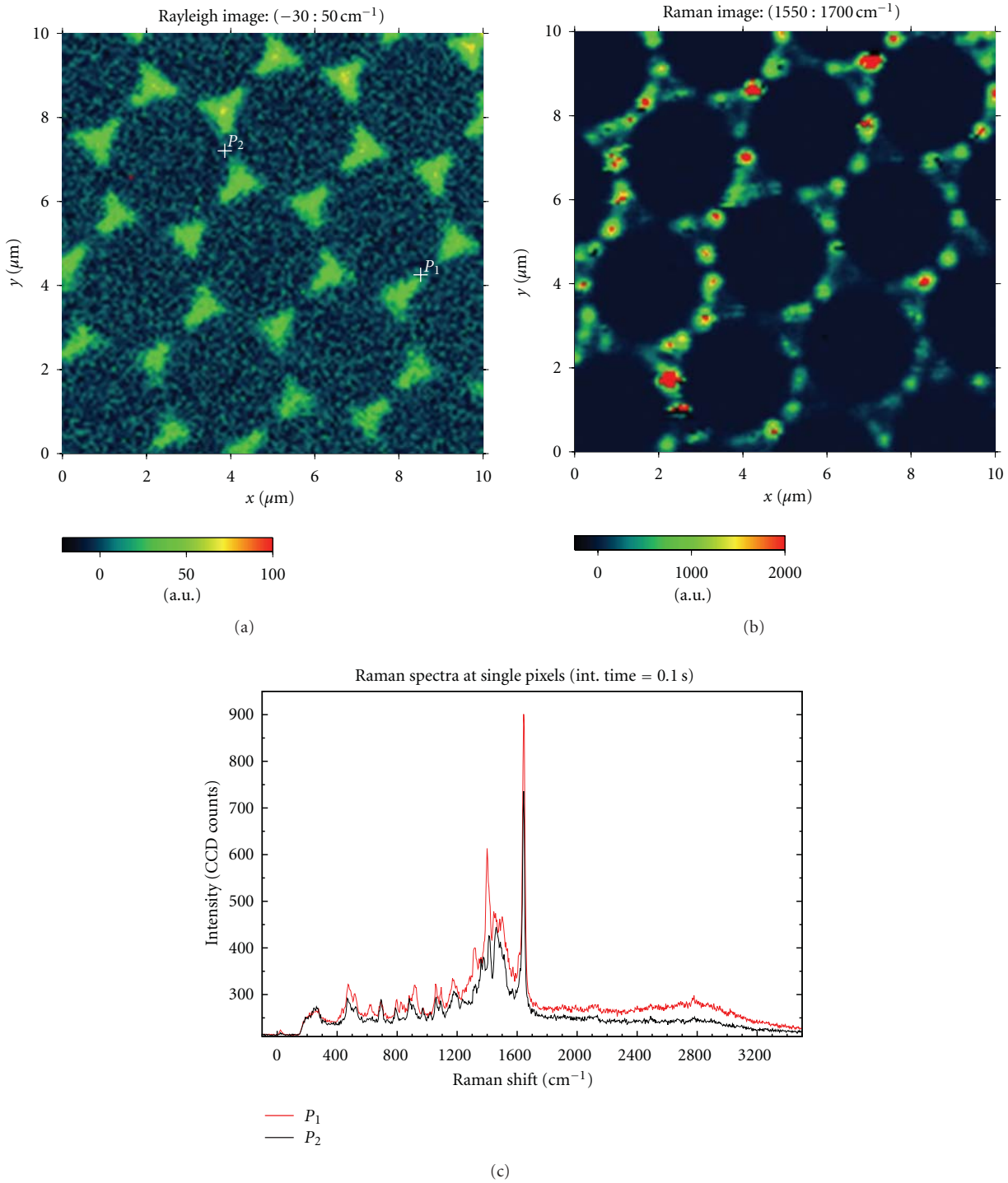

Figure 7: SERS of methylene blue molecules. $\lambda = 532$ nm. $P_{exc} = 9.5\,\mu$W. The spectra below were extracted from the pixels marked.

above) or thiols, which bond covalently to Ag. Noncovalently bond adsorbates can be removed by several successive in pure ethanol, or EMK. Indeed, samples of Ag patterns decorated using a solution containing methylene blue present very rare and weak methylene blue SERS spectra after several sonications in EMK.

5. Discussion

Confocal microscopy combined with Raman spectroscopy can be applied to investigate light scattering in metal micro- and nanostructures and, simultaneously, localize sites of strong near-field enhancement, using SERS. Small molecules

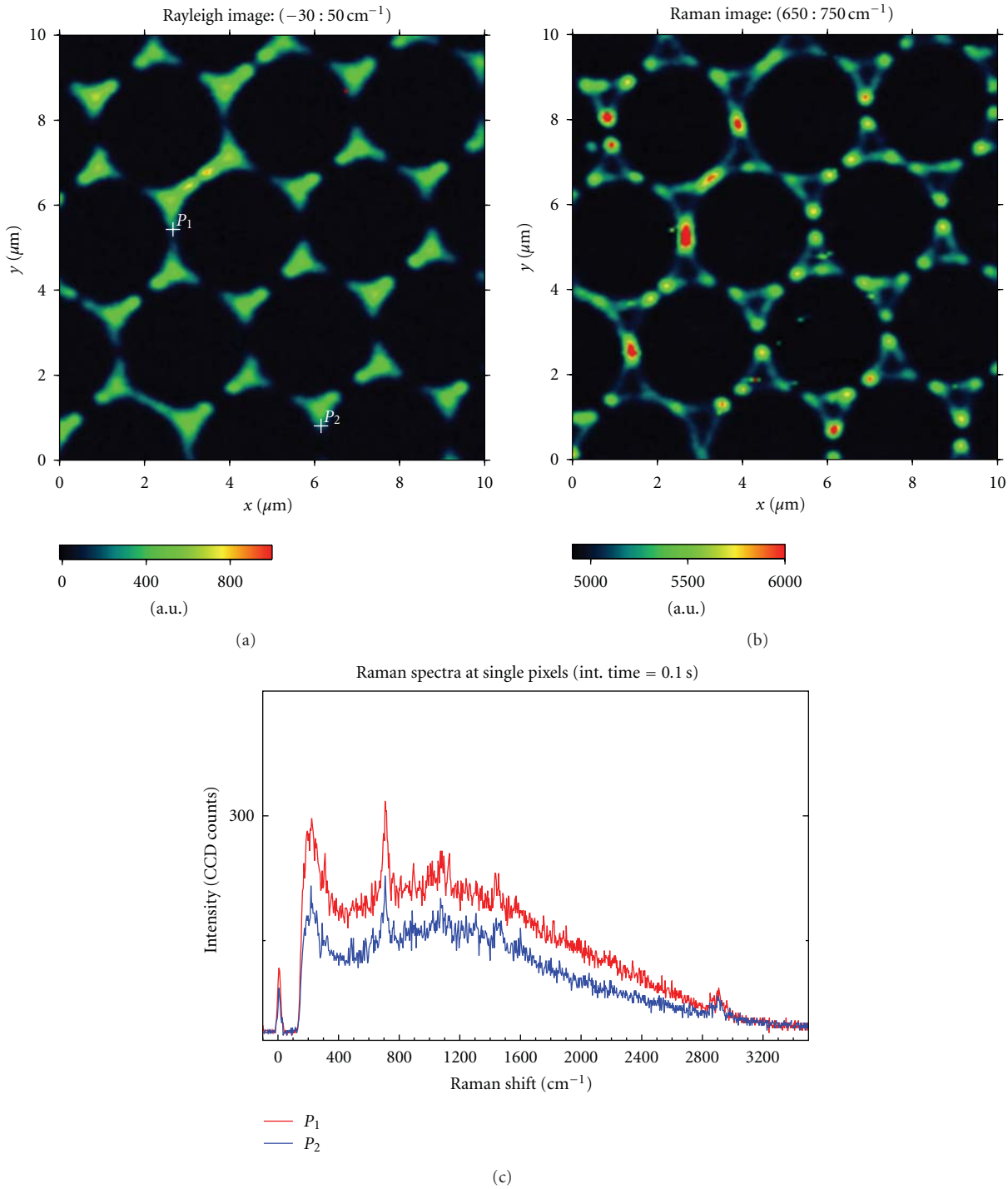

FIGURE 8: SERS of 1-dodecanethiol molecules. $\lambda = 532$ nm. $P_{exc} = 52\,\mu$W. The spectra below were extracted from the pixels marked.

as dyes and thiols are adequate for this purpose. The strong nonlinear dependence of the Raman enhancement on electric field strength is used to find near-field enhancement. Although chemical contributions to Raman scattering cannot be excluded, the electromagnetic contribution usually dominates in SERS [3, 10, 63].

The experimental results presented show that triangular particles of silver are capable of strong SERS activity of different molecules despite the excitation wavelength being far away from the surface-plasmon resonance. FEM simulations of the near-field coupling between a triangular particle and a smaller spherical particles can explain why SERS hotspots can be found at the corners and edges of large silver particles. AFM topography and SEM micrographs of the silver patters reveal small metal clusters formed close to corners of the triangular particles. Calculations of the Raman

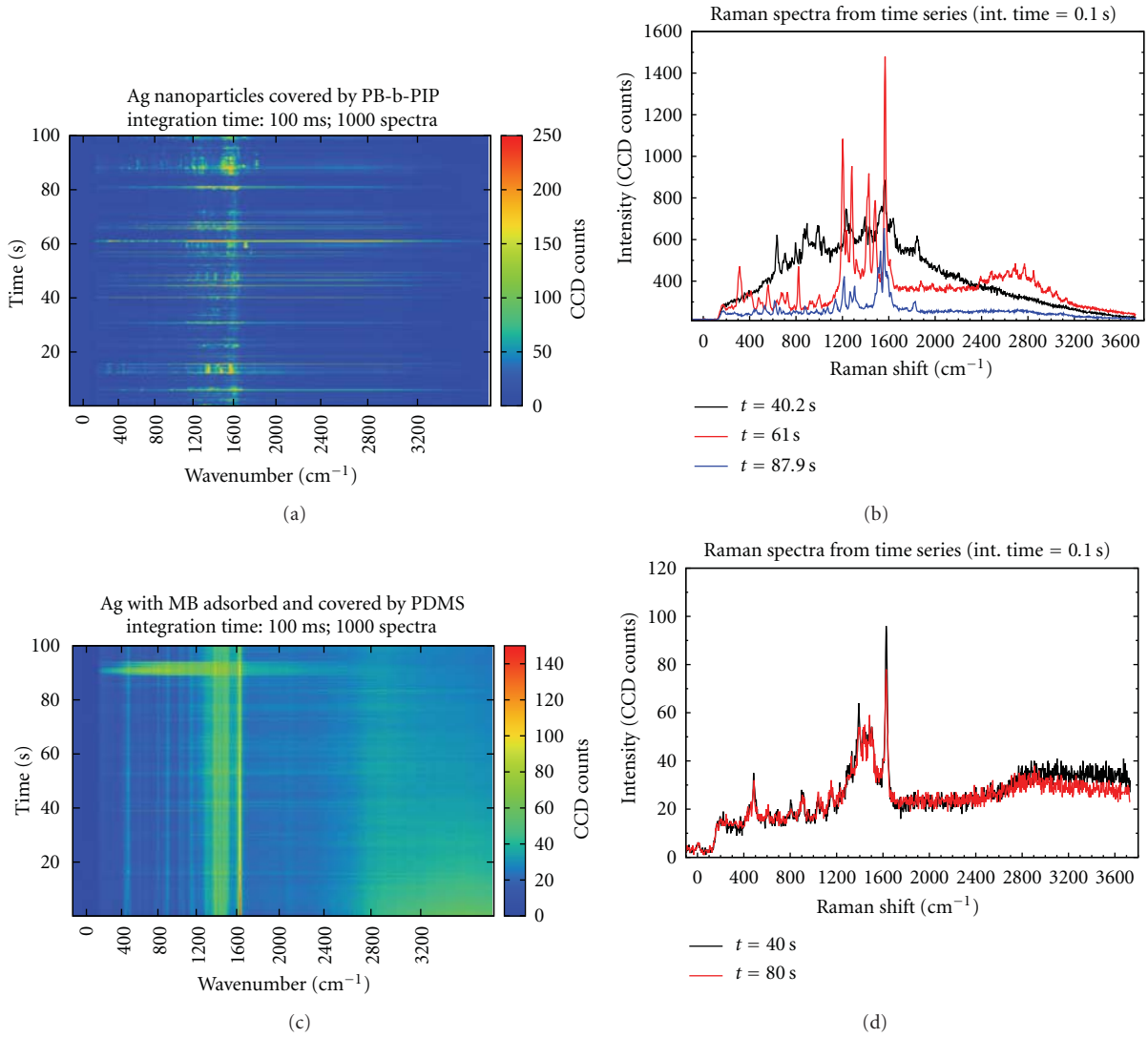

Figure 9: (a) Time series of Raman spectra acquired at a fixed focal point of a sample of Ag nanoparticles covered by a film of the block copolymer PB-b-PIP. Three spectra extracted from the time series are plotted in (b). The strong spectral and intensity fluctuations are not correlated to the Raman spectrum of PB-b-PIP. In (c), a time series of Raman spectra was acquired from a fixed focal point of sample of Ag nanoparticles with methylene blue adsorbed and covered by PDMS. In (d), SERS spectra of MB molecules present stationary behaviour.

enhancement of a molecule placed between two spheres, done by Johansson et al. [12] show that very large cross-section can be achieved. The field enhancement depends on the separation between the spheres. If there are small silver clusters attached to or in the close vicinity of the corners of the particles, molecules can be adsorbed at those sites and contribute to the enhanced Raman scattering. Calculations done by García-Vidal and Pendry [36] and Xiao el al. [64] on corrugated silver structures also present field enhancements leading to Raman enhancement factors of 10^8 or more. In SEM micrographs of Figure 1(c), many clusters surrounding the triangular particle can be seen. FEM calculations show that strong near-fields at the gap between particles are highly dependent on the polarization. The high density of those clusters permits to find many hot-spots at the edges of the triangular particles, even for a fixed polarization direction.

The total experimental Raman enhancement factor can be obtained by

$$G_{\text{SERS}} = \frac{I_R(\overline{\nu})}{N f \sigma I_{\text{exc}}}, \tag{1}$$

where $I_R(\overline{\nu})$ is the count rate at a specific Raman shift, N is the number of molecules contributing to the spectrum, f is the total efficiency of detection, σ_R is the Raman scattering cross-section of the selected vibration mode, and I_{exc} is the power density per solid angle in photons/s/cm ^{2}/rad. N can only be roughly estimated. The total efficiency of detection is of the order 0.2%. The efficiency of the Raman spectrometer is ~0.4. The ratio between the power at the end of the collection fibre and the power measured at the microscope turret is 0.005. Thus, a total efficiency of 0.2% is assumed for the full Raman spectrum. We assume that $N = 100$

molecules contributing to the Raman scattering. Some sites exhibit peaks of the double bond C=C with count rates of $I_R = 10000$ counts/s. A laser power of 10 mW focused onto a spot of less than 1 μm^2 has a photon flux density of 10 μW/cm^2 or 2.68×10^{21} photons/s/cm ^{2}/rad. Assuming that the Raman scattering cross-section of the fluorescein strongest vibration is of the order of 10^{-28} cm ^{2}, the total experimental enhancement is $G_{\text{SERS}}^{\text{exp}} \sim 1.8 \times 10^{11}$. This increases 2 orders of magnitude if only a single molecule contributes to the Raman spectrum and is consistent with theory. However, as discussed above, it is very difficult to know how many molecules are at the hot spot.

6. Conclusion

SERS investigations of several dye and one thiol molecules, adsorbed on silver nanostructures, reveal the sites where the optical near-fields are strongly enhanced. The near-fields of triangular particle dimers and couplings between triangular particles and small cluster were studied by FEM simulations. The large near-field enhancement could explain the Raman spectra by SERS effect. SERS hot-spots were studied with confocal Raman microscopy. The resolution achieved is enough to localize the SERS hot-spots at the corners and, in less extent, at the edges of triangular particles of $\sim$1.2 μm lateral size. These particles have a rim of metal clusters which lead to strong field enhancements. SERS hot-spots were found at the particles rim. These templates are reproducibly fabricated and the hot-spots detected can be resolved with confocal microscopy. Therefore, they can be useful in sensing applications using SERS.

A passivation technique for a major drawback, the amorphous carbon contamination, was presented. Temporal fluctuations and blinking reported by several authors [11, 61, 65–68] are common in SERS. However, effects of amorphous carbon or carbonaceous species adsorbed on fresh evaporated silver particles are discussed only in few papers. The time-scale of spectral fluctuations was briefly discussed.

A limitation of confocal Raman microscopy to localize SERS hot spots is the lateral resolution of $\sim \lambda/2$. The corners of small triangular particles (size length smaller than 300 nm) cannot be resolved. Scanning near-field Raman microscopy could be used to overcome this limitation.

Acknowledgments

The authors thank M. Asbach for the preparation of colloidal crystals and the colleagues of the Institute of Solid State Physics, namely, Alfred Plettl and Paul Ziemann for collaboration and technical support. This work was supported by the Collaborative Research Center SFB-569 (Project C-10) of the Deutsche Forschungsgemeinschaft (DFG).

References

[1] M. Fleischmann, P. J. Hendra, and A. J. McQuillan, "Raman spectra of pyridine adsorbed at a silver electrode," *Chemical Physics Letters*, vol. 26, no. 2, pp. 163–166, 1974.

[2] M. Moskovits, "Surface-enhanced spectroscopy," *Reviews of Modern Physics*, vol. 57, no. 3, pp. 783–826, 1985.

[3] A. Otto, I. Mrozek, H. Grabhorn, and W. Akemann, "Surface-enhanced Raman scattering," *Journal of Physics: Condensed Matter*, vol. 4, no. 5, article 001, pp. 1143–1212, 1992.

[4] J. Gersten and A. Nitzan, "Electromagnetic theory of enhanced Raman scattering by molecules adsorbed on rough surfaces," *The Journal of Chemical Physics*, vol. 73, no. 7, pp. 3023–3027, 1980.

[5] D. S. Wang and M. Kerker, "Enhanced Raman scattering by molecules adsorbed at the surface of colloidal spheroids," *Physical Review B*, vol. 24, no. 4, pp. 1777–1790, 1981.

[6] G. W. Ford and W. H. Weber, "Electromagnetic interactions of molecules with metal surfaces," *Physics Reports*, vol. 113, no. 4, pp. 195–287, 1984.

[7] H. Metiu, "Surface enhanced spectroscopy," *Progress in Surface Science*, vol. 17, no. 3-4, pp. 153–320, 1984.

[8] B. Pettinger, "Light scattering by adsorbates at Ag particles: quantum-mechanical approach for energy transfer induced interfacial optical processes involving surface plasmons, multipoles, and electron-hole pairs," *The Journal of Chemical Physics*, vol. 85, no. 12, pp. 7442–7451, 1986.

[9] A. Otto, "The "chemical" (electronic) contribution to surface-enhanced Raman scattering," *Journal of Raman Spectroscopy*, vol. 36, no. 6-7, pp. 497–509, 2005.

[10] B. N. J. Persson, K. Zhao, and Z. Zhang, "Chemical contribution to surface-enhanced raman scattering," *Physical Review Letters*, vol. 96, no. 20, Article ID 207401, 2006.

[11] S. Nie and S. R. Emory, "Probing single molecules and single nanoparticles by surface-enhanced Raman scattering," *Science*, vol. 275, no. 5303, pp. 1102–1106, 1997.

[12] P. Johansson, H. Xu, and M. Käll, "Surface-enhanced Raman scattering and fluorescence near metal nanoparticles," *Physical Review B*, vol. 72, no. 3, Article ID 035427, pp. 1–17, 2005.

[13] R. M. Stöckle, Y. D. Suh, V. Deckert, and R. Zenobi, "Nanoscale chemical analysis by tip-enhanced Raman spectroscopy," *Chemical Physics Letters*, vol. 318, no. 1–3, pp. 131–136, 2000.

[14] N. Hayazawa, Y. Inouye, Z. Sekkat, and S. Kawata, "Metallized tip amplification of near-field Raman scattering," *Optics Communications*, vol. 183, no. 1, pp. 333–336, 2000.

[15] B. Pettinger, B. Ren, G. Picardi, R. Schuster, and G. Ertl, "Nanoscale probing of adsorbed species by tip-enhanced Raman spectroscopy," *Physical Review Letters*, vol. 92, no. 9, Article ID 096101, 2004.

[16] P. J. Flory, "Conformations of macromolecules in condensed phases," *Pure and Applied Chemistry*, vol. 56, no. 3, pp. 305–312, 1984.

[17] G. Strobl, *The Physics of Polymers*, Springer, 2nd edition, 1997.

[18] H.-G. Elias, *An Introduction to Polymer Science*, Wiley-VCH, 2nd edition, 1997.

[19] A. M. Michaels, M. Nirmal, and L. E. Brus, "Surface enhanced Raman spectroscopy of individual rhodamine 6G molecules on large Ag nanocrystals," *Journal of the American Chemical Society*, vol. 121, no. 43, pp. 9932–9939, 1999.

[20] T. Vosgröne and A. J. Meixner, "Surface- and resonance-enhanced micro-raman spectroscopy of xanthene dyes: from the ensemble to single molecules," *ChemPhysChem*, vol. 6, no. 1, pp. 154–163, 2005.

[21] J. C. Tsang, J. E. Demuth, P. N. Sanda, and J. R. Kirtley, "Enhanced Raman scattering from carbon layers on silver," *Chemical Physics Letters*, vol. 76, pp. 54–57, 1980.

[22] A. Otto, "What is observed in single molecule SERS, and why?" *Journal of Raman Spectroscopy*, vol. 33, no. 8, pp. 593–598, 2002.

[23] A. Kudelski and B. Pettinger, "SERS on carbon chain segments: monitoring locally surface chemistry," *Chemical Physics Letters*, vol. 321, no. 5-6, pp. 356–362, 2000.

[24] A. Kudelski, "Some aspects of SERS temporal fluctuations: analysis of the most intense spectra of hydrogenated amorphous carbon deposited on silver," *Journal of Raman Spectroscopy*, vol. 38, no. 11, pp. 1494–1499, 2007.

[25] K. L. Norrod and K. L. Rowlen, "Removal of Carbonaceous Contamination from SERS-Active Silver by Self-Assembly of Decanethiol," *Analytical Chemistry*, vol. 70, no. 19, pp. 4218–4221, 1998.

[26] N. Félidj, J. Grand, G. Laurent et al., "Multipolar surface plasmon peaks on gold nanotriangles," *Journal of Chemical Physics*, vol. 128, no. 9, Article ID 094702, 2008.

[27] Q. Yu, P. Guan, D. Qin, G. Golden, and P. M. Wallace, "Inverted size-dependence of surface-enhanced Raman scattering on gold nanohole and nanodisk arrays," *Nano Letters*, vol. 8, no. 7, pp. 1923–1928, 2008.

[28] U. C. Fischer and H. P. Zingsheim, "Submicroscopic pattern replication with visible light," *Journal of Vacuum Science & Technology*, vol. 19, no. 4, pp. 881–885, 1981.

[29] J. C. Hulteen and R. P. van Duyne, "Nanosphere lithography: a materials general fabrication process for periodic particle array surfaces," *Journal of Vacuum Science & Technology A*, vol. 13, no. 3, pp. 1553–1558, 1995.

[30] C. L. Haynes and R. P. van Duyne, "Nanosphere lithography: a versatile nanofabrication tool for studies of size-dependent nanoparticle optics," *Journal of Physical Chemistry B*, vol. 105, no. 24, pp. 5599–5611, 2001.

[31] A. Sánchez-Iglesias, I. Pastoriza-Santos, J. Pérez-Juste, B. Rodríguez-González, F. J. García de Abajo, and L. M. Liz-Marzán, "Synthesis and optical properties of gold nanodecahedra with size control," *Advanced Materials*, vol. 18, no. 19, pp. 2529–2534, 2006.

[32] I. Pastoriza-Santos and L. M. Liz-Marzán, "Colloidal silver nanoplates. State of the art and future challenges," *Journal of Materials Chemistry*, vol. 18, no. 15, pp. 1724–1737, 2008.

[33] Y. Wang, P. H. C. Camargo, S. E. Skrabalak, H. Gu, and Y. Xia, "A facile, water-based synthesis of highly branched nanostructures of silver," *Langmuir*, vol. 24, no. 20, pp. 12042–12046, 2008.

[34] X. Lu, M. Rycenga, S. E. Skrabalak, B. Wiley, and Y. Xia, "Chemical synthesis of novel plasmonic nanoparticles," *Annual Review of Physical Chemistry*, vol. 60, pp. 167–192, 2009.

[35] U. Kreibig and M. Vollmer, *Optical Properties of Metal Clusters*, Springer, 1995.

[36] F. J. García-Vidal and J. B. Pendry, "Collective theory for surface enhanced Raman scattering," *Physical Review Letters*, vol. 77, no. 6, pp. 1163–1166, 1996.

[37] E. Hao and G. C. Schatz, "Electromagnetic fields around silver nanoparticles and dimers," *Journal of Chemical Physics*, vol. 120, no. 1, pp. 357–366, 2004.

[38] K. F. Gibson, D. Correia-Ledo, M. Couture, D. Graham, and J.-F. Masson, "Correlated AFM and SERS imaging of the transition from nanotriangle to nanohole arrays," *Chemical Communications*, vol. 47, no. 12, pp. 3404–3406, 2011.

[39] C. Farcau and S. Astilean, "Mapping the SERS efficiency and hot-spots localization on gold film over nanospheres substrates," *Journal of Physical Chemistry C*, vol. 114, no. 27, pp. 11717–11722, 2010.

[40] C. S. Sweetenham and I. Notingher, "Combined atomic force microscopy-Raman mapping of electric field enhancement and surface-enhanced Raman scattering hot-spots for nanosphere lithography substrates," *Journal of Nanophotonics*, vol. 5, no. 1, 2011.

[41] A. Naber, D. Molenda, U. C. Fischer et al., "Enhanced light confinement in a near-field optical probe with a triangular aperture," *Physical Review Letters*, vol. 89, no. 21, pp. 2108011–2108014, 2002.

[42] J. Koglin, U. C. Fischer, and H. Fuchs, "Material contrast in scanning near-field optical microscopy at 1-10 nm resolution," *Physical Review B*, vol. 55, no. 12, pp. 7977–7984, 1997.

[43] M. Rang, A. C. Jones, Z. Fei et al., "Optical Near-Field Mapping of Plasmonic Nanoprisms," *Nano Letters*, vol. 8, no. 10, pp. 3357–3363, 2008.

[44] E. M. Purcell and C. R. Pennypacker, "Scattering and absorption of light by nonspherical dielectric particles," *Astronomy Journal*, vol. 186, p. 705, 1973.

[45] B. T. Draine and P. J. Flatau, "Discrete-dipole approximation for scattering calculations," *Journal of the Optical Society of America A*, vol. 11, no. 4, pp. 1491–1499, 1994.

[46] M. A. Bryant and J. E. Pemberton, "Surface Raman scattering of self-assembled monolayers formed from 1-alkanethiols at silver [electrodes]," *Journal of the American Chemical Society*, vol. 113, pp. 3629–3637, 1991.

[47] P. Hildebrandt and M. Stockburger, "Surface enhanced resonance Raman study on fluorescein dyes," *Journal of Raman Spectroscopy*, vol. 17, p. 55, 1986.

[48] N. Nuntawong, M. Horprathum, P. Eiamchai, K. Wong-Ek, V. Patthanasettakul, and P. Chindaudom, "Surface-enhanced Raman scattering substrate of silver nanoparticles depositing on AAO template fabricated by magnetron sputtering," *Vacuum*, vol. 84, no. 12, pp. 1415–1418, 2010.

[49] M. W. Knight and N. J. Halas, "Nanoshells to nanoeggs to nanocups: optical properties of reduced symmetry core-shell nanoparticles beyond the quasistatic limit," *New Journal of Physics*, vol. 10, Article ID 105006, 2008.

[50] Y. A. Urzhumov, G. Shvets, J. Fan, F. Capasso, D. Brandl, and P. Nordlander, "Plasmonic nanoclusters: a path towards negative-index metafluids," *Optics Express*, vol. 15, no. 21, pp. 14129–14145, 2007.

[51] P. B. Johnson and R. W. Christy, "Optical constants of the noble metals," *Physical Review B*, vol. 6, no. 12, pp. 4370–4379, 1972.

[52] J. D. Jackson, *Classical Electrodynamics*, John Wiley & Sons, 3rd edition, 1999.

[53] J. I. Gersten, "The effect of surface roughness on surface enhanced Raman scattering," *The Journal of Chemical Physics*, vol. 72, no. 10, pp. 5779–5780, 1980.

[54] G. Socrates, *Infrared and Raman Characteristic Group Frequencies*, JohnWiley & Sons, 3rd edition, 2001.

[55] D. A. Long, *Raman Spectroscopy*, McGraw-Hill International Book Company, 1977.

[56] S. A. Meyer, E. C. L. Ru, and P. G. Etchegoin, "Quantifying resonant raman cross sections with SERS," *Journal of Physical Chemistry A*, vol. 114, no. 17, pp. 5515–5519, 2010.

[57] H. Xu, X. H. Wang, M. P. Persson, H. Q. Xu, M. Käll, and P. Johansson, "Unified treatment of fluorescence and Raman scattering processes near metal surfaces," *Physical Review Letters*, vol. 93, no. 24, Article ID 243002, 2004.

[58] J. R. Lakowics, *Principles of Fluorescence Spectroscopy*, Springer, 3rd edition, 2006.

[59] C. S. Levin, B. G. Janesko, R. Bardhan, G. E. Scuseria, J. D. Hartgerink, and N. J. Halas, "Chainlength-dependent vibrational resonances in alkanethiol self-assembled monolayers observed on plasmonic nanoparticle substrates," *Nano Letters*, vol. 6, no. 11, p. 2617, 2006.

[60] K. F. Domke, D. Zhang, and B. Pettinger, "Enhanced Raman spectroscopy: single molecules or carbon?" *Journal of Physical Chemistry C*, vol. 111, no. 24, pp. 8611–8616, 2007.

[61] K. Kneipp, H. Kneipp, I. Itzkan, R. R. Dasari, and M. S. Feld, "Ultrasensitive Chemical Analysis by Raman Spectroscopy," *Chemical Reviews*, vol. 99, no. 10, pp. 2957–2975, 1999.

[62] A. C. Ferrari and J. Robertson, "Interpretation of Raman spectra of disordered and amorphous carbon," *Physical Review B*, vol. 61, no. 20, pp. 14095–14107, 2000.

[63] H. Xu and M. Käll, "Surface-plasmon-enhanced optical forces in silver nanoaggregates," *Physical Review Letters*, vol. 89, no. 24, Article ID 246802, 2002.

[64] S. Xiao, N. A. Mortensen, and A. P. Jauho, "Nanostructure design for surface-enhanced Raman spectroscopy-prospects and limits," *Journal of the European Optical Society*, vol. 3, 2008.

[65] T. Huser, M. Yan, and L. J. Rothberg, "Single chain spectroscopy of conformational dependence of conjugated polymer photophysics," *Proceedings of the National Academy of Sciences of the United States of America*, vol. 97, no. 21, pp. 11187–11191, 2000.

[66] P. C. Andersen, M. L. Jacobson, and K. L. Rowlen, "Flashy silver nanoparticles," *Journal of Physical Chemistry B*, vol. 108, no. 7, pp. 2148–2153, 2004.

[67] H. P. Lu, "Site-specific Raman spectroscopy and chemical dynamics of nanoscale interstitial systems," *Journal of Physics Condensed Matter*, vol. 17, no. 7, pp. R333–R355, 2005.

[68] M. J. Walter, J. M. Lupton, K. Becker, J. Feldmann, G. Gaefke, and S. Höger, "Simultaneous Raman and fluorescence spectroscopy of single conjugated polymer chains," *Physical Review Letters*, vol. 98, no. 13, Article ID 137401, 2007.

Hindawi Publishing Corporation
Journal of Nanotechnology
Volume 2012, Article ID 961216, 10 pages
doi:10.1155/2012/961216

Research Article

Designing Gold Nanoparticle-Ensembles as Surface Enhanced Raman Scattering Tags inside Human Retinal Cells

Sanda Boca,[1] Dumitrita Rugina,[2] Adela Pintea,[2] Nicolae Leopold,[3] and Simion Astilean[1]

[1] *Nanobiophotonics and Laser Microspectroscopy Center, Institute for Interdisciplinary Research in Bio-Nano-Sciences and Faculty of Physics, Babes-Bolyai University, Treboniu Laurian 42, 400271 Cluj-Napoca, Romania*
[2] *Department of Biochemistry, University of Agricultural Sciences and Veterinary Medicine, Manastur 3-5, 400372 Cluj-Napoca, Romania*
[3] *Faculty of Physics, Babes-Bolyai University, Kogalniceanu 1, 400084 Cluj-Napoca, Romania*

Correspondence should be addressed to Sanda Boca, sanda.boca@phys.ubbcluj.ro

Received 10 January 2012; Accepted 15 February 2012

Academic Editor: Brian M. Cullum

Apart from the traditional development of surface-enhanced raman scattering (SERS) substrates for ultrasensitive spectroscopic analysis, an increasing interest is given nowadays to the design of the so-called SERS nanotags which integrate multiple SERS applications into single plasmonic nanoparticles. The fabrication of SERS tags is still a challenging task due to the complicated fabrication process. Typically, SERS tags are hybrid nanoconstructs consisting in a unique plasmonic nanoobject encoded with specific reporter molecules and enveloped in a protective shell that provides both biocompatibility and targeting function. Herein, we produce effective SERS tags consisting in small aggregates of gold nanoparticles (mainly dimers and trimers) which are captured from solution and then transferred into cells to perform as individual plasmonic nanostructures. Actually the small aggregates formed under controlled conditions are stabilized in solution by interlocking into a polymeric envelope made of thiol-modified poly(ethylene) glycol (PEG-SH). No further encoding operation is necessary in our case since part of ascorbic acid used as reducing agent remains attached in the interparticle junctions, providing persistent and strong SERS signal when the fabricated tags are internalized by human retinal cells. Our studies demonstrate a promising potential of new SERS-active nanoparticles to serve as effective reporters for biomedical tracing and imaging.

1. Introduction

The development of various strategies for the preparation of new optical labels as probes for detection and imaging has gained tremendous interest in the past years [1–4]. Among the investigation techniques, Raman spectroscopy presents real advantages due to the unambiguous identity of the encoded probe and the availability of a large pallet of reporter molecules [5]. Although Raman spectroscopy is reliable, the poor efficiency of Raman scattering (the cross-section is equal to 10^{-30} cm^2 molecule^{-1}) has limited its use in biomedical applications. Therefore the enhancement of the vibrational signal of the encoded molecule is required to improve the detection speed and sensitivity. In this context, surface-enhanced Raman scattering (SERS) spectroscopy proved to be a unique solution for the amplification of the vibrational signal by factors of 10^6 and even as high as 10^{14}-10^{15} in some cases [6, 7]. With such a large enhancement of Raman scattering, the use of SERS for imaging applications is an attractive alternative to fluorescence. Unlike fluorescent labels as are organic fluorophores and quantum dots, SERS-encoded probes, composed of a layer of Raman reporter molecules bound onto a metal nanoparticle, have the advantage of being resistant to photobleaching. This is due to the quenching of fluorescence excited states by the metal surface and to the short lifetime of Raman virtual energy states [8]. Furthermore, using SERS technique, different Raman reporters can be simultaneously excited with a single light source of choice (such as near-infrared light for human tissue) to achieve quantitative multiplexed detection [9]. These advantages confer to such SERS labels wide applicability in biomedical systems.

As stated above, the general strategy for designing SERS-encoded nanoparticles or SERS nanotags involves the attachment of one or multiple organic dyes as signature reporters onto a metal enhancer most usefully supplied in the form of a gold or silver nanoparticle, which is further encapsulated by a polymeric, biomolecular, or a glass shell for protection against aggregation and biocompatibilization. The literature is recently abundant with such encoded probes as for example the polymer-stabilized gold nanoparticles reported by Merican et al. [10], protein-capped composite organic-inorganic nanoparticles described by Su et al. [11], silica embedded core-shell nanoparticles reported by Mulvaney et al. [12], or silica-encapsulated Au/Ag nanoshells described by Küstner et al. [13]. More recently an increased attention was given to the implementation of improved substrates for SERS nanoprobes such as anisotropic or multibranched nanoparticles, which exhibit strong plasmon resonances close to the NIR window of biological transparency and, particularly, high electromagnetic field localized at their protrusions [14–16]. Our group succeeded to demonstrate the efficiency of such dye-encoded multi-branched flower-shaped nanoparticles as SERS tags inside living cells [17]. The SERS nano-tags were designed using malachite green oxalate and basic fuchsin as Raman-active molecules and protected against aggregation with thiol-modified poly(ethylene) glycol polymer. As-prepared nanotags were found to be highly stable, to be SERS detectable inside living cells under 633 nm laser excitation, and to present low *in vitro* toxicity when tested inside the cytosol of a line of epithelial cells from human retina.

In this paper, we extend our research and present a new class of nano-tags consisting of gold nanoparticle ensembles (i.e., dimers, trimers, and small aggregates of spherical particles) with real potential to act as SERS-active tags inside living cells. The particles were fabricated by an alternative method of the commonly Turkevich-Frens synthesis, by the use of ascorbic acid as reducer of the gold salt [18]. Notably, this class of nanoparticles does not require any supplementary operation of encoding since ascorbic acid remains attached in between nanoparticles and give a persistent and strong SERS signal when nano-tags are internalized by cells. Therefore we expect that our tags present higher biocompatibility than SERS tags marked with potentially toxic, Raman-active organic dyes. Moreover, our fabrication strategy for the assembly of AuNPs differs from most of the reported techniques which involve crosslinking molecules, like alkanethiols [19, 20], surfactants [21], specific proteins [22], and oligonucleotides [23] and most often destabilizing species like salt or ethanol [24], which might further interfere with the intrinsic particles signal. Herein thiol-modified PEG, a nontoxic, hydrophilic polymer, commonly used to improve particles stability, biocompatibility, and their systemic retention [25], is used for multiple purposes: to link the particles between them and stabilize the formed nanoensembles. To the best of our knowledge, no other reports demonstrate SERS-active tags with high and reproducible intrinsic signal coming from the reducing agent used in particle synthesis. The signal reproducibility in simulated body fluid salted solution, and *in vitro* measurements on human retinal cells highlight the potential of such SERS-active nanoparticles to serve as biomedical imaging tools.

2. Experimental Section

2.1. Chemicals and Materials. Hydrogen tetrachloroaurate (III) trihydrate ($HAuCl_4 \cdot 3H_2O$) was purchased from Sigma-Aldrich (Germany). Analytical-grade L-ascorbic acid ($C_6H_8O_6$) was obtained from Reactivul (Romania). α-Methoxy-ω-mercapto poly(ethylene glycol) (mPEG-SH) of molecular weight 5 kDa was obtained from Iris biotech GmbH (Germany). GIBCO Dulbecco's Modified Eagle's Medium (DMEM) was purchased from Invitrogen (Carlsbad, California, USA). Fetal bovine serum, penicillin, streptomycin, amphotericin B, and 3-(4,5-dimethylthiazol-2-yl)-2,5-diphenyltetrazolium bromide (MTT) were purchased from Sigma (St. Louis, USA). Dimethyl sulfoxide, sodium pyruvate, and all the others chemicals used were of analytical grade and supplied from Merck (Germany). The other reagents used through the experiments were analytical grade and used without further purification. Distilled deionized water (ddH_2O) was used in all aqueous solutions and rinsing procedures.

2.2. Preparation of PEG-Protected Gold Nanoparticle Ensembles. All glassware used in the synthesis was cleaned in a bath of freshly prepared aqua regia solution (3 : 1 (v/v) HNO_3 : HCl) and rinsed thoroughly prior to use. The colloidal gold nanoparticles were synthesized based on a method described elsewhere in detail [18]. Briefly, individual nanoparticles were produced by stirring 10 mL of a solution of $0.5 \cdot 10^{-3}$ M tetrachloroauric acid ($HAuCl_4$) at room temperature for several minutes, followed by the addition of a proper volume of a freshly prepared ascorbic acid ($7.5 \cdot 10^{-3}$ M) solution. Herein, tetrachloroauric acid trihydrated ($HAuCl_4 \cdot 3H_2O$) has a role of nanoparticle initiator while L-ascorbic acid is used as reducer of the gold salt. When the two reactive solutions were mixed, the yellow pale dispersion rapidly turned colorless, dark blue and finally pinkish red. This color transition indicated the reduction of the Au^{3+} ions to gold atoms which undergo nucleation and form the colloidal nanoparticles by diffusional growth.

For designing gold nanoparticles aggregates, increasing volumes of 10^{-6} M mPEG-SH solution (20 μL, 50 μL, and 100 μL) were added to the colloidal solution by dripping and let to sit for several minutes. The ratio between the colloid and polymer solution and the incubation time were carefully chosen so that small aggregates (two to several nanoparticles) would be first formed. Excess polymer stabilized the formed ensembles of nanoparticles. Before being incubated in living cells, the as-prepared probes were purified by centrifugation at low speed.

2.3. Equipments Used for Samples Characterization. Optical extinction spectra were measured with a Jasco V-670 spectrophotometer over a spectral range between 400 and 1000 nm and a spectral resolution of 2 nm. The mean diameter of gold nanoparticles was determined by transmission

electron microscopy (TEM) imaging using a JEOL model JEM1010 microscope. SERS spectra of gold nanoparticles and PEG-capped nanoensembles in aqueous solution were recorded using for excitation NIR (785 nm) laser line from a diode laser using a portable Raman spectrophotometer (R-3000CN from Raman Systems) with 1 cm^{-1} spectral resolution and an integration time of 10 sec. SERS spectra of nanoparticle ensembles inside living cells were recorded using the 633 nm laser line of a He-Ne laser. The 633 nm He-Ne laser delivered a power of 3 mW through a 100x objective (NA = 0.9) of a confocal Raman microscope alpha 300R from WITEC.

2.4. Cell Culture and MTT Viability Assay. Human adult retinal pigment epithelial cells D407 were maintained in Dulbecco's modified eagle medium supplemented with 10% fetal bovine serum, 1 mM sodium pyruvate, 100 U/mL penicillin, 100 μg/mL streptomycin, and 2.5 μg/mL amphotericin B, at 37°C, 5% CO_2, and 95% relative humidity. The cells were seeded in 96 well-plates at a concentration of 1×10^4. After reaching 90% confluence, growth medium was removed and the cells were incubated for 24 h with uncoated nanoparticles (GNPs) and PEGylated gold ensembles (PEG-GENs) by varying the colloidal concentration between 0.3×10^{-11} M and 6×10^{-11} M. The tetrazolium salt was used to quantify living metabolically active cells, based upon the principle that MTT (3-(4,5-dimethylthiazol-2-yl)-2,5-diphenyltetrazolium bromide) is metabolized by mitochondrial dehydrogenase to form a formazan dye. Thereby the end product was measured at a wavelength of 550 nm with background wavelength at 690 nm, with a microplate plate reader HT BioTek Synergy (BioTek Instruments, USA). Briefly, the cells were washed with PBS, and 200 μL MTT solutions in HBSS buffer were added to each well. After 2 h of incubation the MTT reagent was removed and the formazan particles were solubilized with 200 μL DMSO. Viability was expressed as the percentage of actively proliferative cells, and subsequently a relationship between viability and treatment concentrations was plotted as shown in Figure 6. Statistical analysis was conducted using the Tukey multiple comparison test of Graph Pad Prism version 5.00. Data are presented as means and standard errors of the mean (SEM). (*Significant $P < 0.05$, **very significant $P < 0.01$.)

3. Results and Discussion

3.1. Characterization of Gold Nanoparticle Ensembles and Probing Their SERS Activity. The normalized extinction spectrum of as-prepared gold nanoparticles, the building blocks of gold nanoparticle ensembles, is illustrated in Figure 1 (spectrum a) and presents a plasmon resonance band at 540 nm. When few μL of mPEG-SH polymer were added to the colloidal solution, the plasmon peak red-shifted by 3 nm, which is consistent with an increase of the refractive index surrounding the nanoparticles, due to the polymeric capping (magnified image, Figure 1). Together with the observed shift, a slight broadening of the plasmon band occurred and a secondary, smaller-intensity band appeared,

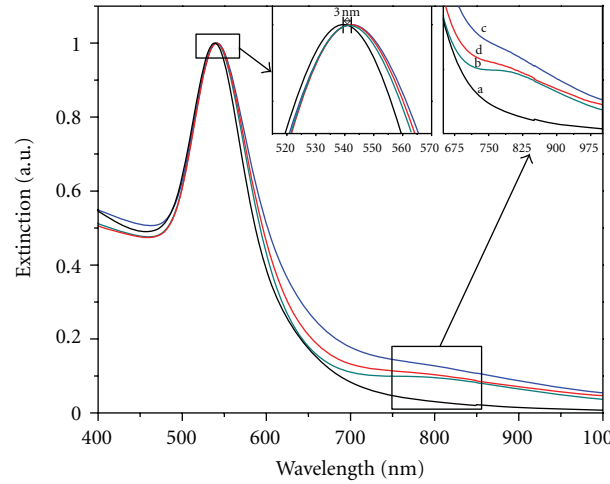

Figure 1: Normalized extinction spectra of individual gold nanoparticles (spectrum a) and of PEGylated gold nano-ensembles obtained by the addition of: 20 μL (spectrum b), 50 μL (spectrum c) and 100 μL (spectrum d), of mPEG-SH polymer into the colloidal solution.

situated at about 800 nm which indicates the formation of few nanoparticle aggregates in the colloidal solution. Further increasing the ratio between the polymer and the colloidal solution determined the broadening of both main (543 nm) and secondary (800 nm) plasmonic band (spectra c and d in Figure 1). Afterward, no more red shift of the main plasmonic band was observed, demonstrating that individual PEGylated nanoparticles were completely capped by the polymer. When the maximum concentration of the polymer was added to the colloidal nanoparticles, the band corresponding to ensembles of nanoparticles featured only negligible red shift, indicating that further aggregation was inhibited and the formed PEG-GENs remained in that aggregation state thereafter. The small intensity drop of the plasmon band observed for this later sample is only caused by the dilution and not by the sedimentation of the aggregates.

The particles morphology and the formation of particle-ensembles were subsequently confirmed by TEM measurements. According to Figure 2(a), as-prepared colloids contain mainly individual, spherical nanoparticles, having a mean diameter of 50 nm. Colloids with added PEGs presented also dimers, trimers, and small clusters (Figures 2(b), 2(c), and 2(d)) which are surrounded by a faint uniform layer of approximately 3 nm of PEG polymeric chains. The clusters of up to five nanoparticles (less than 300 nm) are suitable for intracellular detection due to their small sizes, capable to penetrate through the membrane of a living cell. Moreover, such nanoparticle arrangements in small aggregates are responsible for the strong electromagnetic fields (hot spots) in which trapped Raman-active molecules have scattering signals increased up to 10^{14}.

The general strategy to fabricate SERS-active nano-tags consists in selecting a molecule with a strong Raman signal and binding the selected molecule to a noble metal nanoparticle of suitable optical response [26]. Usually polymers are further involved in that design, in order to increase both

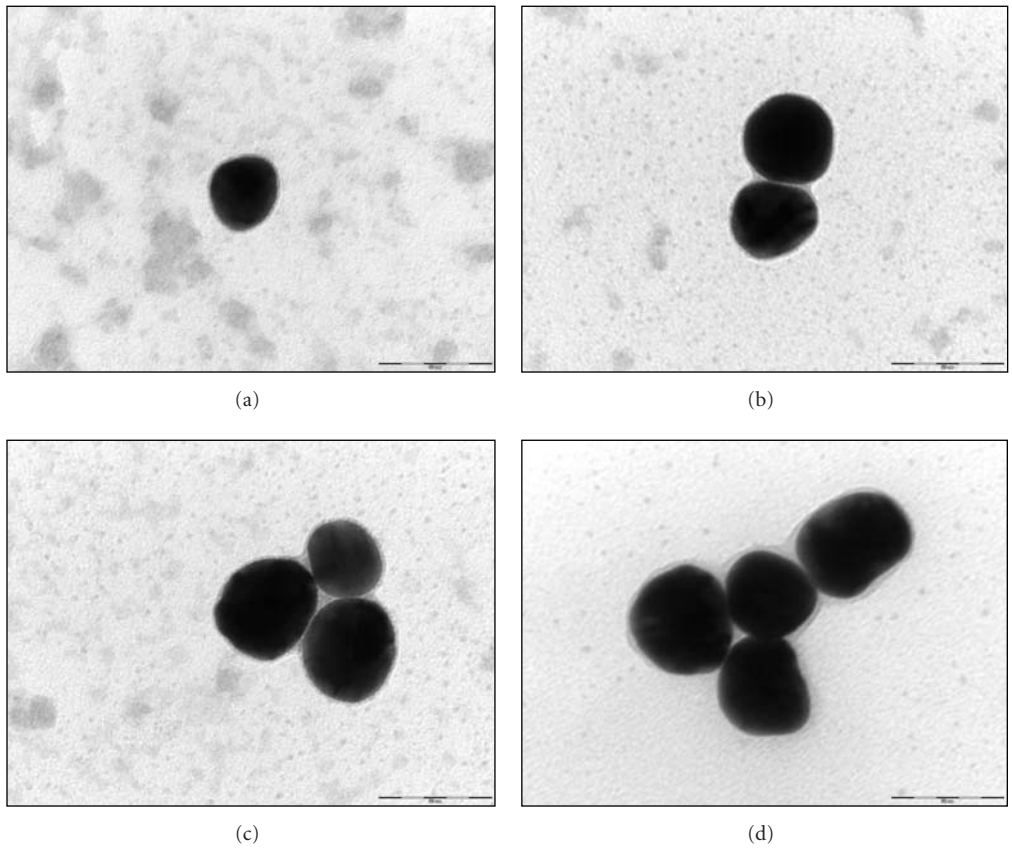

Figure 2: TEM images of single (a), dimer (b), trimer (c), and a small cluster of spherical gold nanoparticles. Scale bar 50 nm.

nanoparticle stability and biocompatibility. For isolated solid spherical Au or Ag nanoparticles with smooth surfaces, the SERS enhancements are reported to be pretty low, with the enhancement factors on the order of 10^3 [27]. Therefore, nanoparticles with bumps and cavities like stars, meatball-like or flower-shaped, were preferred because the localized near-field enhancements on the tip of nanoscale bumps or inside tiny cavities provide SERS enhancements that are significantly larger than those achievable on a solid spherical particle with a smooth surface. Nearly adjacent nanoparticles with nanoscale gaps have been shown to serve as efficient and extremely sensitive SERS substrates [28, 29]. One of the main attributes of such nanoprobes lies in the electronic coupling between the particles which leads to many new properties [30]. For example, this coupling effect has been widely accepted as the cause of the so-called "hot spots" or areas of highly intense electromagnetic fields upon plasmonic excitation in which the efficiency of surface-enhanced Raman scattering (SERS) is dramatically increased [31].

To probe the SERS activity of PEG-GENs, we excited the nano-ensembles in aqueous solution with 785 nm NIR laser line. This excitation wavelength superposes the characteristic plasmon band of the PEG-GENs and also provides maximum light penetrability for further application in biological media such are cells and tissues [32]. We also investigated on which extent the concentration of PEG polymer affects the SERS fingerprint of such nano-ensembles, and we correlated the obtained spectra with the PEG-GENs size and morphology.

SERS spectra of the formed nano-ensembles obtained with increasing concentrations of PEG-SH are illustrated in Figure 3, and the band assignments can be found in Table 1. SERS spectrum of nanospheres (spectrum b) in aqueous solution and Raman spectrum of pure L-ascorbic acid (spectrum a) were also recorded to serve for comparison. The SERS spectra of PEG-GENs (spectra c, d, e) present characteristic vibrational bands of the ascorbic acid molecules. No signal from the PEG polymeric layer is observed which is in agreement with other reports from the literature [33]. Meaningful variations of bands intensities are observed between the three probes, which we correlate with the aggregation degree of individual gold nanoparticles, hence the size and morphology of the nanoaggregates. PEG-GENs prepared with the highest concentration of PEG present the highest SERS signal. We speculate that part of the thiolated polymeric chains links the particles between them when added to the colloidal solution, contributing to the formation of the nano-aggregates, while the polymer in excess stabilizes the formed nano-ensembles, and therefore the SERS signal is conserved.

Few band positions differences from one sample to another are also detected, mostly at higher wave numbers

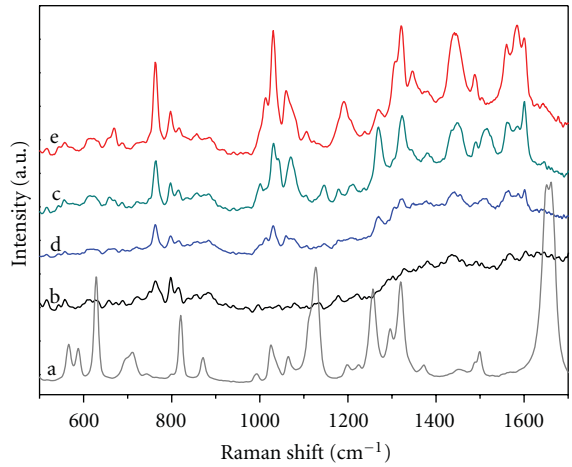

Figure 3: Raman spectrum of solid pure L-ascorbic acid (scaled by factor 0.25)(spectrum a). SERS spectrum of individual gold nanospheres in solution recorded under NIR excitation (spectrum b). SERS spectra of PEG-GENs obtaine with increasing volumes: 20 μL (spectrum c), 50 μL (spectrum d), and 100 μL (spectrum e) mPEG-SH, recorded under NIR excitation.

(1200–1800 cm^{-1}), which arise from different ascorbic acid molecular orientations on the particles surface. A variation of cluster geometry is also responsible for different arrangements of the adsorbed molecules in the formed gaps between particles. The ratios between the intensities of specific vibrational bands such as 1030 cm^{-1} (C–O–H bend) and 1061 cm^{-1} (C–O–C str), 1322 cm^{-1} (C–H bend) and 1270 cm^{-1}, 1488 cm^{-1} (C–H bend) and 1504 cm^{-1} (C–H bend) modify and a triplet band situated at 1584 cm^{-1} appears instead of the intense doublet at 1656 cm^{-1} (C=C str in ring) in the Raman spectrum of pure ascorbic acid. An early study regarding the Raman spectra of ascorbic acid and its related compounds reported by Edsall and Sagall assigns this band to the ascorbate anions of the dissociated ascorbic acid [34]. Herein, this extra band at 1584 cm^{-1}, together with the disappearance of the vibrational bands characteristic to the C=C str in the lactone ring after 1650 cm^{-1} lead us to infer that the SERS spectra of PEG-GENs are assigned in fact to the doubly oxidized, more stable form of the ascorbic acid, dehydroascorbic acid. This stable form arises as a consequence of the ascorbic acid degradation by oxidization in the presence of metal ions, during the nanoparticles synthesis. These molecules are further adsorbed onto nanoparticles surface and then captured in the gaps between nanoparticles through the influence of the polymer, giving rise to strong SERS signal when excited by NIR laser light. Therefore, we demonstrated that we can design PEG-nano-ensembles that are capable to give intrinsic SERS signal in solution without necessitating the addition of supplementary Raman active molecules, potentially toxic to bioenvironments. We mention that the SERS signal is conserved after sample purification while no signal was obtained from individual, as prepared, uncoated nanoparticles in the colloidal suspension (spectrum b in Figure 3).

Table 1: Raman and SERS bands of L-ascorbic acid and their vibrational assignment

Raman	SERS	Vibrational assignment[a]
743w	763s	O–H out of plane def.
798sh	800	O–H out of plane def.
820s	819	C=C str in ring
87 m	883	C=C str in ring
993w	1012	C–H bend; O–H bend
1025m	1030	C–O–H bend
1064w	1061	C–O–C str.
1128vs	1190	C–O–C str.
1198w	1211	C–C(=O)–O str.
1225w		
1256s		C–O–C bend+tw
1295m	1270	
1319s	1322	C–H bend
1372w	1380	C–O–H bend+ CH_2 w
1451w	1441s	C–H bend+ CH_2 sc
1489w	1488m	C–H bend
1498 m	1504w	C–H bend
1656s split	1584 triplet	C=C str in ring

[a] References [34–36].

3.2. Chemical Stability of PEG-GENs in Simulated Biological Fluid. One important requirement for any probe to be used inside living organisms is that it has to retain its properties in salted media as is the cellular medium. Moreover, the investigated probe must provide efficient and distinctive readout (e.g., SERS signal) in these specific conditions. To test the chemical stability of the prepared ensembles and evaluate the protection degree of the PEG shell, we first measured optical extinction spectra of PEG-GENs after the addition of a high molarity solution of sodium chloride, known to induce particle aggregation in the case of unprotected gold colloids [37]. The obtained results were compared with that of uncoated nanoparticles.

Figure 4 illustrates the extinction spectra of uncoated, as-prepared nanoparticles (black curves) and of PEG-GENs obtained with various amounts of PEGs (colored curves) in the absence (full lines) and in the presence (dashed lines) of chloride ions. The appearance of the plasmon resonance band in the case of uncoated nanoparticles was visibly altered after the addition of salt. The peak position shifted to longer wavelengths by several nm, and a secondary band at about 900 nm rapidly developed, demonstrating that, in the absence of PEG protection, the gold nanoparticles rapidly aggregate. Monitored, these aggregated nanoparticles turned into irreversible sediments within hours.

PEG-GENs obtained with low concentration of PEG polymer showed similar behavior with that of unprotected particles. The ratio between the intensity of main plasmonic band at 543 nm and that of the band specific to nanoclusters

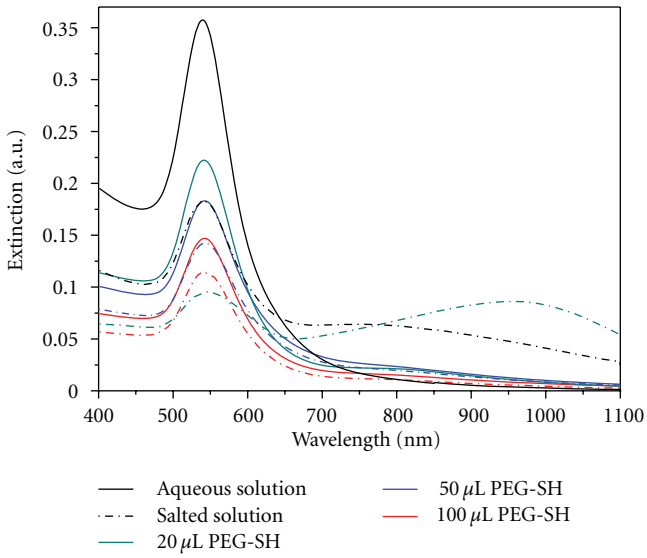

Figure 4: Extinction spectra of gold nanospheres ((GNSs) black line) and of PEGylated gold nanoensembles ((PEG-GENs) colored lines) recorded in the absence (thick lines) and in the presence (dotted lines) of 1 M NaCl solution.

rapidly decreased, due to the formation of more and larger aggregates in the colloidal solution. An increase of PEG polymer concentration contributed to a visible stabilization of the formed GENs, as can be observed from the presented spectra (blue and red curves in Figure 4), which maintained a constant position and band shape, even in the presence of the supplementary aggregation agent. The small drop observed in the extinction intensity is attributed to the sample dilution, caused by the addition of the salted solution. Although slight precipitation might occur after the sample is being kept for a longer time, the sediment can be easily redispersed by sonication.

We further tested the SERS signal stability in the presence of Cl^-ions of the PEG-GENs (Figures 5(b) and 5(c)). Uncoated, individual GNPs (Figure 5(a)) were tested in similar conditions. We found that for both uncoated nanoparticles and for nanoensembles prepared with low concentration of PEG the SERS signal increased after the addition of salt. We corroborate this result with an over-aggregation of the particles, which lack sufficient PEG protection. Although aggregation substantially enhances SERS [38], from an imaging or sensing application standpoint uncontrolled aggregation is undesirable since the resultant SERS signal fluctuates. Moreover large aggregates hardly can penetrate cellular membrane, impeding any use of the particles for *in vivo* applications. In the case of PEG-GENs prepared with higher polymeric concentration, the SERS signal remains almost steady after the addition of sodium chloride (Figure 5(d)). The minor intensity changes might be caused by the modification of the reporter molecules orientation on the gold surface [39]. In our design, the thiol-PEG layer maintains the ascorbate molecules adsorbed onto nanoparticle surface, by steric stabilization. Moreover, the result demonstrates that PEG not only protects the formed ensembles from further aggregation but also controls their aggregation degree by inhibiting the cohesion between particles.

3.3. Viability of D407 Cells Incubated with Nanoparticle Ensembles. The effect of nano-tags toward cell viability was tested using MTT assay. The obtained results were compared with that of uncoated nanoparticles and that of the supernatant solution. The cell survival in the presence of the selected probes is plotted in Figure 6. For all the incubated samples, cells' viability and proliferation are highly dependent on particle concentration. Cells incubated with PEG-GEN have a high (80%) survival rate for nanoparticles concentration maintained up to 2.4×10^{-11} M, after which a steady decrease of cell viability is observed. Significant toxicity for the cells (less than 40% from the total number of cells remain viable after 24 h) appears only for the highest nanoparticle concentration (6×10^{-11} M). At this high concentration bare GNPs gave better survival rate while supernatant was proved to be more cytotoxic than the prepared PEG GENs nano-tags. From the class of hydrophilic polymers used as stabilizing agents for various types of nanoparticles, PEG polymer was generally proved to be biologically inert [40]. Moreover, PEG and PEG-derivatives were largely involved in detoxifying nanoparticles such are for example CTAB-toxic gold nanorods towards use in cellular environment [41, 42]. Bearing this in mind, the increased biocompatibility of naked nanoparticles compared to that of SERS nanotags might appear intriguing. To explain this, we infer a different mechanism of delivery through cells for the two types of nanoprobes. Naked nanoparticles lacking the protection of the PEG coating would aggregate in salted cellular medium forming big clusters, which are unable to penetrate the cellular membrane and therefore would not be delivered through cells. PEG-stabilized nanoensembles on the other hand would be delivered to the cellular compartments in greater amount causing slight toxicity but only at high nanoparticle concentration. The effect of supernatant solution containing only unbound polymer and unreduced gold ions also sustains the above hypothesis.

3.4. PEG-GENs as SERS Tags inside Living Cells. Surface-enhanced Raman scattering is a highly sensitive spectroscopic technique that has been imposed as a convenient and attractive alternative to fluorescence for detection and imaging applications inside living cells [43]. Despite the unique advantages offered by SERS, the huge amount of molecules found in cell cytoplasm is often an impediment towards the extraction of relevant biological information. Moreover, lack of signal reproducibility might occur due to a common tendency of nanoparticles to aggregate in buffer solutions or serum. Although substantial enhancement of SERS is obtained if nanoparticles aggregate, from an imaging and detection standpoint, such phenomenon is hardly desirable, since aggregation cannot be controlled and the resultant SERS signal fluctuates. Also big aggregates hardly can enter the cellular membrane. Recently, more sensitive nano-tags were developed by encapsulating organic dyes as signature reporter molecules between gold nanoparticles and

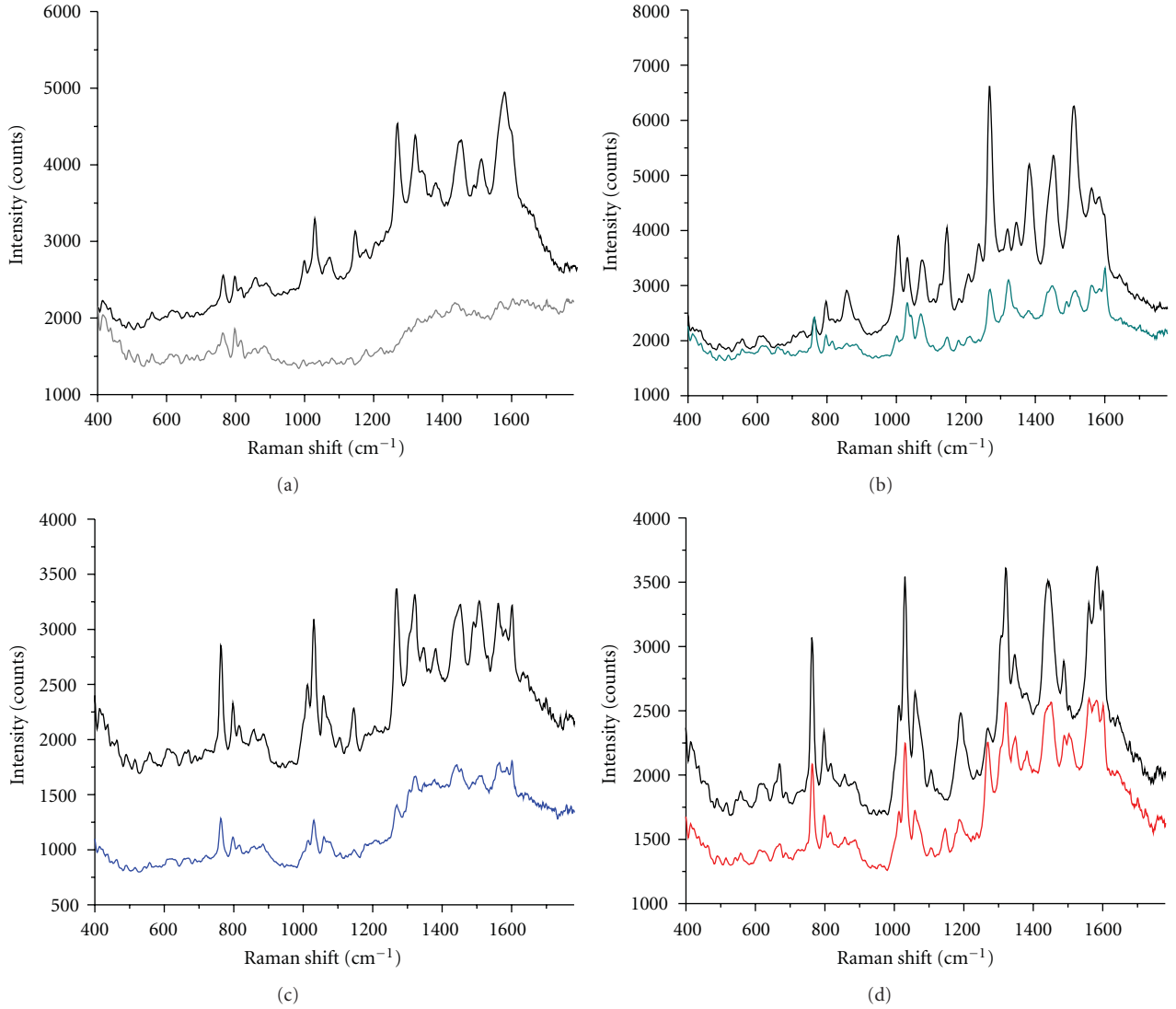

Figure 5: Raman spectrum of gold nanospheres (a) and SERS spectra of PEG-GENs prepared with increasing volumes: 20 μL (b), 50 μL (c), and 100 μL (d) of mPEG-SH polymer, recorded in solution, under NIR excitation. Black spectra are taken in the presence of 1 M salted solution while colored spectra represent the spectra of the nano-probes before the addition of salt.

a polymeric shell for biocompatibilization and stabilization. Such active tags are able to trigger specific phenomena inside cells or can be bound to desired cellular organelles [44, 45].

To determine whether SERS spectra can be acquired from ascorbate-tagged, PEG-protected GENs buried inside cells, we incubated D407 cells with the particles for 24 hours and recorded SERS spectra of tagged nano-probes inside cells. The first optical evaluations of the cellular samples indicate an intracytoplasmic and endoplasmatic reticulum distribution of the probes (Figure 7(a)). The predominant distribution pattern is nearby the nucleus, without triggering any particles in the nuclear region.

SERS detection of the nano-probes inside living cells followed the microscopic visualisation. SERS spectra which highly resemble the Raman-encoded particles signature in solution were obtained at positions in the cells where the particles were located as can be seen in Figure 7(b) (spectrum c). Apart from vibrational bands specific to ascorbic acid reporter molecules, intense SERS bands (the bands marked by asterisks in spectrum c) are also observed in the case of PEGylated GENs inside cells at 672 cm^{-1}, 848 cm^{-1}, and in the 1150–1250 cm^{-1} fingerprint region. These bands can be attributed to phospholipids and cellular proteins (C–C skeletal stretch in proteins and amide III/β-sheet resp.) which intercalate the polymeric chains and adsorb onto some of the nanoparticles surface [43, 46]. Moreover, specific bands (1004 cm^{-1} phenylalanine: ring breathing, 1320 cm^{-1} adenine/proteins: ring stretching/twisting (CH_2, CH_3), 1491 cm^{-1} proteins: deformation (CH_2, CH_3)) superimpose those of the reporter molecules. Therefore, we can fairly assert that the recorded spectra are composite spectra combining the response of encoding ascorbate molecules and cellular constituents. No Raman signal could be obtained from cells in the absence of nanoparticles (spectrum a in

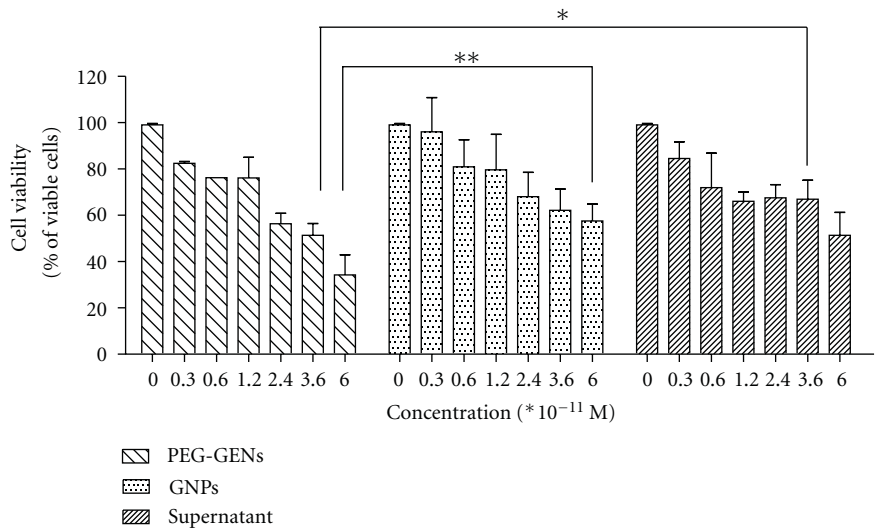

Figure 6: MTT test of epithelial cells from human retina (D407 cells viability (%)) treated with various concentrations of PEG-GENs and GNPs. The effect of supernatant onto cell viability is also presented. Data are presented as means and standard errors of the mean (SEM): *significant $P < 0.05$, **very significant $P < 0.01$.

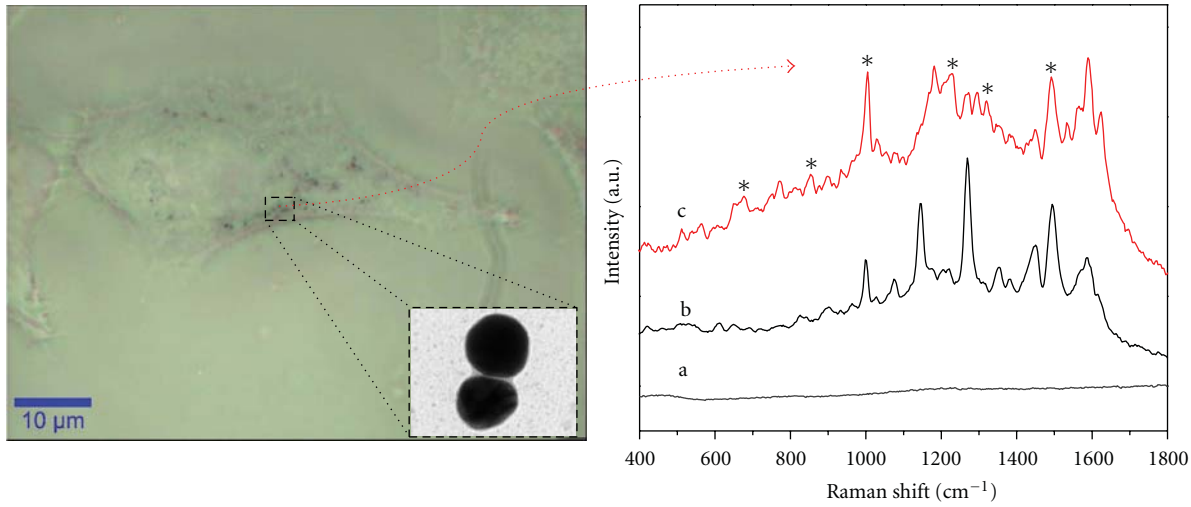

Figure 7: Optical microscopy image of a D407 cell loaded with ascorbate-encoded PEG-GENs (a). SERS spectra of as prepared PEG-GENs in aqueous solution (spectrum b in (b)) and inside the cell (spectrum c in (b)) recorded under 633 nm laser line excitation. The asterisks above spectrum c indicate vibrational modes that correspond to cellular components. Spectrum a in (b) represents the Raman spectrum of an individual cell in the absence of nanoparticles, as control.

Figure 7(b)). The above results demonstrate that our PEG-GENs with intrinsic signal from ascorbic acid drug molecules have the advantage of providing readable SERS response inside cells without involving the aid of any supplementary molecules, potentially toxic to cells.

4. Conclusions

This work presents a new class of SERS-active tags consisting of PEG-protected gold nanoparticles ensembles (PEG-GENs) encoded with trace of ascorbic acid which was previously used as reducing agent in the nanoparticle synthesis. We found that PEG-SH polymer does not only stabilize individual nanoparticles in solution but can also capture, interlock, and stabilize a few number of nanoparticles as dimers, trimers, and small aggregates. The fabrication of SERS tags presents the advantage of easy, single-step encoding procedure by exploiting the presence of ascorbic acid in solution during nanoparticle formation. The PEG-GENs retain both the spectroscopic identity of ascorbic acid and optical activity of aggregates, both in saline solution and inside living cells, without interfering too much with cellular functions. Notably, the polymer coating provides not only good biocompatibility with biological media but exhibits

chemical availability for implementing specific targeting functions.

Acknowledgments

This work was supported by the CNCS-UEFISCDI, Project number PNII-ID_PCCE_129/2008. The authors are grateful to Dr. Lucian Barbu Tudoran for TEM measurements.

References

[1] D. C. Pregibon, M. Toner, and P. S. Doyle, "Multifunctional encoded particles for high-throughput biomolecule analysis," *Science*, vol. 315, no. 5817, pp. 1393–1396, 2007.

[2] J. Yang, M. P. Sena, and X. Gao, "Quantum dot-encoded fluorescent beads for biodetection and imaging," *Reviews in Fluorescence*, vol. 2007, pp. 139–156, 2009.

[3] K. B. Cederquist, S. L. Dean, and C. D. Keating, "Encoded anisotropic particles for multiplexed bioanalysis," *Wiley Interdisciplinary Reviews: Nanomedicine and Nanobiotechnology*, vol. 2, no. 6, pp. 578–600, 2010.

[4] K. T. Thurn, E. M. B. Brown, A. Wu et al., "Nanoparticles for applications in cellular imaging," *Nanoscale Research Letters*, vol. 2, no. 9, pp. 430–441, 2007.

[5] R. A. Alvarez-Puebla and L. M. Liz-Marzán, "SERS-based diagnosis and biodetection," *Small*, vol. 6, no. 5, pp. 604–610, 2010.

[6] R. F. Aroca, *Surface-Enhanced Vibrational Spectroscopy*, John Wiley & Sons, New York, NY, USA, 2006.

[7] M. Moskovits, "Surface-enhanced Raman spectroscopy: a brief retrospective," *Journal of Raman Spectroscopy*, vol. 36, no. 6-7, pp. 485–496, 2005.

[8] X. Qian, X. H. Peng, D. O. Ansari et al., "In vivo tumor targeting and spectroscopic detection with surface-enhanced Raman nanoparticle tags," *Nature Biotechnology*, vol. 26, no. 1, pp. 83–90, 2008.

[9] A. Matschulat, D. Drescher, and J. Kneipp, "Surface-enhanced Raman scattering hybrid nanoprobe multiplexing and imaging in biological systems," *ACS Nano*, vol. 4, no. 6, pp. 3259–3269, 2010.

[10] Z. Merican, T. L. Schiller, C. J. Hawker, P. M. Fredericks, and I. Blakey, "Self-assembly and encoding of polymer-stabilized gold nanoparticles with surface-enhanced Raman reporter molecules," *Langmuir*, vol. 23, no. 21, pp. 10539–10545, 2007.

[11] X. Su, J. Zhang, L. Sun et al., "Composite Organic-Inorganic Nanoparticles (COINs) with chemically encoded optical signatures," *Nano Letters*, vol. 5, no. 1, pp. 49–54, 2005.

[12] S. P. Mulvaney, M. D. Musick, C. D. Keating, and M. J. Natan, "Glass-coated, analyte-tagged nanoparticles: a new tagging system based on detection with surface-enhanced Raman scattering," *Langmuir*, vol. 19, no. 11, pp. 4784–4790, 2003.

[13] B. Küstner, M. Gellner, M. Schütz et al., "SERS labels for red laser excitation: silica-encapsulated SAMs on tunable gold/silver nanoshells," *Angewandte Chemie—International Edition*, vol. 48, no. 11, pp. 1950–1953, 2009.

[14] T. Wang, X. Hu, and S. Dong, "Surfactantless synthesis of multiple shapes of gold nanostructures and their shape-dependent SERS spectroscopy," *Journal of Physical Chemistry B*, vol. 110, no. 34, pp. 16930–16936, 2006.

[15] C. Hrelescu, T. K. Sau, A. L. Rogach, F. Jäckel, and J. Feldmann, "Single gold nanostars enhance Raman scattering," *Applied Physics Letters*, vol. 94, no. 15, Article ID 153113, 2009.

[16] G. H. Jeong, Y. W. Lee, M. Kim, and S. W. Han, "High-yield synthesis of multi-branched gold nanoparticles and their surface-enhanced Raman scattering properties," *Journal of Colloid and Interface Science*, vol. 329, no. 1, pp. 97–102, 2009.

[17] S. Boca, D. Rugina, A. Pintea, L. Barbu-Tudoran, and S. Astilean, "Flower-shaped gold nanoparticles: synthesis, characterization and their application as SERS-active tags inside living cells," *Nanotechnology*, vol. 22, no. 5, Article ID 055702, 2011.

[18] S. C. Boca, M. Potara, F. Toderas, O. Stephan, P. L. Baldeck, and S. Astilean, "Uptake and biological effects of chitosan-capped gold nanoparticles on Chinese Hamster Ovary cells," *Materials Science and Engineering C*, vol. 31, no. 2, pp. 184–189, 2011.

[19] M. G. Bellino, E. J. Calvo, and G. Gordillo, "Adsorption kinetics of charged thiols on gold nanoparticles," *Physical Chemistry Chemical Physics*, vol. 6, no. 2, pp. 424–428, 2004.

[20] A. Hofmann, P. Schmiel, B. Stein, and C. Graf, "Controlled formation of gold nanoparticle dimers using multivalent thiol ligands," *Langmuir*, vol. 27, no. 24, pp. 15165–15175, 2011.

[21] L. Sun, D. Zhao, M. Ding et al., "Controllable synthesis of silver nanoparticle aggregates for surface-enhanced raman scattering studies," *Journal of Physical Chemistry C*, vol. 115, no. 33, pp. 16295–16304, 2011.

[22] M. Ringler, T. A. Klar, A. Schwemer et al., "Moving nanoparticles with Raman scattering," *Nano Letters*, vol. 7, no. 9, pp. 2753–2757, 2007.

[23] D. B. Lukatsky and D. Frenkel, "Surface and bulk dissolution properties, and selectivity of DNA-linked nanoparticle assemblies," *The Journal of chemical physics*, vol. 122, no. 21, Article ID 214904, 11 pages, 2005.

[24] X. Han, J. Goebl, Z. Lu, and Y. Yin, "Role of salt in the spontaneous assembly of charged gold nanoparticles in ethanol," *Langmuir*, vol. 27, no. 9, pp. 5282–5289, 2011.

[25] G. F. Paciotti, D. G. I. Kingston, and L. Tamarkin, "Colloidal gold nanoparticles: a novel nanoparticle platform for developing multifunctional tumor-targeted drug delivery vectors," *Drug Development Research*, vol. 67, no. 1, pp. 47–54, 2006.

[26] J. P. Nolan and D. S. Sebba, "Surface-enhanced raman scattering (SERS) cytometry," *Methods in Cell Biology*, vol. 102, pp. 515–532, 2011.

[27] Z. Zhu, T. Zhu, and Z. Liu, "Raman scattering enhancement contributed from individual gold nanoparticles and interparticle coupling," *Nanotechnology*, vol. 15, no. 3, pp. 357–364, 2004.

[28] J. P. Camden, J. A. Dieringer, Y. Wang et al., "Probing the structure of single-molecule surface-enhanced Raman scattering hot spots," *Journal of the American Chemical Society*, vol. 130, no. 38, pp. 12616–12617, 2008.

[29] H. Ko, S. Singamaneni, and V. V. Tsukruk, "Nanostructured surfaces and assemblies as SERS media," *Small*, vol. 4, no. 10, pp. 1576–1599, 2008.

[30] P. K. Jain and M. A. El-Sayed, "Noble metal nanoparticle Pairs: effect of medium for enhanced nanosensing," *Nano Letters*, vol. 8, no. 12, pp. 4347–4352, 2008.

[31] I. A. Larmour, E. A. Argueta, K. Faulds, and D. Graham, "Design consideration for surface-enhanced (resonance) Raman scattering nanotag cores," *Journal of Physical Chemistry C*, vol. 116, no. 4, pp. 2677–2682, 2012.

[32] X. Huang, I. H. El-Sayed, W. Qian, and M. A. El-Sayed, "Cancer cell imaging and photothermal therapy in the near-infrared region by using gold nanorods," *Journal of the American Chemical Society*, vol. 128, no. 6, pp. 2115–2120, 2006.

[33] L. Rodríguez-Lorenzo, R. A. Álvarez-Puebla, F. J.G. De Abajo, and L. M. Liz-Marzán, "Surface enhanced Raman scattering using star-shaped gold colloidal nanoparticles," *Journal of Physical Chemistry C*, vol. 114, no. 16, pp. 7336–7340, 2010.

[34] J. T. Edsall and E. L. Sagall, "Raman spectra of l-ascorbic acid, tetronic acid and related compounds," *Journal of the American Chemical Society*, vol. 65, no. 7, pp. 1312–1316, 1943.

[35] C. Yohannan Panicker, H. Tresa Varghese, and D. Philip, "FT-IR, FT-Raman and SERS spectra of vitamin C," *Spectrochimica Acta—Part A*, vol. 65, no. 3-4, pp. 802–804, 2006.

[36] H. Yang and J. Irudayaraj, "Rapid determination of vitamin C by NIR, MIR and FT-Raman techniques," *Journal of Pharmacy and Pharmacology*, vol. 54, no. 9, pp. 1247–1255, 2002.

[37] C. Mangeney, F. Ferrage, I. Aujard et al., "Synthesis and properties of water-soluble gold colloids covalently derivatized with neutral polymer monolayers," *Journal of the American Chemical Society*, vol. 124, no. 20, pp. 5811–5821, 2002.

[38] N. Leopold, J. R. Baena, M. Bolboacă, O. Cozar, W. Kiefer, and B. Lendl, "Raman, IR, and surface-enhanced Raman spectroscopy of papaverine: an automated setup for in situ synthesis of the silver substrate and recording of the SER spectra," *Vibrational Spectroscopy*, vol. 36, no. 1, pp. 47–55, 2004.

[39] J. D. Jiang, E. Burstein, and H. Kobayashi, "Resonant raman scattering by crystal-violet molecules adsorbed on a smooth gold surface: evidence for a charge-transfer excitation," *Physical Review Letters*, vol. 57, no. 14, pp. 1793–1796, 1986.

[40] A. W. Basit, F. Podczeck, J. M. Newton, W. A. Waddington, P. J. Ell, and L. F. Lacey, "Influence of polyethylene glycol 400 on the gastrointestinal absorption of ranitidine," *Pharmaceutical Research*, vol. 19, no. 9, pp. 1368–1374, 2002.

[41] S. C. Boca and S. Astilean, "Detoxification of gold nanorods by conjugation with thiolated poly(ethylene glycol) and their assessment as SERS-active carriers of Raman tags," *Nanotechnology*, vol. 21, no. 23, Article ID 235601, 2010.

[42] T. Niidome, M. Yamagata, Y. Okamoto et al., "PEG-modified gold nanorods with a stealth character for in vivo applications," *Journal of Controlled Release*, vol. 114, no. 3, pp. 343–347, 2006.

[43] J. Kneipp, H. Kneipp, B. Wittig, and K. Kneipp, "Novel optical nanosensors for probing and imaging live cells," *Nanomedicine*, vol. 6, no. 2, pp. 214–226, 2010.

[44] J. Kneipp, H. Kneipp, M. McLaughlin, D. Brown, and K. Kneipp, "In vivo molecular probing of cellular compartments with gold nanoparticles and nanoaggregates," *Nano Letters*, vol. 6, no. 10, pp. 2225–2231, 2006.

[45] X. Qian, J. Li, and S. Nie, "Stimuli-responsive SERS nanoparticles: conformational control of plasmonic coupling and surface Raman enhancement," *Journal of the American Chemical Society*, vol. 131, no. 22, pp. 7540–7541, 2009.

[46] C. Matthäus, T. Chernenko, J. A. Newmark, C. M. Warner, and M. Diem, "Label-free detection of mitochondrial distribution in cells by nonresonant Raman microspectroscopy," *Biophysical Journal*, vol. 93, no. 2, pp. 668–673, 2007.

Hindawi Publishing Corporation
Journal of Nanotechnology
Volume 2012, Article ID 840245, 7 pages
doi:10.1155/2012/840245

Research Article

Relationship between Length and Surface-Enhanced Raman Spectroscopy Signal Strength in Metal Nanoparticle Chains: Ideal Models versus Nanofabrication

Kristen D. Alexander,[1] Shunping Zhang,[2] Angela R. Hight Walker,[3] Hongxing Xu,[2] and Rene Lopez[1]

[1] *Department of Physics and Astronomy, University of North Carolina, Chapel Hill, NC 27599, USA*
[2] *Beijing National Laboratory for Condensed Matter Physics, Institute of Physics, Chinese Academy of Sciences, Beijing 100190, China*
[3] *Optical Technology Division, National Institute of Standards and Technology, Gaithersburg, MD 20899, USA*

Correspondence should be addressed to Rene Lopez, rln@physics.unc.edu

Received 5 November 2011; Accepted 18 January 2012

Academic Editor: Mustafa Çulha

We have employed capillary force deposition on ion beam patterned substrates to fabricate chains of 60 nm gold nanospheres ranging in length from 1 to 9 nanoparticles. Measurements of the surface-averaged SERS enhancement factor strength for these chains were then compared to the numerical predictions. The SERS enhancement conformed to theoretical predictions in the case of only a few chains, with the vast majority of chains tested not matching such behavior. Although all of the nanoparticle chains appear identical under electron microscope observation, the extreme sensitivity of the SERS enhancement to nanoscale morphology renders current nanofabrication methods insufficient for consistent production of coupled nanoparticle chains. Notwithstanding this fact, the aggregate data also confirmed that nanoparticle dimers offer a large improvement over the monomer enhancement while conclusively showing that, within the limitations imposed by current state-of-the-art nanofabrication techniques, chains comprising more than two nanoparticles provide only a marginal signal boost over the already considerable dimer enhancement.

1. Introduction

Scientific interest in surface-enhanced Raman spectroscopy (SERS) has increased dramatically since the detection of single molecules was first reported in 1997 [1]. While enhancement factors measured from bulk SERS-active materials typically hover around 10^6 [2, 3], researchers have succeeded in designing "hot spots" on substrates capable of producing values over 10^8 (on the order of the level necessary for detecting single molecules) [4–7]. The prospect of being able to boost sensitivity of SERS measurements at the single molecule level coupled with the fingerprint-like uniqueness of the Raman spectrum makes SERS a sought-after candidate for incorporation into sensor technologies; particularly, for those who are interested in detecting chemical compounds at the trace level.

Although researchers have discovered many nanoscale-textured metallic surfaces capable of producing the strong electromagnetic fields that give rise to SERS enhancements, metal nanoparticle aggregates have long been recognized as ideal materials for the achievement of truly large enhancement factors. Among these, the simplicity of the spherical nanoparticle dimer has made it a structure of choice in many attempts to build arrays of highly sensitive and reproducible SERS-active structures [8]. In a recent study, however, the question has been posed as to whether the two-particle linear aggregate is, indeed, the optimal configuration for generating SERS enhancements, prompting researchers to consider other morphologies [9]. One such configuration is closely spaced metal nanoparticles arranged end to end to form a chain (a natural extension of the dimer configuration). This structure was theoretically investigated by Wang et al. [9],

who carried out finite integral technique (FIT) simulations on gold and silver nanoparticle chains comprised of even numbers of nanoparticles ranging in length from 2 nanoparticles to infinity. The results of the simulations indicate that the field enhancement at the gap between the two centermost particles (Wang refers to this as the "c-point") can reach a maximum at a number larger than two, suggesting that the dimer might not always be the ideal configuration for achieving the maximum field enhancement. In contrast to these predictions, recent theoretical and experimental results by Wustholz et al. [10] suggest that, in most realistic experiments, the signal from the hottest hot spot in a cluster is often extremely dominant and, thus, renders unrealistic the possibility of enhancement due to near-field coupling along the chain as a whole. In this paper, the main aim is to test these conclusions on precisely designed nanoparticle chains. Through the combination of focused ion beam (FIB) milling and capillary forced deposition [11], closely spaced linear nanoclusters were fabricated. The SERS enhancement arising from these structures were measured and subsequently compared with theoretically predicted values.

2. Generalized Mie Theory Simulations

Because it would not be possible for us to measure the SERS enhancement factor (EF) directly at the c-point, we have carried out generalized Mie theory (GMT) [12–15] simulations to map the electromagnetic strength over the entire surface of gold nanospheres chains ranging in length from 1 to 9 nanoparticles with interparticle separations of 1–1.5 nm (these separations still yield reliable results in the frame of classical electromagnetic theory).

The surface Raman enhancement is proportional to the product of the squares of the field enhancement at the incident and Raman frequencies,

$$G = \left| f(\omega_{\text{Raman}}) \right|^2 \left| f\left(\omega_{\text{pump}}\right) \right|^2. \tag{1}$$

Provided that $|\omega_{\text{Raman}} - \omega|$ is smaller than the spectral response of the metal nanostructure and the excitation source is polarized along the axis of the chain, the SERS enhancement can be approximated to scale with the fourth power of the electric field enhancement [16]:

$$G(r) \approx \frac{|E_{\text{loc}}(r)|^4}{|E_0(r)|^4}. \tag{2}$$

Since the molecular species to be detected is assumed to form a monolayer on the surface of the nanospheres, the Raman EF must be averaged over the entire chain surface

$$\langle G(r) \rangle = \frac{1}{\sum_i^N 4\pi R_i^2} \sum_i^N \int_i G(r) d\sigma, \tag{3}$$

where N is the number of nanoparticles in the chain, R_i is the radius of the ith nanoparticle, and the fields were calculated at a distance of 0.5 nm from the surface which, based on the estimated thickness of the benzenethiol monolayer (the reporter molecule used in the experimental part of this study), is the most likely location of the reporter molecule. Here, it is important to note that, although the length of the benzenethiol molecule and bond length on gold are known, the interparticle distance for the structures fabricated in this experiment cannot be known exactly. Similarly, a monolayer of thiophenol molecules surrounding the spheres and the silica/silicon substrate invariably alters the index of refraction of the area immediately surrounding the metal surface. To account for this range in gap size and the effective index of refraction of the surrounding medium, n_{eff}, we calculated the surface averaged enhancement for a gap of 1 nm and $n_{\text{eff}} = 1.0$ (Figure 1(a)) as well as for a gap of 1.5 nm and $n_{\text{eff}} = 1.5$ (Figure 1(b)). As expected, the surface Raman enhancements of the nanochains ($N \geq 2$) reach values on the order of 10^7-10^8 over that of the monomer at resonance. Furthermore, the plasmon resonances shift to longer wavelengths as the particle number increases. Figures 1(c) and 1(d) show the SERS enhancement at the laser line (632.8 nm) as a function of particle number, corresponding to Figures 1(a) and 1(b), respectively. Significantly, a peak is apparent in the SERS enhancement at a chain length of 3 nanoparticles for the 1 nm gap ($n_{\text{eff}} = 1.0$) and 2 nanoparticles for the 1.5 nm gap ($n_{\text{eff}} = 1.5$). It is important to clarify that this simulation approach was designed to produce results that could be compared to experimental measurements of the SERS EF where reporter molecules actually coat all metallic surfaces. This is in contrast to the FIT calculations performed by Wang et al. which by focusing in the field enhancement at the "c-point" cannot be directly compared to a far-field experimental measurement.

3. Finite Difference Time Domain (FDTD) Simulations

To identify the link between nanoparticle chain length and the location of the surface Raman enhancement peak, we also calculated the extinction spectrum for the linear chains. As our GMT code is designed for near-field calculations, we have rather turned to apply a fast and commercially available finite difference time domain (FDTD) method (Lumerical Solutions, Inc) for far-field results. While FDTD cannot compete with the accuracy of GMT for the near field calculations, it is a perfect alternative in the far field. In order to ensure accuracy, simulations were carried out with a mesh override region surrounding the entire structure with cell size limited to 0.8 nm and convergence of the results were confirmed by comparing the results of multiple runs.

Results from these simulations are shown in Figure 2. First, the redshift of the extinction peak with respect to the increased particle number is apparent, indicating as expected, the tight correlation between the optical response and the morphology of the scatterer. Most importantly, however, the location of the highest peak of the extinction with respect to wavelength coincides with the highest EF in the near-field calculations in Figure 1. Here, we note that when we narrow our observations to a fixed wavelength

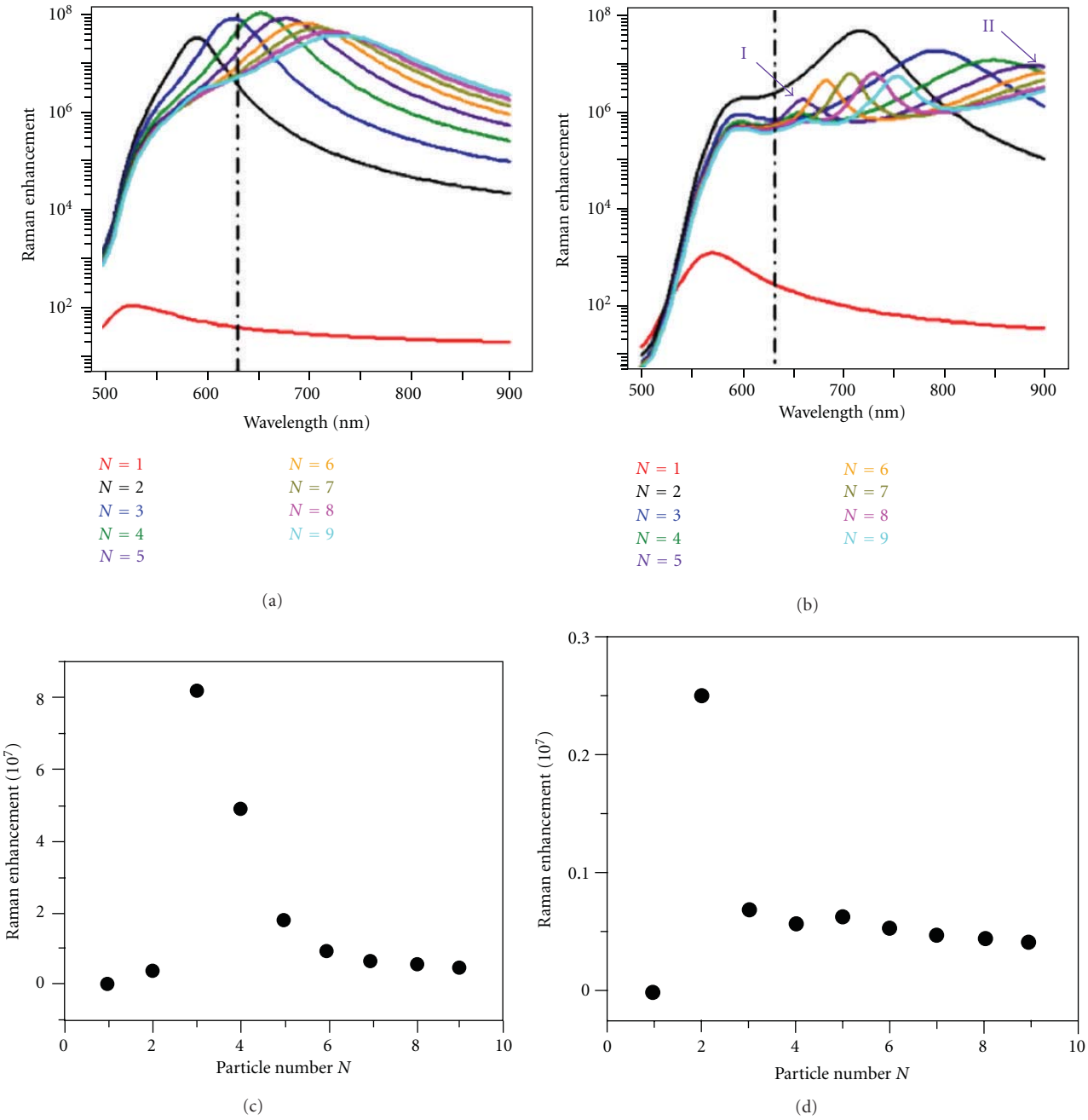

Figure 1: Calculated SERS EFs for Au nanoparticle chains using generalized Mie theory. The EF spectra have been calculated for chains ranging 1–9 nanoparticles in length with excitation source parallel to the long axis of the chain for an interparticle gap of 1 nm and $n_{\text{eff}} = 1.0$ (a) and an interparticle gap of 1.5 nm and $n_{\text{eff}} = 1.5$ (b). The EF for the 632.8 nm excitation source for (a) and (b) are shown, respectively, in (c) and (d). Angular momentum contributions up to the 37th order were included in the GMT calculations. The integral was taken at a distance of 0.5 nm from the particle surface for (a) and 0.75 nm from the particle surface for (b). The two enhancement peaks for the $N = 5$ chain are identified as II and I, respectively, in (b).

(633 nm in this case) small secondary peaks become relevant, making the direct comparison between the far and near fields less direct. Figures 1(c) and 1(d) plot the EF magnitude at the fixed wavelength againts the number of particles in each chain. One can observe that the EF peaks at a particular number of particles, and that number is not necessarily two (Figure 1(c)).

4. Sample Nanofabrication

To experimentally test the simulation results, a templating method was employed to create nanoparticle chains of specific lengths and orientations. FIB milling was used to create trenches in SiO_2 which were approximately 80 nm in width, 70 nm in depth, and ranging from 80 to 560 nm

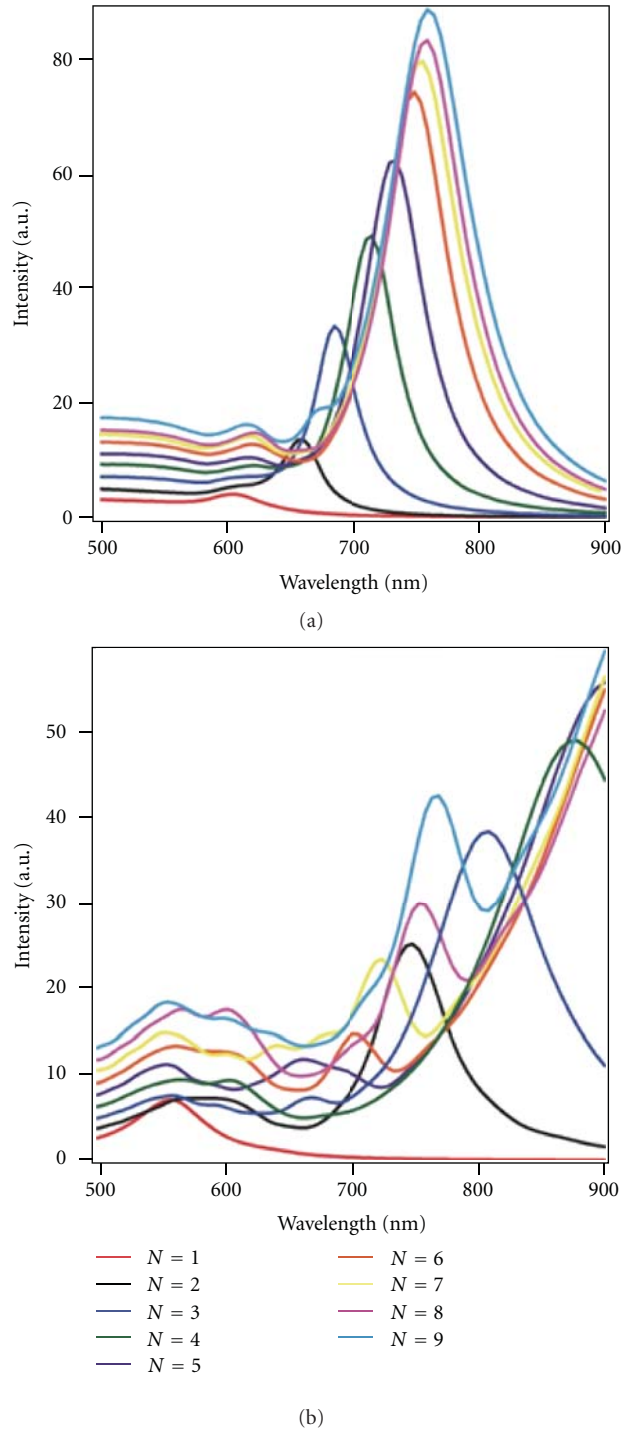

Figure 2: FDTD calculations of the extinction spectra for 60 nm Au nanoparticle chains 1–9 nanoparticles in length. Nanochains in (a) have a 1 nm interparticle separation and are embedded in a medium with refractive index $n_{\text{eff}} = 1.0$. Nanochains in (b) have a 1.5 nm interparticle separation and are embedded in a medium with refractive index $n_{\text{eff}} = 1.5$.

in length. Gold nanospheres (Ted Pella) with a diameter of 60 nm were placed into these trenches using a capillary force deposition method [11]. To accomplish this, the nanopatterned substrate was cleaned in piranha solution and subsequently subjected to a brief plasma treatment to ensure the hydrophilicity of the SiO_2 layer. Next, the SiO_2 was immersed in an aqueous gold colloid which was allowed to evaporate at 70° overnight. As the meniscus slowly recedes across the substrate, nanoparticles concentrate at the three-phase contact line (Figure 3). Because the trenches are designed to host only a specific number and configuration of nanoparticles, this process creates arrays of nanoparticle chains of predetermined lengths. Scanning-electron micrographs of the substrates were taken to identify satisfactory chains. To remove carbonaceous contamination that often accompanies SEM imaging, substrates were subsequently cleaned with piranha solution and treated with O_2 plasma for 10 minutes to remove any unwanted material that the electron beam might have deposited. Finally, nanochains were immersed in a 10 mM solution of benzenethiol overnight, removed, rinsed for 60 seconds with ethanol to remove excess benzenethiol, and then blown dry with N_2.

5. Raman Measurements

Raman spectra of individual chains were obtained using a Leica microscope equipped with a confocal Raman spectroscopic system (Renishaw InVia) and a 30 mW 632.8 nm laser excitation source. All spectra were measured using a 50× objective with a numerical aperture of 0.75. The Raman signal was collected by a TE air-cooled 576 × 400 CCD array preceded by two notch filters (OD > 12) to block the laser line. Preliminary tests concluded that, without sufficient filtering, persistent exposure to the laser beam causes the benzenethiol monolayer to degrade. To avoid photodegradation of the monolayer, the stability of the Raman signal was monitored over a range of beam powers and exposure times. These tests determined that the combination of a 100 μW laser beam power (spot size diameter ~2 μm) delivered on the sample with a 30-second acquisition time yielded sufficiently clear and stable spectra. To account for the possibility that the laser spot was not perfectly aligned over the chain and/or not perfectly uniform, a flat scanning stage was used to raster over the structure. From these measurements, the strongest, most well-defined spectrum from each of the structures was selected for data analysis. A typical spectrum for a nanoparticle heptamer is shown in Figure 4. The most pronounced peaks appear at 1000 cm^{-1} (ring out-of-plane deformation and C–H out-of-plane bending), 1080 cm^{-1} (C–C symmetric stretching and C–S stretching), and 1577 cm^{-1} (C–C symmetric stretching) [17]. Time-stability tests were performed in order to select the most stable Raman peak for comparison in these tests. All the peaks were clear and steady, but the 1080 cm^{-1} peak was found to show the best signal to noise ratio and was, thus, used for all data analyses performed in this study.

6. Summary of Results and Discussion

Experimental results are plotted over GMT simulations for a 1.5 nm interparticle gap in Figure 5. Results from two data sets are shown to delineate the range of outcomes

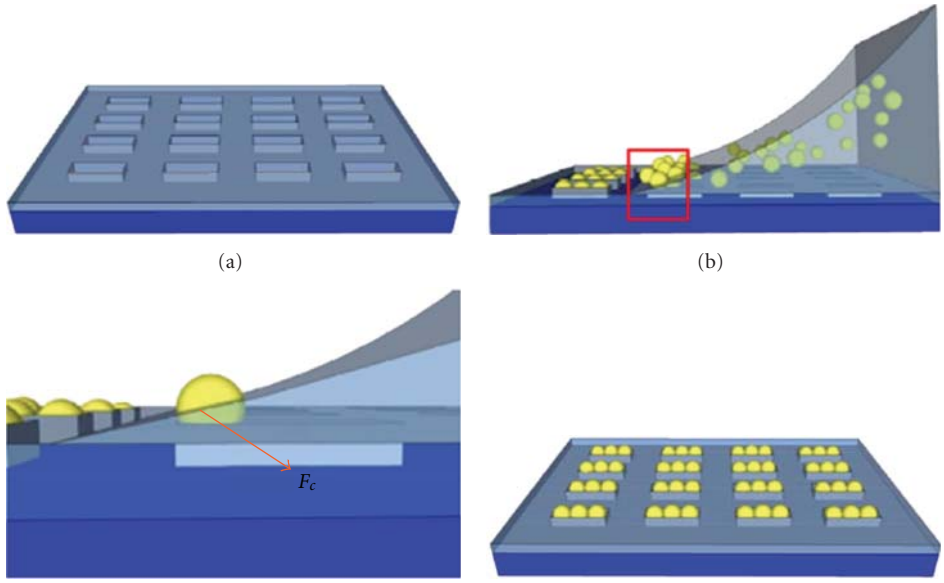

Figure 3: (a) Silicon substrate immediately after FIB milling of SiO_2 layer. (b) Illustration of three-phase contact line dragging nanoparticles across the substrate surface. (c) Close-up illustration of particles pushed into milled trenches via the capillary force. (d) Array of nanosphere trimers after deposition is complete.

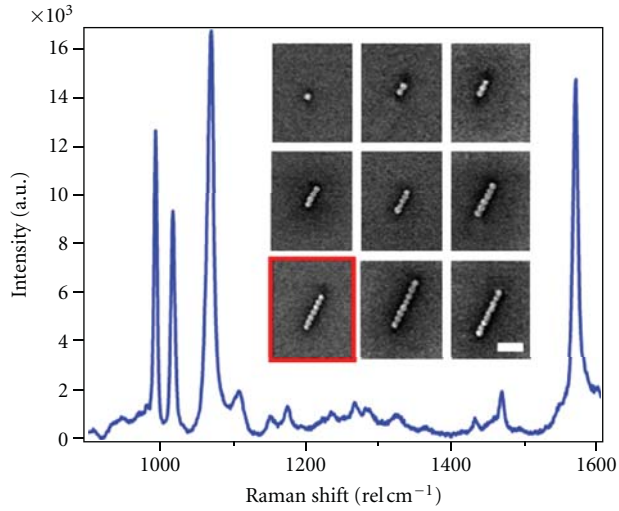

Figure 4: (a) Scanning-electron micrograph of gold nanochains ranging 1–9 particles in length. Scale bar is 300 nm. (b) SERS spectrum of benzenethiol on a nanochain comprised of 60 nm gold nanospheres. Measurements were taken with a 632.8 nm laser source polarized parallel to the nanochain axis. The red box in (a) denotes the heptamer from which this measurement was taken.

for this particular experiment. Specifically, the first set represents the largest measured enhancements (i.e., the best enhancements obtained in this study) for each chain length (red trace), and a second set with the results falling within one standard deviation of the overall data average (blue trace). It can be observed that the second set deviates from theory especially at longer chain lengths, reaching a plateau of enhancement rather than decreasing for larger particle numbers. The large enhancement ratio between the monomer and the dimer is unsurprising, as it is well known that the tiny gaps formed by closely spaced nanoparticles are the source of large electric fields which give rise to large SERS enhancement factors. This situation becomes more complex, however, when the number of gaps in the chain is increased through the addition of nanoparticles. It has been shown that the SERS EF is extremely sensitive to interparticle separation, falling off at the rate of approximately one order of magnitude per nanometer of separation [18]. For longer nanochains, a mixture of coupled and decoupled neighboring particles might coexist. Moreover, the extreme sensitivity of the SERS enhancement to a gamut of factors, including nanoparticle size [19], shape [20], crystal face [21], surface roughness [22], and particle-particle spacing [23–27] is well documented and is known to account for significant variations in EFs arising from seemingly-identical nanoparticle clusters. Taking these two items into consideration, one can see that in practice it is unlikely that the enhancement that would arise from a perfectly coupled nanochain of a specific length is being observed. Moreover, it is quite likely that a single dominant hot spot is accounting for the majority of the enhancement observed for all chain lengths >1. Significantly, these considerations qualitatively explain the plateau of the EF in Figure 5 as well as emphasize the importance of making hot spots through gap formation over additional enhancements achieved through resonances in complex geometries, thereby supporting the Wustholz et al. [10] conclusion.

At the other end of the spectrum of experimental outcomes, the largest enhancement results do show a significant

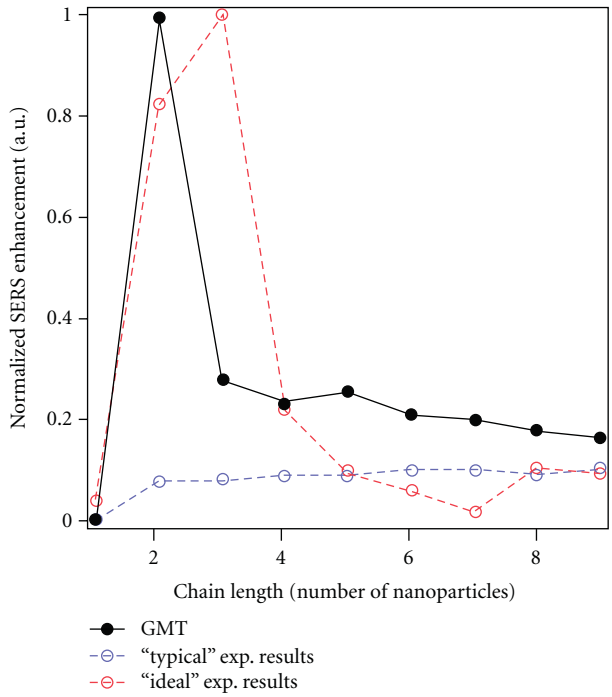

FIGURE 5: Black trace—generalized Mie theory calculations for the SERS EF for 60 nm diameter Au nanochains with a 1.5 nm interparticle separation, embedded in a medium with refractive index $n_{\text{eff}} = 1.5$. Blue trace—experimental SERS EF measurements for 60 nm diameter Au nanochains lying within one standard deviation from the average measured EF value for each chain length (i.e., "typical" results). Red trace—largest values for the SERS EF for each chain length measured in this experiment (i.e., "ideal" results). "Typical" results (blue trace) are normalized against the values for the "ideal" results (red trace) to illustrate the difference in magnitude between the two experimental data sets.

agreement with theory. While it would be impossible to accurately determine whether the peak at a chain length of 3 nanoparticles arises from perfect interparticle coupling along the entire length of the chain, the measurement seems to indicate that this was the case and it is certainly relevant to include a discussion of this ideal situation. Referring back to Figure 1, despite a small redshift, the maximum SERS enhancement for the monomers depicted in Figures 1(a) and 1(b) is located around 525 nm and 570 nm, respectively, corresponding to the far-field LSPR peak. For aggregates consisting of more than two spheres, the hybridized plasmon modes appear as a result of the interaction of primary plasmons in nearby spheres [28, 29]. This coupling dramatically enhances the local electric field, creating an SERS enhancement, that is, orders of magnitude larger than that of a single sphere. In addition to lowering the bonding mode, hybridized plasmon modes of higher angular momentum are also excited by the wave polarized parallel to the long axis of the chain. As the chain length is increased, both EF peaks experience a redshift. These chains demonstrate a sufficiently strong dipole moment and are, thus, able to couple to far field radiation efficiently, thereby creating the peaks in the EF observed in both the simulation and experimental data.

7. Conclusions

In summary, GMT and FDTD simulations were performed to model the surface-averaged electromagnetic field enhancements arising from plasmonic coupling in closely spaced noble metal nanoparticle chains. The simulations suggest that there exists an "ideal" chain length capable of producing modest improvements on the typical dimer enhancement factor. To experimentally test the model, chains of 60 nm gold nanospheres were fabricated using a capillary force deposition technique. Subsequent Raman measurements made from these structures showed modest agreement with the GMT simulations in some cases and a complete lack of agreement in others. In general, the vast majority of the tested nanoparticle chains showed no more enhancement beyond the typical for a two-particle dimmer. From these results, it was concluded that it is unlikely that the individual nanoparticles comprising the chains made using the capillary force deposition method technique are consistently able to couple completely along the entire structure, thereby departing from the ideal situation modeled in the calculations performed in this study. However, comparison of experimental and theoretical results confirms that the formation of dimers provides a large improvement in signal strength over the monomer enhancement. While perfect plasmonic coupling of the ideal number of nanoparticles can provide improvement over the dimer enhancement, it is marginal under the best of circumstances and often introduces more difficulties in the fabrication process than is justifiable by the small boost in signal.

Acknowledgments

This work was supported in part by the Hartley Corporation Fellowship for Graduate Women in Science and the SPIE Graduate Student fellowship. The authors thank Dr. Richard Superfine for many useful conversations.

References

[1] K. Kneipp, Y. Wang, H. Kneipp et al., "Single molecule detection using surface-enhanced raman scattering (SERS)," *Physical Review Letters*, vol. 78, no. 9, pp. 1667–1670, 1997.

[2] J. Lu, D. Chamberlin, D. A. Rider, M. Liu, I. Manners, and T. P. Russell, "Using a ferrocenylsilane-based block copolymer as a template to produce nanotextured Ag surfaces: uniformly enhanced surface enhanced Raman scattering active substrates," *Nanotechnology*, vol. 17, no. 23, pp. 5792–5797, 2006.

[3] A. Gopinath, S. V. Boriskina, W. R. Premasiri, L. Ziegler, B. M. Reinhard, and L. D. Negro, "Plasmonic nanogalaxies: multiscale aperiodic arrays for surface-enhanced Raman sensing," *Nano Letters*, vol. 9, no. 11, pp. 3922–3929, 2009.

[4] J. A. Dieringer, K. L. Wustholz, D. J. Masiello et al., "Surface-enhanced Raman excitation spectroscopy of a single rhodamine 6G molecule," *Journal of the American Chemical Society*, vol. 131, no. 2, pp. 849–854, 2009.

[5] E. C. le Ru, E. Blackie, M. Meyer, and P. G. Etchegoint, "Surface enhanced Raman scattering enhancement factors: a comprehensive study," *Journal of Physical Chemistry C*, vol. 111, no. 37, pp. 13794–13803, 2007.

[6] H. Xu, E. J. Bjerneld, M. Käll, and L. Börjesson, "Spectroscopy of single hemoglobin molecules by surface enhanced Raman scattering," *Physical Review Letters*, vol. 83, no. 21, pp. 4357–4360, 1999.

[7] E. C. le Ru, M. Meyer, E. Blackie, and P. G. Etchegoin, "Advanced aspects of electromagnetic SERS enhancement factors at a hot spot," *Journal of Raman Spectroscopy*, vol. 39, no. 9, pp. 1127–1134, 2008.

[8] J. P. Camden, J. A. Dieringer, Y. Wang et al., "Probing the structure of single-molecule surface-enhanced raman scattering hot spots," *Journal of the American Chemical Society*, vol. 130, no. 38, pp. 12616–12617, 2008.

[9] Z. B. Wang, B. S. Luk'yanchuk, W. Guo et al., "The influences of particle number on hot spots in strongly coupled metal nanoparticles chain," *The Journal of Chemical Physics*, vol. 128, no. 9, Article ID 094705, 2008.

[10] K. L. Wustholz, A. I. Henry, J. M. McMahon et al., "Structure-activity relationships in gold nanoparticle dimers and trimers for surface-enhanced raman spectroscopy," *Journal of the American Chemical Society*, vol. 132, no. 31, pp. 10903–10910, 2010.

[11] Y. Cui, M. T. Björk, J. A. Liddle, C. Sönnichsen, B. Boussert, and A. P. Alivisatos, "Integration of colloidal nanocrystals into lithographically patterned devices," *Nano Letters*, vol. 4, no. 6, pp. 1093–1098, 2004.

[12] G. Mie, "Beitrage zur Optik truber Medien," *Annals of Physics*, vol. 25, pp. 377–445, 1908.

[13] S. Li, D. Wu, X. Xu, and R. Gu, "Theoretical and experimental studies on the adsorption behavior of thiophenol on gold nanoparticles," *Journal of Raman Spectroscopy*, vol. 38, no. 11, pp. 1436–1443, 2007.

[14] H. Xu, "Calculation of the near field of aggregates of arbitrary spheres," *Journal of the Optical Society of America A*, vol. 21, no. 5, pp. 804–809, 2004.

[15] H. X. Xu, "A new method by extending Mie theory to calculate local field in outside/inside of aggregates of arbitrary spheres," *Physics Letters A*, vol. 312, no. 5-6, pp. 411–419, 2003.

[16] L. Novotny and B. Hecht, *Principles of Nano-Optics*, Cambridge University Press, Cambridge, UK, 2006.

[17] J. Hu, B. Zhao, W. Xu, Y. Fan, B. Li, and Y. Ozaki, "Simple method for preparing controllably aggregated silver particle films used as surface-enhanced Raman scattering active substrates," *Langmuir*, vol. 18, no. 18, pp. 6839–6844, 2002.

[18] K. D. Alexander, M. J. Hampton, S. Zhang, A. Dhawan, H. Xu, and R. Lopez, "A high-throughput method for controlled hot-spot fabrication in SERS-active gold nanoparticle dimer arrays," *Journal of Raman Spectroscopy*, vol. 40, no. 12, pp. 2171–2175, 2009.

[19] J. T. Krug, G. D. Wang, S. R. Emory, and S. Nie, "Efficient Raman enhancement and intermittent light emission observed in single gold nanocrystals," *Journal of the American Chemical Society*, vol. 121, no. 39, pp. 9208–9214, 1999.

[20] F. Huang and J. J. Baumberg, "Actively tuned plasmons on elastomerically driven Au nanoparticle dimers," *Nano Letters*, vol. 10, no. 5, pp. 1787–1792, 2010.

[21] P. Kambhampati, C. M. Child, M. C. Foster, and A. Campion, "On the chemical mechanism of surface enhanced Raman scattering: experiment and theory," *The Journal of Chemical Physics*, vol. 108, no. 12, pp. 5013–5027, 1998.

[22] S. Li, M. L. Pedano, S. H. Chang, C. A. Mirkin, and G. C. Schatz, "Gap structure effects on surface-enhanced Raman scattering intensities for gold gapped rods," *Nano Letters*, vol. 10, no. 5, pp. 1722–1727, 2010.

[23] W. Rechberger, A. Hohenau, A. Leitner, J. R. Krenn, B. Lamprecht, and F. R. Aussenegg, "Optical properties of two interacting gold nanoparticles," *Optics Communications*, vol. 220, no. 1–3, pp. 137–141, 2003.

[24] C. Tabor, R. Murali, M. Mahmoud, and M. A. El-Sayed, "On the use of plasmonic nanoparticle pairs as a plasmon ruler: the dependence of the near-field dipole plasmon coupling on nanoparticle size and shape," *The Journal of Physical Chemistry A*, vol. 113, no. 10, pp. 1946–1953, 2009.

[25] L. Gunnarsson, E. J. Bjerneld, H. Xu, S. Petronis, B. Kasemo, and M. Käll, "Interparticle coupling effects in nanofabricated substrates for surface-enhanced Raman scattering," *Applied Physics Letters*, vol. 78, no. 6, pp. 802–804, 2001.

[26] K. Bosnick, M. Maillard, L. Brus, and J. Jiang, "Single molecule Raman spectroscopy at the junctions of large ag nanocrystals," *The Journal of Physical Chemistry B*, vol. 107, no. 37, pp. 9964–9972, 2003.

[27] K. H. Su, Q. H. Wei, X. Zhang, J. J. Mock, D. R. Smith, and S. Schultz, "Interparticle coupling effects on plasmon resonances of nanogold particles," *Nano Letters*, vol. 3, no. 8, pp. 1087–1090, 2003.

[28] E. Prodan, C. Radloff, N. J. Halas, and P. Nordlander, "A hybridization model for the plasmon response of complex nanostructures," *Science*, vol. 302, no. 5644, pp. 419–422, 2003.

[29] P. Nordlander and E. Prodan, "Plasmon hybridization in nanoparticles near metallic surfaces," *Nano Letters*, vol. 4, no. 11, pp. 2209–2213, 2004.

Hindawi Publishing Corporation
Journal of Nanotechnology
Volume 2012, Article ID 745390, 7 pages
doi:10.1155/2012/745390

Research Article

Sensing Properties of a Fabry-Perot Dielectric Structure and Dimer Nanoparticles

A. Polemi and K. L. Shuford

Department of Chemistry, Drexel University, 3141 Chestnut Street, Philadelphia, PA 19104, USA

Correspondence should be addressed to A. Polemi, alessia.polemi@drexel.edu

Received 30 November 2011; Accepted 18 January 2012

Academic Editor: Mustafa Çulha

We investigate the use of a Fabry-Perot dielectric structure combined with differently shaped nanoparticles for Surface Enhanced Raman Scattering. In particular, we show how an ideal two-layer Fabry-Perot configuration enhances the local surface field of silver nanoparticles positioned on the surface of the structure. We develop the concept using disc dimers and then extend the discussion to bowtie nanoparticles. The structure is excited by a single emitter, which couples to the nanoparticles through the dielectric layers, producing a wide aperture field that can be used to excite multiple dimers. We show how an array of nanoparticles can be properly arranged in order to increase the total scattering signal generated from the structure. The layered geometry produces robust field properties in between nanoparticles, making the overall sensing characteristics less sensitive to the interparticle seperation distance and incident polarization.

1. Introduction

In the recent years, the utilization of Surface Enhanced Raman Spectroscopy (SERS) has grown dramatically, demonstrating its power and utility as an analytical tool for the selective detection of molecules interacting with metal surfaces [1, 2]. The SERS enhancement is often interpreted as the product of two contributions [3]: an electromagnetic (EM) enhancement mechanism and a chemical enhancement mechanism. It has been shown that the electromagnetic enhancement is dominant, and it produces the larger contribution [4–6]. This contribution is due to the localized surface plasmon resonance (LSPR), which excites the molecule under study when near a plasmonic surface. An LSPR occurs when the collective oscillation of conduction electrons in a metal nanoparticle is in resonance with the frequency of incident light. When the excitation field is resonant with a plasmon, the metal particle will emit coherent electromagnetic radiation. This radiation increases the local field intensity, $|E|$, that molecules feel when located near the plasmonic structure. It has been established that the Raman scattering enhancement scales approximately as $|E|^4$ [6]. Thus, the use of a proper plasmonic nanostructure is essential to maximize the electromagnetic effect, reaching typical values of SERS gain in the range 10^5–10^6. On the other side, the chemical enhancement, which is primarily due to the excitation of adsorbate localized electronic resonances or metal-to-adsorbate charge-transfer resonances, does not usually exceed 10^2–10^3 [7, 8].

Both theoretical calculations and experiments have shown how the plasmon frequency and resulting EM field are extremely dependent on the nanoparticle composition, size, shape, and dielectric environment [9, 10]. In particular, in a recent paper [11], we have investigated the use of a Fabry Perot (FP) dielectric structure to improve the local field coupled to a nanodisc dimer. The FP concept is well known in the literature and widely used in the radio frequency domain. In [11], we have used an FP planar dielectric structure formed by a superstrate with a high permittivity placed on a substrate with very low permittivity. This substrate/superstrate structure, once properly designed, has been demonstrated to establish a resonance condition, which maximizes antenna gain, radiation resistance, and radiation efficiency [12–14]. In particular, we have focused

on dimer nanoparticles formed by a pair of silver discs placed on top of the double-layer FP structure. A quantum emitter, treated as a classical dipole [15], excites the dimer through the dielectrics by means of a wide aperture field generated on top of the superstrate. Since the source is linearly polarized, the aperture field is also linearly polarized [16], and it is used as a secondary feeding source for the dimer nanoparticles. In [11], we focused primarily on the far field properties of the system, described as an antenna at optical frequencies, and only briefly showed how this structure can be also used for sensing. In the present paper, we focus our attention on the sensing properties, with particular reference to SERS. Here, we will expand our investigation on the disc dimer and will explore the possibility of employing differently shaped nanoparticles, such as bowtie arrangement. At the same time, we will also investigate the effect of losses of realistic dielectric materials on the sensing performance. Then, we will discuss how disc dimers and bowtie nanoparticles can be arranged in an array configuration, within the wide aperture field provided by the FP structure, and how this improves the SERS gain. Finally, we will show how the FP structure is quite robust to changes of the source polarization, and how different orientations of the dipolar emitter can be used to increase the overall field enhancement.

2. Fabry-Perot Cavity and Nanoparticles

The Fabry-Perot dielectric structure is composed of two dielectric slabs (substrate/superstrate) with dielectric permittivity ε_{r1} and ε_{r2}, respectively (see Figure 1). In order to obtain a substantial FP cavity effect, $\varepsilon_{r2} \gg \varepsilon_{r1}$, typically $\varepsilon_{r2} \sim \varepsilon_{r1}$. Initially for simplicity, we assume that the substrate is free space ($\varepsilon_{r1} = 1$), and the superstrate is a lossless material with permittivity $\varepsilon_{r2} = 10$. This assumption can be removed, and other materials can be used with permittivities that fulfill the FP requirements. We will show in the following sections how the use of realistic materials does not alter the general behavior of the structure. The structure is designed at the operating wavelength $\lambda = 633$ nm. At this frequency, the substrate and the superstrate must have thickness $h_1 = \lambda_1/2 = 316.5$ nm and $h_2 = \lambda_2/4 = 50$ nm, where $\lambda_1 = \lambda/\sqrt{\varepsilon_{r1}}$ and $\lambda_2 = \lambda/\sqrt{\varepsilon_{r2}}$ are the wavelengths in the dielectrics with permittivity ε_{r1} and ε_{r2}, respectively, and λ is the wavelength in free space. The substrate is grounded by a silver plate (optical constants taken from [17]), with a thickness greater than the skin depth in order to ensure total reflectivity. We have utilized silver for the sake of fabrication continuity (the nanoparticles are made of silver). The quantum emitter, represented here as a dipole oriented along y with unit current and length of 5 nm (dipole moment $\overline{p} = 5 \cdot 10^{-9}\hat{y}$ Cm), is placed in the substrate in a location that maximizes the electric field inside the cavity. For the ideal case of a perfectly conducting ground plane, this occurs when $h = h_1/2 = 158.25$ nm. In our case, due to the presence of the silver ground plane, the ideal dipole position has been found to be $h = 143$ nm [11]. Note that in a real experiment, an external source excites the quantum emitter, which couples to the dimer through the FP structure. This could be implemented, for example, by means of a nanoemitter on top of a focusing plasmonic tip source. How this affects the FP excitation efficiency is not presented here but is being investigated currently.

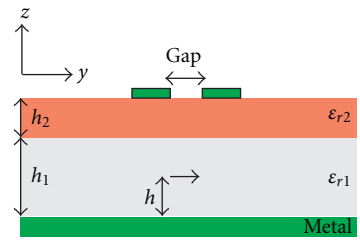

Figure 1: Reference geometry of the structure. The dipolar source is embedded in the substrate, which has permittivity ε_{r1} and height h_1. The superstrate is characterized by permittivity ε_{r2} and height h_2. The nanoparticles are placed on top of the superstrate.

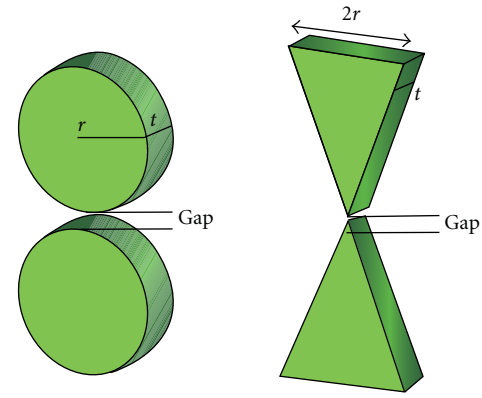

Figure 2: Geometry of the two nanoparticle configurations: disc dimer and bowtie structure.

2.1. Disc Dimers and Bowtie Nanoparticles. In [11], we have shown how the wide linearly polarized aperture field can be used as a secondary field source to feed a pair of disc nanoparticles, composed of silver with radius r, thickness t, and separation gap, placed on the top of the superstrate. Here, we want to investigate their sensing capability compared to a silver bowtie structure. The base of the triangle forming the bowtie is set to $2r$, and the remaining dimensions are assigned in order to have the same total surface area as the disc dimer. The two nanoparticle configurations are shown in Figure 2.

Under the assumption that the Raman signal is only slightly shifted in frequency with respect to the source frequency, the SERS enhancement factor can be calculated as

$$EF_{\text{SERS}} = \left| \frac{E}{E_0} \right|^4, \tag{1}$$

where the electric field around the particles E and the source field E_0 are calculated at $\lambda = 633$ nm in this case. It is well known that the local field of the nanoparticle spikes in the proximity of its edges. When employing grid-based numerical simulations, the value of the field close to the

metal boundary is sensitive to the size of the grid. For these reasons, we have introduced a more representative figure of merit, which is the average of the electric field over the particle surface area [11, 18, 19]. In particular, we define E_{surf} as the total absolute field integrated over the surface ($S = S_{\text{disc}}, S_{\text{bowtie}}$) of the nanoparticles accessible to molecules

$$E_{\text{surf}} = \frac{1}{S}\int_S \left|\overline{E}(x,y,z)\right| dS, \tag{2}$$

and we use this in place of $|E|$ in (1). The value of E_{surf} will be notably less than the maximum surface field but will likely be more in line with what one might actually measure in an experiment. In order to obtain a consistent definition of EF_{SERS}, we equivalently define the source field E_0 in (1) as the average of the electric field over the same particle surface area as in (2), but produced by the dipole in free space, that is,

$$E^0_{\text{surf}} = \frac{1}{S}\int_S \left|\overline{E_0}(x,y,z)\right| dS, \tag{3}$$

where $\overline{E_0}(x,y,z)$ is the dipole source in the absence of the dielectric structure and of the nanoparticles. This allows us to compare the fields around the nanoparticles without including the effect of the spherical spreading factor associated with a dipole field. Thus, the SERS enhancement factor can be redefined as

$$EF^{\text{avg}}_{\text{SERS}} = \left|\frac{E_{\text{surf}}}{E^0_{\text{surf}}}\right|^4. \tag{4}$$

Notice that E^0_{surf} differs for the disc dimer and the bowtie since the area where the surface integral is performed is geometrically different.

Calculations have been performed with CST Microwave Studio [20] using the time domain solver. Within this approach, Maxwell's equations are solved by performing a Finite Integration Technique [21], which relies on the discretization of the geometrical domain in terms of hexahedrons. In our case, the mesh size is set to 1 nm. Perfect Matching Layer boundary conditions are applied to the walls of the domain box.

In Figure 3, we show the $E_{\text{surf}}/E^0_{\text{surf}}$ ratio for the disc dimer (blue line) and the bowtie (red line) on top of the FP structure, with the dimer axis aligned along the dipole source (see Figure 1). The ratio is presented as a function of the gap distance for a radius $r = 40$ nm (Figure 3(a)), and as a function of the radius r when $gap = 5$ nm (Figure 3(b)). In general, the sensing properties of the disc dimer and the bowtie are very similar, except that the bowtie works slightly better when the value of r increases. At this excitation wavelength, smaller particles of both varieties tend to generate larger fields as shown in Figure 3(b). Notice that the variation of r affects the bowtie geometry as well, since both the particles are designed in order to have the same total surface area. Although one would expect that the bowtie geometry provides a larger field because of the sharp tips, we must stress again that we are presenting the integral of the electric field on the particle surface, not in the gap area. Presumably for many SERS applications, the molecules being sensed bind only to the metallic surface, negating most of the potential benefits of any nanojunction hot spots.

Finally, in Figure 3(a), we also include the $E_{\text{surf}}/E^0_{\text{surf}}$ ratio for a bowtie on an FP structure with realistic lossy materials. In particular, we use SiO_2 as substrate ($n_{SiO_2} = 1.45$) and Si as superstrate, whose refractive index at 633 nm is $n_{\text{Si}} = 3.87 + j0.03$ [17]. The double-layered cavity is modified in order to fulfill the Fabry-Perot condition: $h_1 = \lambda_1/2 = 218.4$ nm and $h_2 = \lambda_2/4 = 40.8$ nm, where $\lambda_1 = \lambda/\sqrt{\varepsilon_{r1}}$ and $\lambda_2 = \lambda/\sqrt{\varepsilon_{r2}}$ are the wavelengths in the dielectrics with permittivity $\varepsilon_{r1} = n^2_{SiO_2}$ and $\varepsilon_{r2} = \text{Re}(n_{\text{Si}})^2$, respectively. Since the relation $\varepsilon_{r2} \gg \varepsilon_{r1}$ still holds (in particular $\varepsilon_{r2} \sim 7\varepsilon_{r1}$), we expect that the resonant effect is maintained. Although the presence of losses in the silicon affects the amount of field that reaches the particles and then reduces the $E_{\text{surf}}/E^0_{\text{surf}}$ ratio, the enhancement is still almost constant over the range of gap values. It is clear that the general trends are not affected by dielectric losses. Therefore, in the following, we will only focus on the ideal case. This will allow us to demonstrate the general principle of operation of the structure with fewer circuitous effects.

2.2. Multiple Dimer Configuration. One of the advantages of the FP multilayered structure is that the aperture field on top of the superstrate, provided by the dipolar source, is circularly wide and linearly polarized along the source. We have shown in [11] that this aperture field remains almost unchanged when the dimer is placed in the middle of the field (except for the immediate region where the dimer is placed). This feature can be used for arranging multiple nanoparticle dimers in an array configuration. A possible geometry is shown in Figure 4 for 3 nanodisc dimers. Of course, the disc dimers can be equivalently replaced by the bowtie. The $E_{\text{surf}}/E^0_{\text{surf}}$ ratio is shown in Figure 5 for disc dimer (blue line) and bowtie (red line) as a function of the interelement distance d, for a radius $r = 40$ nm and $gap = 5$ nm. In particular, we compare the case of 3- and 5-dimer elements with the single-element configuration, which is a constant value. As expected, the enhancement of the surface field is increased significantly even though the arrays are all fed by a single dipole source. This means that wide aperture field is still strong enough over a large spatial region to excite multiple nanoparticles. This effect is particularly visible for the 3-element case, where their range of variation of the ratio $E_{\text{surf}}/E^0_{\text{surf}}$ in terms of d is quite moderate. In the 5-element case, the exterior dimers begin to fall out of the aperture field more rapidly as d increases causing the field enhancement to decrease, especially for the discs when $d >$ 100 nm. From Figure 5, it is clear that the bowtie array has an overall better field enhancement, which was also observed for the single-element case, but is amplified here for the array configuration. The larger enhancement results from the geometry of the bowtie, which supports a stronger dipolar field coupling between the bases. This creates a wider area on the sides of the bowtie surface where the field is stronger compared to the discs, which is visible in Figure 6. Here, we show the absolute value of the field distribution for arrays with 1, 3, and 5 elements, for both disc dimer and bowtie

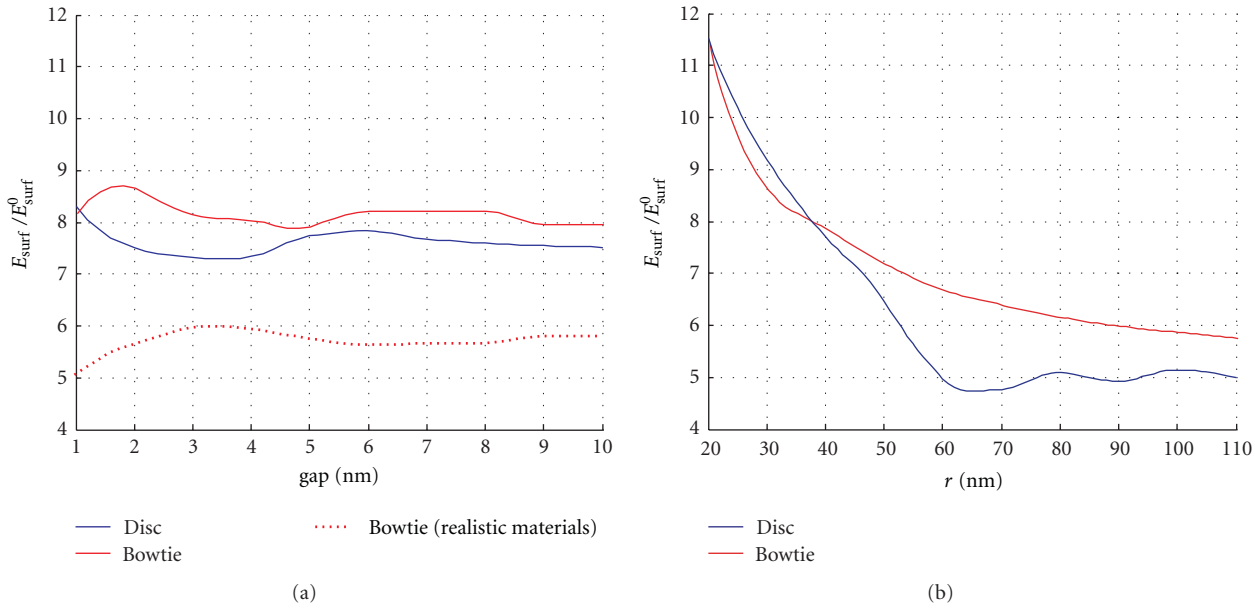

FIGURE 3: (a) Field enhancement for the disc dimer (blue line) and the bowtie (red line) on top of the Fabry-Perot structure as a function of the gap distance for a radius $r = 40$ nm. The effect of realistic lossy materials is also shown (red dotted line) for the bowtie configuration. (b) Field enhancement as a function of the radius r when $gap = 5$ nm. For both panels, the dimer and the bowtie are both oriented along the dipole source (see Figure 1).

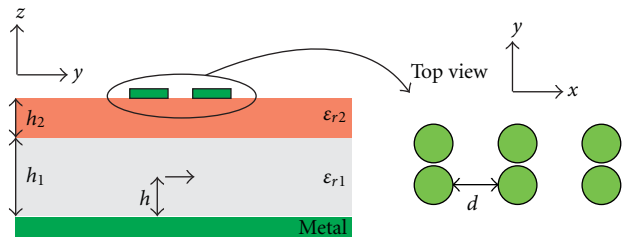

FIGURE 4: Multiple dimer configuration. The nanodisc dimer array can equivalently be replaced by an array of bowtie.

($r = 40$ nm, $gap = 5$ nm). It is clear that the disc dimers contribute to the sensing field predominantly along the side surface and the rim, while the bowtie shows a strong field distribution also on the top surface, which is more accessible to molecules.

2.3. Effect of the Source Polarization. In this section, we explore how the orientation of the dipolar source influences the enhancement of the electric field on the surface of the nanoparticles. We show here, as an example, the results for the 3-element arrays of disc dimers and bowties when the dipole is oriented along the alignment axis of the nanoparticle dimers (along y), and when the dipole is oriented perpendicularly to the dimer axis (along x). See Figure 4 for the reference system. The enhancement factor is shown in Figure 7 as a function of the interelement distance d. The $xpol$ label refers to the case when the dipole is oriented perpendicularly to the main axis of the nanoparticle dimer. This result is very interesting. First,

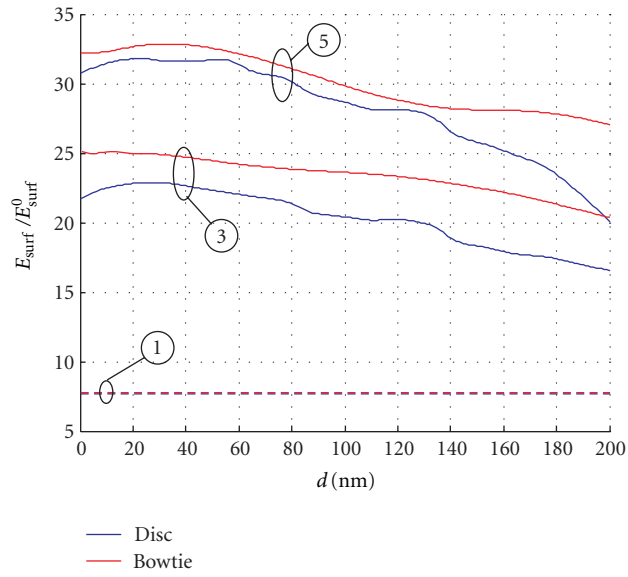

FIGURE 5: Enhancement ratio for the multiple (3 and 5) dimer configurations compared with a single dimer. In particular, the disc dimer case (blue line) and the bowtie case (red line) are plotted as a function of the interelement distance d, for a radius $r = 40$ nm and $gap = 5$ nm. The disc dimer and the bowtie are both oriented along the dipole source (see Figure 4).

we notice that $xpol$ (dashed line) yields better behavior in terms of enhancement, although, for the disc dimers, the improvement is not as substantial. Nevertheless, it shows a clear trend. In this particular configuration, the $xpol$

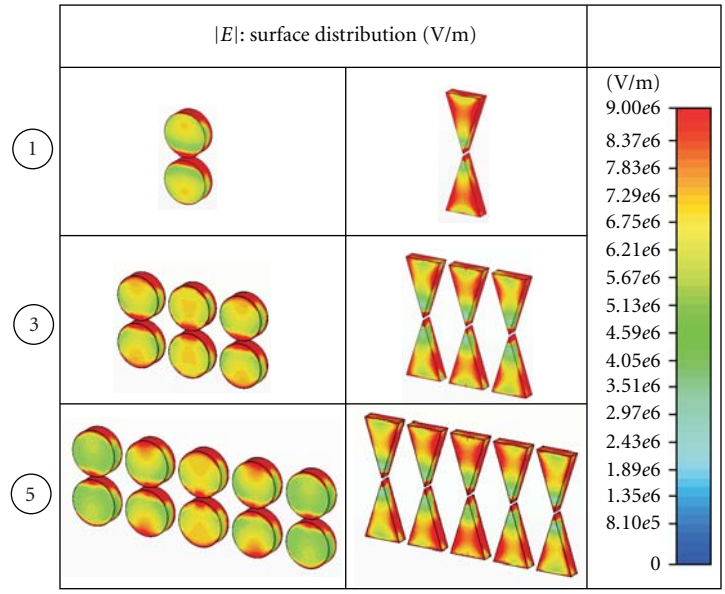

Figure 6: Absolute value of the field distribution for 1-, 3-, and 5-element arrays, for both the disc dimer and bowtie ($r = 40$ nm, $gap = 5$ nm). The field is generated by a dipole with length 5 nm and current 1 A.

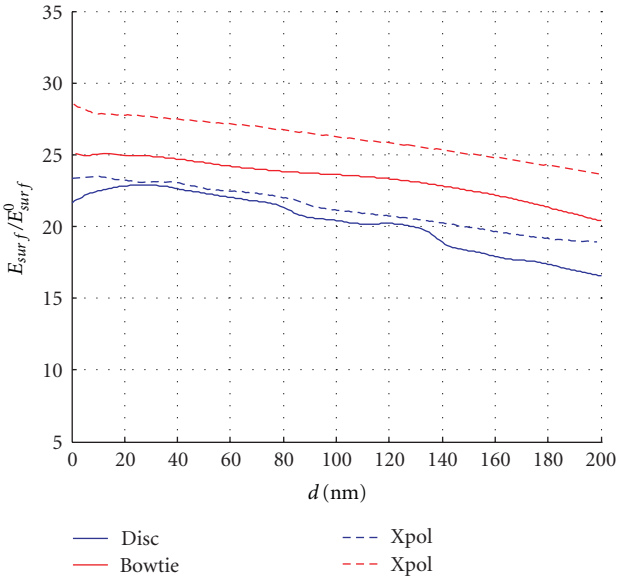

Figure 7: Enhancement ratio for 3-element arrays when the dipolar source is oriented along the alignment axis of the dimers (solid line) and perpendicularly to the alignment axis (dashed line), which is labelled as xpol. The disc dimer case (blue line) and the bowtie case (red line) are plotted as a function of the interelement distance d, for a radius $r = 40$ nm and $gap = 5$ nm.

polarization excites a greater number of equivalent dipolar field distributions over all of the array configuration. This is not particularly evident for the disc dimer but is more conspicuous for the bowtie elements. In order to accentuate this mechanism, Figure 8 shows the absolute value of the field distribution for both disc dimer and bowtie ($r = 40$ nm, $gap = 5$ nm), when the dipole is oriented along the main axis or when it oriented perpendicularly. It is clear that when the dipole is perpendicular to the alignment axis, the bowtie configuration matches the aperture field distribution well, creating a stronger field on the particle surface. This particular excitation facilitates interelement coupling between tips of adjacent dimers yielding a more robust field. This result suggests that the FP structure is quite flexible to different nanoparticle geometries and configurations, since the polarization change can be used as an advantage in the SERS gain optimization process. This will be an area of future study.

3. Conclusions

We have investigated the sensing properties of a Fabry-Perot structure coupled to plasmonic nanoparticles. The Fabry-Perot structure is composed of a double layer of dielectric materials—a superstrate with a high permittivity placed on a substrate with very low permittivity. This substrate/superstrate structure has been demonstrated to establish a resonance condition, which is here used to maximize the aperture field on top of the superstrate, where the nanoparticles are located for sensing. The field is generated by a quantum emitter, treated here as a dipole, residing in the substrate. We have examined two different nanoparticle shapes, specifically disc dimers and bowtie nanostructures. A figure of merit has been defined, which allows the calculation of SERS gain based on the average surface field of the nanoparticles. We have shown that an array configuration of disc dimers and bowties can effectively increase the SERS gain, still within the excitation of a single emitter. We have also investigated how this structure can be used under different polarization conditions and find that good field enhancements can be obtained for different

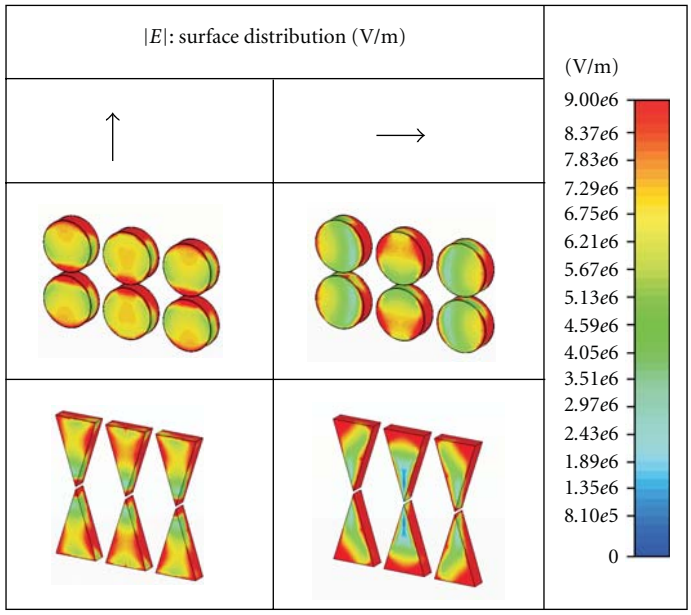

Figure 8: Absolute value of the field distribution for 3-element arrays of both disc dimers and bowties ($r = 40$ nm, $gap = 5$ nm) when the dipolar field is oriented along or perpendicular to the alignment axis of the dimers. The field is generated by a dipole with length 5 nm and current 1 A.

orientations of the dipolar source. This is a promising result, suggesting that other nanoparticle geometries and new array arrangements could be incorporated without detrimental effects to the sensing process.

Acknowledgment

This material is based upon work supported by the Department of Energy under Award Number DE-SC0006922.

References

[1] S. Nie and S. R. Emory, "Probing single molecules and single nanoparticles by surface-enhanced Raman scattering," *Science*, vol. 275, no. 5303, pp. 1102–1106, 1997.

[2] K. Kneipp, Y. Wang, H. Kneipp et al., "Single molecule detection using surface-enhanced Raman scattering (SERS)," *Physical Review Letters*, vol. 78, no. 9, pp. 1667–1670, 1997.

[3] R. Aroca, *Surface-Enhanced Vibrational Spectroscopy*, John Wiley and Son, Chichester, UK, 2006.

[4] H. C. Kim and X. Cheng, "SERS-active substrate based on gap surface plasmon polaritons," *Optics Express*, vol. 17, no. 20, pp. 17234–17241, 2009.

[5] L. C. T. Shoute, A. J. Bergren, A. M. Mahmoud, K. D. Harris, and R. L. McCreery, "Optical interference effects in the design of substrates for surface-enhanced raman spectroscopy," *Applied Spectroscopy*, vol. 63, no. 2, pp. 133–140, 2009.

[6] M. J. Banholzer, J. E. Millstone, L. Qin, and C. A. Mirkin, "Rationally designed nanostructures for surface-enhanced Raman spectroscopy," *Chemical Society Reviews*, vol. 37, no. 5, pp. 885–897, 2008.

[7] A. Campion, J. E. Ivanecky III, C. M. Child, and M. Foster, "Chemical enhancement in surface-enhanced raman scattering," *Journal of the American Chemical Society*, vol. 117, no. 47, pp. 11807–11808, 1995.

[8] P. Kambhampati, C. M. Child, M. C. Foster, and A. Campion, "On the chemical mechanism of surface enhanced Raman scattering: experiment and theory," *Journal of Chemical Physics*, vol. 108, no. 12, pp. 5013–5026, 1998.

[9] K. L. Kelly, E. Coronado, L. L. Zhao, and G. C. Schatz, "The optical properties of metal nanoparticles: the influence of size, shape, and dielectric environment," *Journal of Physical Chemistry B*, vol. 107, no. 3, pp. 668–677, 2003.

[10] R. Boyack and E. C. Le Ru, "Investigation of particle shape and size effects in SERS using T-matrix calculations," *Physical Chemistry Chemical Physics*, vol. 11, no. 34, pp. 7398–7405, 2009.

[11] A. Polemi and K. L. Shuford, "Fabry-Perot effect on dimer nanoantennas," *Photonics and Nanostructures* , vol. 10, no. 1, pp. 36–45, 2012.

[12] N. G. Alexopoulos and D. R. Jackson, "Fundamental superstrate (cover) effects on printed circuit antennas," *IEEE Transactions on Antennas and Propagation*, vol. 32, no. 8, pp. 807–816, 1984.

[13] D. R. Jackson and N. G. Alexopoulos, "Gain enhancement methods for printed circuit antennas," *IEEE Transactions on Antennas and Propagation*, vol. AP-33, no. 9, pp. 976–987, 1985.

[14] D. R. Jackson and A. A. Oliner, "Leaky-wave analysis of the high-gain printed antenna configuration," *IEEE Transactions on Antennas and Propagation*, vol. 36, no. 7, pp. 905–910, 1988.

[15] L. Allen and J. H. Eberly, *Optical Resonance and Two-Level Atoms*, Dover Publications, Dover, Del, USA, 1987.

[16] A. Polemi and S. Maci, "On the polarization properties of metamaterial lenses," *IEEE Antennas and Wireless Propagation Letters*, vol. 5, no. 1, pp. 306–310, 2006.

[17] E. D. Palik, *Handbook of Optical Constants of Solids*, Academic Press, Orlando, Fla, USA, 1985.

[18] A. Polemi, S. M. Wells, N. V. Lavrik, M. J. Sepaniak, and K. L. Shuford, "Local field enhancement of pillar nanosurfaces for SERS," *Journal of Physical Chemistry C*, vol. 114, no. 42, pp. 18096–18102, 2010.

[19] A. Polemi, S. M. Wells, N. V. Lavrik, M. J. Sepaniak, and K. L. Shuford, "Dispersion characteristics in Diskon-Pillar array nanostructures for surface enhanced Raman spectroscopy," *The Journal of Physical Chemistry C*, vol. 115, no. 28, pp. 13624–13629, 2011.

[20] "CST Computer Simulation Technology AG," Darmstadt, Germany, 2011, http://www.cst.com.

[21] T. Weiland, "Discretization Method for the Solution of Maxwell's Equations for Six-Component Fields," *AEU-Archiv fur Elektronik und Ubertragungstechnik*, vol. 31, no. 3, pp. 116–120, 1977.